R63-5

DASA-1358

STATIC AND DYNAMIC BEHAVIOR OF REINFORCED CONCRETE CIRCULAR ARCHES (PART I)

Written by
Vijay N. Gupchup
Jayendrakumar K. Shah

Supervised by
John M. Biggs

Sponsored by
DEFENSE ATOMIC SUPPORT AGENCY
NWER Subtask 13.106
Contract No. DA-49-146-XZ-105

March, 1963

R63-5

DASA-1358

DEPARTMENT OF CIVIL ENGINEERING

STATIC AND DYNAMIC BEHAVIOR OF REINFORCED CONCRETE CIRCULAR ARCHES

(PART I)

Written by

Vijay N. Gupchup

Indravadan K. Shah

Supervised by

John M. Biggs

March, 1963

Sponsored by

DEFENSE ATOMIC SUPPORT AGENCY

NWER Subtask 13.106

Contract DA-49-146-XZ-105

DSR 8984

School of Engineering

MASSACHUSETTS INSTITUTE OF TECHNOLOGY

Cambridge, 39, Massachusetts

PREFACE

This research was carried out in the Structures Division of the Department of Civil Engineering, under Contract DA-49-146-XZ-105 with the Defense Atomic Support Agency. The research was supervised and directed by Professor John M. Biggs and was carried out by Vijay N. Gupchup, Indravadan K. Shah, Leon R. Wang, Charles R. Nelson and Shui Ho. The Structural Dynamics Laboratory, where the experiments were carried out, is under the the overall supervision of Professor R. J. Hansen.

Appreciation is extended to E. F. McCaffery, E. N. Brinkerhoff, R. J. Cronin, R. E. Brooks, and J. P. Brown for their help in performing the experiments.

Special thanks are due to the Defense Atomic Support Agency for sponsoring the research and to the Computation Center of M.I.T. for the use of the computer facilities.

SUMMARY

OBJECTIVE

The main objectives of this research program are (1) to obtain an analytical solution for the nonlinear response and ultimate loads of two hinged reinforced concrete circular arches, subjected to static and dynamic loads; (2) to determine experimentally the static and dynamic ultimate loads of two-hinged semicircular reinforced concrete arches under certain typical loading conditions and (3) to estimate experimentally as well as analytically the values of the ductility factor μ at failure, μ being defined as the ratio of maximum deflection at failure to the elastic limit deflection.

The nonlinearity of the response is due to the nonlinear stress-strain curve of concrete and also due to the effect of large deflections on the strains and equilibrium of an element of the arch.

SCOPE

The analytical part of this research program includes the formulation of the governing equations and boundary conditions for both static and dynamic cases, taking into account the nonlinear stress-strain curve of concrete and the effects of large deformations on the strains and equilibrium of the arch element. The governing equations are obviously nonlinear and discontinuous and are solved by numerical methods. Programs for the IBM 7090 digital computer are prepared for computing the response and the ultimate loads, using these numerical methods.

The experimental program includes the testing of small scale semi-circular arches to determine the static and dynamic ultimate loads and the ductility factor μ

for the following loading conditions:

1. Uniformly distributed symmetric radial loads.
2. A concentrated load at the crown.
3. Antisymmetric concentrated loads at quarter points.

CONCLUSIONS

The experimental and analytical studies indicate that the approximate conventional theory based on limit analysis is quite adequate to predict the static ultimate loads of the underreinforced arches. The dynamic ultimate loads for compression mode loading can also be predicated by approximate theory provided that an appropriate dynamic increase factor (based on the increase in material properties) is used. However, it is not clear whether a satisfactory approximate theory can be developed to predict the ultimate dynamic load carrying capacity of the arch, subjected to a concentrated dynamic load at the crown or antisymmetric concentrated dynamic loads at quarter points.

The experimental and analytical investigations also indicate that the natural periods of the arches have a significant influence on the dynamic load carrying capacity of the arches in the cases of a concentrated load at the crown and antisymmetric concentrated loads at quarter points. The mode of failure under both static and dynamic loads is quite ductile in these cases as compared to the compression mode loading.

TABLE OF CONTENTS

		Page
Summary		i
Table of Contents		iii
List of Figures		vii
List of Tables		xi
List of Symbols		
CHAPTER I	INTRODUCTION	
1.1	Objective	1
1.2	Previous Work	
1.2.1	Analytical Work	1
1.2.2	Experimental Work	3
1.3	Scope	
1.3.1	Analytical Study	4
1.3.2	Experimental Study	5
1.3.3	Comparison of Analytical and Experimental Studies	6
CHAPTER 2	THEORETICAL INVESTIGATION	
2.1	Material Properties	
2.1.1	Concrete	7
2.1.2	Reinforcing Steel	11
2.1.3	Failure Criterion	13
2.2	Geometry of the Arch	14
2.3	Static Response	
2.3.1	Governing Equations	15
2.3.2	Nondimensionalization of the Equations	23
2.3.3	Finite Difference Formulation	26
2.3.4	Numerical Method of Solution	30

TABLE OF CONTENTS (Cont'd)

		Page
2.3.5	Calculation of Ultimate Load	34
2.3.6	Digital Computer Program	35
2.3.7	Convergence	35
2.4	Dynamic Response	
2.4.1	Governing Equations	38
2.4.2	Nondimensionalization of the Equations	41
2.4.3	Finite-Difference Formulation	46
2.4.4	Numerical Method of Solution	50
2.4.5	Calculation of the Ultimate Load	52
2.4.6	Digital Computer Program	58
2.4.7	Selection of Space and Time Intervals	58
2.5	Conventional Theory for Predicting Ultimate Loads and Deflections	
2.5.1	Uniformly Distributed Symmetric Radial Load	61
2.5.2	Concentrated Load at Crown	63
2.5.3	Antisymmetric Concentrated Loads at Quarter Points	65
2.6	Ductility Factor	66
2.7	Comparison of Dynamic Ultimate Loads - Non-Linear Theory and Approximate Theoretical Analysis	67
CHAPTER 3	EXPERIMENTAL INVESTIGATION	
3.1	Test Specimen	72
3.2	Material Properties	
3.2.1	Concrete	73
3.2.2	Steel	74

TABLE OF CONTENTS (Cont'd)

		Page
	3.3 Loading Conditions	75
	3.4 Experimental Set Up	
	3.4.1 Modification of the Existing Loading Machine	75
	3.4.2 Instrumentation and Measurements	79
	3.5 Testing Technique	
	3.5.1 Static Tests	84
	3.5.2 Dynamic Tests	85
CHAPTER 4	EXPERIMENTAL RESULTS	
	4.1 Introduction	107
	4.2 General	
	4.2.1 General	107
	4.2.2 Static Tests	108
	4.2.3 Dynamic Tests	109
	4.3 Summary of Test Results - Type II Loading	
	4.3.1 General	111
	4.3.2 Static Tests	111
	4.3.3 Dynamic Tests	113
	4.4 Summary of Test Results - Type III Loading	
	4.4.1 General	114
	4.4.2 Static Tests	115
	4.4.3 Dynamic Tests	117
	4.5 Natural Period of Arch Specimens	125
CHAPTER 5	COMPARISON OF THEORETICAL AND EXPERIMENTAL RESULTS	
	5.1 Introduction	141
	5.2 Theoretical and Experimental Results and their Comparison	
	5.2.1 Type I - Loading	141

TABLE OF CONTENTS (Cont'd)

		Page
5.2.2	Type II - Loading	145
5.2.3	Type III - Loading	146
CHAPTER 6	CONCLUSIONS	170
APPENDIX I	VARIOUS CONSIDERATIONS FOR FORCE-STRAIN RELATIONS BASED ON LINEAR CONCRETE STRESS-STRAIN CURVE	173
APPENDIX II	'NEWTON-RAPHSON ITERATION' FOR SOLVING NONLINEAR SIMULTANEOUS ALGEBRAIC EQUATIONS	177
APPENDIX III	CONCISED FLOW-CHART AND DIGITAL COMPUTER PROGRAM STATIC CASE	188
APPENDIX IV	CONCISED FLOW-CHART AND DIGITAL COMPUTER PROGRAM - DYNAMIC CASE	214
BIBLIOGRAPHY		230

LIST OF FIGURES

		Page
Figure 2.1	Static and Dynamic Stress-Strain Curves for Concrete	8
2.2	Static and Dynamic Stress-Strain Curves for Steel.	11
2.3	Geometry of the Arch	14
2.4	Forces Acting on a Deformed Element	15
2.5	Arch Section and Possible Strain Distributions	19
2.6	The Discrete System	27
2.7	Arch with External Reactions	30
2.8	Semi-circular Arch under a Uniform Antisymmetrical Load	36
2.9	Dynamic Forces Acting on a Deformed Element	39
2.10	Load-Time Curves	51
2.11	Selection of Time Interval	60
2.12	Triangular Load Pulse	68
2.13	Comparison of Analytical Results with Approximate Analysis	71
3.1	Type A Specimen	87
3.2	Type B Specimen	88
3.3	Wooden Formwork for Type A Specimens	89
3.4	Device for Making Reinforcement Cages for Type A Specimen	89

LIST OF FIGURES (Continued)

			Page
Figures	3.5	Stress-Strain Curve - No. 7 Wires	90
	3.6	Stress-Strain Curve - No. 12 Wires	91
	3.7	Type of Loading	92
	3.8	Push Side Reservoir	93
	3.9	Pull Side Reservoir	94
	3.10	Schematic Diagram of Loading Unit	95
	3.11	Experimental Set Up - Type I Loading	96
	3.12	Experimental Set Up - Type II Loading	97
	3.13	Experimental Set Up - Type III Loading	98
	3.14	Hinge Supports for Test Specimen	99
	3.15	Supporting Detail "X" For Type A Specimen	100
	3.16	Supporting Detail "X" for B Specimen	101
	3.17	Supporting Detail "Y" for B Specimen	102
	3.18	Load Cells for Measuring Applied Load	103
	3.19	Reaction Load Cells	104
	3.20	L.V.D.T. Locations	105
	3.21	Attachment for L. V. D. T.	106
	4.1	Appearance of Specimen A-4 after Test - (Static Test - Type I Loading)	126
	4.2	Appearance of Specimen B-10 after Test - (Static Test - Type I Loading)	127
	4.3	pu_{EXP} vs pu_{THST} - Type I Loading	128
	4.4	Appearance of Specimen A-17 after Test (Dynamic Test - Type I Loading)	129

LIST OF FIGURES (Continued)

			Page
Figure	4.5	Appearance of Specimen B-13 after Test (Dynamic Test - Type I Loading)	130
	4.6	Appearance of Specimen A-21 after Test (Static Test - Type II Loading)	131
	4.7	Appearance of Specimen B-21 after Test (Static Test Type II Loading)	132
	4.8	$P_{u_{EXP}}$ vs. $P_{u_{TH_{ST}}}$ - Type II Loading	133
	4.9	Appearance of Specimen A-25 after Test (Dynamic Test - Type II Loading)	134
	4.10	Appearance of Specimen B-22 after Test (Dynamic Test - Type II Loading)	135
	4.11	Appearance of Specimen A-30 after Test (Static Test - Type III Loading)	136
	4.12	Appearance of Specimen B-26 after Test (Static Test - Type III Loading)	137
	4.13	$P_{u_{EXP}}$ vs. $P_{u_{TH_{ST}}}$ - Type III Loading	138
	4.14	Appearance of Specimen A-35 after Test (Dynamic Test - Type III Loading)	139
	4.15	Appearance of Specimen B-31 after Test (Dynamic Test - Type III Loading)	140
	5.1	Specimen A-5	155
	5.2	Specimen A-11 (Failure Pulse)	156

LIST OF FIGURES (Continued)

			Page
Figure	5.3	Specimen A-17 (Failure Pulse)	157
	5.4	Specimen A-17 (Partial Pulse)	158
	5.5	Specimen B-14 (Failure Pulse)	159
	5.6	Load-Deflection (Dynamic Case)	160
	5.7	Specimen A-21	161
	5.8	Specimen B-21	162
	5.9	Specimen A-24	163
	5.10	Specimen B-24	164
	5.11	Specimen A-28	165
	5.12	Specimen A-34	166
	5.13	Specimen B-26	167
	5.14	Specimen A-37	168
	5.15	Specimen B-32	169

LIST OF TABLES

		Page
Table 4.1	Summary of Type A Specimens - Type I Loading	119
4.2	Summary of Type B Specimens - Type I Loading	120
4.3	Summary of Type A Specimens - Type II Loading	121
4.4	Summary of Type B Specimens - Type II Loading	122
4.5	Summary of Type A Specimens - Type III Loading	123
4.6	Summary of Type B Specimens - Type III Loading	124
4.7	Natural Periods	125
5.1a	Comparison of Theoretical and Experimental Results - Type I Loading, Type A Specimens	150
5.1b	Comparison of Theoretical and Experimental Results - Type I Loading, Type B Specimens	151
5.2	Comparison of Theoretical and Experimental Results - Type III Loading	152
5.3	Comparison of Static and Dynamic Behavior - Type I Loading	153

LIST OF TABLES

		Page
TABLE 5.4	Comparison of Static and Dynamic Behavior	154

LIST OF SYMBOLS

A_g	Gross area of the reinforced concrete section
A_s	Area of tension steel
A'_s	Area of compression steel
b	Width of the cross-section of the arch
C_s	Seismic velocity in concrete
d	Distance from extreme compressive fibre to the centroid of tensile steel
d'	Distance between the centroids of tension and compression steels
DIF	Dynamic Increase Factor
e_o	Strain in the middle surface of the cross-section
e_1	Strain in the innermost (bottom) fibre of the cross-section
e_2	Strain in the inner (bottom) steel
e_3	Strain in the outer (top) steel
e_4	Strain in the outermost (top) fibre of the cross-section
e_c	Static compressive strain in concrete
e_c	Static strain rate of concrete

LIST OF SYMBOLS (continued)

e'_c	Concrete compressive strain corresponding to a stress = f''_c
e_{dc}	Dynamic compressive strain in concrete
$\dot{e}_{dc}$	Dynamic strain rate of concrete
e'_{dc}	Concrete compressive strain corresponding to a stress = f''_{dc}
e_s	Static strain in steel
e_{ds}	Dynamic strain in steel
e_u	Ultimate strain in concrete
e_y	Static yield strain in steel
e_{dy}	Dynamic yield strain in steel
E_c	Initial tangent modulus of concrete
$\bar{E}_c$	Secant modulus of concrete
E_s	Modulus of elasticity of steel
f'_c	Static ultimate compressive stress of concrete, as obtained from cylinder tests
f''_c	$0.85\ f'_c$

f'_{dc}	Dynamic ultimate compressive stress of concrete
f''_{dc}	$0.85\, f''_{dc}$
f_y	Static yield stress of steel
f_{dy}	Dynamic yield stress of steel
f_u	Ultimate stress of steel
H_A, H_B	Horizontal reactions of the arch at the left and the right supports
i	Index denoting a section on the discretized arch
I_{av}	Average of moments of inertia of the cracked and the uncracked sections
I_g	Gross moment of inertia of the uncracked reinforced concrete section
j	Index denoting a segment of the discretized arch
k	Index denoting time interval, also a constant
m	Number of discrete sections
M	Bending moment on the cross-section of the arch
n	Modular Ratio $= \frac{E_s}{E_c}$
N	Axial thrust on the cross-section of the arch

p	$\frac{A_s}{bd}$
p_m	Dynamic ultimate load having a triangular load-time dependence and zero rise time (lbs/inch)
p_r	Radial load on the arch in lbs/inch
p_θ	Tangential load on the arch in lbs/inch
p_t	$\frac{(A_s + A_s')}{bt}$
$p_{u_{ANA}}$	Analytical ultimate load (lbs/inch) compression mode loading
$p_{u_{EXP}}$	Experimental ultimate load (lbs/inch) compression mode loading
$p_{u_{TH_{ST}}}$	Conventional theoretical static ultimate load (lbs/inch) - compression mode loading
Pu_{ANA}	Analytical ultimate load (lbs) - Antisymmetric quarter point loading
Pu_{EXP}	Experimental ultimate load (lbs) -
$P_{u_{TH_{ST}}}$	Conventional theoretical static ultimate load (lbs)

LIST OF SYMBOLS (continued)

Q	Shear force on the cross-section
r_o	Mean radius of the arch
t	Depth of the cross-section of the arch, also variable time
Δt	Time interval
t_r	Rise time of the dynamic load
t_1	Duration of a triangular dynamic load pulse with zero rise time
T	Natural period of the arch
u	Tangential deflection of an arch element
V_A, V_B	Vertical reactions of the arch at the left and the right support
w	Radial deflection of an arch element
W	Nondimensional radial deflection of an arch element
Σw_m	Sum of the radial deflections at crown and at 54° points in the case of compression mode loading
w_q	Deflection at quarter point

LIST OF SYMBOLS (continued)

θ	Angle subtended at the center of the arch by an arc between the left support and any point on the arch
$\Delta\theta$	Angle subtended at the center of the arch by an element of the discretized arch
ϕ_o	Half the central angle of the arch
μ	Ductility Factor
ρ	Density of reinforced concrete
χ	Change in the curvature of an arch element

CHAPTER 1

INTRODUCTION

1.1 OBJECTIVE

This research program has the following threefold objectives:

a) To obtain an analytical solution for the non-linear response and the ultimate loads of two-hinged circular reinforced concrete arches under static and dynamic loading. The nonlinearity of the response is obtained by including the effects of the nonlinear stress-strain curve of concrete under compression and those of large deflections on the strains and the equilibrium of an element of the arch.

b) To determine experimentally the static and dynamic ultimate loads of two-hinged semicircular reinforced concrete arches under certain conditions of loading.

c) To obtain the analytical and the experimental values of the ductility-factor μ at failure, μ being defined as the ratio of the maximum deflection at failure to the elastic limit deflection.(Refer to § 2.6)

1.2 PREVIOUS WORK

1.2.1 Analytical Work:

In 1932, Cross and Morgan[1]* summarized

* Superscripted numbers in parentheses refer to references given in the bibliography.

methods of analysis and design of reinforced concrete arches under static loading. These methods were based on the conventional linear elastic theory for reinforced concrete structures. In 1951, a special committee of the American Concrete Institute published a joint report[2] on plain and reinforced concrete arches. This report recommends a numerical procedure to account for the moments caused by the axial thrust and the deflection of the arch. It also suggests the use of Whitney's stress block method for obtaining the ultimate strength of the cross-section of the arch. In 1953, Onat and Prager published a paper[3] concerning limit analysis of arches constructed from homogeneous elastic-plastic materials. This paper proposes a theory to account for the reduction of the plastic moment of a section which is subjected to both a moment and a thrust. However, since in this paper the properties of materials are considered to be identical in compression and tension, the proposed theory cannot be applied to reinforced concrete arches. In 1960, Jain published a paper[4] on ultimate strength of reinforced concrete arches. In this paper the author has employed a

bilinear elastic-plastic stress-strain curve for concrete and obtained the ultimate loads making use of an iterative procedure to account for large plastic deformations of the arch.

In the field of dynamic response, Love[5] has presented the mathematical formulation of the vibration of a circular elastic ring and obtained the normal functions of free vibrations. In 1960, Eppink and Veletsos published a paper[6] on dynamic analysis of circular elastic arches. Later this work was continued to include inelastic effects[7]. The authors have considered a material with bilinear stress-strain curve and identical properties in compression and tension. They have developed a set of governing equations to include the effects of large deflections and have used a numerical method to solve these equations.

1.2.2 Experimental Work:

A series of large scale static tests on reinforced concrete arch ribs[15] and three span reinforced concrete arch bridges[16] were conducted by Wilson. In this work the measured values of the reactions and stresses due to unit loads were found to be in close agreement with the theoretical values based on linear elastic theory. Jain[4] tested two-hinged reinforced concrete arches to failure and showed good agreement between results obtained from the tests and those obtained by using his proposed theory.

In the field of dynamic testing Technical Report No. 2-590 of Corps of Engineers discusses the results of tests conducted on underground and buried fixed-end and two-hinged reinforced concrete arches. This test program was a part of operation PLUMBBOB in 1957.

1.3 SCOPE

1.3.1 Analytical Study :

A set of equations and boundary conditions governing the behavior of a reinforced concrete arch are formulated. The equations are derived from the conditions of equilibrium, strain-displacement relations and force-strain relations. The equations in cases of the static and the dynamic response differ in that in the latter case, the equilibrium equations include the effects of inertial forces and the dynamic properties of both concrete and steel are used to obtain the force-strain relations.

A simultaneous solution of the governing equations yields the response of the reinforced concrete arch. The equations being nonlinear and discontinuous* they are solved by numerical methods. Programs for the IBM 7090 digital computer are prepared for computing the response using these methods. The ultimate load of the arch is obtained as a load

---

*The force-strain relations are discontinuous since they consist of three groups (Figs. 2.5b, 2.5c, and 2.5d), each valid for a different strain distribution.

under which the maximum compressive strain in the arch reaches or exceeds the ultimate strain e_u, of concrete. The small reserve strength which exists in the arch at this stage is neglected. Because of the particular definition of ultimate load used in this work, the analytical methods developed can predict the ultimate loads of only the following types of loadings:

a) Uniformly distributed compression mode loading

b) Anti-symmetrically distributed deflection mode loading

and c) Symmetrical and antisymmetrical concentrated loads except a single concentrated load at the crown. This aspect is discussed in detail in § 2.1.3.

1.3.2 Experimental Study:

The scope of the experimental program included the testing of small scale model arches and the determination of the static and dynamic ultimate loads and the ductility-factor μ at failure for the following conditions of loading:

a) Uniformly distributed symmetric radial loads

b) A concentrated load at the crown

and c) Antisymmetric concentrated loads at quarter points.

In the dynamic cases, a failure load pulse of triangular shape

having a rise time between ten and twenty milliseconds was applied. Dynamic tests were also conducted under partial loads for the uniformly distributed symmetrical loading case.

1.3.3 Comparison of Analytical and Experimental Studies:

Within the scope outlined above a comparison between analytical and experimental investigations is obtained. Also, the static and dynamic behaviors of two-hinged reinforced concrete arches are compared.

CHAPTER 2

THEORETICAL INVESTIGATION

2.1 MATERIAL PROPERTIES

In this article the nonlinearity of the stress-strain curve of concrete under compressive loading is discussed. Also the effects of rapid rates of straining on both concrete and reinforcing steel are presented herein.

2.1.1 Concrete:

a) Static Behavior: A typical stress-strain curve for a concrete cylinder under static compressive loading is shown in Fig. 2.1. Hognestad[8] suggested that Ritter's parabola was a good approximation for the curve up to ultimate stress and that Inge Lyse's equation for the initial tangent modulus was satisfactory, provided that f_c' in that equation was replaced by $0.85\, f_c'$. Hognestad assumed the descending portion of the curve to be a straight line. However, the shape and the extent of this portion of the curve is both uncertain and difficult to measure. Hence, Hognestad's expressions are used to describe the stress-strain curve upto failure. The expressions are

$$f_c'' = 0.85\, f_c' \qquad (2.1a)$$

$$E_{soc} = E_c = 1800000 + 460\, f_c'' \text{ psi.} \qquad (2.1b)$$

$$e_c' = \frac{2f_c''}{E_c} \qquad (2.1c)$$

$$f_c = f_c'' \left[\frac{2e_c}{e_c'} - \left(\frac{e_c}{e_c'} \right)^2 \right] \qquad (2.1d)$$

and $$e_u = 0.0038 \qquad (2.1e)$$

where f_c' = Static ultimate stress of concrete obtained from cylinder tests

e_c' = Strain corresponding to stress f_c''

e_u = Static ultimate strain of concrete

E_{soc} = Static initial tangent modulus of concrete

and f_c and e_c = Corresponding stress and strain on the static curve

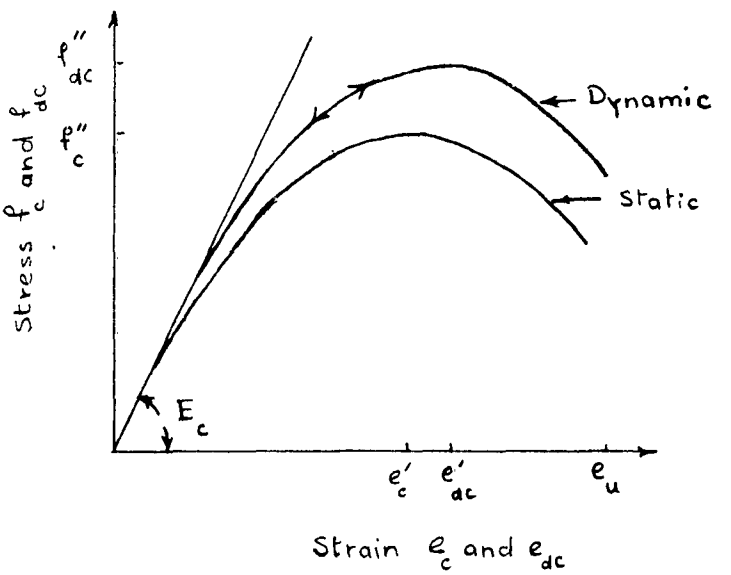

Figure 2.1 Static and Dynamic Stress-Strain Curves for Concrete

The tensile stresses in concrete under static loading are neglected.

b) Dynamic Behavior: A typical stress-strain curve for a concrete cylinder under compressive loading with a rapid strain rate is also shown in Fig. 2.1. Watstein[9] compared the compressive strengths of concrete cylinders tested at rates of strain varying from a low value of 10^{-6} in./(in.)(sec.) to a very high value of 10 in./(in.)(sec.). His work indicates that, with very high rates of strain, the dynamic ultimate strength can be much greater than the static ultimate strength. Yang, et al[10] suggest that the parameters associated with the dynamic stress-strain curve may be obtained by using

$$\frac{f'_{dc}}{e'_{dc}} = \frac{f'_c}{e'_c} \qquad (2.2a)$$

$$e'_{dc} = e'_c \left[1 + \frac{1}{300}\left(\log_{10} \frac{\dot{e}_{dc}}{\dot{e}_c}\right)^2\right] \qquad (2.2b)$$

and $$E_{doc} = E_{soc} = E_c \qquad (2.2c)$$

where f'_{dc} = Dynamic ultimate stress of concrete obtained from cylinder tests conducted at rapid strain rates

e'_{dc} = Strain corresponding to stress f''_{dc}

E_{doc} = Dynamic initial tangent modulus of concrete

$\dot{e}_{dc}$ = Dynamic strain rate of concrete

$\dot{e}_{c}$ = Static strain rate of concrete

Making use of relations similar to those used for static behavior we obtain the following expressions:

$$f''_{dc} = 0.85 f'_{dc} \qquad (2.3a)$$

$$f_{dc} = f''_{dc} \left[\frac{2 e_{dc}}{e'_{dc}} - \left(\frac{e_{dc}}{e'_{dc}} \right)^2 \right] \qquad (2.3b)$$

$$e_{du} = e_{u} = 0.0038 \qquad (2.3c)$$

where f_{dc} and e_{dc} = Corresponding stress and strain on the dynamic curve

and e_{du} = Dynamic ultimate strain of concrete.

Stress-strain curve for unloading and reloading of concrete is assumed to be the same as that for the initial loading. Also, the tensile stresses in concrete are assumed to be negligible.

2.1.2 Reinforcing Steel:

a) Static Behavior: The stress-strain curve for steel under static compressive and tensile loading is shown in Fig. 2.2. The following expressions are used to describe the stress-strain relation.

$$\left.\begin{aligned} & f_s = E_s e_s \qquad \text{for} \quad e_s < e_y \\ \text{and} \quad & f_s = f_y \qquad \text{for} \quad e_s > e_y \end{aligned}\right\} \quad (2.4)$$

where f_y = Static yield stress of steel

e_y = Static yield strain of steel

E_s = Modulus of elasticity of steel

and f_s and e_s = Corresponding stress and strain on the static curve.

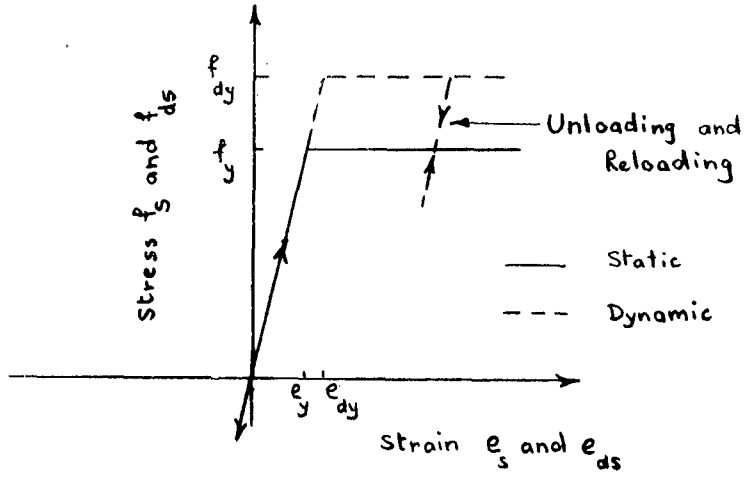

Figure 2.2 Static and Dynamic Stress-Strain Curves for Steel

b) Dynamic Behavior: The effect of rapid strain rates is to increase the yield stress of steel above the values obtained under static loading. The modulus of elasticity remains practically unaffected. Figure 2.5 of Ref.[11] shows the effect of strain rate on the dynamic yield stress of steel. It can be seen that for both structural and intermediate grades, the increase in the yield stress above the static value varies between 20 and 40% when the time to reach this yield stress varies between 0.001 and 0.1 seconds. Hence in this work the dynamic yield stress is assumed to be 30% larger than the static yield stress. Behavior of steel in tension and compression is assumed to be identical.

The dynamic stress-strain curve for steel is also shown in Fig. 2.2. The following expressions describe the stress-strain relationship.

$$\left.\begin{aligned} f_{ds} &= E_s\, e_{ds} && \text{for} \quad e_{ds} < e_{dy} \\ \text{and} \quad f_{ds} &= f_{dy} && \text{for} \quad e_{ds} > e_{dy} \end{aligned}\right\} \qquad (2.5)$$

The stress-strain curve for unloading is assumed to be linear (Fig. 2.2), the slope being equal to E_s.

The reloading curve is assumed to be linear with a slope equal to E_s when the dynamic strain is less than the previous maximum dynamic strain; however, when the dynamic

strain is greater than the previous maximum dynamic strain, the reloading curve is assumed to be indentical with the initial loading curve.

2.1.3 Failure Criterion:

A failure criterion based on excessive compressive strain in concrete has been used. It is assumed that failure occurs when at any section of the arch the combination of the thrust and the moment produces a compressive strain which exceeds the ultimate strain for concrete, e_u. Such a criterion would indicate failure when the strain in the extreme fibre of any section becomes greater than e_u.

This criterion neglects a certain reserve strength in the structure because even after the strain in the extreme fibre exceeds e_u, the inner fibres up to the neutral axis have low compressive strains. Further, in a statically indeterminate structure, more sections than one have to fail before the structure collapses. If the load distribution on the structure is such that the failure of the necessary number of sections (the number depending upon the degree of indeterminancy) occurs at a load which differs only a little from the load at which the first section fails, the failure criterion used here would be adequate. Such load distributions on a two-hinged circular arch are,

a) uniformly distributed symmetrical loads

b) uniformly distributed antisymmetrical loads

and c) symmetrical and antisymmetrical concentrated loads, except a concentrated load at the crown.

This failure criterion is inadequate when a single concentrated load is considered because when the maximum compressive strain at the section under the load exceeds e_u, the other sections of the arch have low compressive strains and hence the arch has a considerable reserve strength.

The failure criterion thus gives a lower bound of the ultimate load for the above-mentioned distributions. However, for design purposes this may be a realistic limit.

2.2 GEOMETRY OF THE ARCH

The two-hinged arch under consideration is shown in Fig.2.3. The geometry of the arch is described by the following:

r_o = Mean radius of the arch

ϕ_o = Half the central angle

b = Width of the cross section

t = Depth of the cross section

and θ = Angle subtended at the center by an arc between the left support and any point on the arch.

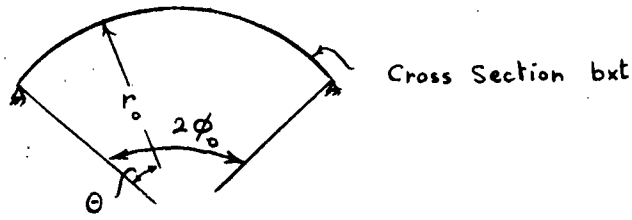

Figure 2.3 Geometry of the Arch

2.3 STATIC RESPONSE

2.3.1 Governing Equations:

a) Equations of Equilibrium: Fig. 2.4 shows the geometry of deformation of an element of the arch and the forces acting on it.

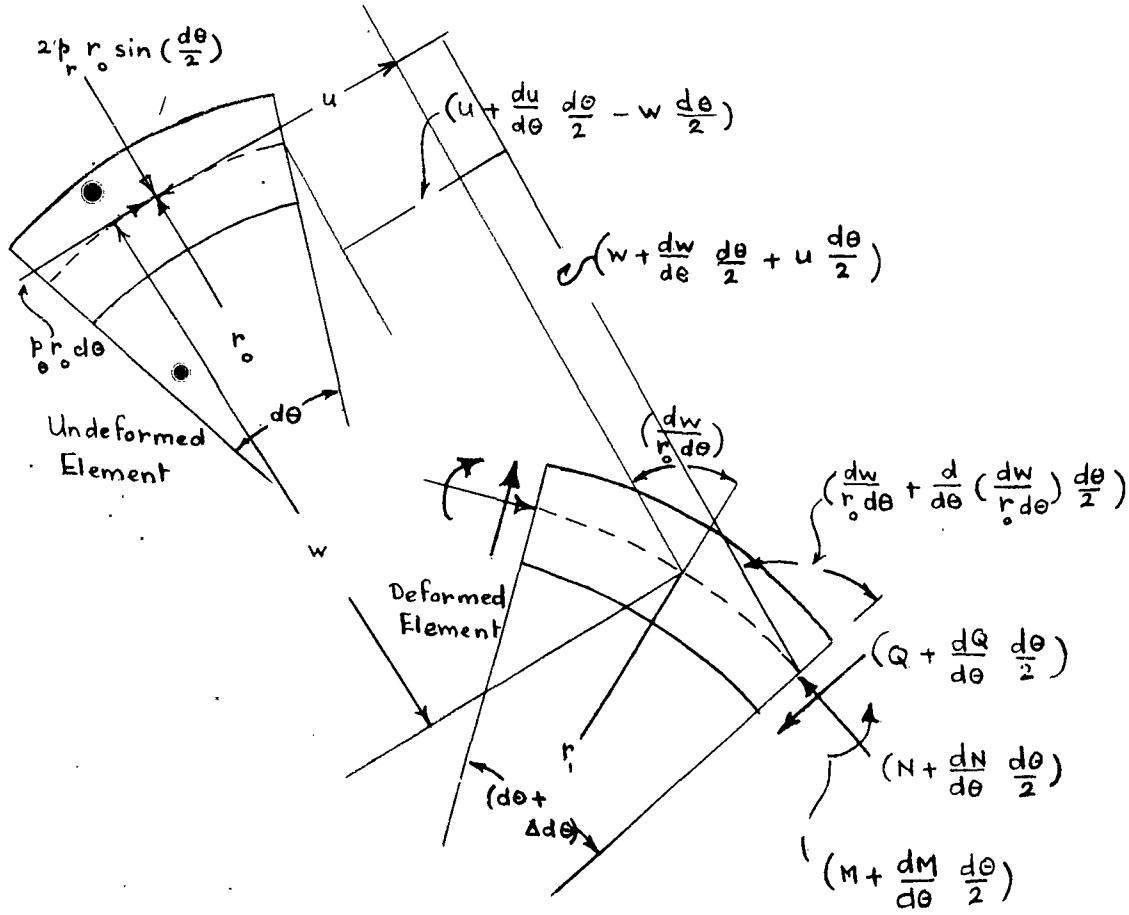

Forces and Displacements are Shown in Positive Sense

Figure 2.4 Forces Acting on a Deformed Element

Considering the equilibrium of the forces in r and θ directions and the moment equilibrium, the following equations are obtained:

$$2 p_r r_o \sin\left(\frac{d\theta}{2}\right) - 2Q \sin\left(\frac{d\theta}{2}\right) \sin(\Delta d\theta) - 2N \sin\left(\frac{d\theta}{2}\right) \cos(\Delta d\theta) + \frac{dQ}{d\theta} d\theta \cos\left(\frac{d\theta}{2}\right) \cos(\Delta d\theta) - \frac{dN}{d\theta} d\theta \cos\left(\frac{d\theta}{2}\right) \sin(\Delta d\theta) = 0 \qquad (2.6)$$

$$p_\theta r_o d\theta + 2N \sin\left(\frac{d\theta}{2}\right) \sin(\Delta d\theta) - 2Q \sin\left(\frac{d\theta}{2}\right) \cos(\Delta d\theta) - \frac{dN}{d\theta} d\theta \cos\left(\frac{d\theta}{2}\right) \cos(\Delta d\theta) - \frac{dQ}{d\theta} d\theta \cos\left(\frac{d\theta}{2}\right) \sin(\Delta d\theta) = 0 \qquad (2.7)$$

and $$\frac{dM}{d\theta} - Q r_o \cos\left(\frac{d\theta}{4}\right) + \frac{dN}{d\theta} r_o \sin\left(\frac{d\theta}{4}\right) = 0 \qquad (2.8)$$

where

p_r	= Radial component of load per unit length of the arc
p_θ	= Tangential component of load per unit length of the arc
$d\theta$	= Angle subtended at the center by the element before deformation
$\Delta d\theta$	= Change in $d\theta$ due to deformation
N	= Axial force on the section
M	= Bending moment on the section
Q	= Shear force on the section

b) Strain-displacement Relations: Assuming that the normals to the middle surface remain normal after the deformation and that the shear strains are negligible, expressions for the strain in the middle surface, e_o and the change in curvature χ are obtained as follows (Fig. 2.4):

The length and the curvature of the undeformed element are

$$ds = r_o\, d\theta \quad ; \quad \frac{d\theta}{ds} = \frac{1}{r_o} \qquad (a)$$

The square of the length of the deformed element is

$$(ds + \Delta ds)^2 = \left(\frac{du}{d\theta}\, d\theta + (r_o - \omega)\, d\theta\right)^2 + \left(\frac{d\omega}{d\theta} + \frac{u}{2}\, d\theta\right)^2 \qquad (b)$$

where u = Tangential displacement of the element, measured positive when the element moves clockwise

and w = Radial displacement of the element, measured positive when the element moves toward the center.

Since the compressive strain in the middle surface is

$$e_o = -\frac{\Delta ds}{ds}$$

we get,

$$(1 - e_o)^2 (r_o\, d\theta)^2 = (ds + \Delta ds)^2 \qquad (c)$$

From equations (b) and (c), neglecting the higher order terms we obtain,

$$e_o = \frac{1}{r_o}\left(w - \frac{du}{d\theta}\right) - \frac{1}{r_o^2}\left[\frac{1}{2}\left(\frac{dw}{d\theta}\right)^2 + u\frac{dw}{d\theta}\right] \qquad (2.9)$$

The linear expression,

$$\Delta d\theta = \frac{1}{r_o}\frac{d^2w}{d\theta^2}\,d\theta \qquad (d)$$

is used to obtain the change in angle $d\theta$ due to deformation.

Again, since the nonlinear terms contribute insignificantly to the quantity $\varkappa$, a linear expression is obtained as follows:

The curvature of the deformed element is

$$\frac{1}{r_1} = \frac{(d\theta + \Delta d\theta)}{(ds + \Delta ds)} \qquad (e)$$

Using linear expressions for $\Delta d\theta$ and ΔdS, equation (e) becomes

$$\frac{1}{r_1} = \frac{\left(d\theta + \frac{1}{r_o}\frac{d^2w}{d\theta^2}d\theta\right)}{r_o\,d\theta + \left(\frac{du}{d\theta} - w\right)d\theta}$$

Or, neglecting the quantities of higher order,

$$\frac{1}{r_1} = \frac{1}{r_o} + \frac{w}{r_o^2} + \frac{1}{r_o^2}\cdot\frac{d^2w}{d\theta^2} - \frac{1}{r_o^2}\cdot\frac{du}{d\theta}$$

Hence, the change in curvature,

$$\chi = \left(\frac{1}{r_1} - \frac{1}{r_o}\right) = \frac{1}{r_o^2}\left(w + \frac{d^2w}{d\theta^2} - \frac{du}{d\theta}\right) \qquad (2.10)$$

c) Force-strain Relations: Fig. 2.5a shows a symmetrically reinforced rectangular concrete section of an arch, acted upon by a positive bending moment M and a positive thrust N. Depending upon the relative magnitudes of M and N, the strain distribution across the section will be as shown in either Fig. 2.5b or Fig. 2.5c. It is assumed that the ratio of r_o/t is large enough to neglect the nonlinearity of the strain distribution across the depth of section. If the thrust N is negative, it is possible that the entire section will be in tension. (Fig. 2.5d)

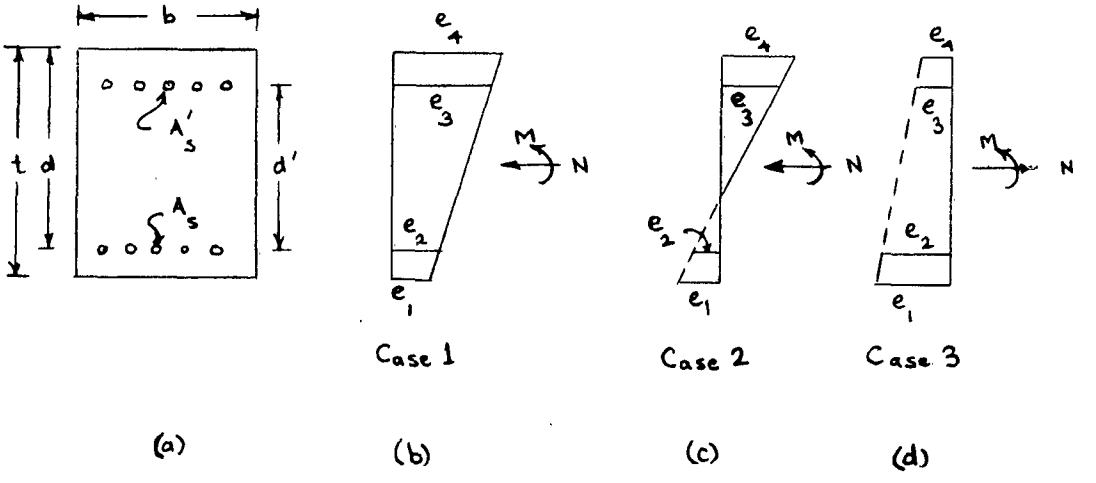

Figure 2.5 Arch Section and Possible Strain Distributions

Noting that positive bending moment causes a decrease in the initial curvature of the arch, we have

$$\left.\begin{aligned} e_o &= \frac{(e_1 + e_4)}{2} \\ \text{and} \quad \chi &= \frac{(e_1 - e_4)}{t} \end{aligned}\right\} \qquad (2.11)$$

Using the stress-strain properties of concrete and steel described in § 2.1.1a and 2.1.2a respectively, the following relations between M, N, e_1, e_2, e_3 and e_4 are obtained,

Case 1 - Section completely in compression

i.e., $e_4 \leqslant e_u$ and $e_1 \geqslant 0$

$$\frac{N}{f''_c bt} = \frac{E_s p_t}{2 f''_c} \left(1 - \frac{1}{n}\right)(e_2 + e_3) + \frac{A_1}{(e_4 - e_1)} \qquad (2.12)$$

$$\text{and} \quad \frac{M}{f''_c bt^2} = \frac{E_s p_t}{4 f''_c} \cdot \frac{d'}{t} \left(1 - \frac{1}{n}\right)(e_3 - e_2) + \frac{B_1}{(e_4 - e_1)^2}$$

$$- \frac{(e_1 + e_4)}{2(e_4 - e_1)^2} A_1 \qquad (2.13)$$

where A_s = Area of tension steel

A_s' = Area of compression steel = A_s

$p_t = \frac{(A_s + A_s')}{bt}$

n = Modular ratio, E_s/E_{sc}

E_{sc} = Secant modulus of concrete

$$A_1 = \frac{(e_4^2 - e_1^2)}{e_c'} - \frac{(e_4^3 - e_1^3)}{3e_c'^2}$$

and $$B_1 = \frac{2(e_4^3 - e_1^3)}{3e_c'} - \frac{(e_4^4 - e_1^4)}{4e_c'^2}$$

Case 2 - Section partly in compression and partly in tension.
i.e., $e_4 \leq e_u$ and $e_1 < 0$

$$\frac{N}{f_c'' bt} = \frac{E_s p_t}{2f_c''}\left[e_2 + e_3\left(1 - \frac{1}{n}\right)\right] + \frac{A_2}{(e_4 - e_1)} \qquad (2.14)$$

and $$\frac{M}{f_c'' bt^2} = \frac{E_s p_t}{4f_c''} \cdot \frac{d'}{t}\left[e_3\left(1 - \frac{1}{n}\right) - e_2\right] + \frac{B_2}{(e_4 - e_1)^2}$$

$$- \frac{(e_1 + e_4)}{2(e_4 - e_1)^2} A_2 \qquad (2.15)$$

where $$A_2 = \frac{e_4^2}{e_c'} - \frac{e_4^3}{3e_c'^2}$$

and $$B_2 = \frac{2}{3}\frac{e_4^3}{e_c'} - \frac{e_4^4}{4e_c'^2}$$

The steel strain e_2 or e_3 in the equations (2.12) through (2.15) is replaced by e_y when either the bottom or the top steel yields.

Case 3 - Section completely in tension
i.e. $e_4 \leq 0$ and $e_1 \leq 0$

$$\frac{N}{f_c'' bt} = \frac{E_s p_t}{2f_c''}(e_2 + e_3) \qquad (2.16)$$

and $$\frac{M}{f_c'' bt^2} = \frac{E_s p_t}{4f_c''}\frac{d'}{t}(e_3 - e_2) \qquad (2.17)$$

It is evident that in order to satisfy both (2.16) and (2.17) simultaneously, the tensile strains $-e_2$ and $-e_3$ must be below the tensile yield strain $-e_y$.

d) Boundary Conditions: The boundary conditions which govern the solution of the two-hinged arch problem are

At $\theta = 0$ and $\theta = 2\phi_o$

$u = w = M = 0 \qquad (2.18)$

2.3.2 Nondimensionalization of the Equations:

The governing equations (2.6) through (2.18) are converted into nondimensional form using the following notation:

$$\left.\begin{aligned} \bar{\Theta} &= \frac{\Theta}{\phi_o} & \bar{Q} &= \frac{Q}{f''_c bt} \\ U &= \frac{u}{r_o} & \bar{N} &= \frac{N}{f''_c bt} \\ W &= \frac{w}{r_o} & \bar{M} &= \frac{M}{f''_c bt^2} \\ P_r &= \frac{p_r}{f''_c t} & e &= e \\ P_\theta &= \frac{p_\theta}{f''_c t} & \bar{\chi} &= \chi r_o \end{aligned}\right\} \qquad (2.19)$$

The nondimensional equations are:

Conditions of equilibrium:-

$$2P_r - \frac{2b}{r_o}\left[\sin(\Delta d\Theta)\,\bar{Q} + \cos(\Delta d\theta)\,\bar{N}\right] + \frac{b}{r_o} d\bar{\theta} \cot\left(\frac{d\Theta}{2}\right)\left[\cos(\Delta d\theta)\,\frac{d\bar{Q}}{d\bar{\theta}} - \sin(\Delta d\theta)\,\frac{d\bar{N}}{d\bar{\theta}}\right] = 0 \qquad (2.20)$$

$$\phi_o \, d\bar{\theta} \, \text{cosec}\left(\frac{d\theta}{2}\right) P_\theta + \frac{2b}{r_o}\left[\sin(\Delta d\theta)\,\bar{N} - \cos(\Delta d\theta)\,\bar{Q}\right]$$

$$- \frac{b}{r_o} d\bar{\theta} \cot\left(\frac{d\theta}{2}\right)\left[\cos(\Delta d\theta)\frac{d\bar{N}}{d\bar{\theta}} + \sin(\Delta d\theta)\frac{d\bar{Q}}{d\bar{\theta}}\right]$$

$$= 0 \qquad (2.21)$$

$$\frac{d\bar{M}}{d\bar{\theta}} - \frac{r_o \phi_o}{t}\cos\left(\frac{d\theta}{4}\right)\bar{Q} + \frac{r_o \phi_o \, d\bar{\theta}}{2t}\sin\left(\frac{d\theta}{4}\right)\frac{d\bar{N}}{d\bar{\theta}}$$

$$= 0 \qquad (2.22)$$

Strain-displacement relations:

$$e_o = W - \frac{1}{\phi_o}\frac{dU}{d\bar{\theta}} - \frac{1}{2}\left(\frac{dW}{\phi_o d\bar{\theta}}\right)^2 - \frac{U}{\phi_o}\frac{dW}{d\bar{\theta}} \qquad (2.23)$$

$$\bar{\chi} = \bar{W} + \frac{1}{\phi_o^2}\cdot\frac{d^2W}{d\bar{\theta}^2} - \frac{1}{\phi_o}\frac{dU}{d\bar{\theta}} \qquad (2.24)$$

Force-strain relations:

$$\left.\begin{aligned} e_o &= \frac{(e_1 + e_4)}{2} \\ \text{and} \quad \bar{\chi} &= \frac{r_o}{t}(e_1 - e_4) \end{aligned}\right\} \qquad (2.25)$$

Case 1 : If $e_4 \leqslant e_u$ and $e_1 \geqslant 0$

$$\bar{N} = \frac{E_s p_t}{2 f''_c} \left(1 - \frac{1}{n}\right)(e_2 + e_3) + \frac{A_1}{(e_4 - e_1)} \qquad (2.26)$$

$$\bar{M} = \frac{E_s p_t}{4 f''_c} \cdot \frac{d'}{t} \left(1 - \frac{1}{n}\right)(e_3 - e_2) + \frac{B_1}{(e_4 - e_1)^2}$$

$$- \frac{(e_1 + e_4)}{2(e_4 - e_1)^2} A_1 \qquad (2.27)$$

Case 2 : If $e_4 \leqslant e_u$ and $e_1 < 0$

$$\bar{N} = \frac{E_s p_t}{2 f''_c} \left[e_2 + e_3 \left(1 - \frac{1}{n}\right)\right] + \frac{A_2}{(e_4 - e_1)} \qquad (2.28)$$

$$\bar{M} = \frac{E_s p_t}{4 f''_c} \frac{d'}{t} \left[e_3 \left(1 - \frac{1}{n}\right) - e_2 \right] + \frac{B_2}{(e_4 - e_1)^2}$$

$$- \frac{(e_1 + e_4)}{2(e_4 - e_1)^2} A_2 \qquad (2.29)$$

Case 3 : If $e_4 \leqslant 0$ and $e_1 \leqslant 0$

$$\bar{N} = \frac{E_s p_t}{2 f_c''} (e_2 + e_3) \qquad (2.30)$$

$$\bar{M} = \frac{E_s p_t}{4 f_c''} \frac{d'}{t} (e_3 - e_2) \qquad (2.31)$$

and boundary conditions:

At $\bar{\theta} = 0$ and $\bar{\theta} = 2$

$$U = W = \bar{M} = 0 \qquad (2.32)$$

2.3.3 Finite-difference Formulation:

In order to obtain a numerical solution, the differential equations (2.20) through (2.24) are converted into difference equations. The form of the difference equations chosen is suitable for the numerical method described in the next article. The difference equations represent a discrete system consisting of (m-1) segments denoted as j-1, j, j+1, etc. The ends of the segments are denoted as i-1, i, i+1, etc. (Fig. 2.6). Each of the segments subtends a nondimensional angle $\Delta\bar{\theta}$ at the center of the arch. The unknowns $\bar{M}$, $\bar{N}$, $\bar{Q}$, e_o, $\bar{\chi}$, U and W at each section are denoted by subscripting them, $\bar{M}_i$, $\bar{N}_i$, etc. The loads P_r and P_θ on each segment are denoted as P_{rj}, $P_{\theta j}$, etc.

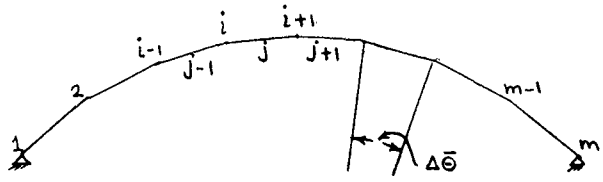

Figure 2.6 The Discrete System

From equation (d) of §2.3.1b,

$$\Delta d\Theta = \frac{1}{r_o} \cdot \frac{d^2w}{d\Theta^2} \cdot d\Theta$$

$$= \frac{d^2W}{\phi_o \, d\bar{\Theta}^2} \cdot d\bar{\Theta}$$

Using forward differences,

$$\left(\Delta d\Theta\right)_j = \frac{\left(W_{i+2} - 2W_{i+1} + W_i\right)}{\phi_o \cdot \Delta\bar{\Theta}} \qquad (2.33)$$

Using the averages of the values of $\bar{N}$ and $\bar{Q}$ at Sections i and i+1 and the forward differences for the derivatives of $\bar{N}$, $\bar{Q}$ and $\bar{M}$, the differential equations (2.20), (2.21) and (2.22) are transformed into the following difference equations,

$$A\bar{Q}_{i+1} + B\bar{N}_{i+1} = C\bar{Q}_i + D\bar{N}_i - 2P_{rj} \qquad (2.34)$$

$$-B\bar{Q}_{i+1} + A\bar{N}_{i+1} = -D\bar{Q}_i + C\bar{N}_i + C_3 P_{\theta j} \qquad (2.35)$$

and $$\bar{M}_{i+1} = \bar{M}_i + C_4 (\bar{Q}_i + \bar{Q}_{i+1}) + C_5 (\bar{N}_i - \bar{N}_{i+1}) \qquad (2.36)$$

where

$$C_1 = \frac{b}{r_o}$$

$$C_2 = C_1 \cot\left(\frac{\phi_o \Delta\bar{\theta}}{2}\right)$$

$$C_3 = \phi_o \Delta\bar{\theta} \operatorname{cosec}\left(\frac{\phi_o \Delta\bar{\theta}}{2}\right)$$

$$C_4 = \frac{r_o \phi_o \Delta\bar{\theta}}{2t} \cos\left(\frac{\phi_o \Delta\bar{\theta}}{4}\right)$$

$$C_5 = \frac{r_o \phi_o \Delta\bar{\theta}}{2t} \sin\left(\frac{\phi_o \Delta\bar{\theta}}{4}\right)$$

$$A = C_2 \cos(\Delta d\theta) - C_1 \sin(\Delta d\theta)$$

$$B = -C_2 \sin(\Delta d\theta) - C_1 \cos(\Delta d\theta)$$

$$C = C_2 \cos(\Delta d\theta) + C_1 \sin(\Delta d\theta)$$

$$D = -C_2 \sin(\Delta d\theta) + C_1 \cos(\Delta d\theta) \qquad (2.37)$$

The strain-displacement relations (2.23) and (2.24) are used to obtain difference equations which relate displacements at sections i and i+1.

Defining $\bar{e}_{,} = e_{,} + \frac{1}{2}\left(\frac{dW}{\phi_o d\bar{\theta}}\right)^2 + \frac{U}{\phi_o}\cdot\frac{dW}{d\bar{\theta}}$,

$$\left.\begin{aligned} \bar{e}_{oi} &= e_{oi} + \frac{(W_{i+1}-W_{i-1})^2}{8(\phi_o \Delta\bar{\theta})^2} + \frac{U_i (W_{i+1}-W_{i-1})}{2\phi_o \Delta\bar{\theta}} \\ &\qquad (i = 2,\cdots,m-1) \\ \bar{e}_{o1} &= e_{o1} + \frac{W_2^2}{2(\phi_o \Delta\bar{\theta})^2} \quad , \quad \bar{e}_{om} = e_{om} - \frac{W_{m-1}^2}{2(\phi_o \Delta\bar{\theta})^2} \end{aligned}\right\} \quad (2.38a)$$

$$U_i' = \left[\frac{dU}{d\bar{\theta}}\right]_i = \phi_o (W_i - \bar{e}_{oi}) \quad (2.38b)$$

$$U_i'' = \left[\frac{d^2U}{d\bar{\theta}^2}\right]_i = \phi_o (W_i' - \bar{e}_{oi}') \quad (2.38c)$$

$$\left.\begin{aligned} \bar{e}_{oi}' &= \frac{(\bar{e}_{o\,i+1} - \bar{e}_{o\,i-1})}{2\Delta\bar{\theta}} \quad , (i = 2,\cdots,m-1) \\ \bar{e}_{o1}' &= \frac{(\bar{e}_{o\,2} - \bar{e}_{o1})}{\Delta\bar{\theta}} \quad , \quad \bar{e}_{om}' = \frac{(\bar{e}_{om} - \bar{e}_{o\,m-1})}{\Delta\bar{\theta}} \end{aligned}\right\} \quad (2.38d)$$

$$W_i'' = \left[\frac{d^2W}{d\bar{\theta}^2}\right] = \phi_o^2 (\bar{\chi}_i - \bar{e}_{oi}) \quad (2.38e)$$

Also, using Taylor series,

$$W_i' = W_{i-1}' + W_{i-1}''(\Delta\bar{\theta}) + \cdots \quad (2.38f)$$

$$U_{i+1} = U_i + U_i'(\Delta\bar{\theta}) + U_i''\frac{(\Delta\bar{\theta})^2}{2} + \cdots \quad (2.39)$$

and $$W_{i+1} = W_i + W_i'(\Delta\bar{\theta}) + W_i''\frac{(\Delta\bar{\theta})^2}{2} + \cdots \quad (2.40)$$

The finite-difference approach used above was chosen as the most suitable to obtain a good numerical solution after making a preliminary study of various possible approaches.

2.3.4 Numerical Method of Solution:

A two-hinged circular arch has a degree of static indeterminancy equal to one. The structure is analysed by treating the reaction at the right hand support as the redundant (Fig. 2.7). The magnitude of the redundant is determined by first assuming a certain value and then refining it by successive iterations until all the governing equations are adequately satisfied.

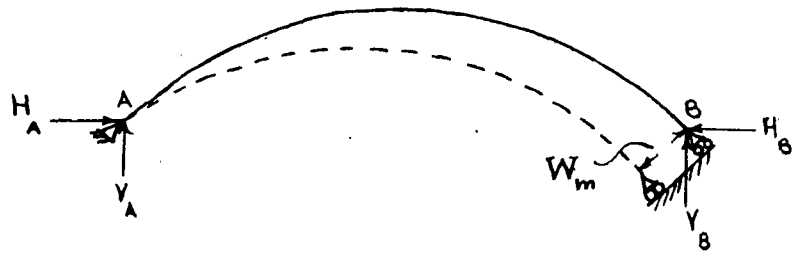

Figure 2.7 Arch with External Reactions

The method can be described as follows:

Trial 1 -

(a) The arch is divided in (m-1) segments and the nondimensionalized radial and tangential components of the load, distributed on each segment, are obtained.

(b) An initial nondimensional value H_{B1} is assumed for the horizontal reaction at the right support. A good initial value can be obtained from the linear elastic analysis of the arch.

(c) Using equations of static equilibrium for the entire structure, the nondimensionalized values of the other three reactions, viz. H_A, V_A, and V_B are obtained.

(d) Equations (2.37) are now evaluated assuming $(\Delta d\Theta)_j = 0$. Making use of V_A, H_A, M_A and the constants c_1, c_2, ..., equations (2.34), (2.35) and (2.36) are solved for (m-2) segments. Thus the forces $\bar{N}$ and $\bar{Q}$ and the moments $\bar{M}$ are known at all the m sections.

(e) At all the m sections, the values of concrete strains at the top and the bottom of the section are calculated assuming that the concrete stress-strain curve is linear in compression and that the tensile stresses in concrete are negligible. The considerations used for this purpose are given in Appendix I.

(f) Using the strains obtained above, each of the m sections is classified as either Case 1 (Fig. 2.5b), Case 2 (Fig. 2.5c) or Case 3 (Fig. 2.5d). Governing equations (2.26) and (2.27), (2.28) and (2.29) or (2.30) and (2.31) are chosen for each section in accordance with

the above classification. The first two pairs of the equations can be solved by the 'Newton-Raphson iteration' method[12]. (If $\bar{M}$ is negative the terms e_1 and e_4 are interchanged and the same equations are employed along with the absolute value of $\bar{M}$.) This method as applied to the present problem is explained in Appendix II. The strain values obtained in step (e) are used as initial values to start the iterations. The last pair of equations being linear, the strains obtained in step (e) satisfy these equations. Thus the solution of the proper pair of equations gives strains e_4 and e_1 for all the m sections.

(g) Using the concrete strains e_4 and e_1, the steel strains e_3 and e_2 are obtained. If $|e_3|$ or $|e_2|$ or both are greater than $|e_y|$, the governing force-strain relations are altered as explained in 2.3.1c and the nonlinear equations are once again solved by the 'Newton-Raphson iteration' method. The initial values for starting the iterations are the solutions obtained in step (f). The values of e_4 and e_1 thus obtained take into account the yielding of steel.

(h) The quantities e_o and $\bar{\varkappa}$ are obtained using equations (2.25) for all the m sections.

(i) Using equations (2.38a) through (2.38f), U_i', U_i'', W_i'' (i = 1,...,m) and W_i' (i = 2,...,m) are evaluated in terms of one unknown viz. W_1'. Since, in the first trial, values of U_i's and W_i's are not known,

e_{oi}'s in equation (2.38a) are assumed to be equal to $\bar{e}_{oi}$'s. This amounts to neglecting the non-linear terms in the strain-displacement relations for this cycle of trial 1. Equations (2.39) and (2.40) are now written for (m-1) sections to obtain a set of (2m-2) equations involving (2m+1) unknowns viz. m U_i's, W_i's and W_i'. From equation (2.32) we know that $U_1 = W_1 = U_m = 0$. Thus the unknowns are reduced to (2m-2). On solving these equations simultaneously the values of deflections U and W are obtained for all the m sections.

(j) Making use of equations (2.33) and (2.38a) $(\Delta d\Theta)_j$, (j = 1,..., m-2) and $\bar{e}_{oi}$ (i = 1,..., m) are calculated and steps (d) through (i) are repeated using the newly calcualted values of $(\Delta d\Theta)_j$, and $\bar{e}_{oi}$. The deflections U's and W's thus calculated include large deflection effects. These deflections are found to be satisfactory and a second repetition of this step is not needed.

Trial 2 -

(a) If the value of W_m obtained in Trial 1 - (j), does not satisfy the condition $W_m \approx 0$ (equation 2.32)*,

---

*In the present method a tolerance of (- 1/500 inch $< w_m <$ 1/500 inch) is considered to be satisfactory.

the assumed value H_{B1} is changed by a small percentage to a new value H_{B2}.

(b) Steps (c) through (j) of Trial 1 are now repeated, the only difference being that the values of $(\Delta d\Theta)_j$ in step (d) [equation (2.33)] and those of $\bar{e}_{oi}$ in step (i) [equation (2.38a)] are obtained by using the values of U_i's and W_i's calculated in step (j) of trial 1.

(c) If the most recent value of $W_m \neq 0$, the value of H_{B2} is modified once again. The new value H_{B3} is obtained by extrapolating linearly on the basis of H_{B1}, H_{B2} and the deflections W_m's associated with each respectively.

Using H_{B3}, steps (c) through (j) of Trial 1 are repeated and the deflection W_m is checked. This procedure is continued until the deflection falls within the tolerance limits.

2.3.5 Calculation of Ultimate Load:

The ultimate load carrying capacity of an arch for a particular distribution of loading can be obtained by using the method described in the previous article. The procedure consists of analysing the arch for increasing values of load until the ultimate is obtained. The ultimate load is assumed as that which causes the maximum compressive

strain in the arch to exceed e_u, the ultimate concrete strain, (§ 2.1.3).

2.3.6 Digital Computer Program:

A computer program prepared to handle the extensive calculations involved in obtaining a numerical solution by the above method is presented in Appendix III. The program consists of a main routine and six subroutines. The flow-chart of the program is also presented in Appendix III.

2.3.7 Convergence:

a) Number of Discrete Segments:

Semicircular arches were divided into 16, 20, 24 and 28 segments and analysed for various load distributions. It was found that the results obtained from the last three cases were essentially similar and a choice of 20 segments (each subtending an angle of 9° at the center of the arch) was made to approximate a semicircular arch.

b) Convergence of Iterations:

In the numerical method described in § 2.3.4, two different iterative procedures are used. The first one concerns the solutions by means of 'Newton-Raphson iteration' [steps (f) and (g) of Trial 1]. Certain difficulties experienced in obtaining convergence with this iteration have been explained in Appendix II (§ A2.3).

The second iteration involves successive choice of the horizontal reaction until sufficient convergence is

obtained in as few as four to six cycles of iteration. However, for certain load distributions, as the load approaches the ultimate small changes in the assumed value of the redundant cause large changes in displacement and it becomes difficult to obtain the convergence. Consider, for example, a semicircular arch under the action of a uniformly distributed antisymmetrical loading (Fig. 2.8a).

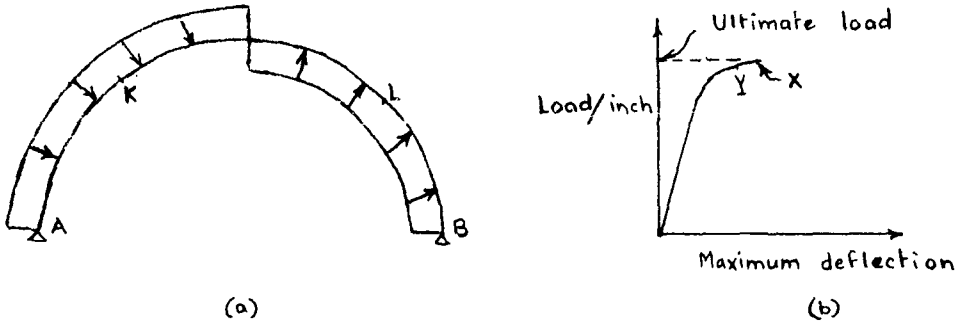

Figure 2.8 Semicircular Arch under a Uniform Antisymmetrical Load

For points below Y on the load-deflection curve in Fig. 2.8b the convergence is satisfactory. When the load is increased to that at point X, the combination of moment M and thrust N for a certain trial value of the

horizontal reaction say H_{B1}, causes the maximum compressive strain at sections K and L (quarter points) to exceed e'_c. That is, the strains in many fibres at these sections correspond to the drooping part of the concrete stress-strain curve. With such large strains, the change in curvature at the sections K and L is large and its contribution to the end deflection W_m is large. As the value of the horizontal reaction is changed, the moments and the thrusts on the sections change. These changes, though small, may be sufficient to cause a change in the strain distribution at either K or L or both, such that the maximum compressive strain is less that e'_c. Such a drastic change in strains can occur because the concrete stress-strain curve has been assumed to be parabolic with a drooping part, the slope of which increases very rapidly. The net effect of this large change in the strains at K or L is to affect the curvature at these points considerably and consequently to change the end deflection W_m by a large amount. On account of such a sensitivity of the deflection W_m to the changes in the value of the redundant, the solution tends to oscillate or even diverge. However, it is seen from Fig. 2.8b that such

a difficulty in convergence occurs only in the vicinity of X, where the load-deflection curve is almost horizontal. Therefore, it is reasonable to take the load at X as the ultimate load of the arch, and a good convergence is not necessary. The method thus yields a close approximation of the value of the ultimate load, but is unable to predict the load-deflection curve beyond X.

2.4 DYNAMIC RESPONSE

2.4.1 Governing Equations:

The forces acting on an element of the arch deformed under the action of time-dependant loads are shown in Fig. 2.9. In addition to the external loads and the internal forces, radial and tangential inertia forces are shown to act on the element. The rotational inertia has been neglected. The geometry of deformation of the arch element is similar to that in the static case (Fig. 2.4). Also, the force-strain relation now depend on the dynamic stress-strain properties of both concrete and steel.

a) Equations of Equilibrium: By considering the equilibrium of forces in r and θ directions and the moment equilibrium, the following equations of dynamic equilibrium of the arch element are obtained:

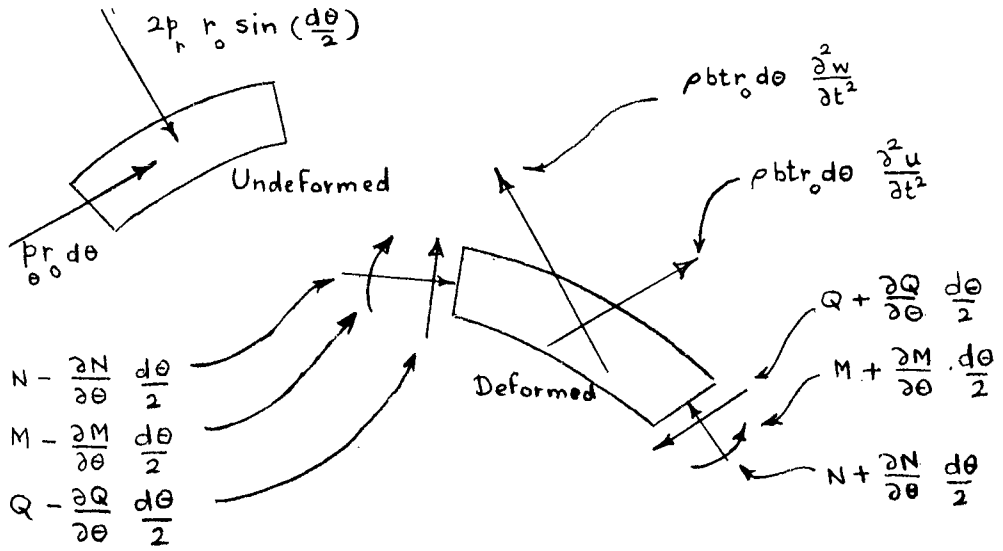

Figure 2.9 Dynamic Forces Acting
on a
Deformed Element

$$2p_r r_o \sin\left(\frac{d\theta}{2}\right) - 2Q \sin\left(\frac{d\theta}{2}\right)\sin(\Delta d\theta) - 2N \sin\left(\frac{d\theta}{2}\right)\cos(\Delta d\theta)$$

$$+ \frac{\partial Q}{\partial \theta} d\theta \cos\left(\frac{d\theta}{2}\right)\cos(\Delta d\theta) - \frac{\partial N}{\partial \theta} d\theta \cos\left(\frac{d\theta}{2}\right)\sin(\Delta d\theta)$$

$$- \rho b t r_o d\theta \frac{\partial^2 w}{\partial t^2} = 0 \qquad (2.41)$$

$$p_\theta r_o d\theta + 2N \sin\left(\frac{d\theta}{2}\right)\sin(\Delta d\theta) - 2Q \sin\left(\frac{d\theta}{2}\right)\cos(\Delta d\theta)$$

$$- \frac{\partial N}{\partial \theta} d\theta \cos\left(\frac{d\theta}{2}\right)\cos(\Delta d\theta) - \frac{\partial Q}{\partial \theta} \cos\left(\frac{d\theta}{2}\right)\sin(\Delta d\theta)$$

$$-\rho b t r_o d\theta \frac{\partial^2 u}{\partial t^2} = 0 \qquad (2.42)$$

and $$\frac{\partial M}{\partial \theta} - Q r_o \cos\left(\frac{d\theta}{4}\right) + \frac{\partial N}{\partial \theta} r_o \frac{d\theta}{2} \sin\left(\frac{d\theta}{4}\right) = 0 \qquad (2.43)$$

where, in addition to the notations used in § 2.3.1, the density of reinforced concrete is denoted by ρ and the time by t.

b) Strain-displacement Relations: Since the geometry of the deformed element is similar to the one in the static case, the strain-displacement relations are similar to equations (2.9) and (2.10) except that the total derivatives are replaced by partial derivatives:

$$e_o = \frac{1}{r_o}\left(w - \frac{\partial u}{\partial \theta}\right) - \frac{1}{r_o^2}\left[\frac{1}{2}\left(\frac{\partial w}{\partial \theta}\right)^2 + u\frac{\partial w}{\partial \theta}\right] \qquad (2.44)$$

and $$\chi = \frac{1}{r_o^2}\left(w + \frac{\partial^2 w}{\partial \theta^2} - \frac{\partial u}{\partial \theta}\right) \qquad (2.45)$$

Also equation (d) of §2.3.1b becomes

$$\Delta d\theta = \frac{1}{r_o^2} \cdot \frac{\partial^2 w}{\partial \theta^2} d\theta \qquad (2.46)$$

c) Force-strain Relations: The force-strain relations also are similar to those in the static case except that the dynamic properties of both concrete and steel are to be used. That is, in equations (2.11) through (2.17) f''_c and e'_c are to be replaced by f''_{dc} and e'_{dc} respectively. The dynamic force-strain relations are given in a nondimensional form in § 2.4.2.

d) Boundary Conditions: The boundary conditions governing the dynamic case are the same as in the static case, viz.

$$\text{At} \quad \theta = 0 \quad \text{and} \quad \theta = 2\phi_o$$
$$u = w = M = 0 \qquad (2.47a)$$

e) Initial Conditions: The initial conditions specify that the arch be undeformed at the start of the response, i.e. at time $t = 0$,

$u = w = M = N = Q = 0$ everywhere on the arch (2.47b)

2.4.2 Nondimensionalization of the Equations:

For the purpose of converting the governing equations into nondimensional form, the following notation is used in addition to that defined in §2.3.2 [equations (2.19)],

$$\bar{f}''_{dc} = \frac{f''_{dc}}{f''_c} \qquad \text{and} \qquad \bar{t} = \frac{t}{T} \qquad (2.48)$$

where T = Natural period of the arch.

Hence, the nondimensional governing equations are,

Equations of equilibrium :-

$$2P_r - \frac{2b}{r_o}\left[\sin(\Delta d\theta)\bar{Q} + \cos(\Delta d\theta)\bar{N}\right] + \frac{b}{r_o} d\bar{\theta} \cot\left(\frac{d\theta}{2}\right)\left[\cos(\Delta d\theta)\frac{\partial \bar{Q}}{\partial \bar{\theta}} - \sin(\Delta d\theta)\frac{\partial \bar{N}}{\partial \bar{\theta}}\right] = \rho b \frac{r_o}{T^2} \cdot \frac{\phi_o\, d\bar{\theta}}{f_c'' \sin\left(\frac{d\theta}{2}\right)} \cdot \frac{\partial^2 W}{\partial \bar{t}^2} \qquad (2.49)$$

$$\phi_o\, d\bar{\theta}\, \mathrm{cosec}\left(\frac{d\theta}{2}\right) P_\theta + \frac{2b}{r_o}\left[\sin(\Delta d\theta)\bar{N} - \cos(\Delta d\theta)\bar{Q}\right] - \frac{b}{r_o} d\bar{\theta} \cot\left(\frac{d\theta}{2}\right)\left[\cos(\Delta d\theta)\frac{\partial \bar{N}}{\partial \bar{\theta}} + \sin(\Delta d\theta)\frac{\partial \bar{Q}}{\partial \bar{\theta}}\right] = \rho b \frac{r_o}{T^2} \frac{\phi_o\, d\bar{\theta}}{f_c'' \sin\left(\frac{d\theta}{2}\right)} \cdot \frac{\partial^2 U}{\partial \bar{t}^2} \qquad (2.50)$$

$$\frac{\partial \bar{M}}{\partial \bar{\theta}} - \frac{r_o \phi_o}{t} \cos\left(\frac{d\theta}{4}\right)\bar{Q} + \frac{r_o \phi_o\, d\bar{\theta}}{2t} \sin\left(\frac{d\theta}{4}\right)\frac{\partial \bar{N}}{\partial \bar{\theta}} = 0 \qquad (2.51)$$

Strain-displacement relations:

$$e_o = W - \frac{1}{\phi_o} \cdot \frac{\partial U}{\partial \bar{\theta}} - \frac{1}{2}\left(\frac{\partial W}{\phi_o \partial \bar{\theta}}\right)^2 - \frac{U}{\phi_o}\frac{\partial W}{\partial \bar{\theta}} \qquad (2.52)$$

$$\bar{\chi} = W + \frac{1}{\phi_o^2} \cdot \frac{\partial^2 W}{\partial \bar{\theta}^2} - \frac{1}{\phi_o} \cdot \frac{\partial U}{\partial \bar{\theta}} \qquad (2.53)$$

$$\text{and} \quad \Delta d\theta = \frac{\partial^2 W}{\phi_o \partial \bar{\theta}^2} \, d\bar{\theta} \qquad (2.54)$$

Force-strain relations:

As stated earlier, the force-strain relations are obtained by the substitution of f''_{dc} and e'_{dc} in place of f''_{ε} and e'_{c} respectively in equations (2.11) through (2.17). The form of equation (2.11) is altered to suit the numerical method described in 2.4.4. Thus, the force-strain relations are,

$$\left.\begin{aligned} e_4 &= e_o - \frac{t}{2r_o}\bar{\chi} \\ \text{and} \quad e_1 &= e_o + \frac{t}{2r_o}\bar{\chi} \end{aligned}\right\} \qquad (2.55a)$$

Also, $e_2 = e_1 + (e_4 - e_1)(t-d)/t$

and $e_3 = e_1 + (e_4 - e_1)\, d/t$ (2.55b)

Case 1 : If $e_4 \leq e_u$ and $e_1 \geq 0$

$$\bar{N} = \frac{E_s p_t}{2 f''_c}\left(1 - \frac{1}{n}\right)(e_2 + e_3) + \bar{f}''_{dc}\,\frac{A_3}{(e_4 - e_1)} \qquad (2.56)$$

$$\bar{M} = \frac{E_s p_t}{4 f''_c} \cdot \frac{d'}{t}\left(1 - \frac{1}{n}\right)(e_3 - e_2) + \bar{f}''_{dc}\,\frac{B_3}{(e_4 - e_1)^2}$$

$$- \bar{f}''_{dc}\,\frac{(e_1 + e_4)}{2(e_4 - e_1)^2}\,A_3 \qquad (2.57)$$

where $A_3 = \dfrac{(e_4^2 - e_1^2)}{e'_{dc}} - \dfrac{(e_4^3 - e_1^3)}{3 e'^2_{dc}}$

and $B_3 = \dfrac{2(e_4^3 - e_1^3)}{3 e'_{dc}} - \dfrac{(e_4^4 - e_1^4)}{4 e'^2_{dc}}$

Case 2 : If $e_A \leqslant e_u$ and $e_1 < 0$

$$\bar{N} = \frac{E_s p_t}{2 f''_c} \left[e_2 + e_3 \left(1 - \frac{1}{n}\right) \right] + \bar{f}''_{dc} \frac{A_A}{(e_A - e_1)} \qquad (2.58)$$

$$\bar{M} = \frac{E_s p_t}{4 f''_c} \cdot \frac{d'}{t} \left[e_3 \left(1 - \frac{1}{n}\right) - e_2 \right] + f''_{dc} \frac{B_A}{(e_A - e_1)^2}$$

$$- f''_{dc} \frac{(e_1 + e_A)}{2(e_A - e_1)^2} A_A \qquad (2.59)$$

where $A_A = \frac{e_A^2}{e'_{dc}} - \frac{e_A^3}{3 e'^2_{dc}}$

and $B_A = \frac{2}{3} \cdot \frac{e_A^3}{e'_{dc}} - \frac{e_A^4}{4 e'^2_{dc}}$

Case 3 : If $e_A \leqslant 0$ and $e_1 \leqslant 0$

$$\bar{N} = \frac{E_s p_t}{2 f''_c} (e_2 + e_3) \qquad (2.60)$$

$$\bar{M} = \frac{E_s p_t}{4 f''_c} \cdot \frac{d'}{t} (e_3 - e_2) \qquad (2.61)$$

In cases 1 and 2, the steel strain e_2 or e_3 is replaced by e_{dy} when either the bottom or the top steel yields. However, in Case 3, both the tensile strains $-e_2$ and $-e_3$ need to be below the tensile yield strain $-e_{dy}$ in order to satisfy equations (2.60) and (2.61) simultaneously.

The boundary conditions in nondimensional form are,

At $\bar{\Theta} = 0$ and $\bar{\Theta} = 2$

$$U = W = \bar{M} = 0 \qquad (2.62a)$$

The initial conditions are,

at $\bar{t} = 0$, $U = W = \bar{M} = \bar{N} = \bar{Q} = 0$ everywhere on the arch (2.62b)

2.4.3 Finite-difference Formulation:

In order to solve the governing equations using numerical techniques, the differential equations (2.49) through (2.54) are converted into difference

equations, suitable for the method presented in 2.4.4. The formulation of the difference equations is accomplished by using a discrete system shown in Fig. 2.6. The notation followed in § 2.3.3 denoting the discrete sections by i-1, i, i+1 etc., and the discrete segments by j-1, j, j+1 etc., is also used in the present case. In addition, successive time intervals are denoted by k-1, k, k+1 etc. Therefore, each unknown carries two subscripts - either subscript i or j depending upon whether the unknown pertains to a section or to a segment and the subscript k specifying the time interval.

The difference equations obtained are as follows:

Using forward differences, equation (2.54) becomes,

$$(\Delta d\Theta)_{j,k} = \frac{\left(W_{i+2,k} - 2W_{i+1,k} + W_{i,k}\right)}{\phi_o \, \Delta\bar{\theta}} \qquad (2.63)$$

By using central differences for sections away from the boundaries and forward differences for boundary sections, equations (2.52) and (2.53) become,

$$e_{o\,i,k} = W_{i,k} - \frac{(U_{i+1,k} - U_{i-1,k})}{2\phi_o \Delta\bar{\theta}} - \frac{(W_{i+1,k} - W_{i-1,k})^2}{8(\phi_o \Delta\bar{\theta})^2} - \frac{U_{i,k}(W_{i+1,k} - W_{i-1,k})}{2\phi_o \Delta\bar{\theta}} \qquad (i = 2, \cdots, m-1)$$

$$e_{o\,1,k} = -\frac{U_{2,k}}{\phi_o \Delta\bar{\theta}} - \frac{W_{2,k}^2}{2(\phi_o \Delta\bar{\theta})^2}$$

$$e_{o\,m,k} = \frac{U_{m-1,k}}{\phi_o \Delta\bar{\theta}} + \frac{W_{m-1,k}^2}{2(\phi_o \Delta\bar{\theta})^2} \qquad (2.64)$$

$$\bar{\chi}_{i,k} = e_{o\,i,k} + \frac{(W_{i+1,k} - 2W_{i,k} + W_{i-1,k})}{(\phi_o \Delta\bar{\theta})^2} + \frac{(W_{i+1,k} - W_{i-1,k})^2}{8(\phi_o \Delta\bar{\theta})^2} + \frac{U_{i,k}(W_{i+1,k} - W_{i-1,k})}{(2\phi_o \Delta\bar{\theta})} \qquad (i = 2, \cdots, m-1)$$

$$\bar{\chi}_{1,k} = e_{o\,1,k} + \frac{W_{2,k}^2}{2(\phi_o \Delta\bar{\theta})^2}$$

$$\bar{\chi}_{m,k} = e_{o\,m,k} - \frac{W_{m-1,k}^2}{2(\phi_o \Delta\bar{\theta})^2} \qquad (2.65)$$

Using the notation defined by equation (2.37), equations (2.49), (2.50) and (2.51) are converted into difference equations. The quantities $\bar{N}$ and $\bar{Q}$ are substituted by their average values at sections i and i+1, while forward differences are used in place of the derivatives of $\bar{N}$, $\bar{Q}$ and $\bar{M}$. The difference equations are,

$$C_6 (WT'')_{j,k} + C\bar{Q}_{i,k} - A\bar{Q}_{i+1,k} = -D\bar{N}_{i,k} + B\bar{N}_{i+1,k} + 2P_{rj,k} \tag{2.66}$$

$$C_6 (UT'')_{j,k} + D\bar{Q}_{i,k} - B\bar{Q}_{i+1,k} = C\bar{N}_{i,k} - A\bar{N}_{i+1,k} + C_3 P_{\theta j,k} \tag{2.67}$$

$$C_4\bar{Q}_{i,k} + C_4\bar{Q}_{i+1,k} = -\bar{M}_{i,k} + \bar{M}_{i+1,k} - C_5(\bar{N}_{i,k} - \bar{N}_{i+1,k}) \tag{2.68}$$

where $$C_6 = \rho b \frac{r_o}{T^2} \frac{\phi_o \Delta\bar{\theta}}{f_c'' \sin\left(\frac{d\theta}{2}\right)}$$

$$WT'' = \frac{\partial^2 W}{\partial \bar{t}^2}$$

$$UT'' = \frac{\partial^2 U}{\partial \bar{t}^2}$$

2.4.4 Numerical Method of Solution:

The solution is started out from the specified initial conditions and then information is obtained at successive time intervals, Δt apart. The method is as follows:

(a) The arch is divided in (m-1) segments as shown in Fig. 2.6. The ordinates of the radial and tangential components of the load pulse acting on each segment are computed at time intervals Δt apart so that the values of loads at discrete times t_o, t_1, ..., t_k are known as shown in Fig. 2.10a or 2.11b. These load values are nondimensionalized. The natural period, T is calculated as follows[13],

Compression mode

$$T = \frac{r_o}{1800}$$

where T is in seconds

and r_o is in feet.

Flexural mode

$$T = \frac{\phi_o^2 r_o^2}{425000\, d\sqrt{p}} \cdot \left[\frac{(\pi/\phi_o)^2 + 1.5}{(\pi/\phi_o)^2 - 1}\right]$$

where T is in seconds

and r_o and d are in inches.

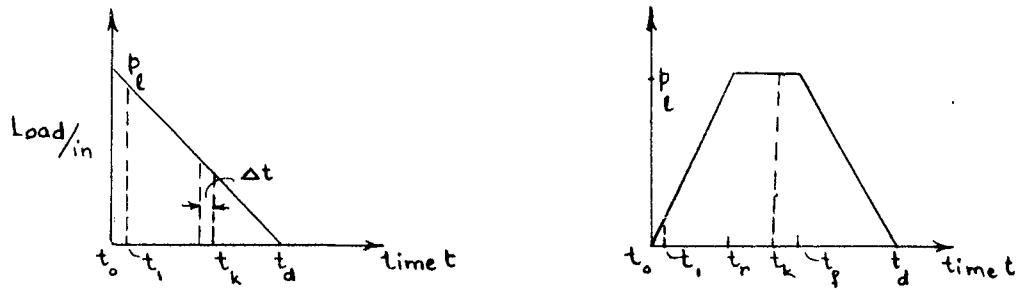

t_r = Rise time of the load.

$(t_f - t_r)$ = Time for which load is constant

$(t_d - t_f)$ = Decay time of the load.

Figure 2.10 Load-Time Curves

(b) Starting with the undeformed arch equation (2.62b) at time t_o, the solution for the response is launched by using the 'Acceleration-pulse' method[11]. In this method the following formulae are used for extrapolating the displacements $W_{i,k}$ and $U_{i,k}$ of a secion $i(i = 2,3,\ldots,m-1)$ at time t_k, $(k = 2,3,\ldots)$.

$$\bar{W}_{i,k} = 2W_{i,k-2} - W_{i,k-1} + (WT'')_{i,k-1} (\Delta\bar{t})^2 \qquad (2.69)$$

$$\text{and} \quad U_{i,k} = 2\,U_{i,k-2} - U_{i,k-1} + (UT'')_{i,k-1}\,(\Delta\bar{t})^2 \qquad (2.69)$$

where $\Delta\bar{t} = \frac{\Delta t}{T}$, the nondimensional time interval.

At time t_1, for any section i (i = 2,3,..., m-1) the following two types of extrapolation formulae are used.

(1) If the load-time curve is as shown in Fig. 2.10a,

$$\left.\begin{aligned} W_{i,1} &= \tfrac{1}{2}\,(WT'')_{i,0}\,(\Delta\bar{t})^2 \\ \text{and} \quad U_{i,1} &= \tfrac{1}{2}\,(UT'')_{i,0}\,(\Delta\bar{t})^2 \end{aligned}\right\} \qquad (2.70a)$$

(2) If the load-time curve is as shown in Fig. 2.10b,

$$\left.\begin{aligned} W_{i,1} &= \tfrac{1}{6}\,(WT'')_{i,1}\,(\Delta\bar{t})^2 \\ \text{and} \quad U_{i,1} &= \tfrac{1}{6}\,(UT'')_{i,1}\,(\Delta\bar{t})^2 \end{aligned}\right\} \qquad (2.70b)$$

In cases when equations (2.70b) are used, an iteration on the values of both $(WT")_{i,1}$ and $(UT")_{i,1}$ becomes necessary.

(c) At time t_o, equation (2.62b) indicates that

$$U_{i,o} = W_{i,o} = \bar{M}_{i,o} = \bar{N}_{i,o} = \bar{Q}_{i,o} = 0 \qquad (i = 1, \cdots, m)$$

Using load $P_{rj,o}$, $P_{j,o}$ and equilibrium equations (2.66), (2.67) and (2.68), the values of $(WT")_{j,o}$ and $(UT")_{j,o}$ ($j = 1,\ldots, m-1$ - segments) are obtained. Also, approximating the radial and tangential accelerations of section i by the average of the corresponding accelerations of segments j-1 and j,

$$\left.\begin{aligned} (WT")_{i,k} &= \frac{1}{2}\left[(WT")_{j-1,k} + (WT")_{j,k}\right] \\ \text{and} \quad (UT")_{i,k} &= \frac{1}{2}\left[(UT")_{j-1,k} + (UT")_{j,k}\right] \end{aligned}\right\} \qquad (2.71)$$

where ($i = 2,3,\ldots, m-1$),

the values of $(WT")_{i,o}$ and $(UT")_{i,o}$ are obtained.

(d) At time $t_1 = t_o + \Delta t$,

(i) Using either equations (2.70a) or (2.70b)* as need be, values of $W_{i,1}$ and $U_{i,1}$, ($i = 2,\ldots, m-1$) are obtained. The boundary conditions [equation (2.62a)] require that,

$$W_{1,1} = U_{1,1} = \bar{M}_{1,1} = W_{m,1} = U_{m,1} = \bar{M}_{m,1} = 0$$

(ii) Using equations (2.63), (2.64) and 2.65), values of $e_{oi,1}$ and $\bar{\chi}_{i,1}$ ($i = 1,\ldots,m$) and $(\Delta d\theta)_{j,1}$ ($j = 1,\ldots, m-1$) are obtained.

(iii) For each section i, equations (2.55a) and (2.55b) are employed to obtain concrete strains e_1, e_4 and steel strains e_2, e_3.

---

*When equations (2.70b) are used, the values of $(WT")_{i,1}$ and $(UT")_{i,1}$ ($i = 1,\ldots,m$) are not available. Hence, certain reasonable values are assumed; at first operations (i) through (vii) are performed and values obtained in step(vii) are compared with the assumed values. If the agreement between them is not satisfactory, the newly obtained values of $(WT")_{i,1}$ and $(UT")_{i,1}$ are employed in step (i) and steps (i) through (vii) are repeated. This process is continued until a satisfactory agreement between the values used in step (i) and those obtained in step (vii) is achieved.

(iv) Based on the values of e_1 and e_4, each section is classified as Case 1 [equations (2.56), (2.57)], Case 2 [equations (2.58), (2.59)] or Case 3 [equations (2.60), (2.61)]. Also, strains e_2 and e_3 for each section i, are compared with the yield strain of steel e_{dy} and are replaced by e_{dy} (with proper sign) if found to be greater than e_{dy} in magnitude.

(v) Making use of the equations (2.56), (2.57) or (2.58), (2.59) or (2.60), (2.61) values of $\bar{N}_{i,1}$ and $\bar{M}_{i,1}$ (i =1,...,m) are obtained.

(vi) Loads $P_{rj,1}$, $P_{\theta j,1}$ and $(\Delta d\theta)_{j,1}$ calculated in step (ii), (j =1,...,m-1) and equations (2.66), (2.67), (2.68) are used to calculate $(WT")_{j,1}$, $(UT")_{j,1}$ (j = 1,...,m-1) and $\bar{Q}_{i,1}$ (i = 1,...,m). For the (m-1) segments, (3m-3) equations are now available while the unknowns form a total of (3m-2), i.e., (m) $\bar{Q}$s, (m-1) WT"s and (m-1) UT"s. In order to overcome this difficulty, it is assumed that

$$(WT")_{j,1} = 0 \quad \text{where} \quad j = 1 \quad \text{and} \quad m\text{-}1$$

This assumption implies that the radial accelerations of segments nearest to the two supports are neglected. This

leaves (3m-4) quantities as unknown. Excluding equation (2.66) as applied to segment (m-1), a total of (3m-4) equations are available. Solving these equations, values of $(WT")_{j,1}$, $(UT")_{j,1}$ (j " 2,...,m-2) and $\bar{Q}_{i,1}$ (i = 1,...,m) are obtained.

However, in the case of uniformly distributed symmetrical loading, making use of the fact that the shear $\bar{Q}$ at the crown is zero, equations (2.66), (2.67) and (2.68) are simultaneously solved for half the arch. The solutions of of these equations yield the values of (WT"), (UT") and $\bar{Q}$ for one-half of the arch: the corresponding values for the other half are obtained by using symmetry.

(vii) Finally, using equations (2.71) for k = 1, values of $(WT")_{i,1}$ and $(UT")_{i,1}$ (i = 2,...,m-1-sections) are obtained.

At the end of step (vii) all the information regarding the internal forces $\bar{M}$, $\bar{N}$ and $\bar{Q}$, the radial and tangential displacements W and U, and the corresponding accelerations WT" and UT" is available at time t_1 for all the m sections.

(e) At each successive time t_2, t_3,... t_k the seven steps of (d) are used to obtain all the information about the arch at the discrete sections, the only difference being that in step (i) equations (2.69) are used to calculate displacements $W_{i,k}$ and $U_{i,k}$ (i = 2,..., m-1 - sections).

The steps (a) through (e) thus give the response of the arch to a time-dependent load.

2.4.5 Calculation of Ultimate Load:

The ultimate load of an arch is once again

leaves (3m-4) quantities as unknown. Excluding equation (2.66) as applied to segment (m-1), a total of (3m-4) equations are available. Solving these equations, values of $(WT")_{j,1}$, $(UT")_{j,1}$ (j " 2,...,m-2) and $\bar{Q}_{i,1}$ (i = 1,...,m) are obtained.

However, in the case of uniformly distributed symmetrical loading, making use of the fact that the shear $\bar{Q}$ at the crown is zero, equations (2.66), (2.67) and (2.68) are simultaneously solved for half the arch. The solutions of of these equations yield the values of (WT"), (UT") and $\bar{Q}$ for one-half of the arch: the corresponding values for the other half are obtained by using symmetry.

(vii) Finally, using equations (2.71) for k = 1, values of $(WT")_{i,1}$ and $(UT")_{i,1}$ (i = 2,...,m-1-sections) are obtained.

At the end of step (vii) all the information regarding the internal forces $\bar{M}$, $\bar{N}$ and $\bar{Q}$, the radial and tangential displacements W and U, and the corresponding accelerations WT" and UT" is available at time t_1 for all the m sections.

(e) At each successive time t_2, t_3,... t_k the seven steps of (d) are used to obtain all the information about the arch at the discrete sections, the only difference being that in step (i) equations (2.69) are used to calculate displacements $W_{i,k}$ and $U_{i,k}$ (i = 2,..., m-1 - sections).

The steps (a) through (e) thus give the response of the arch to a time-dependent load.

2.4.5 Calculation of Ultimate Load:

The ultimate load of an arch is once again

defined to be that load under which the maximum compressive strain in concrete exceeds the ultimate strain e_u. Therefore, as explained in § 2.3.5, this method gives ultimate loads for certain distributions of loading such as (a) uniformly distributed symmetrical loads, (b) uniformly distributed antisymmetrical loads, and (c) symmetrical and antisymmetrical concentrated loads, except a concentrated load at the crown.

For a given distribution of loading and for a given load pulse such as the one shown in Fig. 2.10b (defining t_r, t_f and t_d) the ultimate load is obtained as follows:

(1) Starting at a low value of the peak load p_ℓ the arch is analysed at discrete times $t_o, t_1, \ldots, t_k$ using the procedure outlined in § 2.4.4. At each time the maximum value of the concrete compressive strain is compared with the concrete ultimate strain to check for failure. The analysis is continued either until $t_k = t_d$ (if $t_d > T$) or until $t_k = T$ (if $t_d < T$). Since the maximum response of the arch occurs at a time $t_m < T$ (usually $t_m \approx 0.5T$ to $0.75T$)[11], the analysis of the arch upto $t_k \geqslant T$ is sufficient for investigation of the possibility of failure under the load p_ℓ.

(2) The peak load p_ℓ is increased by a certain percentage and the analysis as explained in step (1) is repeated.

(3) This process of increasing the peak load p_ℓ and analysing the arch is continued until the ultimate strain e_u is exceeded. The value of p_ℓ at which this excessive strain is produced is the ultimate load of the arch for a given distribution of loading and a given load-time dependence.

2.4.6 Digital Computer Program:

A digital computer program prepared to perform the calculations involved in the methods outlined in articles 2.4.4 and 2.4.5 is presented in Appendix IV. A flow-chart of the program is also presented in Appendix IV.

2.4.7 Selection of Space and Time Intervals:

Before the numerical method presented in 2.4.4 can be used, it is necessary to determine the approximate values for the parameters $\Delta\Theta$ and Δt used for discretization of the continuous system. As in § 2.3.7. again a semicircular arch is divided into 20 segments so that $\Delta\Theta$ is equal to nine degrees.

In order to establish the time interval Δt, information regarding the problem of wave propogation in a one dimensional elastic system proves to be useful. Crandall[14] has shown that in a one dimensional elastic system, the time interval Δt is related to the ratio of the space interval ΔX and the seismic velocity, C_s in the medium. This relation says that for the stability of the numerical method of solution,

$$\Delta t \leqslant \frac{\Delta X}{C_s} \tag{2.72}$$

Crandall has also suggested that if Δt is much smaller than $\frac{\Delta X}{C_s}$, the accuracy of the numerical method deteriorates.

$$\left.\begin{aligned} &\text{With} \quad \Delta X = r_o \, \Delta\Theta \\ &\text{and} \quad C_s = \sqrt{\frac{E_c}{\rho}} \end{aligned}\right\} \tag{2.73}$$

Semicircular arches of Type A (refer to § 3.3) under different distributions of loading with different load-time functions have been analysed. It is found (Fig. 2.11)

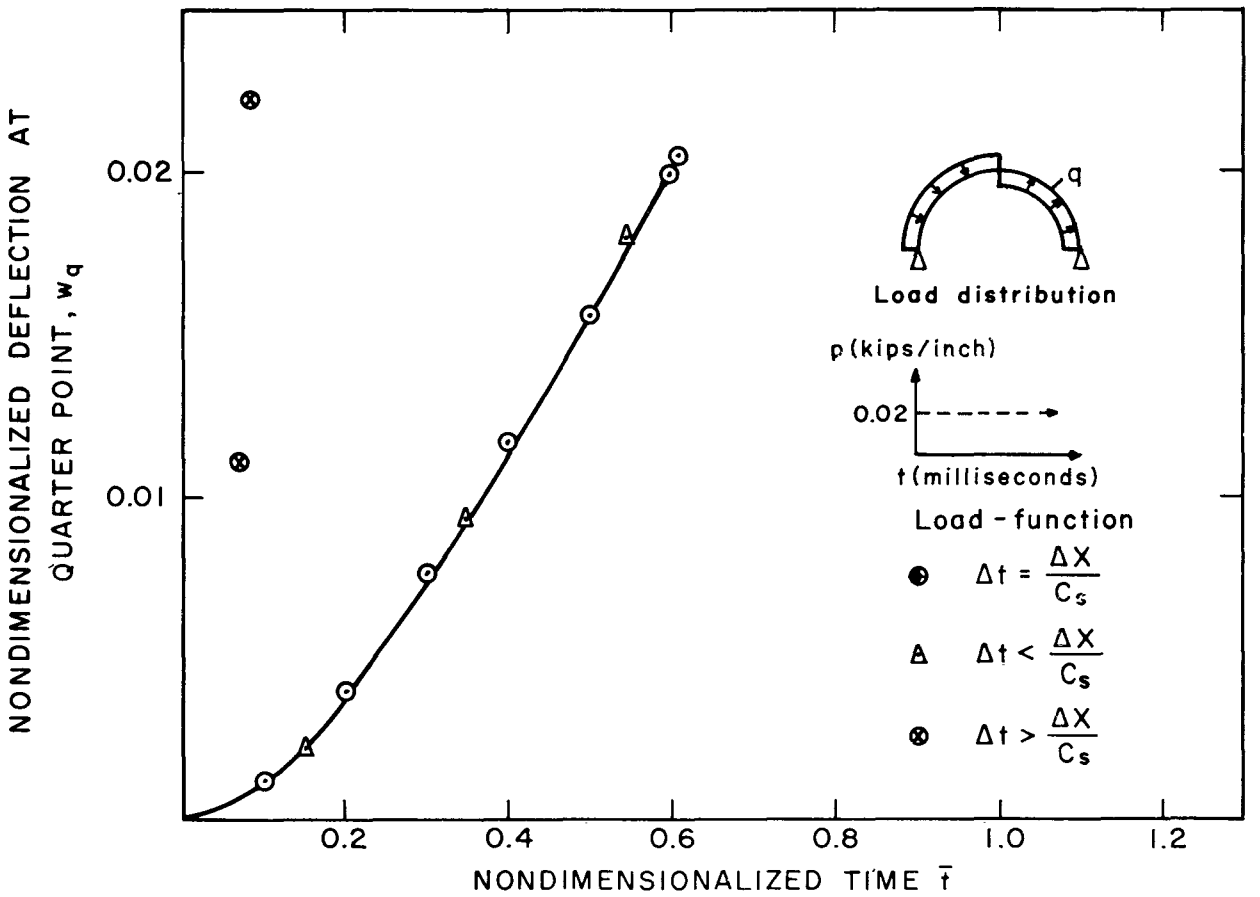

FIGURE 2.11 — SELECTION OF TIME INTERVAL

that for $\Delta t = \frac{\Delta X}{C_s}$ or $< \frac{\Delta X}{C_s}$, the convergence is adequate and satisfactory deflection-time curves are obtained. However, for $\Delta t > \frac{\Delta X}{C_s}$ the deflection-time curves show erroneous trends. Therefore, for all the dynamic cases the criterion $\Delta t = \frac{\Delta X}{C_s}$ is used, permitting the use of the largest time interval without causing numerical instability.

2.5 CONVENTIONAL THEORY FOR PREDICTING ULTIMATE LOADS AND DEFLECTIONS

In this section a brief review is given of the conventional methods of predicting the ultimate loads of arches under (1) uniformly distributed symmetric radial load, (2) concentrated load at the crown and (3) antisymmetric loads at the quarter points. The expressions for deflection at the points where the deflections are measured in tests (refer section 3.4.2 (c) in following chapter), are also given. The initial tangent modulus of concrete is to be used in these expressions. The expressions for deflections are derived by assuming linearly elastic material, using the usual virtual work approach.

2.5.1 Uniformly Distributed Symmetric Radial Load:

(a) Ultimate Load: If the secondary bending effects are neglected, the ultimate load is given by the

following expression.

$$p_{u_{TH}} = (0.85 f_c' + p_t f_y) \frac{bt}{r_o} \qquad (2.74)$$

where t = Total depth of arch in inches

r_o = Radius of arch in inches

b = Width of arch in inches

$p_{u_{TH}}$ = Ultimate load in lbs/inch

p_t = Total steel percentage = $\frac{A_s + A_s'}{bt}$

(b) Deflection: The radial deflections of the arch at crown and at points 54° from the supports are given by the following expressions.

$$w_c = 1.636 \frac{p_{TH} r_o^2}{A E_c} \qquad (2.75)$$

$$w_q = 1.20 \frac{p_{TH} r_o^2}{A E_c} \qquad (2.76)$$

where $A = A_c [1 + (n-1) p_t]$

$E_c = (1800000 + 390 f_c')$ in psi.

p_{TH} = Distributed load in lbs/inch

A_c = Area of concrete section in sq. inches

n = Modular ratio = $\frac{E_s}{E_c}$ = 10 (assumed)

w_c = Radial deflection at the crown in inches

w_q = Radial deflection at 54° points

2.5.2 Concentrated Load at Crown:

(a) Ultimate Load: The ultimate load of the arch under concentrated load can be calculated by using the conventional plastic theory as the test specimens of the test program are underreinforced. It can be shown that the arch will collapse with the formation of three hinges, one at the crown and two others at 38° from the supports. It is not easy to derive an explicit formula for the ultimate load because the effect of thrust on the moment capacity of the section has to be considered. An iterative procedure described below can be used.

In the first cycle, the ultimate load can be calculated by using equilibrium conditions and neglecting the effect of thrust. Two unknowns - horizontal reaction H and ultimate load P_u can be found by using the conditions that the moments at two hinges should be the ultimate moment M_u, which is given by

$$M_u = A_s f_y (d - a/2) \qquad (2.77)$$

where $$a = \frac{A_s f_y}{(0.85 f'_c b)}$$

Once this ultimate load is calculated, it can be used to calculate the thrust at the crown and at the 38° points. With these values of thrusts, new values of moment capacities

at crown and at 38° points can be found from the graph of P/P_u vs. M/M_u. (See for example Fig. 5A - 10.2, Reference No. 13, in bibliography.) With these values of moment capacities a second cycle of iteration will give a new value of H and P_u. This process can be repeated until a satisfactory convergence is obtained. Usually two or three cycles should give satisfactory results.

(b) Deflection: The expression for the radial deflection at crown is as follows.

$$w_c = 0.021 \frac{P_{TH} r_o^3}{E_c I_{AV}} \qquad (2.78)$$

where I_{AV} = Average of the moments of inertia of the cracked and uncracked sections in $in.^4$

E_c = $(1800000 + 390 f'_c)$ in psi

P_{TH} = Concentrated load at crown in pounds.

w_c = Radial deflection at crown in inches.

It is uncertain as to what value of the moment of inertia of reinforced concrete section should be used. However, as recommended in references 11 (Section 2.6) and 19 in bibliography, it is decided to use an average of the moments of inertia of the cracked and uncracked sections (i.e., I_{AV}).

2.5.3 Antisymmetric Concentrated Loads at Quarter Points:

(a) Ultimate Load: The ultimate load in this case can be calculated also by using plastic theory. Under this type of loading it can be shown that the arch collapses by the formation of two hinges, one at each quarter point. To take into account the effect of thrust on the moment capacity of the section, the following iterative procedure can be used.

In the first cycle of iteration, if the effect of thrust is neglected, the ultimate load P_u is given by

$$P_u = \frac{2 M_u}{r_o} \qquad (2.79)$$

where $M_u = A_s f_y (d - a/2)$

and $a = \frac{A_s f_y}{0.85 f_c' b}$

With this value of ultimate load, thrust at two quarter points can be calculated. These thrust values can be used to determine the new values of moment

deflection is calculated by using formulae presented in § 2.5 and the analytically predicted ultimate load. The experimental value of μ is calculated by using the value of the maximum deflection under the ultimate load measured as described in § 3.4.2 (c) and the elastic deflection obtained by using again the formulae given in § 2.5 and the experimentally determined ultimate load.

2.7 COMPARISON OF DYNAMIC ULTIMATE LOADS - NONLINEAR THEORY AND APPROXIMATE THEORETICAL ANALYSIS

The nonlinear theory developed so far is used to obtain ultimate loads of arches under a triangular dynamic load pulse with zero rise time (Fig. 2.12). The distributions of loading along the arch are

a) Compression mode type

and b) Deflection mode type

The geometry and material properties of the arches is as follows:

$b = 10"$, $t = 15"$ $r_o = 300"$

$\phi_o = 90°$, $p_t = 0.025$ $d = 13.5"$

$f'_{dc} = 4000$ psi, $f_{dy} = 40{,}000$ psi,

$E_s = 30 \times 10^6$ psi

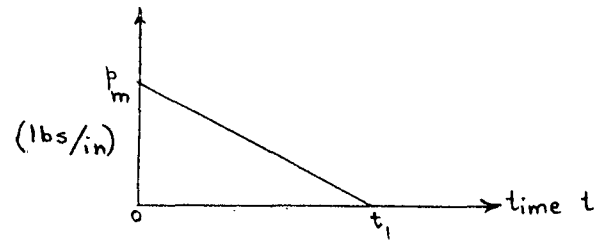

Figure 2.12 Triangular Load Pulse

Various values of the ultimate loads, p_m are obtained for different duration of loading t_1, with both types of distributions.

Approximate analysis based on a single-degree freedom system is also conducted for the same arches. The following formulae[13], [19] are used for this purpose:

Compression mode loading -

$$p_m = r_c \left[\frac{1 - \frac{1}{2\mu}}{1 + \frac{2}{\pi}\frac{T}{t_1}} + \frac{T}{\pi t_1} \left(2 \cdot \mu - 1 \right)^{0.5} \right]$$

where p_m = Dynamic load (lbs/in)

$$r_c = (0.85\, f'_{dc} + p_t\, f_{dy}) \frac{bt}{r_o} \quad \text{(lbs/in)}$$

T = Natural period of the arch in compression mode (milliseconds)

$$= \frac{r_o}{21.6}$$

r_o = Mean radius of the arch (inches)

μ = Ductility factor

Here, p_m is calculated for two values of μ, viz. μ = 1.3 and 2, and various values of t_1.

Deflection mode loading

$$p_m = r_f \left[\frac{1 - \frac{1}{2\mu}}{1 + \frac{2}{\pi} \frac{T}{t_1}} + \frac{T}{\pi t_1} (2 \cdot \mu - 1)^{0.5} \right]$$

where $r_f = 7.2\ p\ f_{dy} \frac{d^2}{(\phi_o\ r_o)^2}$

$$p = \frac{A_s}{bd}$$

T = Natural period of the arch in flexural mode (milliseconds)

$$= \frac{(\phi_o \cdot r_o)^2}{425\ d \sqrt{p}} \cdot \left[\frac{(\pi/\phi_o)^2 + 1.5}{(\pi/\phi_o)^2 - 1} \right]$$

Here various values of t_1 and two values of μ, viz. μ = 2 and 5 are used for calculating p_m.

The analytical results obtained from the nonlinear theory are compared with results obtained from the approximate analysis (20). This comparison is shown in Fig. 2.13. There is a good agreement between these results when the duration of loading t_1 is greater than about half the

natural period, T. However, the approximate analysis seems to give unconservative results for t_1 less than about 0.5 T. A possible explanation for such results may lie in the fact that under loads of short duration, more than one mode of vibration are excited and analysis based on a single-degree freedom system becomes inadequate.

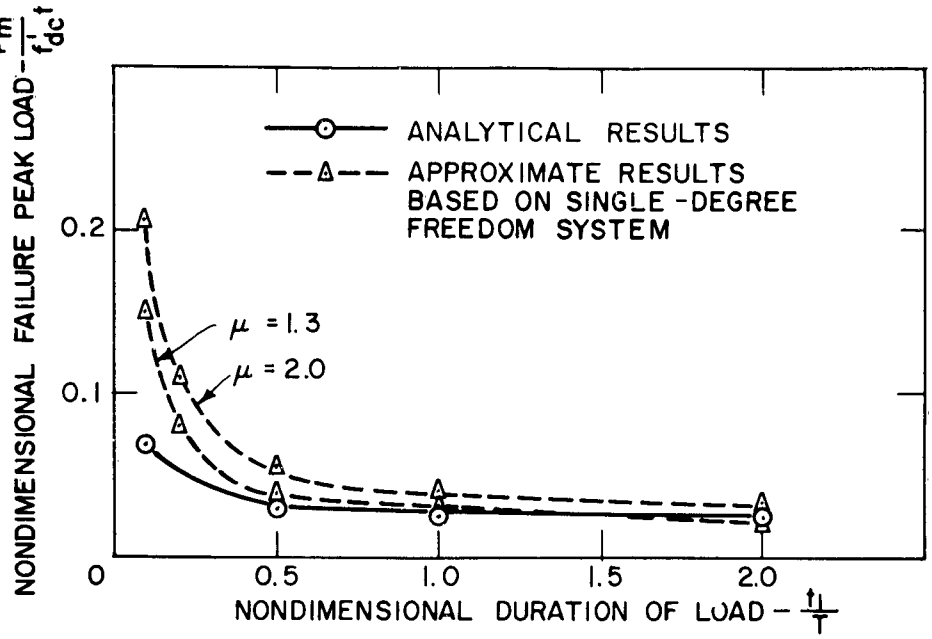

(a) COMPRESSION MODE LOADING

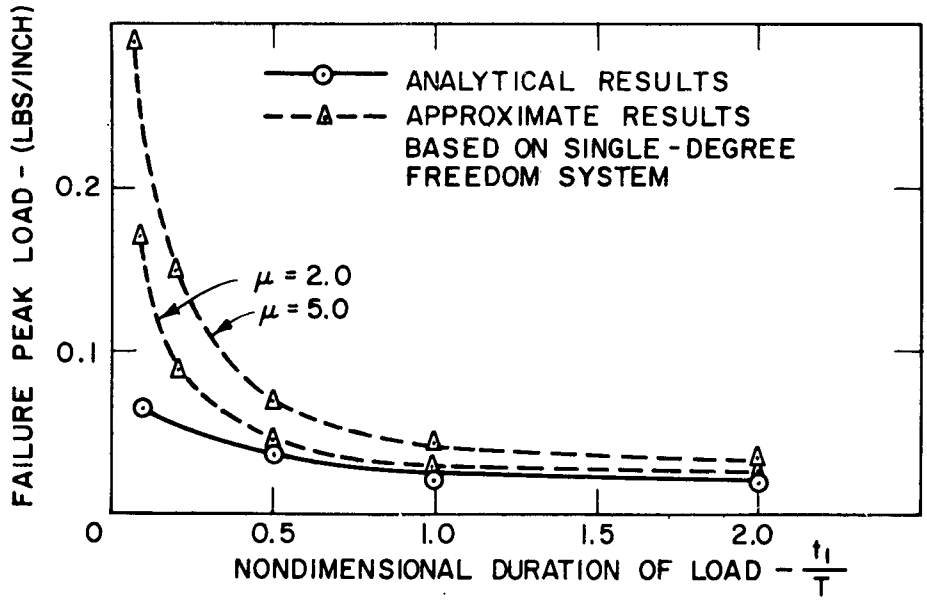

(b) DEFLECTION MODE LOADING

FIGURE 2.13- COMPARISON OF ANALYTICAL RESULTS WITH APPROXIMATE ANALYSIS

CHAPTER 3

EXPERIMENTAL INVESTIGATION

3.1 TEST SPECIMENS

All test specimens are reinforced concrete, semi-circular arches of radius 18" and of rectangular cross-section. For the purpose of these tests, two sizes, one with a cross-section of 2" x 2" and the other with a cross-section of 1" x 2" were chosen. The purpose of choosing two sizes was to detect if possible, the influence of the natural period on the dynamic response of the arch for a given rise time of the dynamic load. The details of the geometry, cross-section and reinforcement of the arches are shown in Table 3.1 and Figs. 3.1 and 3.2. The specimens with 2" x 2" cross-section are designated as Type A, and those with 1" x 2", as Type B.

TABLE 3.1

Specimen Type	Cross-section	Reinforcement	A_s (sq.in.)	A'_s (sq.in.)
A	2" deep x 2" wide	4 #7 wires (diameter = 0.177")	0.0492	0.0492
B	1" deep x 2 wide	4 #12 wires (diameter = 0.105"	0.0173	0.0173

Suitable wooden forms were used to cast the specimens. (Fig.3.3) A simple device as shown in Fig. 3.4 was used to make the reinforcement cages. The wires were first bent to the required radius in a wire bending machine, and then inserted into the device mentioned above. Stirrups were tied at predetermined spacing.

The concrete was mixed for 2 to 3 minutes in a nine cubic feet capacity tilting drum type mixer. The specimens were left in the formwork for about 48 hours, after which they were removed from the forms and cured in the air of the laboratory until tested. With each specimen, three 6" x 12" control cylinders were also cast and cured under the same conditions. These control cylinders were used to determine the ultimate compressive strength f'_c of the concrete, at the time the specimen was tested.

3.2 MATERIAL PROPERTIES

3.2.1 Concrete:

The concrete mix was designed for an f'_c of 3000 psi at seven days. The proportions by weight of the cement, sand, gravel and water were as follows:

1 part by weight of high early portland cement,

2.64 part by weight of sand,

2.10 part by weight of coarse aggregate,

7.25 gallons of water per sack of cement.

With these proportions it was expected to obtain f'_c equal to 3000 psi at seven days. However, for some test specimens, the actual f'_c obtained from the test cylinders was higher because it was not possible to test the specimens exactly at seven days. In some cases, specimens were tested after as much as thirty days, due to unexpected delays. The actual value of f'_c of each specimen is given in Chapter 4.

The sand used had a fineness modulus of about 2.5. The maximum aggregate size for Type A specimens was 3/8", while for Type B specimens 3/16".

3.2.2 Steel:

Black annealed mild steel wires were used as the reinforcement. For Type A specimens, #7 wires (diameter = 0.177") were used, while for Type B Specimens #12 wires (diameter = 0.105") were used. The strength properties of these wires were as follows:

(a) #7 Wires:

Static yield stress f_y = 40 ksi

Static ultimate stress f_u = 51 ksi

Modulus of elasticity E_s = 34.1 x 10^3 ksi

The stress-strain curve of this wire is given in Fig. 3.5.

(b) #12 Wires:

Static yield stress f_y = 40 ksi

Static ultimate stress f_u = 49.5 ksi

Modulus of elasticity E_s = 31.6 x 10^3 ksi

The stress-strain curve of this wire is given in Fig. 3.6.

3.3 LOADING CONDITIONS

In this test program, static and dynamic tests were conducted for the following three types of loading conditions.

Type I - Uniformly distributed symmetric radial load: This was simulated by ten point loads, spaced at equal intervals on the periphery of the arch as shown in Fig. 3.7. Each interval subtends an angle of 18° at the center.

Type II - Concentrated load at the crown of the arch.

Type III - Antisymmetric concentrated loads at quarter points on the arch.

These three loading conditions are shown in Fig. 3.7.

3.4 EXPERIMENTAL SET UP

3.4.1 Modification of the Existing Loading Machine:

The dynamic loading machine[18], constructed by the Department of Civil Engineering, M.I.T., under the contract DA-49-129-ENG-325, had to be modified to suit

the loading conditions described in section 3.3. With the earlier version of the machine it was possible only to apply a single point load on the test specimen. The modification essentially consisted of mounting ten jacks on a suitable frame, and in connecting these jacks through rubber hoses to the auxiliary oil reservoirs. In what follows, a short description of loading jacks, rubber hoses, oil reservoirs and the details of their connection with the previously existing apparatus is given. For a detailed description of the components of the original machine and the principal of its operation, reference is made to [18].

(a) Loading Jacks: The preliminary estimate of the dynamic resistance of the Type A arch specimens showed that the failure load under compression mode loading (i.e., Type I loading condition) would be about 6.5 to 7 kips per jack. Therefore, it was decided to design the loading jacks to develop a load of 12 kips at the maximum working oil pressure of 4000 psi. The details of design were based on considerations similar to those given in reference (18) (Chap. V, Art c). It was found that Hannifin Series "H" square type hydraulic cylinders (manufactured by Haniffin Company, Des Plaines, Illinois) with the following requirements, were suitable for the purpose and accordingly adopted.

1. Bore diameter = $2\frac{1}{2}$"
2. Piston rod diameter = $1\frac{3}{8}$"
3. Stroke = 4"
4. Maximum Working Pressure = 4000 psi

These jacks are double acting - double rod end, with cushions on both ends of the jack.

(b) Reservoir: In the modified loading system, two reservoirs are used. One of them is interposed between the pump and the push side of the loading jacks while the other is placed between the pull side of the jacks and the dump valve of the original dynamic loading machine. These reservoirs are in the form of cylindrical containers with a sufficient number of outlets which can be connected to the jacks. These reservoirs are shown in Figs. 3.8 and 3.9. Various details, such as the diameter of cylindrical container, number of outlets, etc., are also marked in Figs. 3.8 and 3.9. The reservoirs are designed to withstand an oil pressure of 5000 psi. The main purpose of these reservoirs is to provide the means of supplying oil to all the jacks at the same pressure so that the jacks can develop equal loads.

(c) Rubber Hoses: In order to have the flexibility in connections between the reservoirs and the jacks, rubber hoses were used instead of metal tubing. These hoses are 3 wire braid high pressure hoses (working pressure = 5000 psi,

and bursting pressure = 20,000 psi) with $\frac{1}{2}$" internal diameter.

(d) Hydraulic Connection: The hydraulic connections between various components of the loading system are shown in Fig. 3.10.

The main cylinder of the machine is connected to the push side reservoir which in turn is connected to the push side of the jacks. The main dump valve is connected to the pull side reservoir which in turn is connected to the pull side of the jacks. Heavy duty steel pipes are used for connecting the main cylinder with the push side reservoir and the dump valve with the pull side reservoir. Connections between the reservoirs and the loading jacks are through high pressure rubber hoses as already mentioned.

The pull and push side reservoirs are interconnected by $\frac{3}{4}$" tubing so that equal pressure can be built up and maintained initially on the pull and push side of the jack. A needle valve is placed in this line, so that by closing the valve, the two reservoirs can be disconnected before dumping the pull side reservoir through the dump valve.

(e) Frame: The structural frame in which the jacks and the specimen are mounted, consists of WF I

sections. Fig. 3.11 shows this frame with ten jacks mounted for Type I loading. For Type II loading, only one jack is mounted at the proper place on the frame as shown in Fig. 3.12. Two jacks are mounted on the frame as shown in Fig. 3.13 for Type III loading. In order to ensure that the applied load remains radial, as the arch deforms under load, the jacks are mounted so as to allow them to rotate with the arch. This is done by using pin connections between the jacks and the frame and between jacks and the specimen.

The pinned supports for the test specimen is simulated by using specially fabricated devices as shown in Figs. 3.14, 3.15, 3.16 and 3.17.

3.4.2 Instrumentation and Measurements:

In order to study the behavior of the test specimens, it is necessary to measure the following quantities:

(a) Applied Loads,

(b) Reactions,

(c) Radial deflection at crown and at $\frac{1}{4}$ points,

(d) Natural frequency of the test specimens.

(a) Applied Loads: The applied loads were measured by mounting suitable load cells on the piston rod of the jacks. The range of failure loads between type A specimens under compression mode loading (Type I) and type B specimens under deflection mode loading (Type I_{II}) was quite large. Type A specimen under compression mode had an estimated failure load of about 7000 lbs. per jack, while the estimated failure load for type B specimen under deflection mode was as low as 100 lbs. per jack. Therefore three different types of load cells had to be made for each of the three load types. These load cells are shown in Fig. 3.18.

Load cells for Type I and Type II loadings were essentially hollow circular aluminum rods on which are mounted eight C-7 strain gages (4 active gages and 4 dummy gages, resistance of each gage = 500 ohms). Load cells for Type III loading were in the form of a u-shaped aluminum frame on the vertical sides of which are mounted eight C-7 strain gages. These strain gages are connected to form a suitable wheatstone bridge circuit. The signal from this strain gage bridge was fed into an eighteen channel recording oscillograph, Type 5-114-P3, manufactured by the Consolidated Electrodynamics Company. (Hereafter in this report this equipment will be referred to as the C. E. C. recorder). The traces of the galvanometers

of the C.E.C. recorder were recorded on photographic paper in both dynamic and static tests.

Initially a few pilot tests were made on type "A" specimens under Type I loading and in these tests all ten jack loads were measured to determine whether the loads developed by all jacks were equal or not. These pilot tests did confirm that the loads were equal and as a consequence, it was decided to measure only five jack loads during the tests.

(b) Reactions: Vertical and horizontal reactions were measured by the load cells as shown in Fig. 3.14. Again for the reasons mentioned above [article 3.4.2 (a)] various types of load cells had to be made. These load cells are in the form of solid or hollow aluminum rods of suitable diameter, with square aluminum plates at their ends. These load cells were useful for measuring relatively large reactions. The ring type load cells which essentially consisted of an aluminum ring between two square plates were used to measure relatively small reactions. Eight C-7 strain gages were mounted at suitable places on these load cells as shown in Fig. 3.19. The gages were connected to form a suitable wheatstone bridge circuit. The output of the load cell was measured by the C.E.C. recorder in both static and dynamic tests.

The power to all the load cells was supplied by a Sorenson Transisterized D.C. Power Supply (Model No. QR-36-4A). The range of output voltage and output current of this power supply unit is 0 - 36 volts and 0 - 4 amps. respectively, with a % regulation of 0.02.

(c) Measurement of Deflections: In all tests, radial deflections of the test specimen were measured at the following points.

For Type I loading, radial deflections were measured at the crown and at the points 54 degrees from the supports (Fig. 3.20). Deflections were measured at these 54° points rather than at the quarter points because it was difficult to attach the deflection measuring device at the latter due to the presence of the loading jack. In Type I loading, it was found during pilot tests that the supporting frame also deflected appreciably and therefore deflections of the support were also measured. Electric inductance gages of the moving core solenoid type, commonly known as Linear Variable Differential Transformers (L.V.D.T.), were used to measure the deflections. These gages were of the type 1000 - SS - L (manufactured by Schaevitz Engineering Corportation) with a linear range

of ± 1.0". The core and the transformer of the L.V.D.T. were mounted on a special attachment shown in Fig. 3.21. One end of this attachment was connected to the specimen, while the other end was connected at a suitable point independent of the supporting frame. These connections were such as to allow the attachment to rotate so that it remained radial when the arch deformed under load. Fig. 3.11 shows the set up of L.V.D.T.'s.

For Type II loading, radial deflections were measured at the crown and at two quarter points (Fig. 3.20). At quarter points the attachments as described in the above paragraph were used to mount the L.V.D.T.'s while at the crown the L.V.D.T. was mounted directly on the jack. The setup of L.V.D.T.'s is shown in Fig. 3.12.

For Type III loading, radial and tangential deflections were measured at the two quarter points. Type 2000 - SS - L L.V.D.T.'s with a linear range of ± 2.0" were used to measure the radial deflections, while tangential deflections were measured by type 1000 - SS - L L.V.D.T.'s. The L.V.D.T.'s measuring the radial deflections were mounted directly on the jack while the L.V.D.T.'s, measuring tangential deflections, were mounted on an attachment as

shown in Fig. 3.13.

(d) Measurement of Natural Period: The natural periods of types A and B specimens in the first bending mode (i.e., antisymmetric mode) and in the second bending mode (i.e., mode corresponding to the configuration of the arch under a point load at the crown) were measured. For this purpose displacements corresponding to each mode were given to the arch specimens, released suddenly, and the resulting vibrations measured by very sensitive L.V.D.T.'s, (Type 020 MS - L, linear range = $\pm$ 0.02") connected to the C.E.C. recorder.

3.5 TESTING TECHNIQUE

In this section a brief description of the method of static and dynamic testing is given.

3.5.1 Static Tests:

The specimens were mounted in the frame and connected to the loading jacks as shown in Figs. 3.11, 3.12 and 3.13. The specimens were loaded by continuously building up the oil pressure on one side of the jacks, until the specimens failed. A continuous record of all the measurements was obtained by running the C.E.C. recorder at the slow speed of 0.80 in/sec. The duration of test on an average was 3 to 4 minutes.

3.5.2 Dynamic Tests:

The specimens were mounted in the frame and connected to the loading jacks as in static tests. Equal oil pressure was built up on both sides of the jacks. In order that no load be applied to the specimen, while the pressures were being increased to the required value, it was necessary to maintain an equal pressure on both sides of the jacks at all times. This was done by keeping the valve which interconnects the pull and push side reservoirs, open. This valve was closed after the required pressure was attained on two sides of the jack and then the pull side was "dumped" by opening the dump valve. The latter was operated by sending a predetermined command signal to the servo valve which controls the dump valve. In this way the dynamic loads with a rise time between 10 to 20 milliseconds were applied to the test specimens. A record of all measurements such as applied load, deflections, etc. with respect to time was obtained on the C.E.C. recorder running at the high speed of 21.6 inches/sec.

In all cases a failure pulse slightly greater than the estimated failure resistance of the specimens under each type of loading, was applied. Due to limitations of the loading machine, it was not possible to apply

partial loads on test specimens except for type "A" specimens under compression mode loading (Type I), because the failure loads were too low in other cases. Partial loads with a rise time between 10 to 20 milliseconds and a flat peak of considerably longer duration (about 1000 milliseconds) were applied to some of these type "A" specimens.

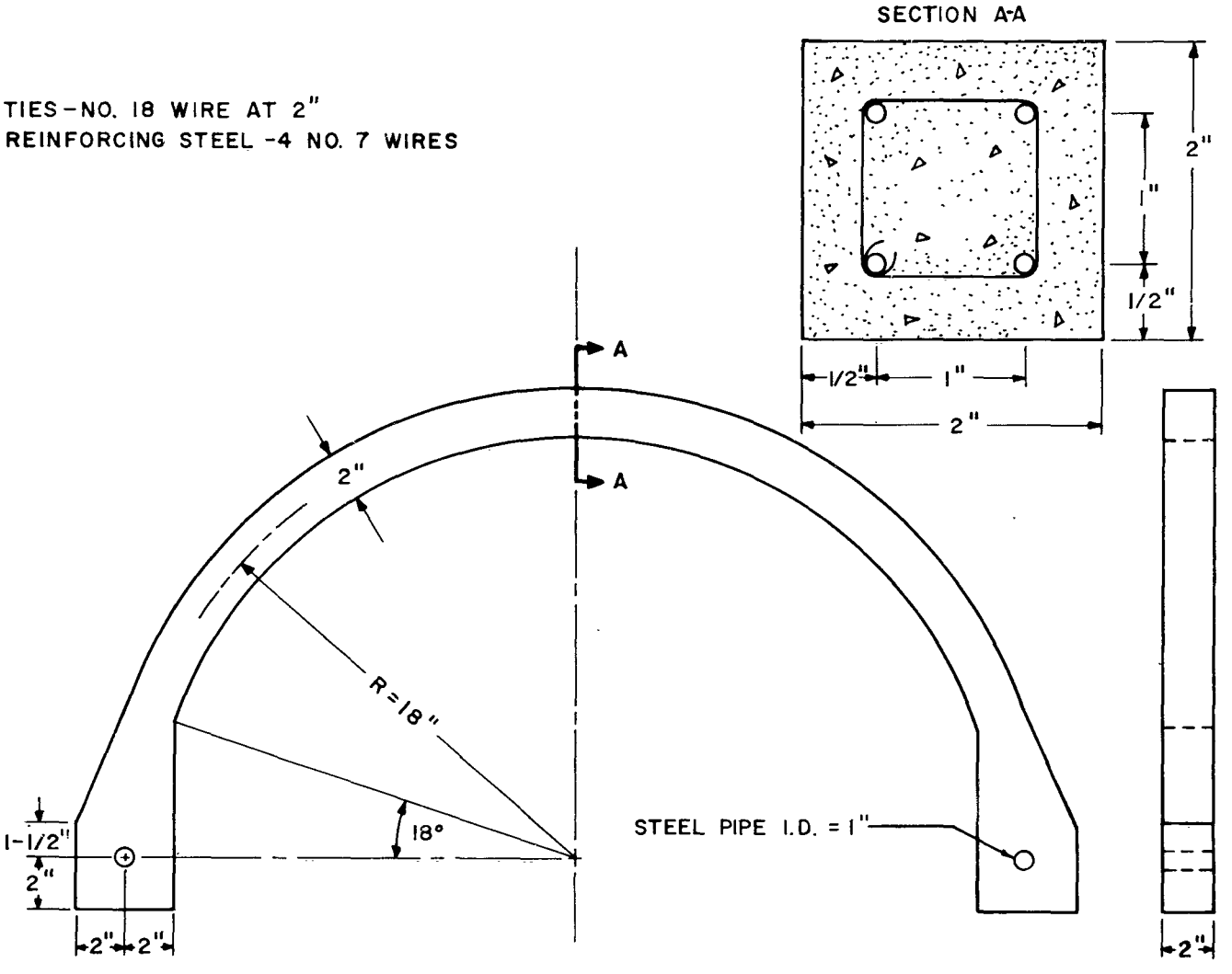

FIGURE 3.1 - TYPE A SPECIMEN

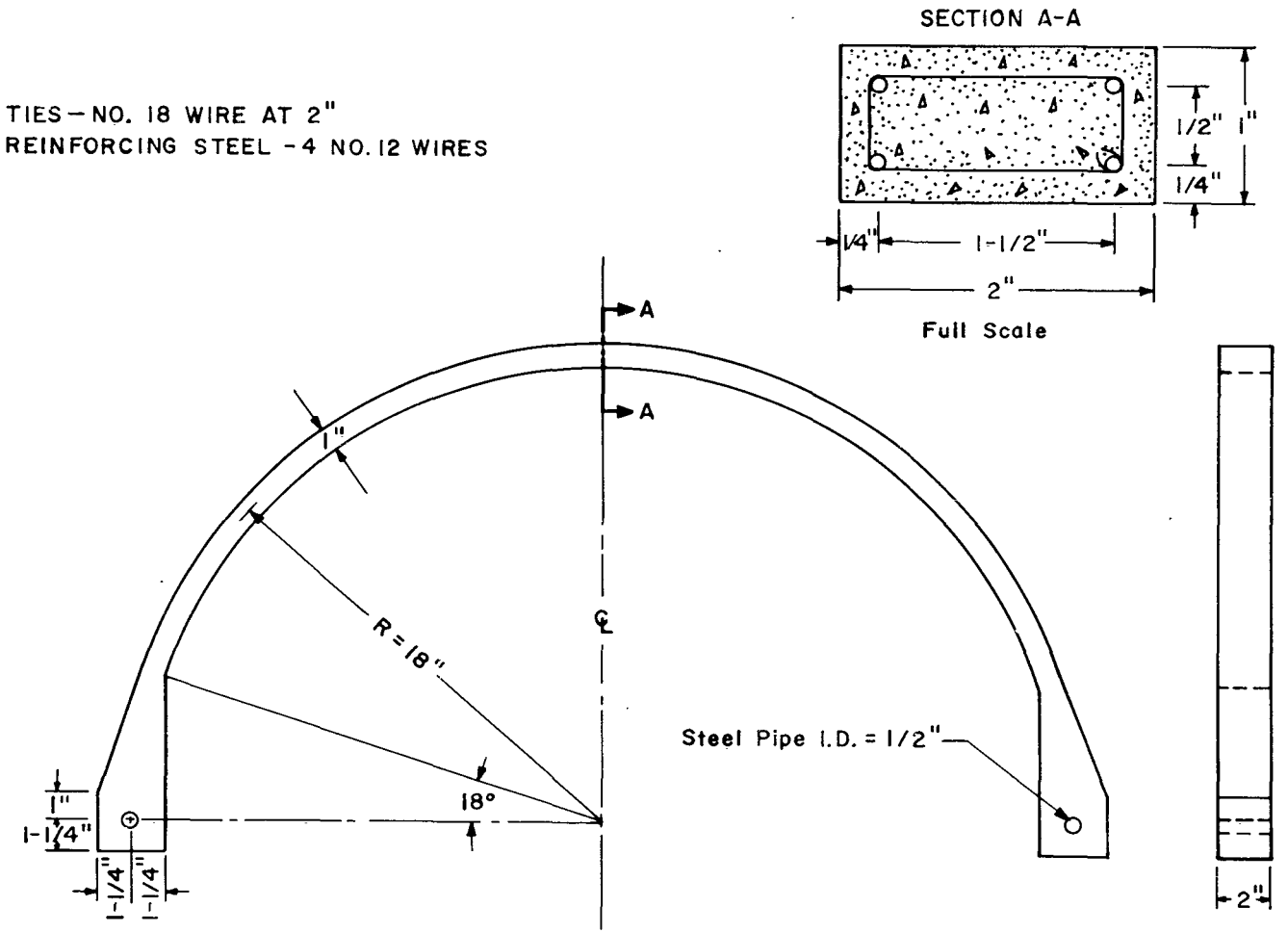

FIGURE 3.2 – TYPE B SPECIMEN

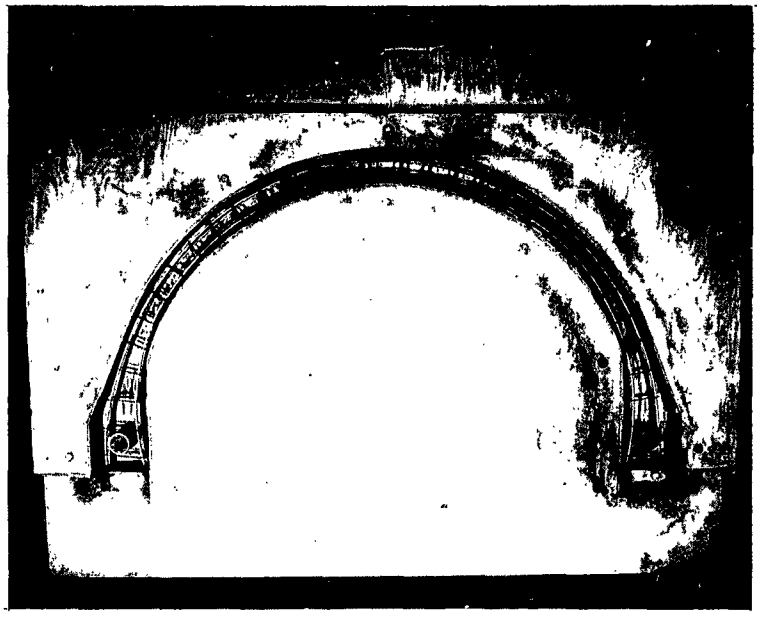

Figure 3.3 - Wooden Form Work for Type A Specimens.

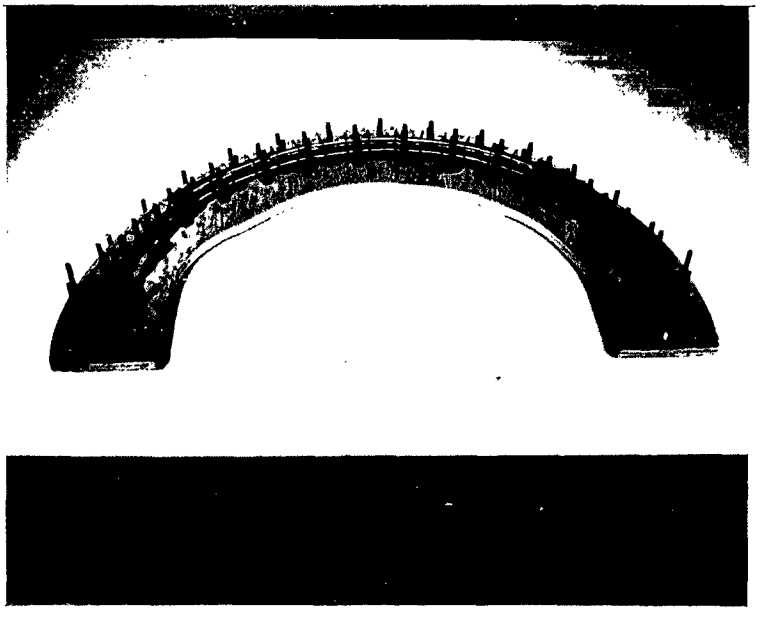

Figure 3.4 - Device for Making Reinforcement Cages for Type A Specimen.

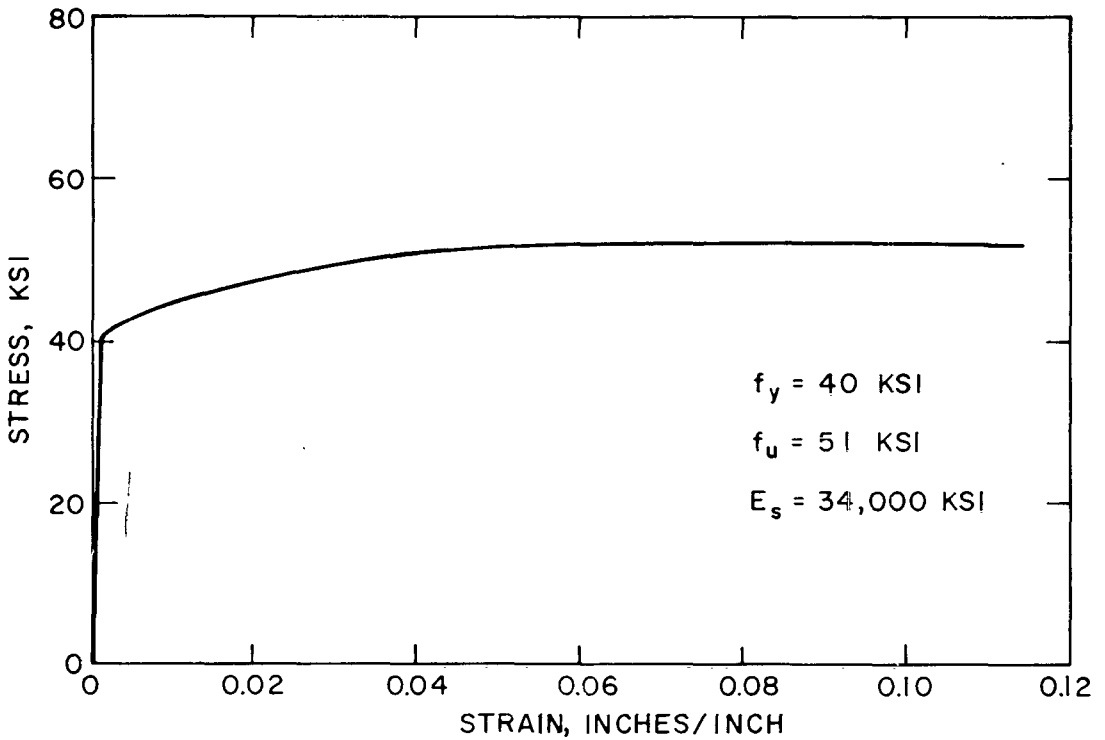

FIGURE 3.5 - STRESS-STRAIN CURVE - NO. 7 WIRES

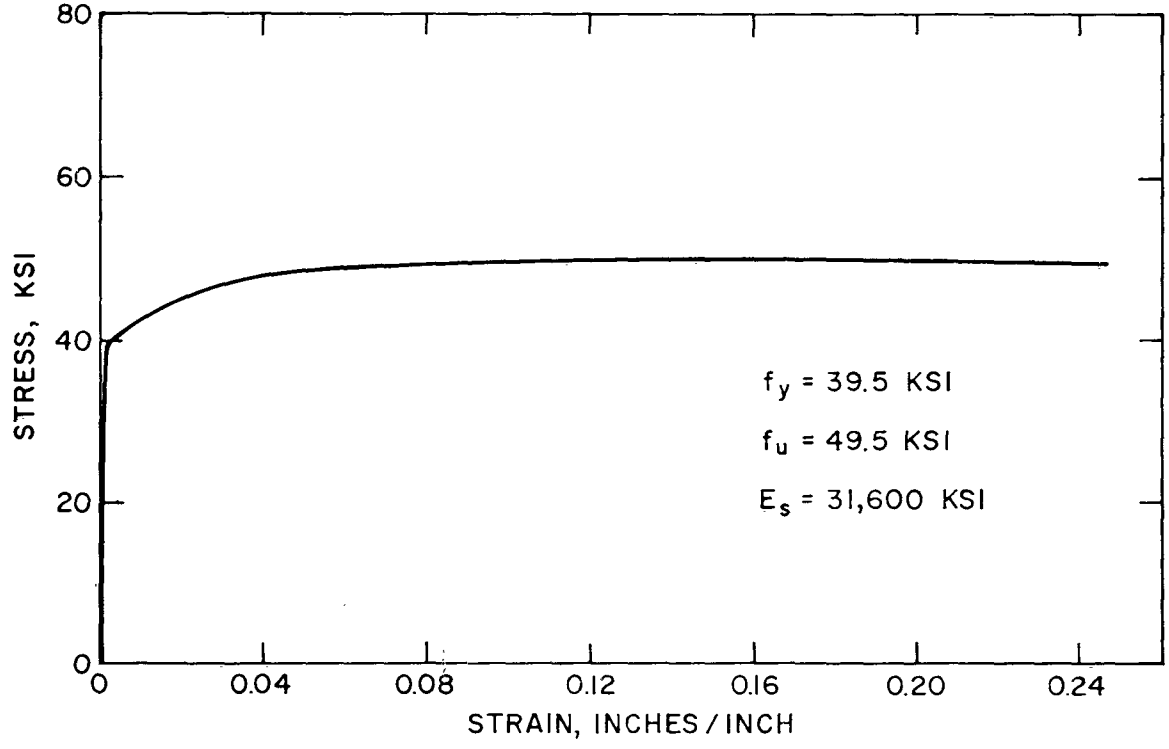

FIGURE 3.6 - STRESS-STRAIN CURVE - NO. 12 WIRES

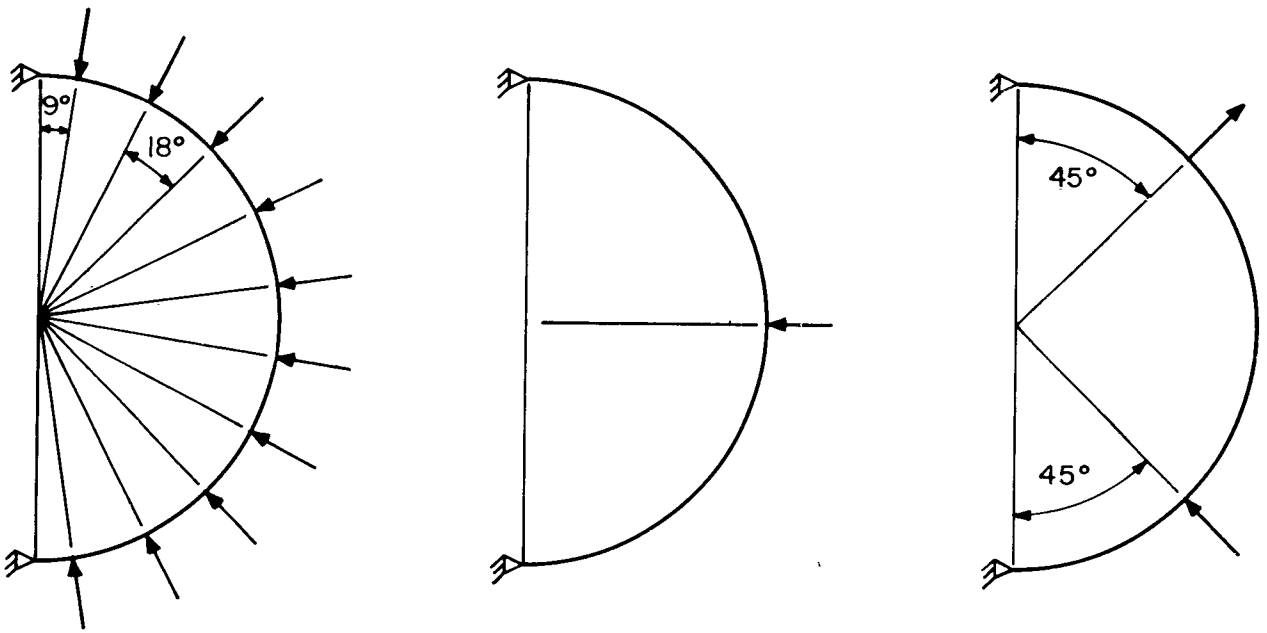

FIGURE 3.7- TYPE OF LOADING

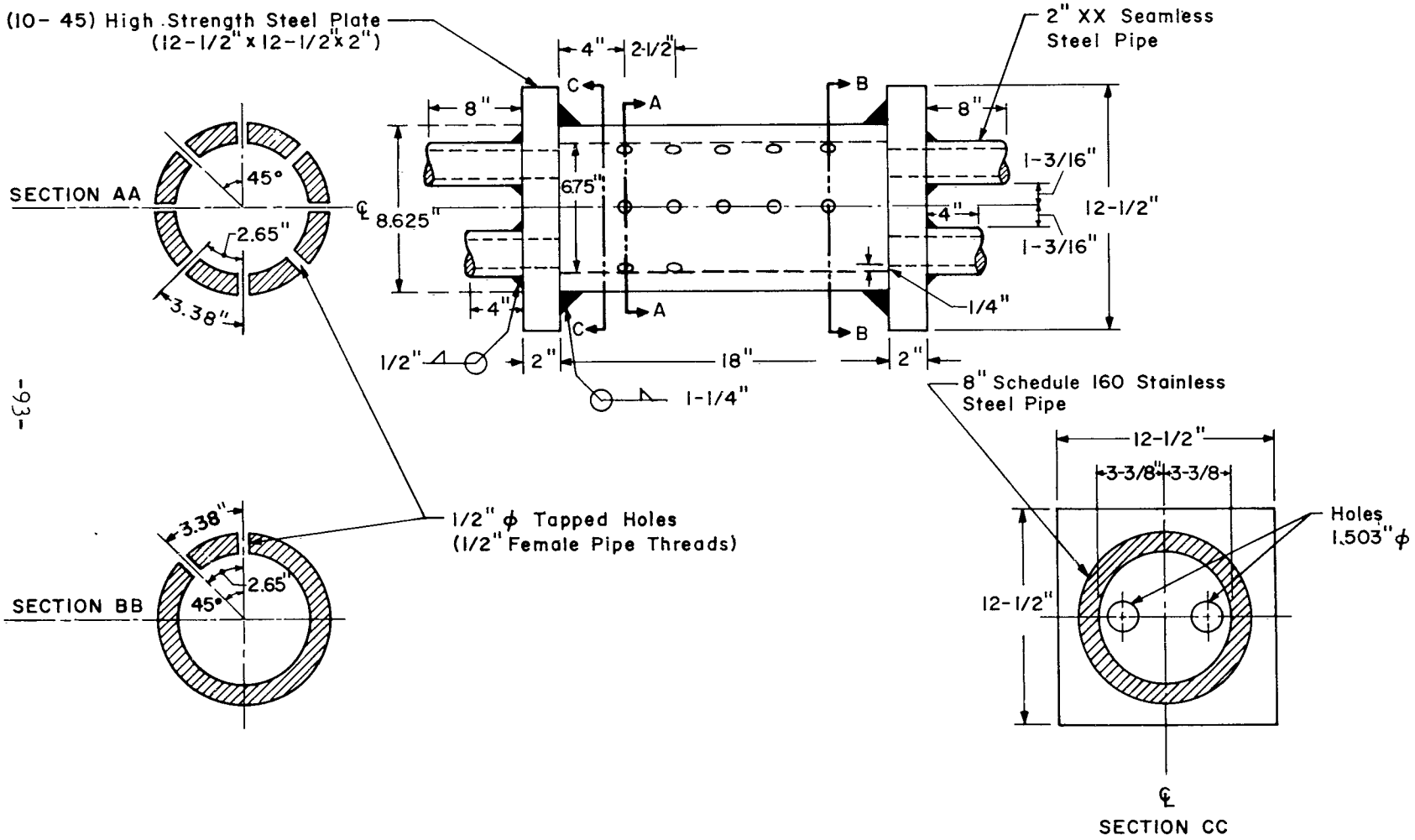

FIGURE 3.8 - PUSH SIDE RESERVOIR

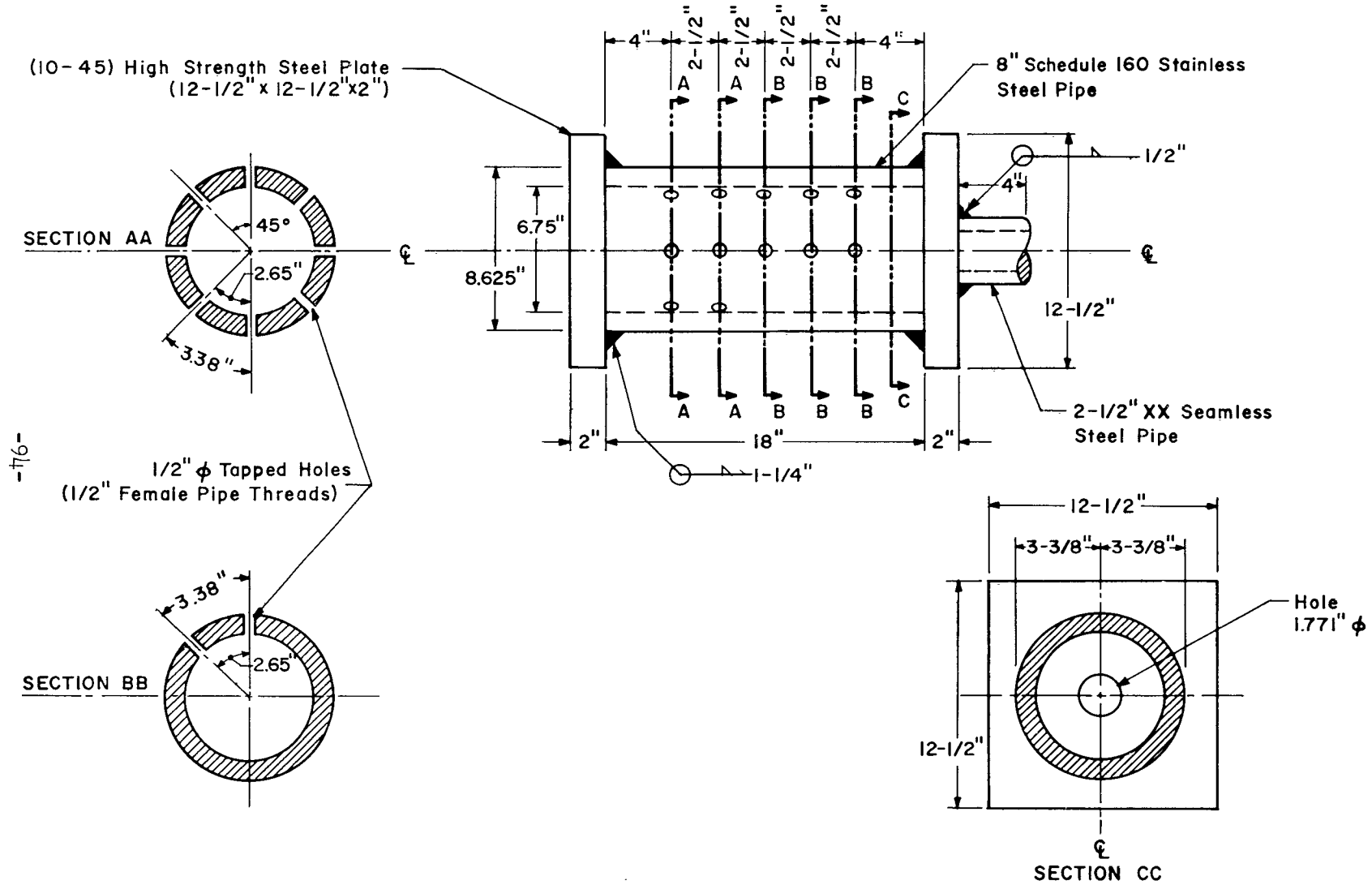

FIGURE 3.9 PULL SIDE RESERVOIR

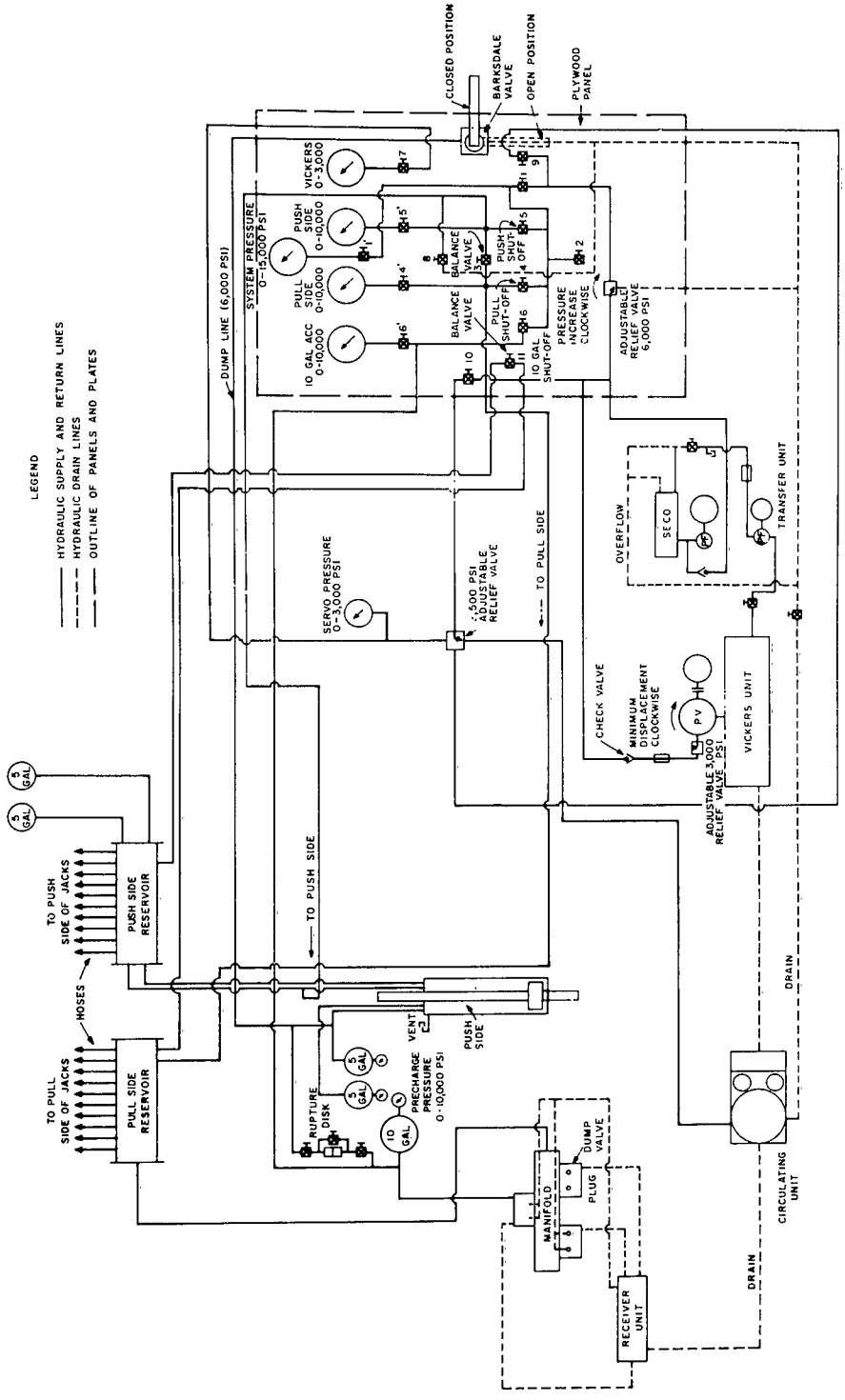

FIGURE 3.10-SCHEMATIC DIAGRAM OF LOADING UNIT

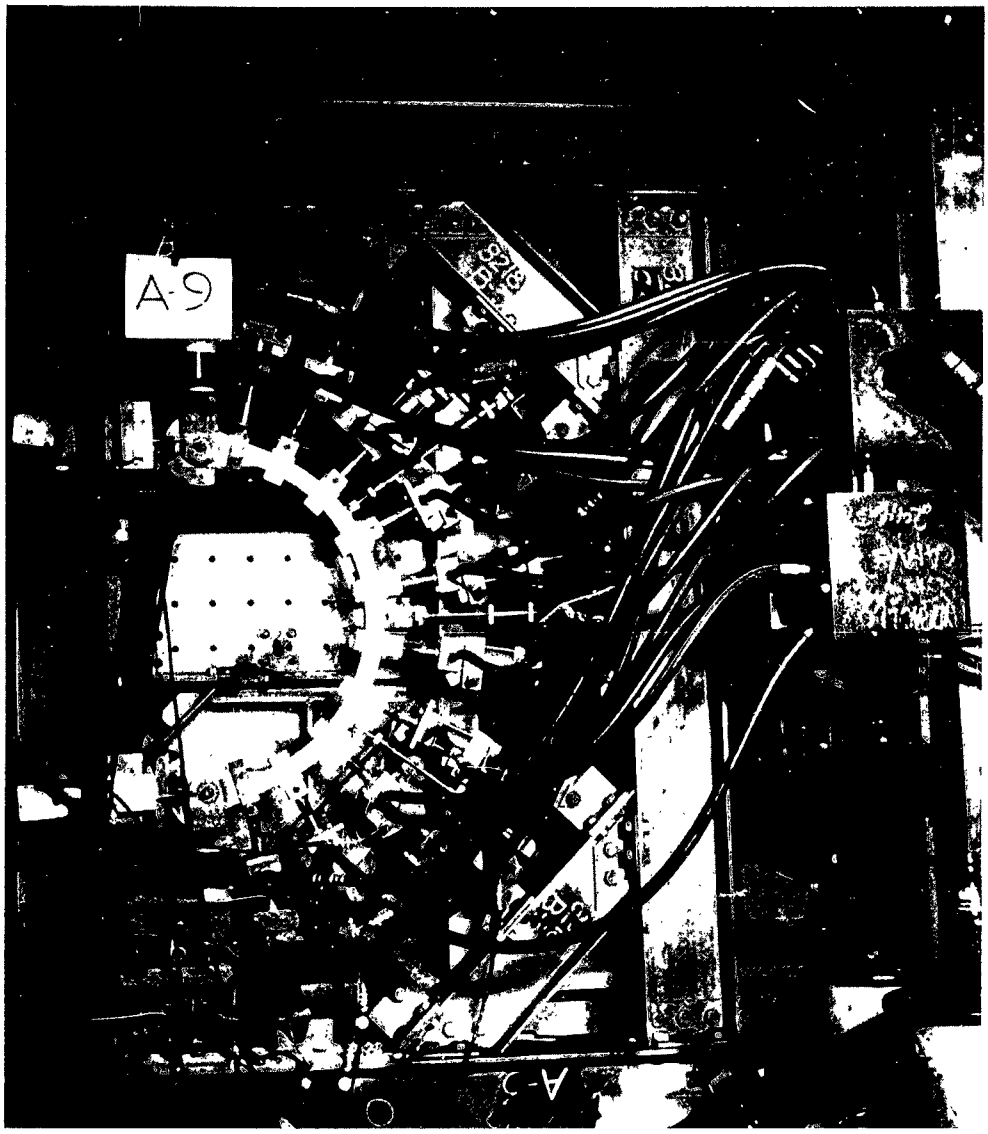

Figure 3.11 - Experimental Set Up -
Type I Loading.

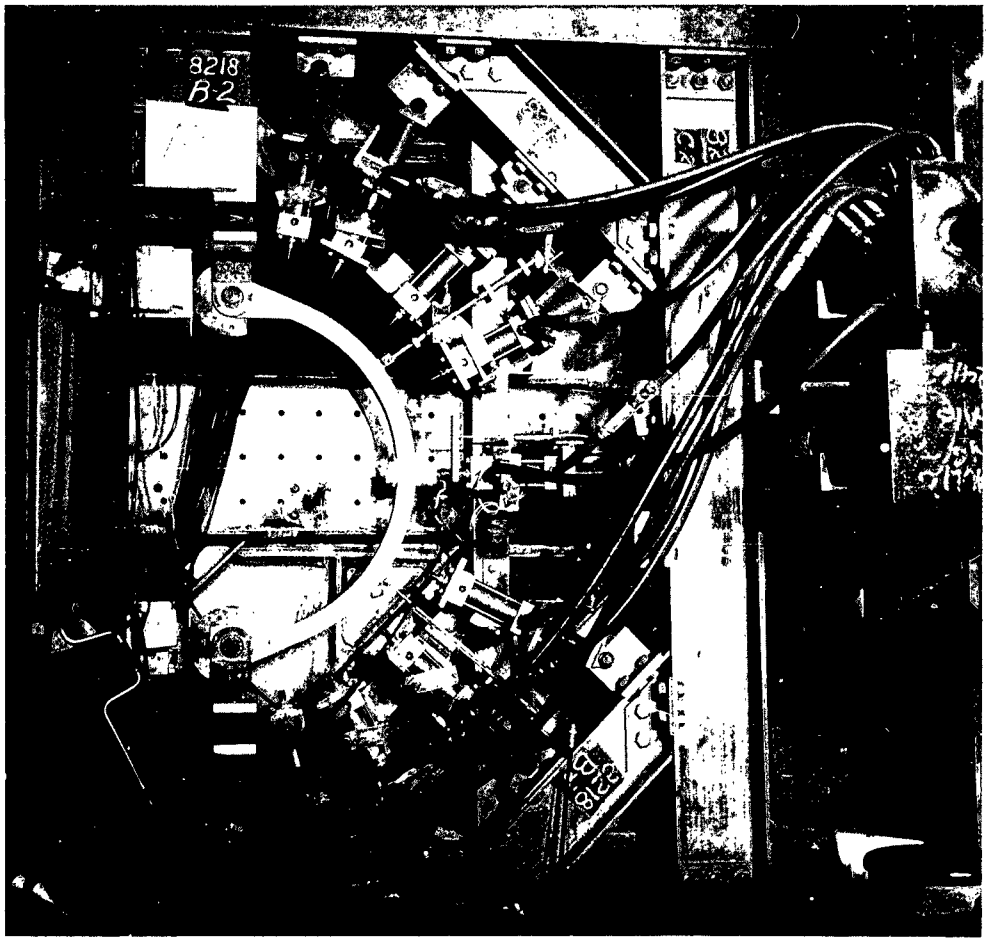

Figure 3.12 - Experimental Set Up -
Type II Loading.

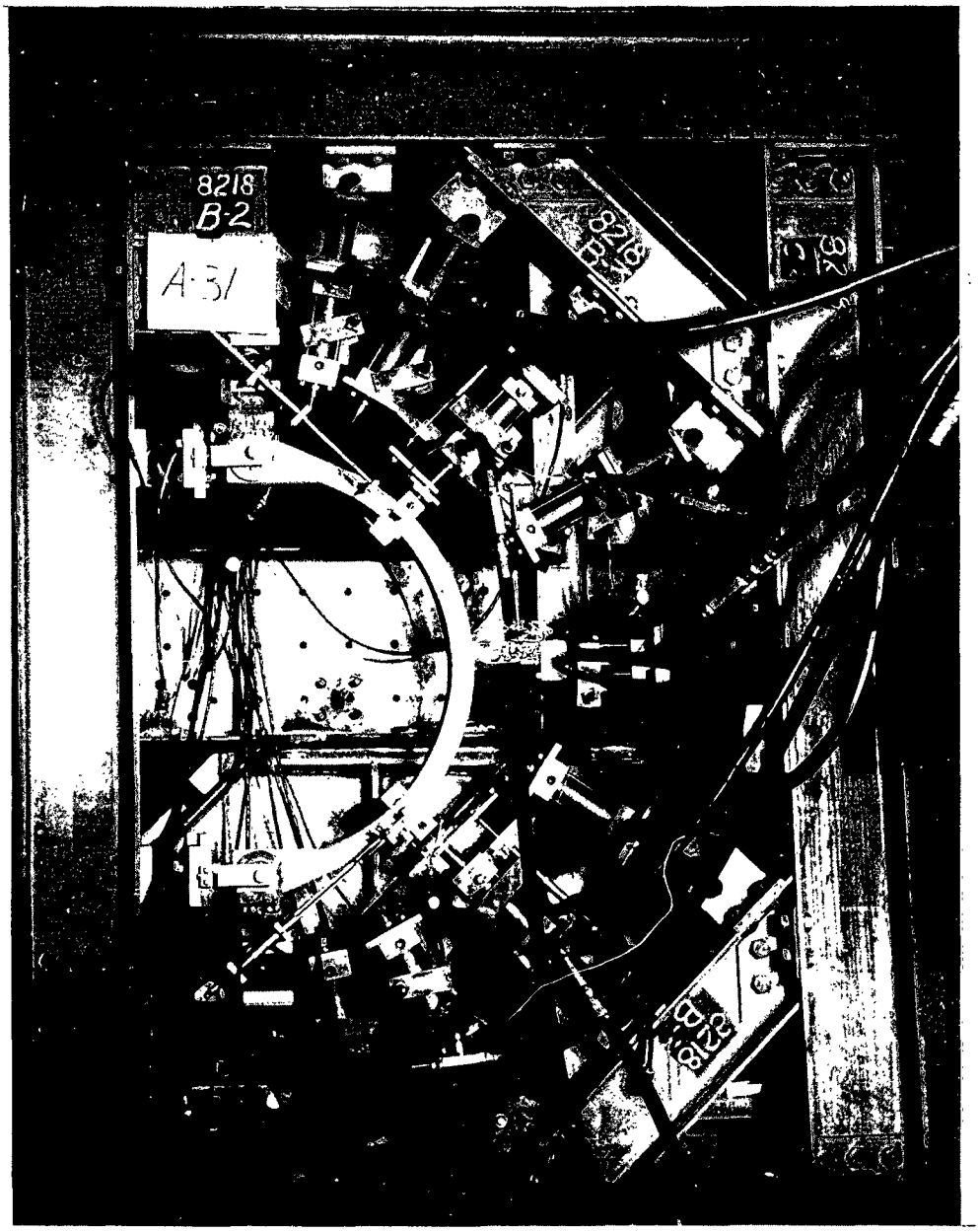

Figure 3.13 - Experimental Set Up -
Type III Loading.

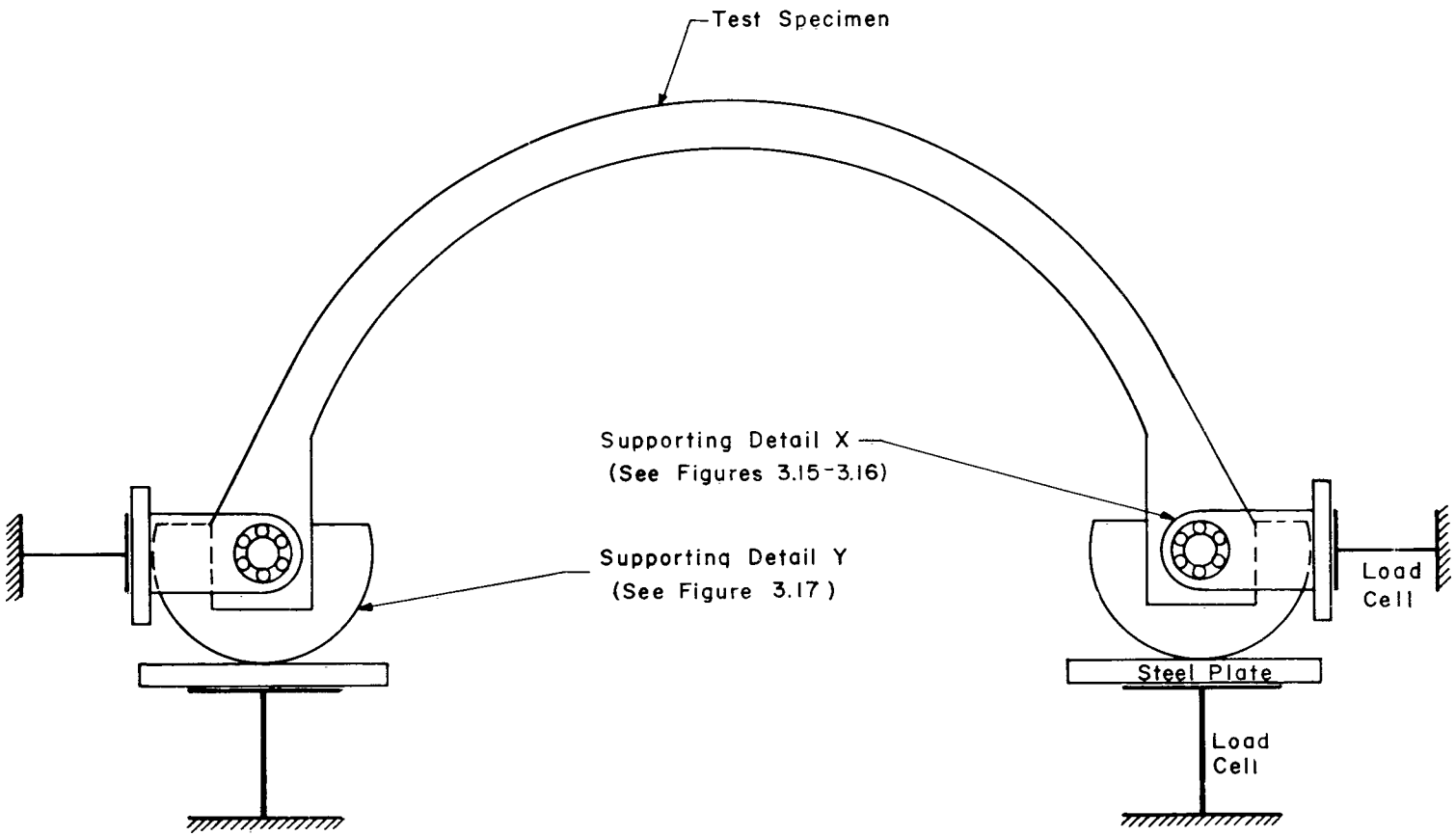

FIGURE 3.14 – HINGE SUPPORTS FOR TEST SPECIMEN

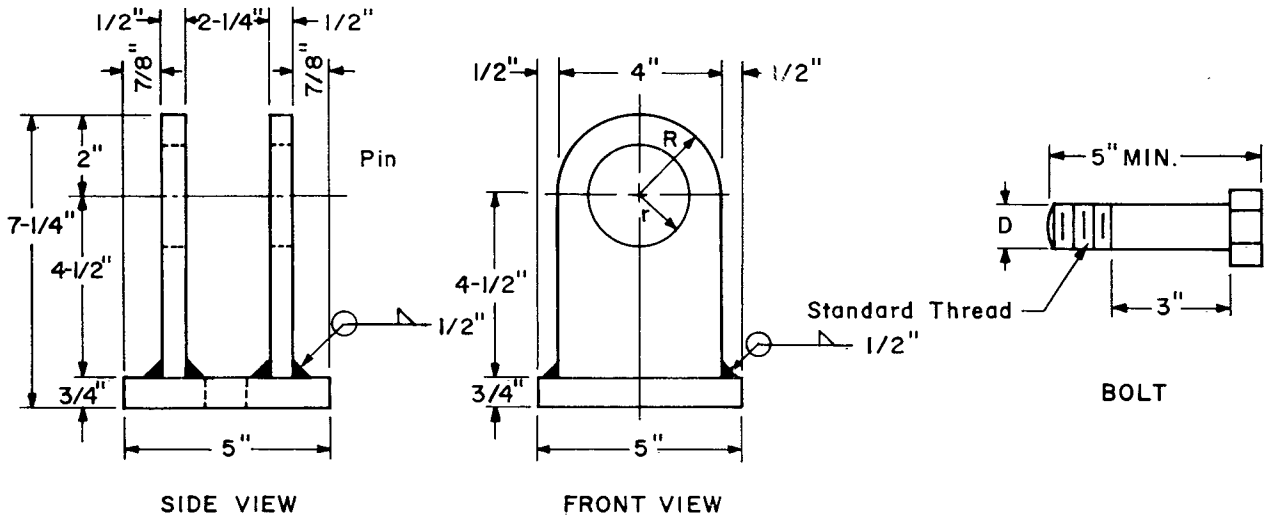

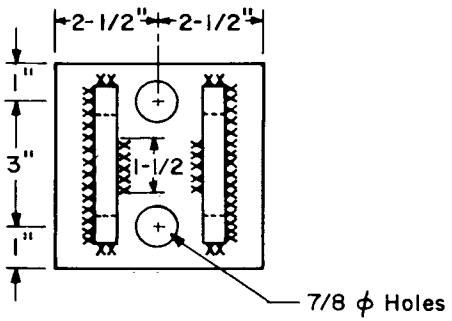

NOTES :

R = 2"

r ≈ 1.2205" TO FIT NO. 20206 BALL BEARING

D ≈ 1.1811" TO FIT NO. 20206 BALL BEARING

MATERIAL - STEEL

FIGURE 3.15 - SUPPORTING DETAIL "X" FOR TYPE A SPECIMEN

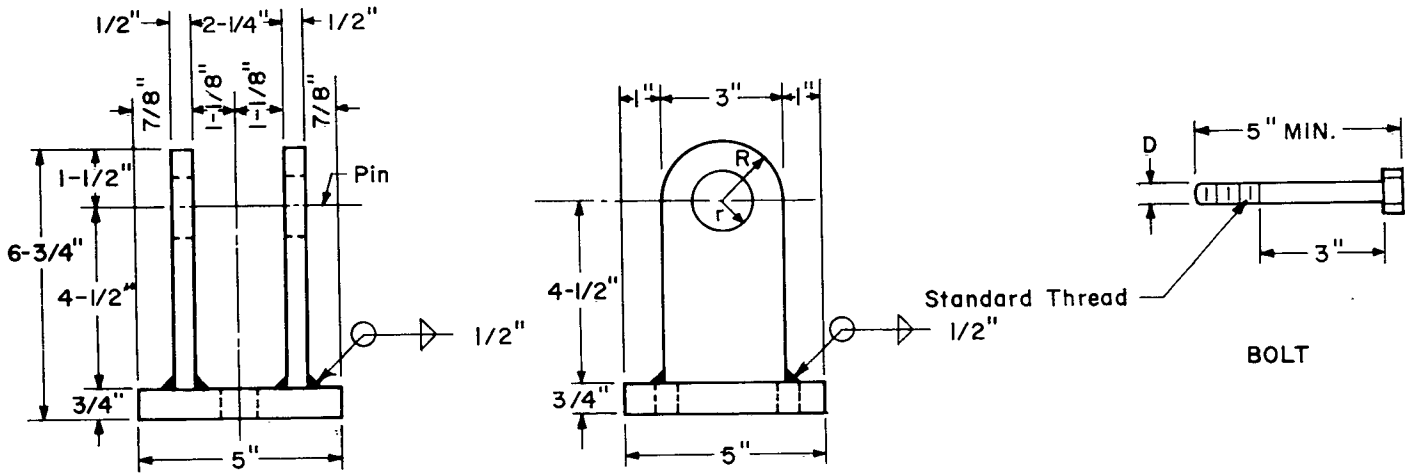

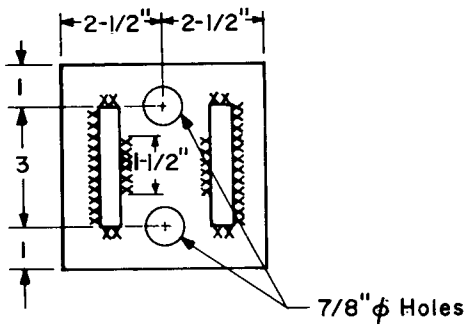

NOTES:

R = 1-1/2"

r ≈ 0.7284" TO FIT NO. 3301 NEW DEPARTURE BALL BEARING

D ≈ 0.4724" TO FIT BALL BEARING

MATERIAL-STEEL

FIGURE 3.16 - SUPPORTING DETAIL "X" FOR B SPECIMEN

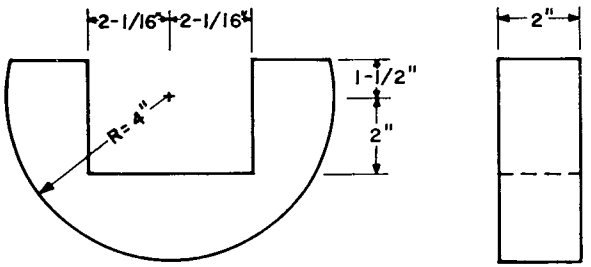

FOR TYPE "A" SPECIMEN

MATERIAL USED – STEEL

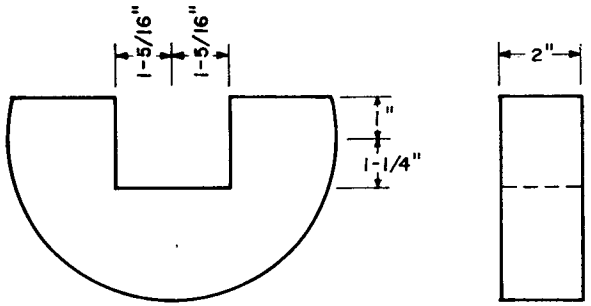

FOR TYPE "B" SPECIMEN

FIGURE 3.17 – SUPPORTING DETAIL Y

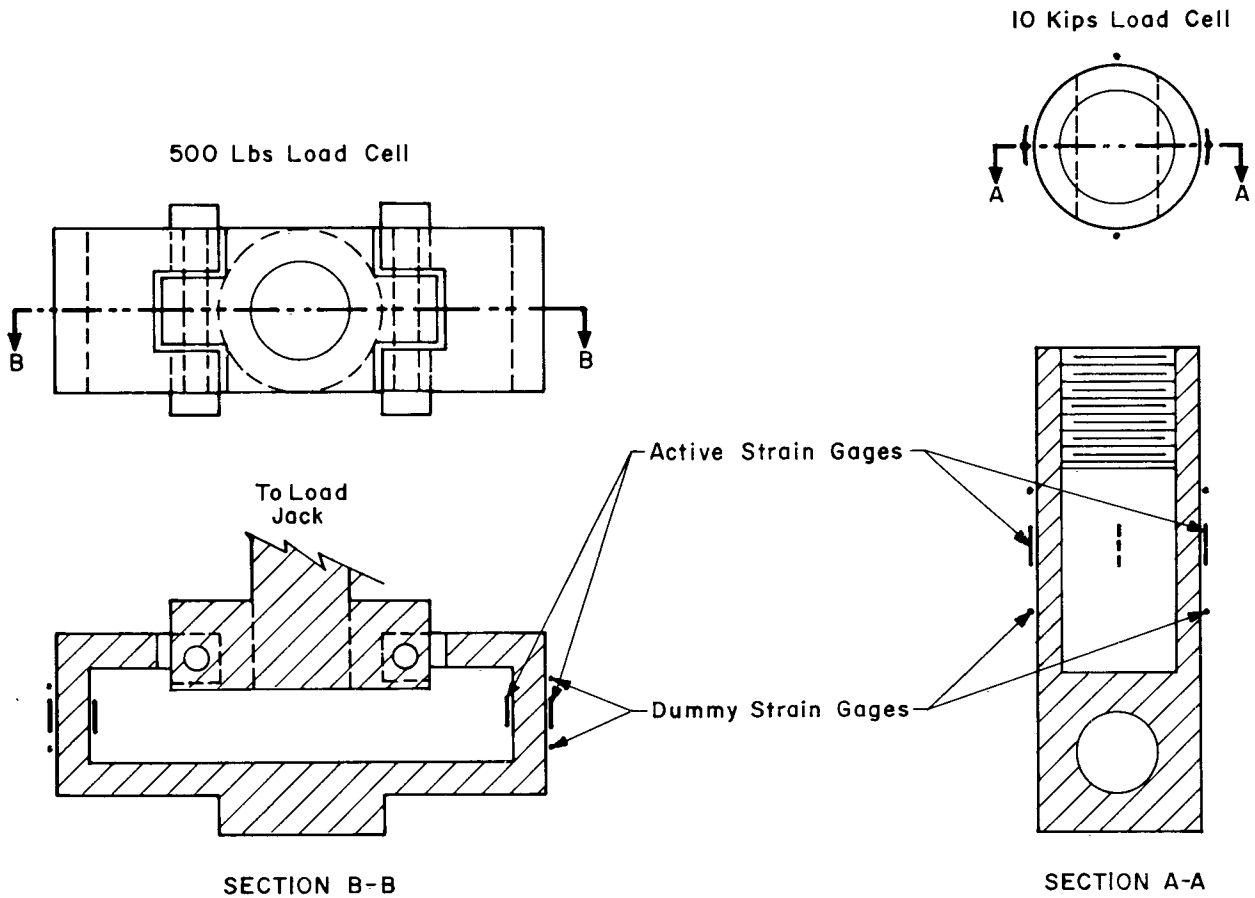

NOTE

1. 2.5 Kips Load Cell Similar to the 10 Kip Load Cell.
2. Material of Load Cells–Aluminum.

FIGURE 3.18 LOAD CELLS FOR MEASURING APPLIED LOAD

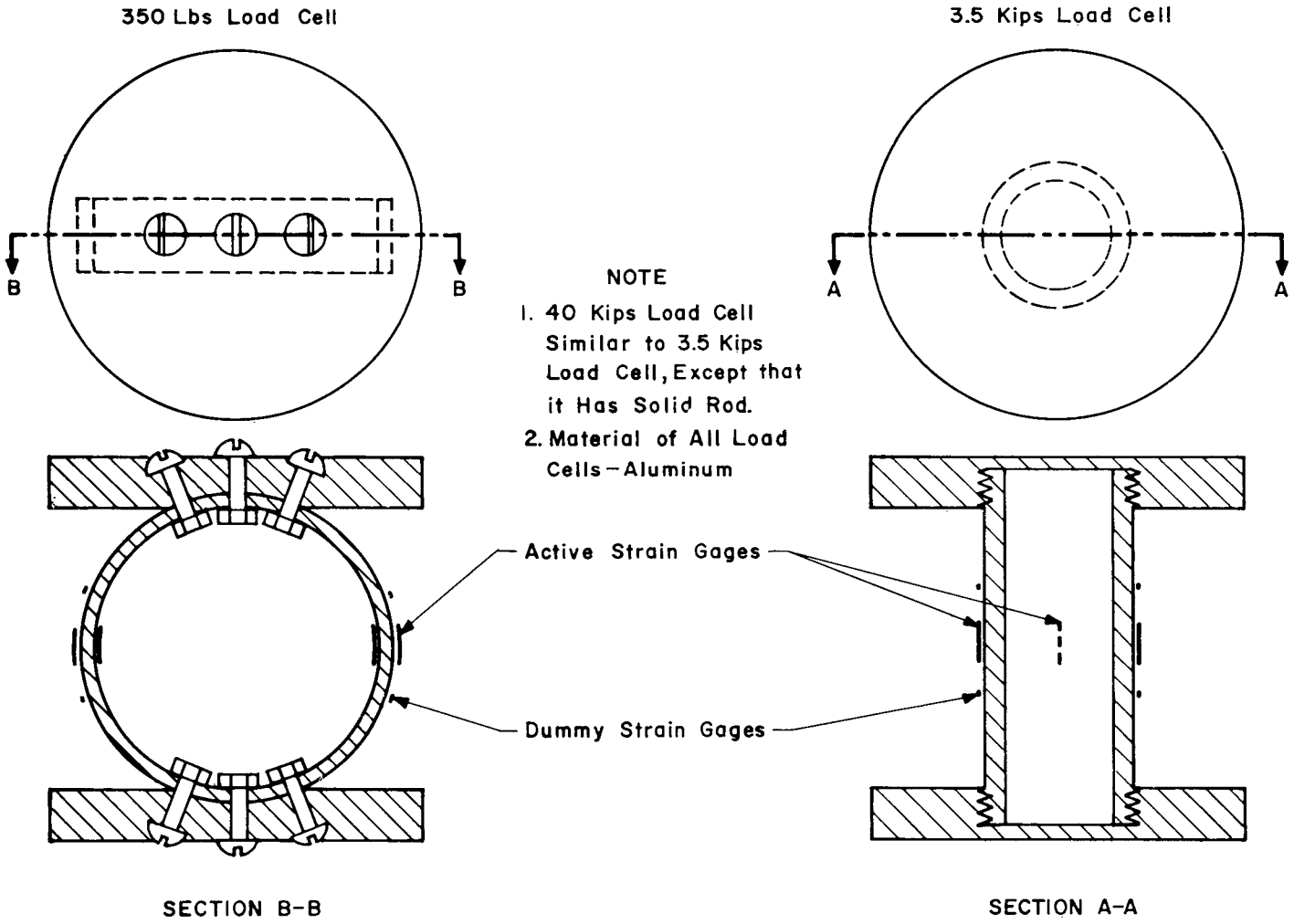

FIGURE 3.19 - REACTION LOAD CELLS

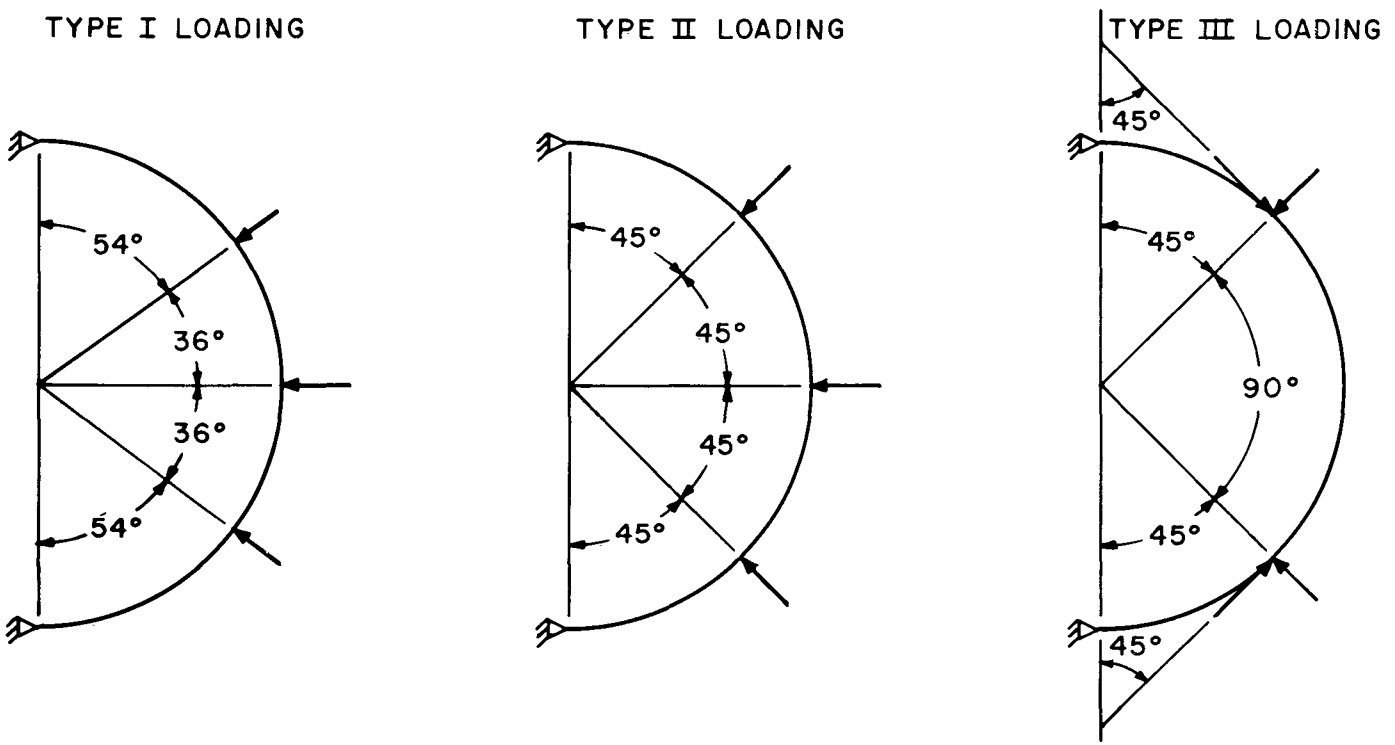

FIGURE 3.20– L.V.D.T. LOCATIONS

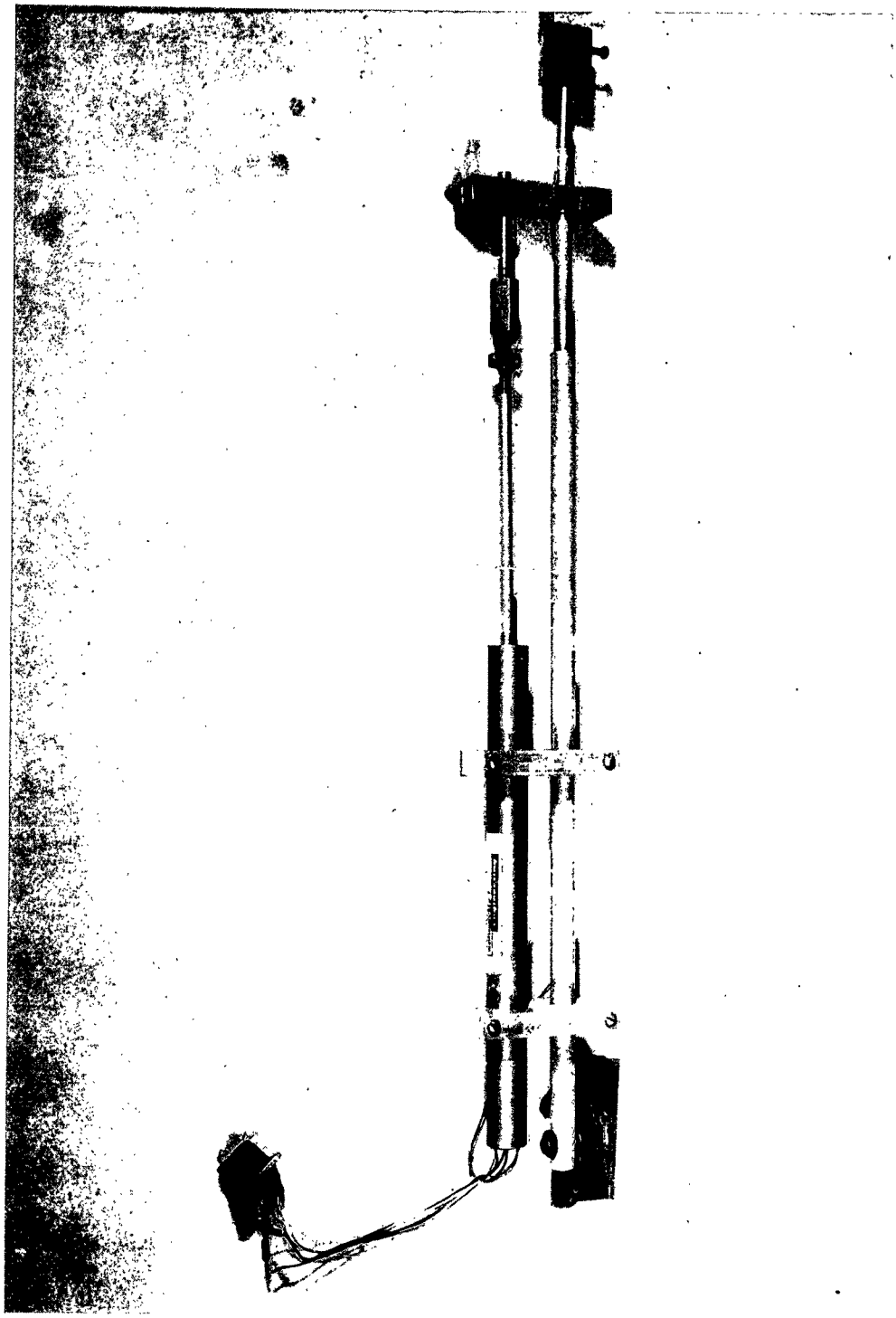

Figure 3.21 - Attachment for L.V.D.T.

CHAPTER 4

EXPERIMENTAL RESULTS

4.1 INTRODUCTION

In this chapter the test results of all specimens are presented in tabular form (Tables 4.1 to 4.6). In these tables values of f'_c, experimental failure load, experimental deflections, and rise time of the failureload in the case of dynamic tests are given. Theoretical failure load and deflections for each specimen, calculated on the basis of conventional theory presented in Section 2.5 of Chapter 2, are also given. It should be noted that the values of the theoretical deflections given in each table are the elastic limit values based on the failure load obtained from the tests. Comparisons between the experimental results and those obtained by the analysis presented in Chapter 2 are made and discussed in Chapter 5.

4.2 SUMMARY OF TEST RESULTS - TYPE I LOADING

4.2.1 General:

The test results of type "A" and type "B" specimens are summarized in Tables 4.1 and 4.2, respectively. As mentioned in Section 3.3 of Chapter 3, the radial distributed load was simulated by ten points loads on the arch specimen. These point loads are converted into equivalent distributed load per inch and these equivalent

values are presented in Tables 4.1 and 4.2. Instead of presenting the measured radial deflections at crown and at 54° points separately, the summation of these measured deflections is presented in Tables 4.1 and 4.2 and compared to the corresponding theoretical values. This was done in order to eliminate unsymmetric behavior of the test specimen, which occured due to unavoidable irregularities in the test specimens and in the loading apparatus. Certain specimens such as A-3, A-9, A-10 etc., or B-3, B-18 etc. are not included in Tables 4.1 and 4.2 because some of these specimens were not tested due to excessive honeycombing in the concrete, while for certain other specimens reliable results were not obtained due to malfunctioning of the loading device or measuring equipment.

4.2.2 Static Tests:

The results of the static tests seem quite satisfactory. The variation in experimental failure loads is well within $\pm$ 15% of the loads predicted by the conventional theory except for specimens B-1 and B-2. In these latter cases the concrete may have had less strength than that indicated by the test cylinders. It is also interesting to note that, except for specimens A-1 and B-10, the experimental failure loads are lower than those predicted by the conventional theory. This is probably due to

secondary bending effects introduced for many reasons. The detailed discussion on the comparison between test results and the theoretical results is deferred until Chapter 5.

The failure of the specimens was mainly by the crushing of concrete at a few points along the arch. In a few cases, the specimen failed by crushing at only one spot, while in other specimens the evidence of failure was distributed. Photographs of typical specimens after failure are shown in Figs. 4.1 and 4.2.

For a few specimens such as A-1, A-2, B-1, etc., reliable deflection measurements were not obtained and therefore these results are not given in Tables 4.1 and 4.2. Load deflection curves of typical specimens are given in Fig. 5.1 (Chapter 5). Comparison between theoretical and experimental failure loads is shown in Fig. 4.3 to indicate the scatter in the test results.

4.2.3 Dynamic Tests:

In the dynamic tests of type "A" arches, specimens A-8 and A-11 were tested by applying only one pulse corresponding to the failure pulse. On specimens A-12, A-13, and A-17, a partial pulse was first applied and measurements obtained. These specimens were then tested under a

failure pulse. On specimen A-19 two partial pulses were applied before applying a failure pulse. It was not possible to apply partial loads to the type "B" specimens because the failure loads are considerably lower and the loading apparatus is not capable of producing partial dynamic pulses sufficiently small.

Type "A" specimens show an average dynamic increase of about 18% in failure load over the theoretical static failure loads. Type "B" specimens show an average increase of about 27% if specimens B-12 and B-13 which show exceptionally large increases are not considered. This percentage increase in the failure loads seems reasonable on the basis of the expected increase in material strength. The increase of about 100% in the failure loads for specimens B-12 and B-13 cannot be fully explained on the basis of the increase of material properties and inertial effects.

The failure in all specimens was mainly by the crushing of concrete simultaneously at a few points along the arch. Photographs of typical specimens after failure are shown in Figs. 4.4 and 4.5.

The load-time curves and deflection-time curves of typical specimens are given in Figs. 5.2, 5.3, 5.4 and 5.5 of Chapter 5, and the load-deflection curve of type "A" specimens is shown in Fig. 5.6 Chapter 5. In this curves the partial and failure loads of each specimen are non-dimensionalized with respect to the theoretical static failure loads. These non-dimensionalized values are plotted against the corresponding experimental deflections values given in Table 4.1. The experimental failure loads are plotted vs. theoretical static loads in Fig. 4.3 to indicate the scatter in test results and the general difference between static and dynamic results.

4.3 SUMMARY OF TEST RESULTS - TYPE II LOADING

4.3.1 General:

The test results for type "A" and type "B" specimens are summarized in Tables 4.3 and 4.4, respectively.

4.3.2 Static Tests:

The results of the static tests seem quite reasonable. The failure load of B-19 is within 2% of the failure load predicted by the conventional theory. While for specimens B-21, A-21, and A-22, the experimental values are higher by 10 to 15%. There are several factors which could have caused the higher experimental values. One

reason could be that the supports may not behave like perfect hinges and may introduce some restraint, which would tend to increase the experimental failure load. Secondly, the yield stress f_y in the steel is taken at 40 ksi, while predicting the conventional theoretical loads. The stress-strain curve of the steel (See Figs. 3.5 and 3.6) is not exactly bi-linear but follows a flat curve after 40 ksi. It is obvious that the strain in the steel at failure in both "A" and "B" specimens is much greater than the yield strain at 40 ksi, which suggests that at failure the stress could be higher than 40 ksi. Therefore, the experimental failure loads could be higher than that predicted by conventional theory using f_y = 40 ksi.

The failure of the specimens occured by the formation of three hinges, one at the crown and the other two in the vicinity of the quarter points. The locations of these latter hinges almost coincided with the theoretical prediction of hinge formation at points 38° from the supports. Photographs of typical specimens after failure are shown in Figs. 4.6 and 4.7.

The failure of the specimens seemed quite ductile. The maximum radial deflection at the crown was of the order of 0.45" for type "A" and 0.85" for type "B" specimens.

The load-deflection curves of typical specimens are given in Fig. 5.7 and 5.8 Chapter 5. To represent the scatter in test results the experimental failure loads are plotted against conventional theoretical loads in Fig. 4.8.

4.3.3 Dynamic Tests:

All specimens were tested for failure only. Because the failure loads were extremely small, no attempt was made to apply partial loads.

Type "A" specimens show an average dynamic increase of about 55% in the failure loads over conventional theoretical static failure loads. For Type "B" specimens the increase is of the order of 70%. Part of this rather large dynamic increase can be attributed to the larger than expected static strength as discussed in the preceeding section. The remaining increase is due to the increase in material properties due to very rapid strain rates and to inertial effects. On this basis, the test results seem quite reasonable.

The failure of the specimens was similar to that observed in static tests as described in Section 4.3.2. Photographs of typical specimens after failure are shown in Figs. 4.9 and 4.10.

The failure of the specimens seemed quite ductile. The maximum radial deflection at the crown was about 0.5" for type A and about 0.9 for type B specimens.

The load-time and deflection-time curves of typical specimens are shown in Figs. 5.9 and 5.10 Chapter 5. The scatter in test results is indicated by Fig. 4.8.

4.4 SUMMARY OF TEST RESULTS - TYPE III LOADING

4.4.1 General:

The test results for type A and type B specimens are summarized in Tables 4.5 and 4.6, respectively. The results for specimen B-28 are not given in Table 4.6, because no reliable results were obtained.

The deflection data in Tables 4.5 and 4.6, clearly indicate that the strain in the steel wires at failure must have been considerably higher than the strain corresponding to a stress of 40 ksi, at which yielding begins. Therefore, as explained in Section 4.3.2, it seems reasonable to assume a higher value of f_y while

calculating the failure load based on conventional theory. A value of 46 ksi is used in the calculation of these conventional theoretical failure loads.

4.4.2 Static Tests:

The results of the static tests of type "A" specimens seem quite reasonable. Experimental failure loads on an average are about 9% higher than the conventional theoretical failure loads, except specimen A-33, for which the failure load is lower by about 9%. The latter specimen was actually loaded twice. The first run was terminated after about 60% of the failure load had been applied, due to difficulties in the loading device. It was then loaded to failure. The preloading could have damaged the specimen and caused failure under a lower load. The increase in the failure load of all other specimens over the conventional theoretical load seems partly due to the restraint at the support as explained in Section 4.3.2 and partly due to the effect of the weight of the loading jacks on the test specimen as explained below.

It is clear from Fig. 3.13 that about half the weight of the jack is applied to the arch at the loading points. Theoretical considerations indicate that if the top jack was "pulling" the arch and the bottom jack "pushing"

(see Fig. 3.13), the failure load increases by the same amount as the applied weight of the jack. On the other hand, with the top jack "pushing" and the bottom jack "pulling", the failure load decreases by the same amount.

This effect is more severe in the case of type B specimens because the failure loads are only six to seven times the applied weight of the jack (which is about 10 lbs) as compared to 40 times the applied weight in the case of type A specimens. In order to eliminate this effect, specimens B-26 and B-27 were tested with the top jack "pulling" and the bottom jack "pushing", while the reverse was done for B-29 and B-30. Table 4.6 indicates that the average of the failure loads of B-26 and B-27 is 91 lbs. and of B-29 and B-30 is 52 lbs. Therefore, an average of these two values or about 71 lbs. should be considered as the experimental failure load. The average conventional theoretical load for these specimens is about 60 lbs., and the eleven-pound increase in the experimental load can easily be due to the various factors mentioned previously, or small errors in measurement. The test results are therefore considered quite reasonable.

The failure of the specimens occurred by the formation of hinges very nearly at the quarter points. Photo-

graphs of typical specimens after failure are shown in Figs. 4.11 and 4.12. The failures were quite ductile with maximum radial deflection at the quarter points of the order of 1.5" for type A specimens and about 2" for type B specimens.

The load deflection curves of typical specimens are given in Figs. 5.11, 5.12 and 5.13, Chapter 5. The experimental failure loads are plotted against conventional theoretical loads in Fig. 4.13 to indicate the scatter in experimental results.

4.4.3 Dynamic Tests:

All specimens were tested for failure only. No attempt was made to apply partial loads for the reasons already mentioned.

Type A specimens show an average increase of about 8% in failure loads over the conventional theoretical static failure loads. Out of this about 10% is probably due to partial support restraint and the effect of the weight of jacks on the failure loads, as already explained in previous sections. The remaining increase is attributed to the increase in the material properties due to rapid strain rates and inertial effects. This is discussed in more detail in the next chapter.

Dynamic tests on type B specimens were performed with the top jack "pulling" and the bottom jack "pushing". No tests were performed in the reverse condition as was done in static tests. Therefore, the results of dynamic tests of these specimens should be compared with the corresponding results of the static tests, i.e., the results for specimen B-26 and B-27. This type of comparison shows an average increase of 180% in dynamic failure loads. This increase seems to be due to the increase in the material properties under very rapid strain rates and inertial effects. This aspect is discussed further in the next chapter.

The failure of the specimen occurred by the formation of hinges very nearly at the quarter points, as in the static tests. Photographs of typical specimens after failure are shown in Figs. 4.14 and 4.15. The failure of the specimen was quite ductile. The maximum radial deflection at quarter points is about 1.25" for type A and 1.7" for type B specimens.

The load-time and deflection-time curves for typical specimens are shown in Fig. 5.14 and 5.15 in Chapter 5. To indicate the scatter of experimental results, experimental failure loads are plotted against theoretical static failure loads in Fig. 4.13.

TABLE 4.1

SUMMARY OF TYPE "A" SPECIMENS - TYPE I LOADING

Type of Test	Specimen No.	Type of Pulse	f'_o (psi)	$p_{u_{EXP}}$ (lbs/in)	$p_{u_{TH_{ST}}}$ (lbs/in)	$\frac{p_{u_{EXP}}}{p_{u_{TH_{ST}}}}$	t_r (milli-seconds)	Σw_m (inch)	$\Sigma w_{m_{TH}}$ (inch)	$\mu_{EXP} = \frac{\Sigma wm}{\Sigma wm_{TH}}$
STATIC	A-1		4300	1215	1030	1.18				
	A-2		3460	765	875	0.875				
	A-4		4010	970	980	0.99		0.086	0.077	1.12
	A-5		3800	920	930	0.99		0.135	0.076	1.78
DYNAMIC	A-8	Failure Pulse	4160	1130	1005	1.13	8	0.235	0.088	2.67
	A-11	Failure Pulse	3500	1010	880	1.15	10	0.253	0.085	2.98
	A-12	Partial Pulse I	3400	415*			15	0.076°		
		Failure Pulse		1108	860	1.29	11	0.213	0.095	2.24
	A-13	Partial Pulse I	3160	478*			12	0.174°		
		Failure Pulse		980	815	1.20	10	0.290	0.086	3.38
	A-17	Partial Pulse I	3440	700*			19	0.130°		
		Failure Pulse		920	870	1.06	11	0.176	0.078	2.26
	A-19	Partial Pulse I	2640	565*			16	0.153°		
		Pulse II		735*			20	0.182°		
		Failure Pulse		880	715	1.23	11	0.118 x	0.061 x	1.94

* These are loads representing flat peak of the partial pulse.

x This is the summation of radial deflection at crown and at one 54° point

° These are the summations of max. deflection at crown and at 54° points, at load corresponding to the flat peak at partial pulse.

$p_{u_{EXP}}$ - Experimental failure load.

$p_{u_{TH_{ST}}}$ - Theoretical static failure load.

Σw_m - Summation of maximum experimental radial deflections at crown and at two 54° points.

$\Sigma w_{m_{TH}}$ - Summation of theoretical elastic radial deflection at crown and at two 54° points, at experimental failure load.

t_r - Rise time of the load.

TABLE 4.2[x]

SUMMARY OF TYPE "B" SPECIMENS - TYPE I LOADING

Type of Test	Specimen No.	Type of Pulse	f'_c (psi)	$p_{u_{EXP}}$ (lbs/in)	$p_{u_{TH_{ST}}}$ (lbs/in)	$\frac{p_{u_{EXP}}}{p_{u_{TH_{ST}}}}$	t_r (milliseconds)	Σw_m (inch)	$\Sigma w_{m_{TH}}$ (inch)	$\mu_{EXP} = \frac{\Sigma w_m}{\Sigma w_{m_{TH}}}$
STATIC	B-1		3700	304	405	0.75				
	B-2		3880	286	420	0.68				
	B-10		3010	443	380	1.15				
	B-11		3280	350	385	0.91				
	B-15		3150	330	375	0.88		0.085	0.062	1.37
	B-16		3790	380	430	0.89		0.043*	0.040*	1.08
DYNAMIC	B-4	Failure Pulse	3800	473	412	1.15	9	0.234	0.081	2.88
	B-12	"	2590	645	322	2.0	10	0.144	0.128	1.13
	B-13	"	2630	640	324	1.98	11	0.163	0.129	1.26
	B-14	"	3720	480	428	1.12	11	0.200	0.083	2.41
	B-17	"	3420	530	400	1.33	17	0.184	0.095	1.94
	B-20	"	3740	648	429	1.50	30	0.160	0.111	1.45

*This is the summation of radial deflections at two 54° points only.

[x]Notations used in this table are same as in Table 4.1.

TABLE 4.3

SUMMARY OF TYPE "A" SPECIMENS - TYPE II LOADING

Type of Test	Specimen No.	f'_c (psi)	$P_{u_{EXP}}$ (lbs)	$P_{u_{TH_{ST}}}$ (lbs)	$\frac{P_{u_{EXP}}}{P_{u_{TH_{ST}}}}$	t_r (milli-seconds)	w_{mc} (inch)	w_{mq} (inch)	$w_{mc_{TH}}$ (inch)	$\mu_{EXP} = \frac{w_{mc}}{w_{mc_{TH}}}$
STATIC	A-21	3050	1470	1335	1.10		0.443	0.047*	0.057	7.78
	A-22	4000	1630	1415	1.15		0.480	0.075*	0.056	8.60
DYNAMIC	A-24	3900	2165	1407	1.54	43	0.559	0.125*	0.076	7.36
	A-25	3050	2200	1335	1.65	48	0.518	0.085	0.085	6.08
	A-26	3300	1940	1355	1.46	26	0.474	0.200	0.073	6.50

* This is the average of the deflections at points 2.3" away from the quarter points, towards crown.

$P_{u_{EXP}}$ - Experimental failure load.

$P_{u_{TH_{ST}}}$ - Theoretical static failure load.

w_{mq} - Average of the experimental radial deflections at failure, at two quarter points.

w_{mc} - Maximum experimental radial deflection at crown.

$w_{m_{TH}}$ - Theoretical elastic radial deflection at crown, at experimental failure load.

t_r - Rise time of the load

TABLE 4.4*

SUMMARY OF TYPE "B" SPECIMENS - TYPE II LOADING

Type of Test	Specimen No.	f'_c (psi)	$P_{u_{EXP}}$ (lbs)	$P_{u_{TH_{ST}}}$ (lbs)	$\frac{P_{u_{EXP}}}{P_{u_{TH_{ST}}}}$	t_r (milli-seconds)	w_{mc}	w_{mq}	$w_{mc_{TH}}$	$\mu_{EXP} = \frac{w_{mc}}{w_{mc_{TH}}}$
STATIC	B-19	3680	242	237	1.02		0.775	0.350	0.076	10.2
	B-21	3820	277	238	1.16		0.999	0.267	0.085	10.6
DYNAMIC	B-22	3750	386	238	1.62	18	0.950	0.265	0.120	7.90
	B-23	3830	455	238	1.90	18	0.772	0.164	0.130	5.95
	B-24	3860	420	238	1.77	18	0.900	0.383	0.130	6.95
	B-25	2920	363	231	1.57	16	1.00	0.475	0.126	7.95

*Notations used in this table are same as in Table 4.3.

TABLE 4.5

SUMMARY OF TYPE "A" SPECIMENS - TYPE III LOADING

Type of Test	Specimen No.	f'_c (psi)	$P_{u_{EXP}}$ (lbs)	$P_{u_{TH_{ST}}}$ (lbs)	$\frac{P_{u_{EXP}}}{P_{u_{TH_{ST}}}}$	t_r (milli-seconds)	w_{qm} (inch)	$w_{qm_{TH}}$ (inch)	$\mu = \frac{w_{qm}}{w_{qm_{TH}}}$
	A-27	3560	384	348	1.10		1.30	0.096	13.5
S	A-28	4020	394	355	1.11		1.60	0.093	17.2
T	A-29	4100	413	356	1.16		1.86	0.097	19.2
A	A-30	4280	360	359	1.00		1.69	0.082	20.6
T	A-31	4020	381	355	1.07		1.90	0.090	21.1
I	A-32	4270	397	359	1.11		1.64	0.091	18.0
C	A-33	3820	318	352	0.91		1.55	0.077	20.2
	A-34	4200	396	358	1.11		1.68	0.092	18.3
D									
Y	A-35	2750	608	336	1.81	16	1.34	0.168	8.0
N									
A	A-36	2750	650	336	1.93	16	1.24	0.180	6.9
M									
I	A-37	2680	630	335	1.88	16	1.14	0.176	6.5
C									

$P_{u_{EXP}}$ - Average of the experimental failure loads at two quarter points.

$P_{u_{TH_{ST}}}$ - Theoretical static failure load.

w_{qm} - Average of the maximum experimental radial deflections at two quarter points.

$w_{qm_{TH}}$ - Theoretical elastic radial deflection at quarter point at experimental failure load.

t_r - Rise time of the failure load.

TABLE 4.6*

SUMMARY OF TYPE "B" SPECIMEN - TYPE III LOADING

Type of Test	Specimen No.	f'_c (psi)	$P_{u_{EXP}}$ (lbs)	$P_{u_{TH_{ST}}}$ (lbs)	$\frac{P_{u_{EXP}}}{P_{u_{TH_{ST}}}}$	t_r (milli-seconds)	w_{qm} (inch)	$w_{qm_{TH}}$ (inch)	$\mu = \frac{w_{qm}}{w_{qm_{TH}}}$
STATIC	B-26	4030	93	62	1.50		2.00	0.184	10.9
	B-27	3700	90	60	1.50		2.00	0.164	12.2
	B-29	3920	50	62	0.81			0.104	
	B-30	3460	55	59	0.93		2.20	0.122	18.0
DYNAMIC	B-31	3600	251	60	4.21	20	2.00	0.544	3.68
	B-32	3800	265	61	4.35	20	1.60	0.562	2.85
	B-33	3820	255	61	4.20	16	1.48	0.540	2.74

*Notations used in this table are the same as in Table 4.5.

4.5 NATURAL PERIOD OF ARCH SPECIMENS

The natural periods of the arch for the first bending or antisymmetric mode and the second bending mode (i.e., the mode corresponding to the configuration of the arch, under a point load at the crown) were experimentally determined for one specimen of each type. These values are given in Table 4.7. The natural period for the compression mode* was not determined experimentally.

TABLE 4.7

NATURAL PERIODS

Mode	Natural Period (Milliseconds)	
	Type A Specimen	Type B Specimen
First bending mode	25	59
Second bending mode	6	12

*The natural period in the compression mode is approximately given by r/1800 (see Ref. No. 13 in bibliography, p. 5B-15). Therefore the natural period for both types in the compression mode is about 0.83 milliseconds. In the above formula "r" is the radius in feet.

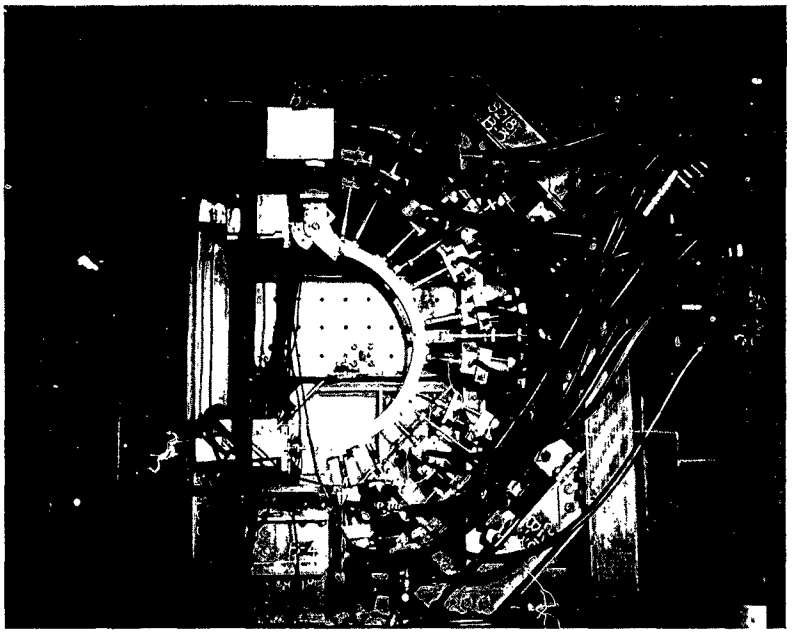

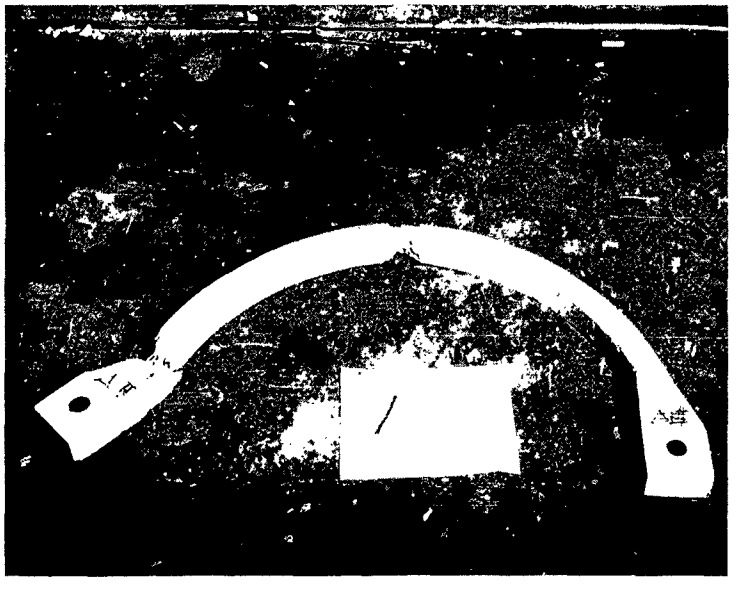

Figure 4.1 - Appearance of Specimen A-4 after Test - (Static Test - Type I Loading).

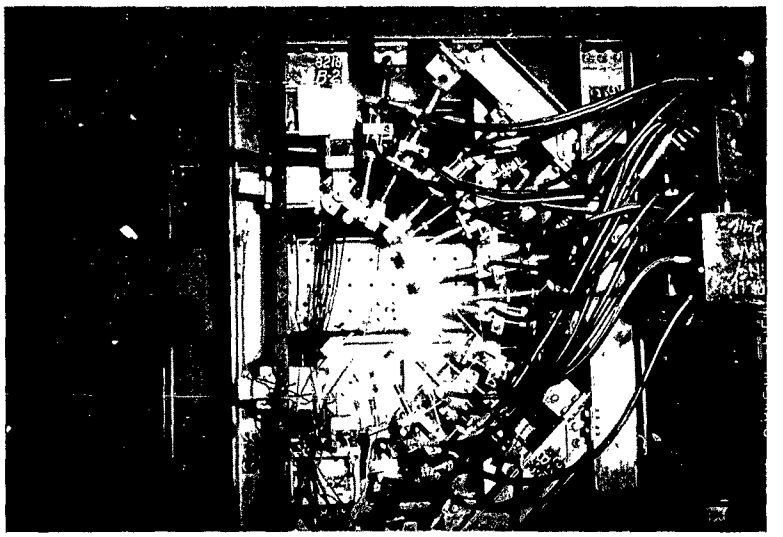

Figure 4.2 - Appearance of Specimen B-10 after Test - (Static Test - Type I Loading).

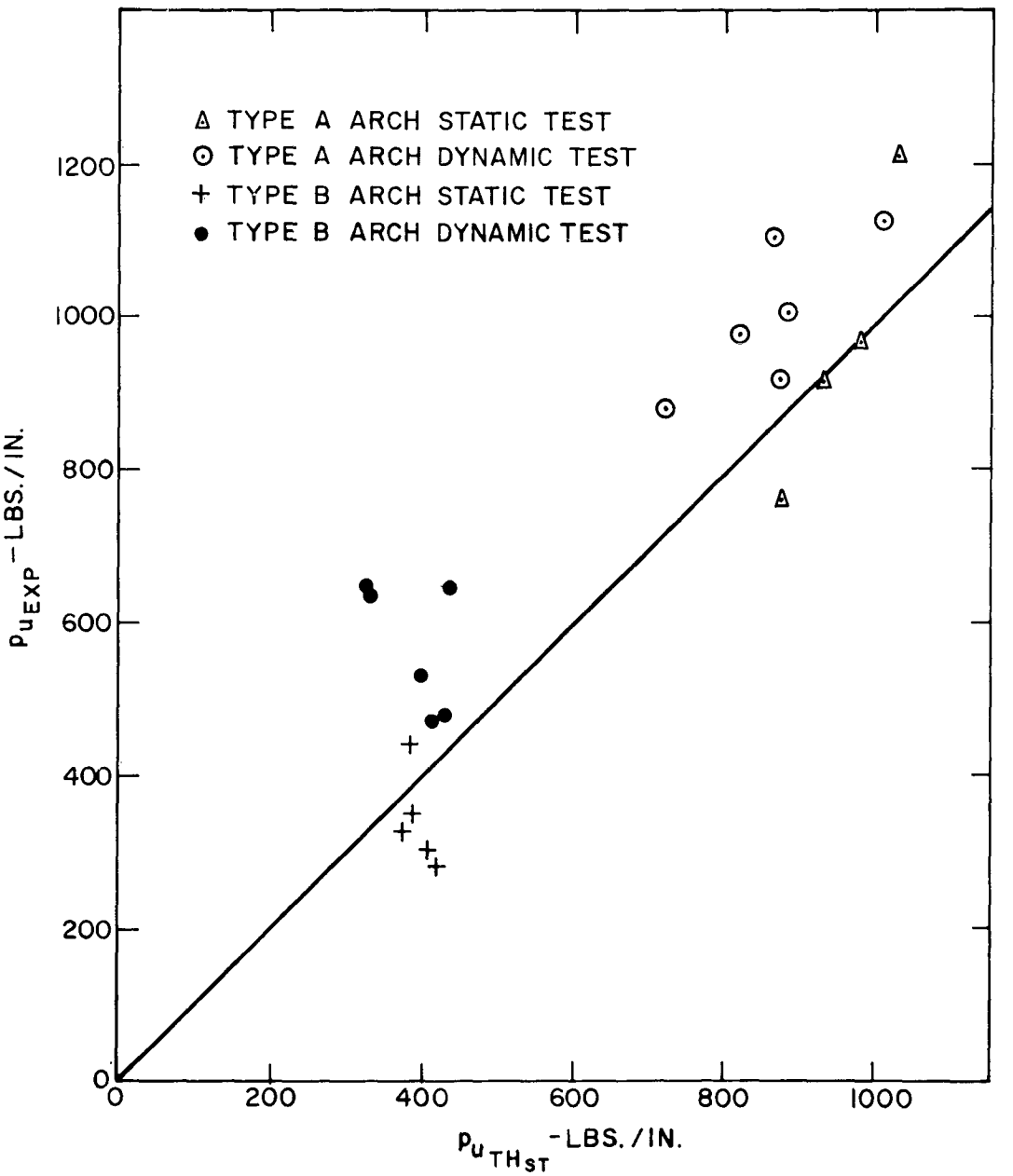

FIGURE 4.3 - $p_{u_{EXP}}$ VS $p_{u_{THST}}$ - TYPE I LOADING

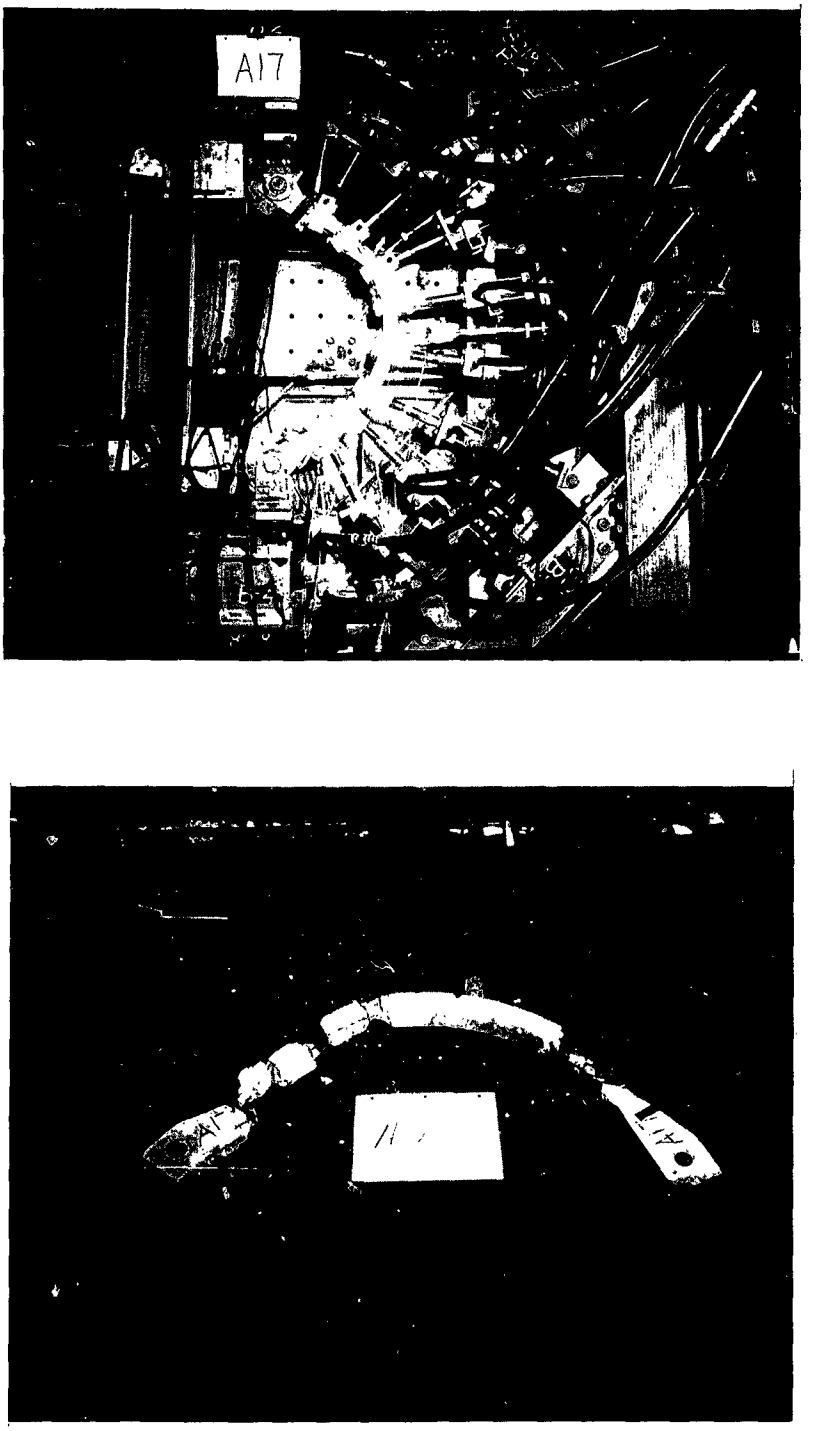

Figure 4.4 - Appearance of Specimen A-17 after Test - (Dynamic Test - Type I Loading).

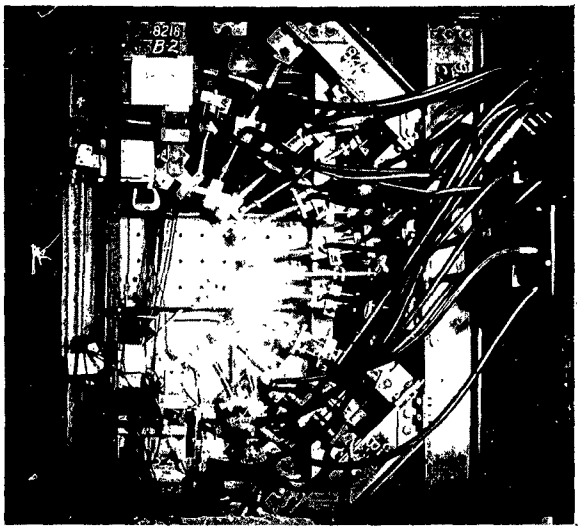

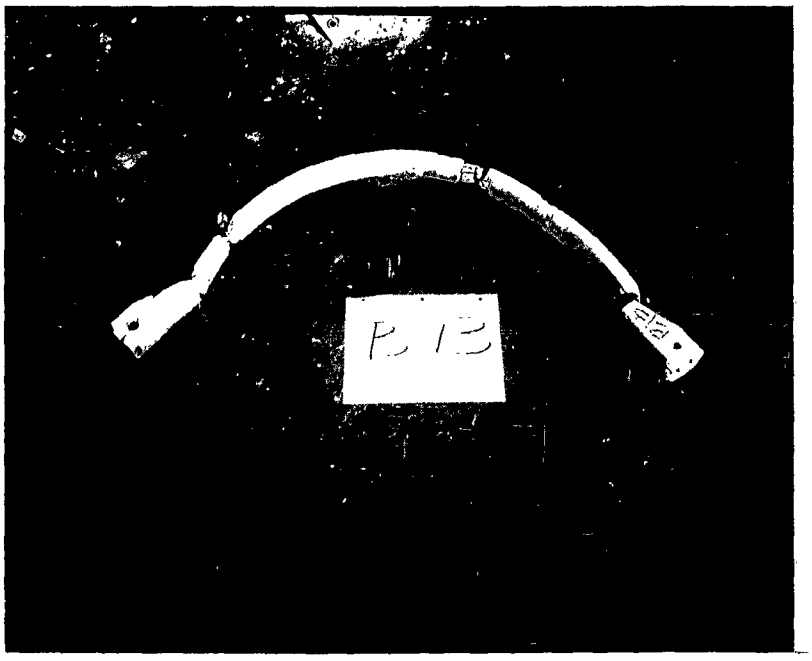

Figure 4.5 - Appearance of Specimen B-13 after Test - (Dynamic Test - Type I Loading).

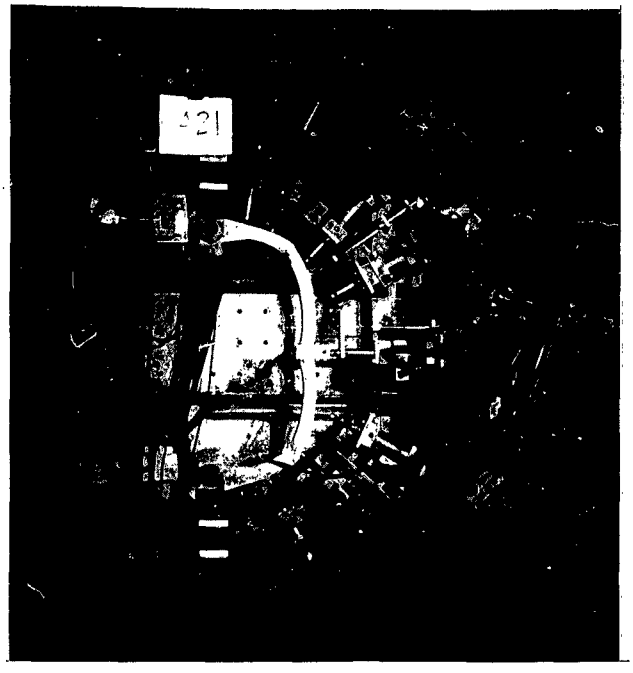

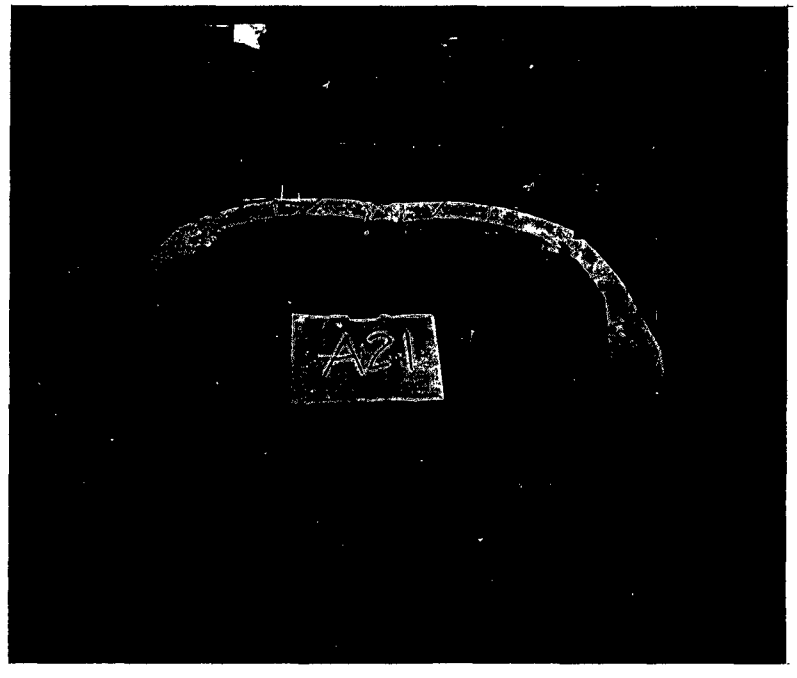

Figure 4.6 - Appearance of Specimen A-21 after Test - (Static Test - Type II Loading).

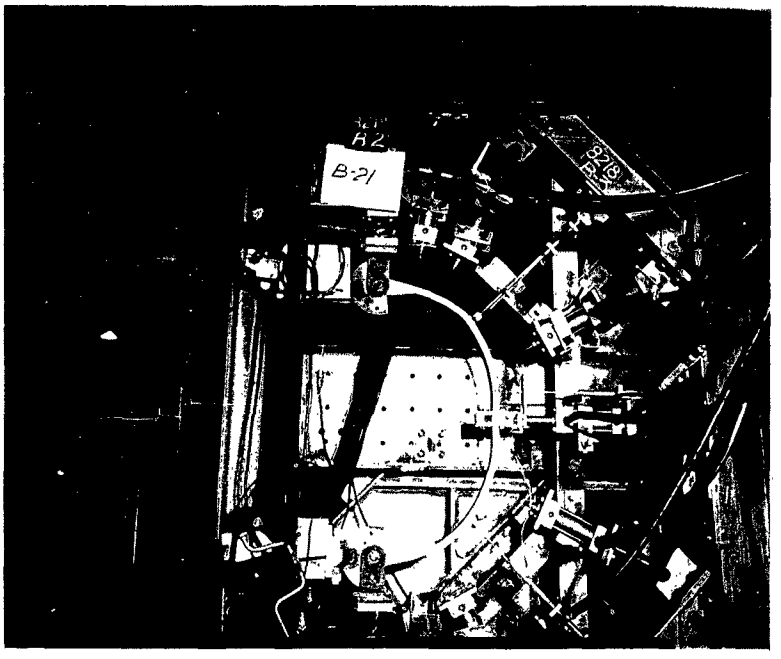

Figure 4.7 - Appearance of Specimen B-21 after Test - (Static Test - Type II Loading).

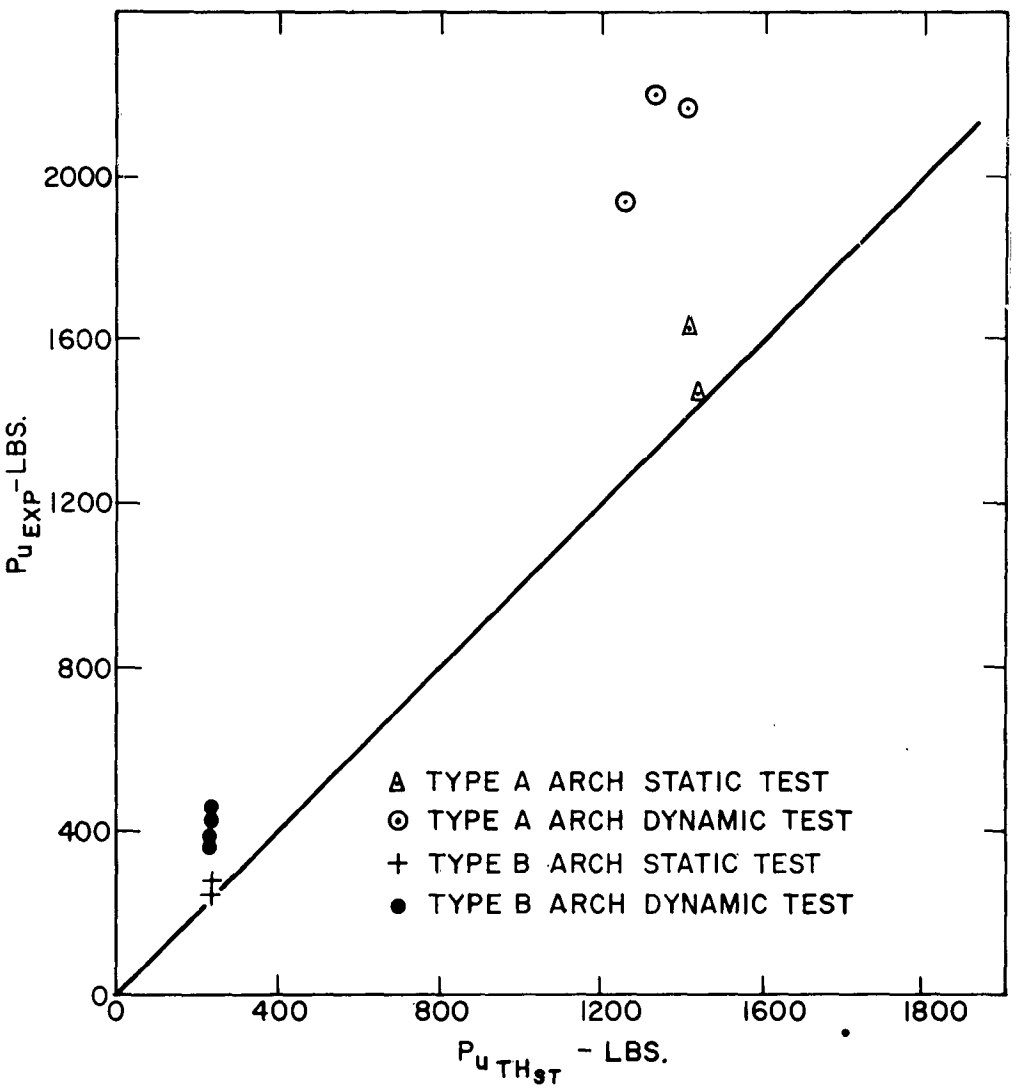

FIGURE 4.8- $P_{u_{EXP}}$ VS. $P_{u_{TH_{ST}}}$ - TYPE II LOADING

Figure 4.9 - Appearance of Specimen A-25 after Test - (Dynamic Test - Type II Loading).

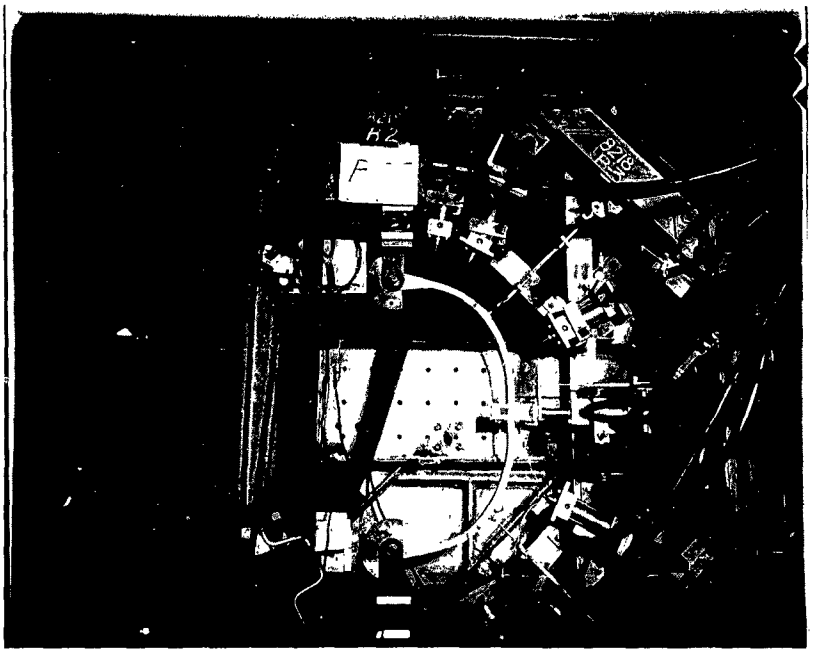

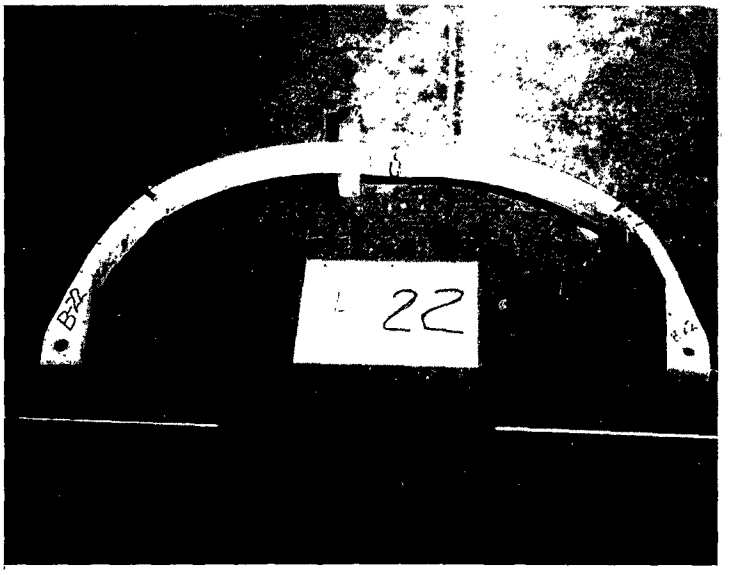

Figure 4.10 - Appearance of Specimen B-22 after Test - (Dynamic Test - Type II Loading).

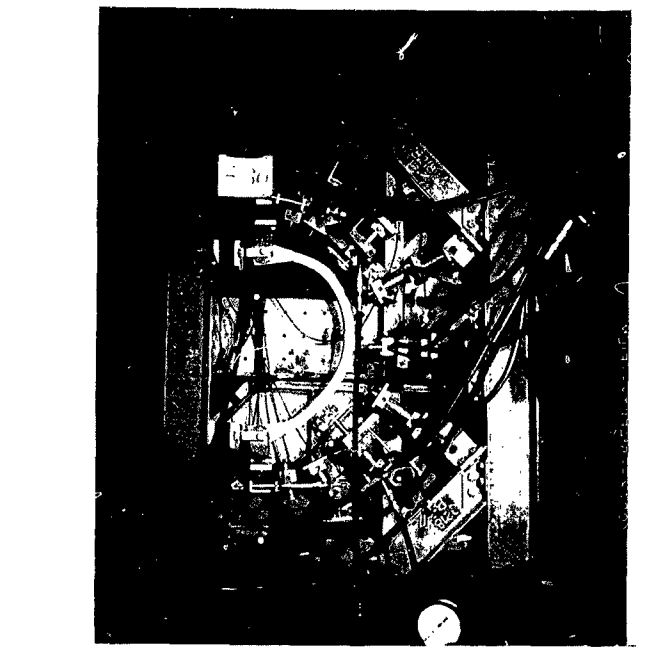

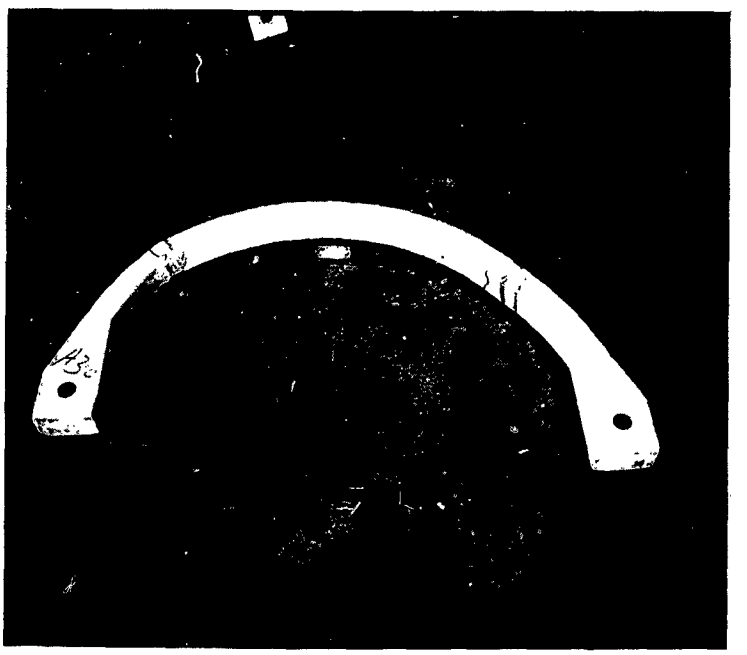

Figure 4.11 - Appearance of Specimen A-30 after Test - (Static Test - Type III Loading).

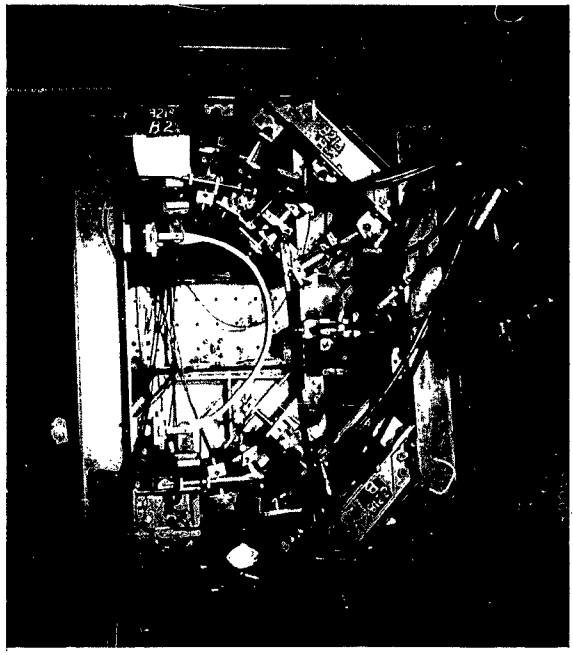

Figure 4.12 - Appearance of Specimen B-26 after Test - (Static Test - Type III Loading)

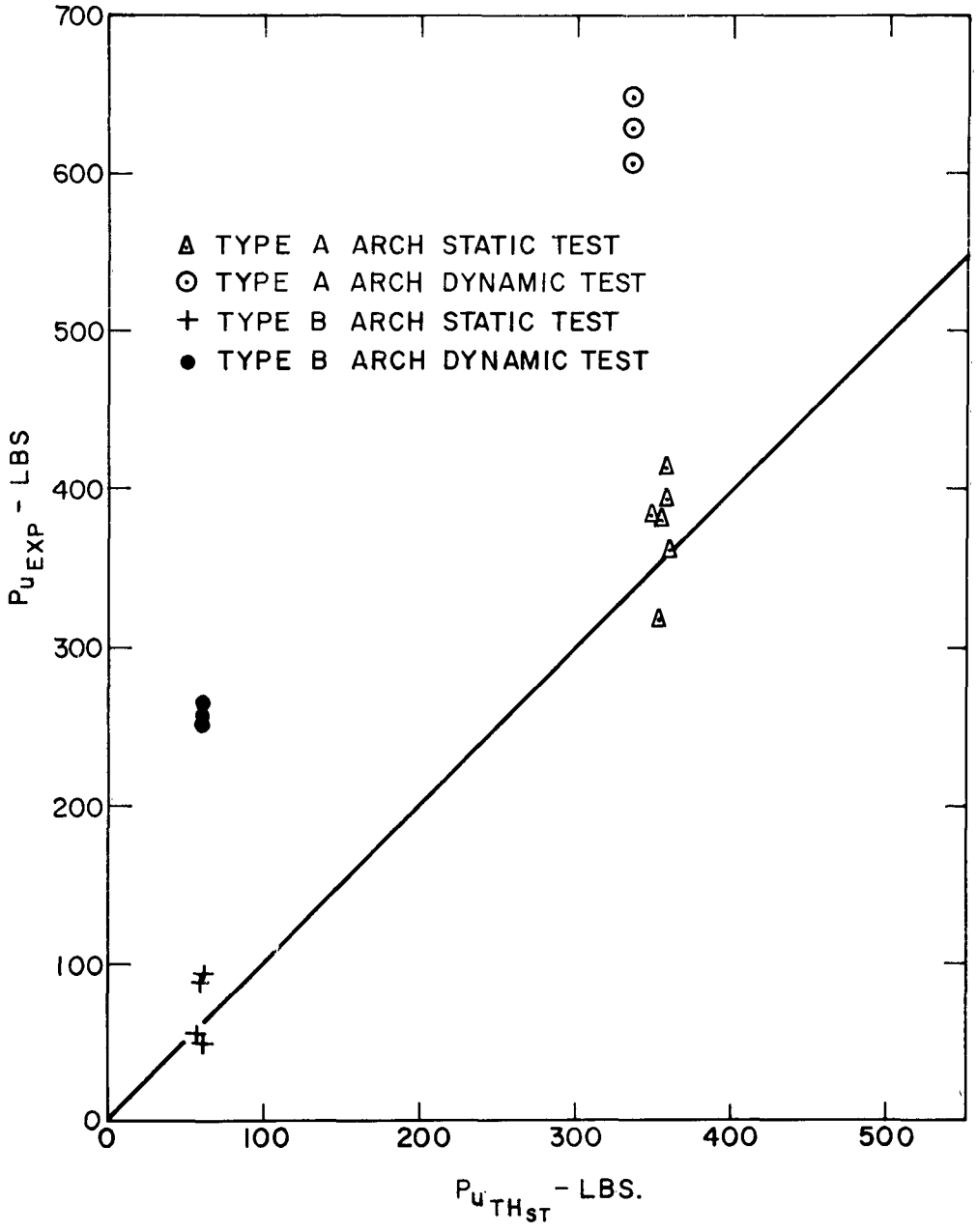

FIGURE 4.13 - $P_{u_{EXP}}$ VS $P_{u_{THST}}$ - TYPE III LOADING

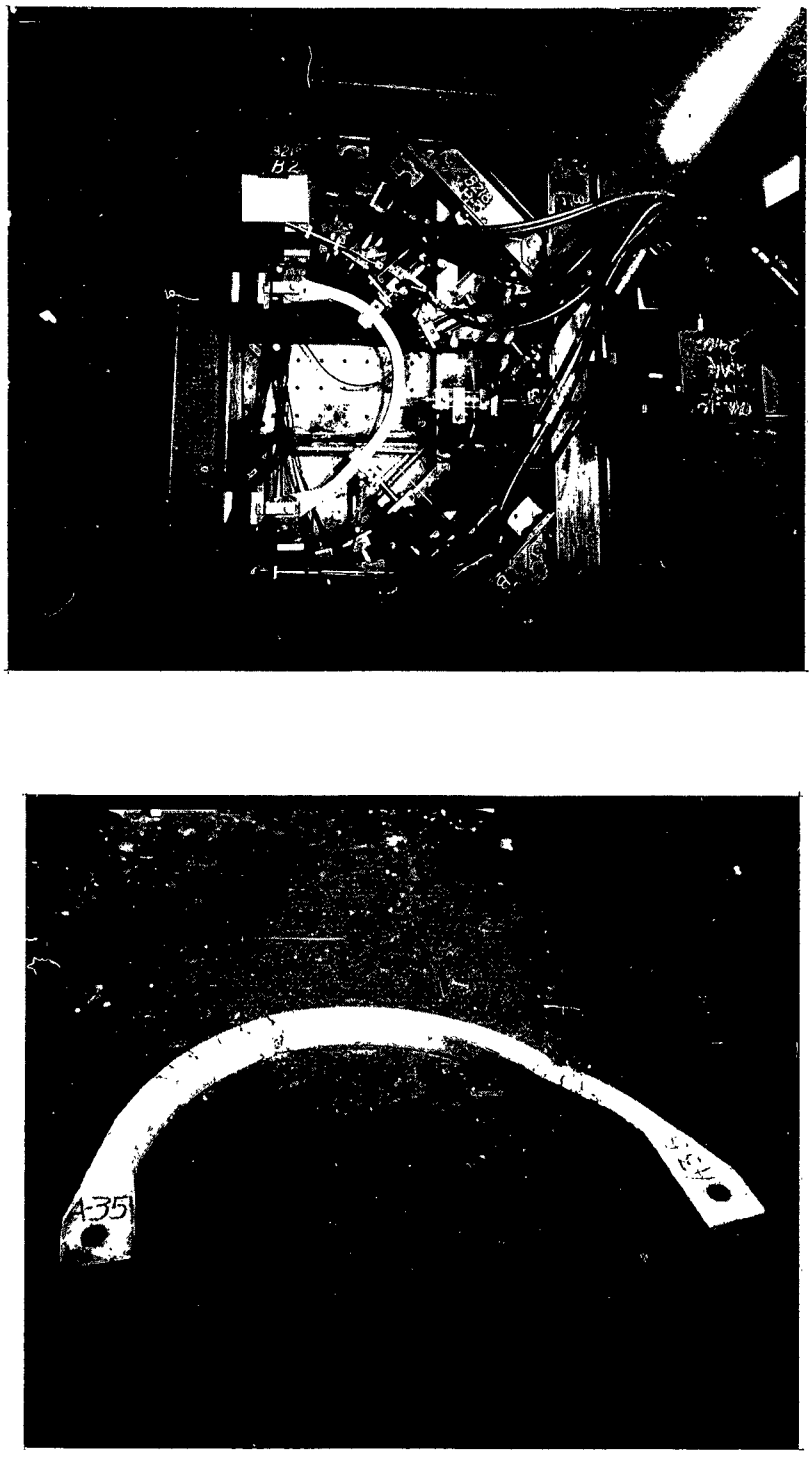

Figure 4.14 - Appearance of Specimen A-35 after Test - (Dynamic Test - Type III Loading).

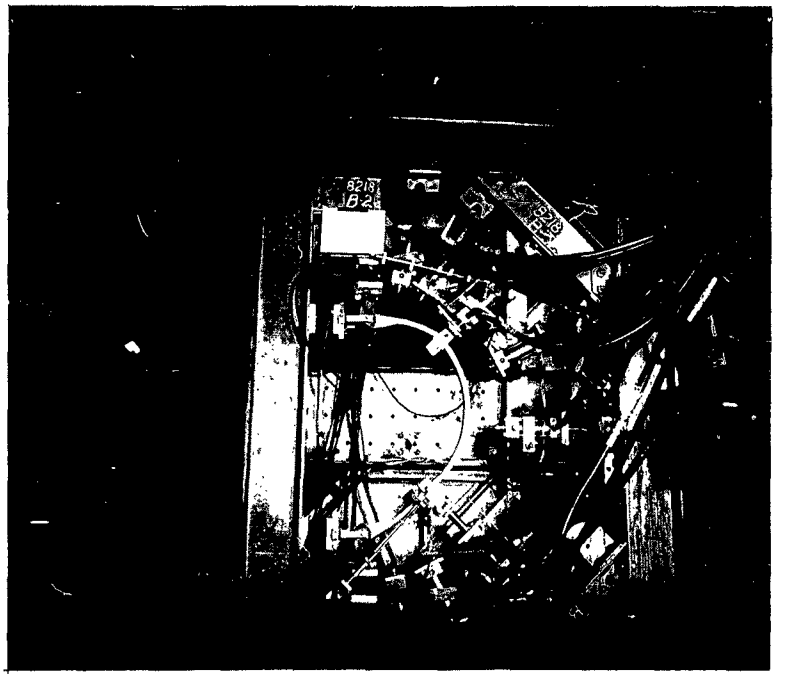

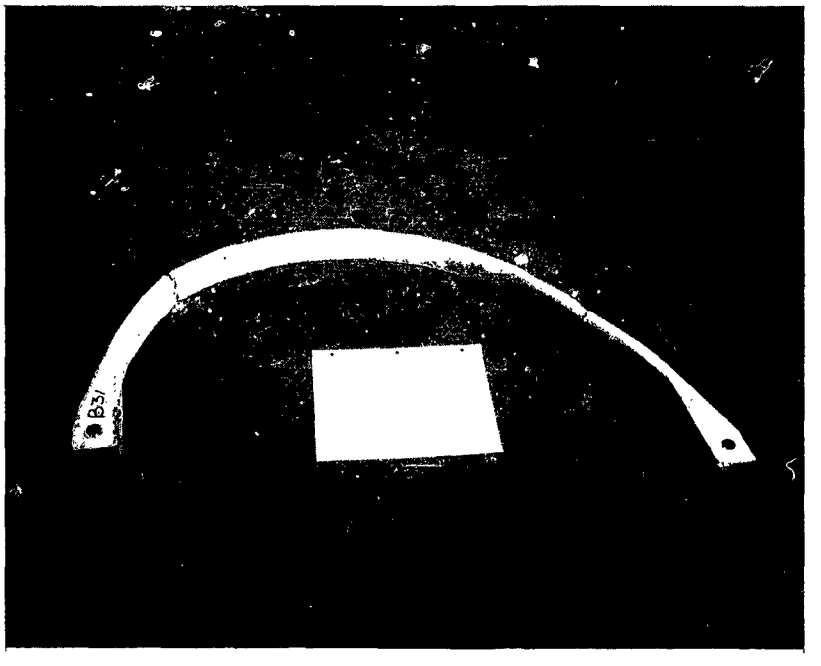

Figure 4.15 - Appearance of Specimen B-31 after Test - (Dynamic Test - Type III Loading).

CHAPTER 5

COMPARISON OF THEORETICAL AND EXPERIMENTAL RESULTS

5.1 INTRODUCTION

For the purpose of comparison, certain experimental specimens of both type A and type B are analysed theoretically. The nonlinear theory developed in § 2.1 through § 2.4 is used to obtain the static and dynamic response, ultimate loads and μ's for type I and type III loading. The average dynamic strain rate $\dot{e}_{dc}$ necessary to obtain the dynamic properties of concrete (equation 2.2b) is calculated as $e_{dc} = e_u/t_r$. These ultimate loads and μ's are called analytical results. The elastic limit deflections needed to calculate the μ's are obtained by using the formulae presented in § 2.5. Further, a set of static ultimate loads for all three types of loading is also obtained from the conventional theory presented in § 2.5. The ultimate loads calculated in this way are referred to as "theoretical ultimate loads".

5.2 THEORETICAL AND EXPERIMENTAL RESULTS AND THEIR COMPARISON.

5.2.1 Type I Loading:

A summary of the experimental and analytical values of the ultimate loads and μ's for certain specimens of type A and type B is given in tables 5.1a and 5.1b

respectively. Also listed in the tables are the theoretical static ultimate loads.

(a) Static Behavior:

Tables 5.1a and 5.1b clearly show that the analytical values of the ultimate loads agree within ten percent with the experimental values for specimens A-2, A-4, A-5, B-11, B-15, and B-16. However, the experimental ultimate loads for specimens B-1 and B-2 are much lower and those for A-1 and B-10 are higher than the analytical values. This may be due to a possible difference between the strength of concrete in the test specimens and that indicated by the test cylinders.

The comparison between the theoretical and experimental ultimate loads has already been made in 4.2.2. However, attention is drawn here to the fact that the experimental failure loads are in practically all cases lower than the theoretical failure loads. This seems to be due to the presence of secondary bending effects which are not considered in the theoretical calculations. The secondary bending effects occur for such reasons as: (1) the shape of the arch does not confirm to the funicular polygon of the compression mode loading; (2) in the tests, the uniformly distributed load is simulated by ten equally spaced point loads; (3) These ten point loads, applied on the test specimen may not be

exactly equal, due to the limitations of the loading apparatus; (4) the arch cross-section may not be exactly uniform along the length.

A comparison between the analytical and theoretical values shows that both agree within ten percent for most of the specimens. The analytical values are, however, consistently lower in all cases; the reason being that the secondary bending effects are not considered in calculating theoretical loads.

Table 5.1 (a) and 5.1 (b) also indicate that except for specimen A-5, the experimental μ - values are lower than the analytical μ - values.

Fig. 5.1 shows the analytical and experimental load-deflection curves for specimen A-5, selected for illustration, to be in fair agreement.

(b) Dynamic Behavior:

It is seen from tables 5.1a and 5.1b that the analytical values of dynamic ultimate load agree within about fifteen percent with the experimental values for all specimens except specimens B-12 and B-20. The high experimental ultimate loads for these specimens may be in part due to an increase in material strength under rapid strain rate, higher than that considered in the analytical approach.

The analytical and experimental μ-values lie within a range of 1.5 to 2.5.

Figures 5.2 5.3 and 5.5 show analytical and experimental load-time and deflection-time curves for specimens A-11, A-17 and B-14. These curves represent a failure load pulse. Specimen A-17 was also tested under partial load pulse and the load-time and deflection-time curves for this partial load pulse are shown in figure 5.4. All the curves show a fair agreement between the analytical and experimental results. Figure 5.6 shows the analytical and experimental dynamic load-deflection curve for type A specimens. The points on the experimental curve are obtained from a number of tests by nondimensionalizing the dynamic load with respect to the corresponding theoretical static ultimate load of each test. The analytical curve pertains to specimen A-17.

(c) Comparison Between Dynamic and Static Behavior:

Table 5.3 shows the experimental and analytical values of the dynamic increase factors (DIF) for both type A and type B specimens. The dynamic increase factor is obtained as a ratio of the average nondimensional dynamic load to the nondimensional static load; the average being obtained from the values given in tables 5.1a and 5.1b. The values of experimental ultimate loads of specimens B-12 and B-13 are not considered in obtaining the average non-dimensional dynamic load because these values seem

unreasonably high. The experimental and analytical dynamic increase factors vary between 1.2 and 1.4. This increase is mainly due to the increase in the properties of materials at very rapid strain rates.

5.2.2 Type II Loading

No comparison between the experimental and analytical results under this type of loading is possible because the non-linear theory cannot be used to predict the ultimate loads for the reasons explained in § 2.1.3. A comparison between the experimental and theoretical failure loads is already made and reasons for the differences in the values, if any, are explained in § 4.3.2. Therefore, in what follows, only a comparison between the experimental static and dynamic behavior is made.

In table 5.4, the values of static and dynamic ultimate loads for the type A and type B arches are given. These are the average values of those given in tables 4.3 and 4.4 for type A and type B specimens respectively. It is reasonable to take such an average, even though the value of f'_c varies, for each specimen in the tests, because the influence of f'_c on the ultimate loads of such underreinforced elements, where the bending moment is predominant compared to the axial thrust, is insignificant. Table 5.4 shows that the dynamic increase

is of the order of 36% for type A arch and about 57% for type B arch. This increase seems to be partly due to the increase in the material properties under very rapid strain rates and partly due to inertial effects.

The load-deflection curves for specimens A-21 and B-21 (static tests) are shown in Figures 5.7 and 5.8, while Figures 5.9 and 5.10 show the load-time and deflection time curves for specimens A-24 and B-24 (dynamic tests).

5.2.3 Type III Loading

The experimental values of the static and dynamic ultimate loads and μ's for type A and type B arches are given in table 5.2. The values of the theoretical static ultimate loads are shown in table 5.2. These values are the averages of those presented in tables 4.5 and 4.6. The analytical values of the static ultimate loads and μ's given in table 5.2 are those obtained for specimens A-34 and B-26, while the corresponding values for dynamic tests are for specimens A-37 and B-32. The analytical values are calculated by taking f_y = 46 ksi, for the reasons explained in article 4.4.1. A comparison between these analytical values and the average experimental values is reasonable, for reasons already mentioned in the previous section.

(a) Static Behavior:

The experimental ultimate loads agree with the analytical and theoretical values within about

ten percent. Table 5.2 also indicates an excellent agreement between theoretical and analytical values of ultimate loads. The analytical values of μ's are much smaller than the experimental μ's because of the convergence difficulties in the analytical approach as explained in § 2.3.7. Figures 5.11, 5.12 and 5.13 show the analytical and the experimental load deflection curve for specimens A-28, A-34 and B-26 respectively.

(b) Dynamic Behavior:

The analytical value of the ultimate load of the type A specimen is 17% lower than the experimental value while for the type B specimen, this difference is as high as 40%. The analytical μ's are lower than the experimental μ's. The lower analytical u-value can be explained on the basis that in the analytical calculations, the arch is considered to have failed when the compressive strain in extreme fibres at any one point in the arch exceeds e_u = 0.0038 inches/ in.: while in tests, the extreme fibre strains at failure could be much larger than e_u. In figures 5.14 and 5.15 are shown the analytical and experimental load-time and deflection-time curves for specimens A-37 and B-32 respectively. These curves indicate a fair agreement between the analytical and experimental results.

(c) Comparison of Dynamic and Static Behavior:

In table 5.4 a comparison between the experimental and analytical dynamic increase factor (DIF) is sought. The value of the experimental static ultimate load for type B arches, given in this table is an average of those of specimens B-26 and B-27; while the specimens B-29 and B-30 are not considered in this average value, in order to have a consistent comparison between static and dynamic behavior as explained in detail in paragraph 3 of § 4.4.3.

The experimental values of the dynamic increase are of the order of 65% and 179% respectively for the type A and type B arches. The corresponding analytical values are 49% and 145%. Thus the agreement between the experimental and analytical values is quite good. This dynamic increase seems to be due to the increase in the material properties under very rapid strain rates and also due to inertial effects. The comparatively larger dynamic increase in the case of type B arches is possibly due to the presence of substantial inertial effects, as compared to type A arches.

The experimental as well as analytical μ-values for the dynamic case are smaller than those for the static case. (See table 5.2). This is, in part, due to the fact that the elastic-limit deflections are calculated at the ultimate loads which are considerably higher in the dynamic

case. Therefore the elastic-limit deflections are considerably higher and the μ-values are lower.

TABLE 5.1a*

COMPARISON OF THEORETICAL AND EXPERIMENTAL RESULTS TYPE I LOADING
TYPE A SPECIMENS

Type of Test	Specimen No.	f'_c (psi)	t_r (ms.)	Pu_{EXP} (lbs/in)	$Pu_{TH_{ST}}$ (lbs/in)	Pu_{ANA} (lbs/in)	μ_{EXP}	μ_{ANA}
S	A-1	4300		1215	1030	910	-	1.65
T	A-2	3460		765	875	813	-	1.72
A	A-4	4010		970	980	903	1.12	1.68
T	A-5	3800		920	930	898	1.78	1.70
I								
C								
	A-8	4160	8	1130		1290	2.67	1.48
D	A-11	3500	10	1010		1120	2.98	1.60
Y	A-12	3400	11	1108		1090	2.24	1.67
N	A-13	3160	10	980			3.38	
A	A-17	3440	16	920		1100	2.26	1.63
M	A-19	2600	11	880			1.94	
I								
C								

* In addition to the notations used in Table 4.1, this table uses the following:

Pu_{ANA} - Failure load obtained by using computer programs presented in Appendices III and IV.

TABLE 5.1b*

COMPARISON OF THEORETICAL AND EXPERIMENTAL RESULTS

TYPE I LOADING, TYPE B SPECIMENS

Type of Test	Specimen No.	f_c' (psi)	t_r (ms.)	$P_{u_{EXP}}$ (lbs/in)	$P_{u_{THST}}$ (lbs/in)	$P_{u_{ANA}}$ (lbs/in	μ_{EXP}	μ_{ANA}
S	B-1	3400		304	405	381		1.82
T	B-2	3880		286	420	391		1.80
A	B-10	3010		443	380	330		1.82
T	B-11	3280		350	385	350		1.73
I	B-15	3150		330	375	339	1.37	1.86
C	B-16	3790		380	430	384	1.08	1.82
D	B-4	3800	9	473		550	2.88	1.48
Y	B-12	2590	10	645		390	1.13	1.88
N	B-13	2630	11	640		-	1.26	
A	B-14	3720	11	480		520	2.41	1.51
M	B-17	3420	17	530		-	1.94	
I	B-20	3740	30	648		490	1.45	1.6
C								

* Notations used in this table are the same as in table 5.1a.

TABLE 5.2*

COMPARISON OF THEORETICAL AND EXPERIMENTAL RESULTS

TYPE III LOADING

Type of Test	Specimen type	Average t_r (ms)	Average $P_{u\ EXP}$ (lbs.)	Average P_{uTHST} (lbs.)	$P_{u\ ANA}$ (lbs.)	μ_{EXP}	μ_{ANA}
STATIC	A	-	380	355	350	18.5	2.83
	B	-	72	60	62	13.7	2.9
DYNAMIC	A	16	629	-	520	7.1	1.92
	B	19	257	-	152	3.1	1.7

* In addition to the notations used in table 4.5, this table uses the following.

$P_{u_{ANA}}$ - Failure load obtained by using computer programs presented in Appendices III and IV

TABLE 5.3

COMPARISON OF STATIC AND DYNAMIC BEHAVIOR

TYPE I LOADING

Specimen Type	Average $\frac{Pu_{EXP_{ST}}}{f'_c\ t}$	Average $\frac{Pu_{EXP_{Dy}}}{f'_c\ t}$	D.I.F. (Experimental) = $\frac{\text{Col.(3)}}{\text{Col (2)}}$	Average $\frac{Pu_{ANA_{ST}}}{f'_c\ t}$	Average $\frac{Pu_{ANA_{Dy}}}{f'_c\ t}$	D.I.F. (Analytical) = $\frac{\text{Col.(6)}}{\text{Col. (5)}}$
(1)	(2)	(3)	(4)	(5)	(6)	(7)
A	0.123	0.150	1.22	0.113	0.157	1.38
B	0.102	0.145	1.42	0.105	0.143	1.36

TABLE 5.4

COMPARISON OF STATIC AND DYNAMIC BEHAVIOR

Loading Type	Specimen Type	Average $P_{u_{EXP_{ST}}}$ (lbs.)	Average $P_{u_{EXP_{Dy}}}$ (lbs.)	D.I.F. (Experimental) = Col.(4) / Col.(3)	$P_{u_{ANA_{ST}}}$ (lbs.)	$P_{u_{ANA_{Dy}}}$ (lbs.)	D.I.F. (Analytical) Col.(7) / Col.(6)
	(2)	(3)	(4)	(5)	(6)	(7)	
II	A	1550	2101	1.36			
	B	259	406	1.57			
III	A	380	629	1.65	350	520	1.49
	B	92	257	2.79	62	152	2.45

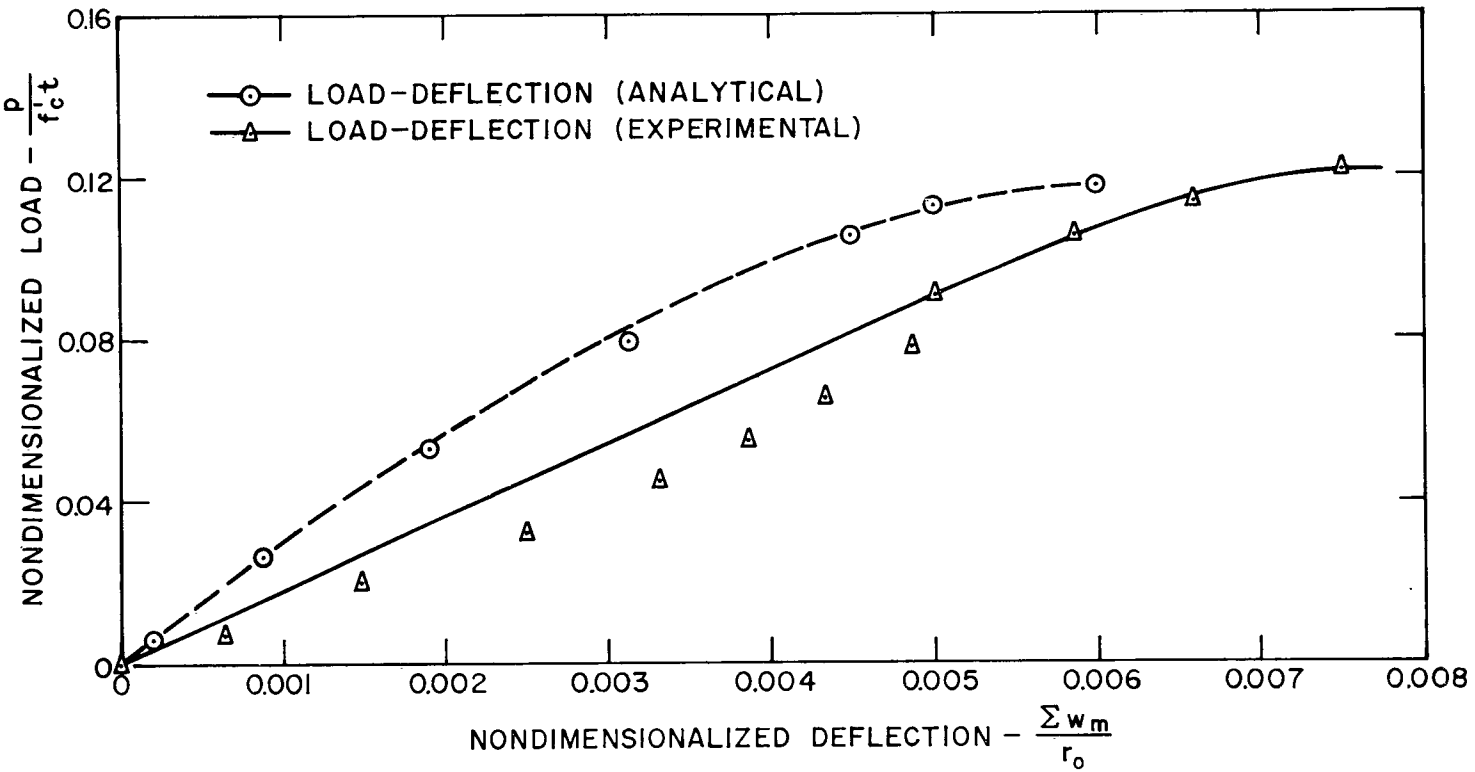

FIGURE 5.1-SPECIMEN A-5

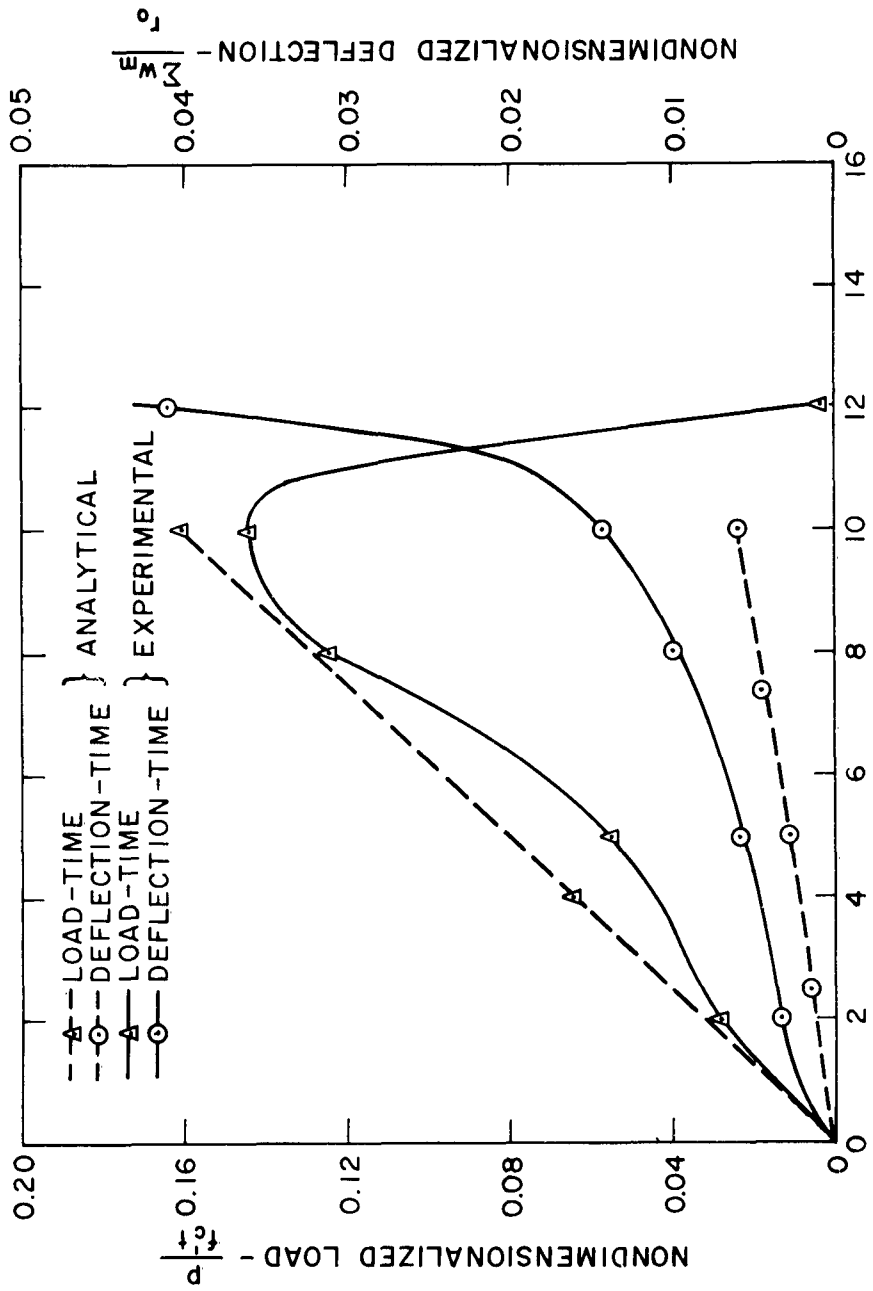

FIGURE 5.2-SPECIMEN A-II (FAILURE PULSE)

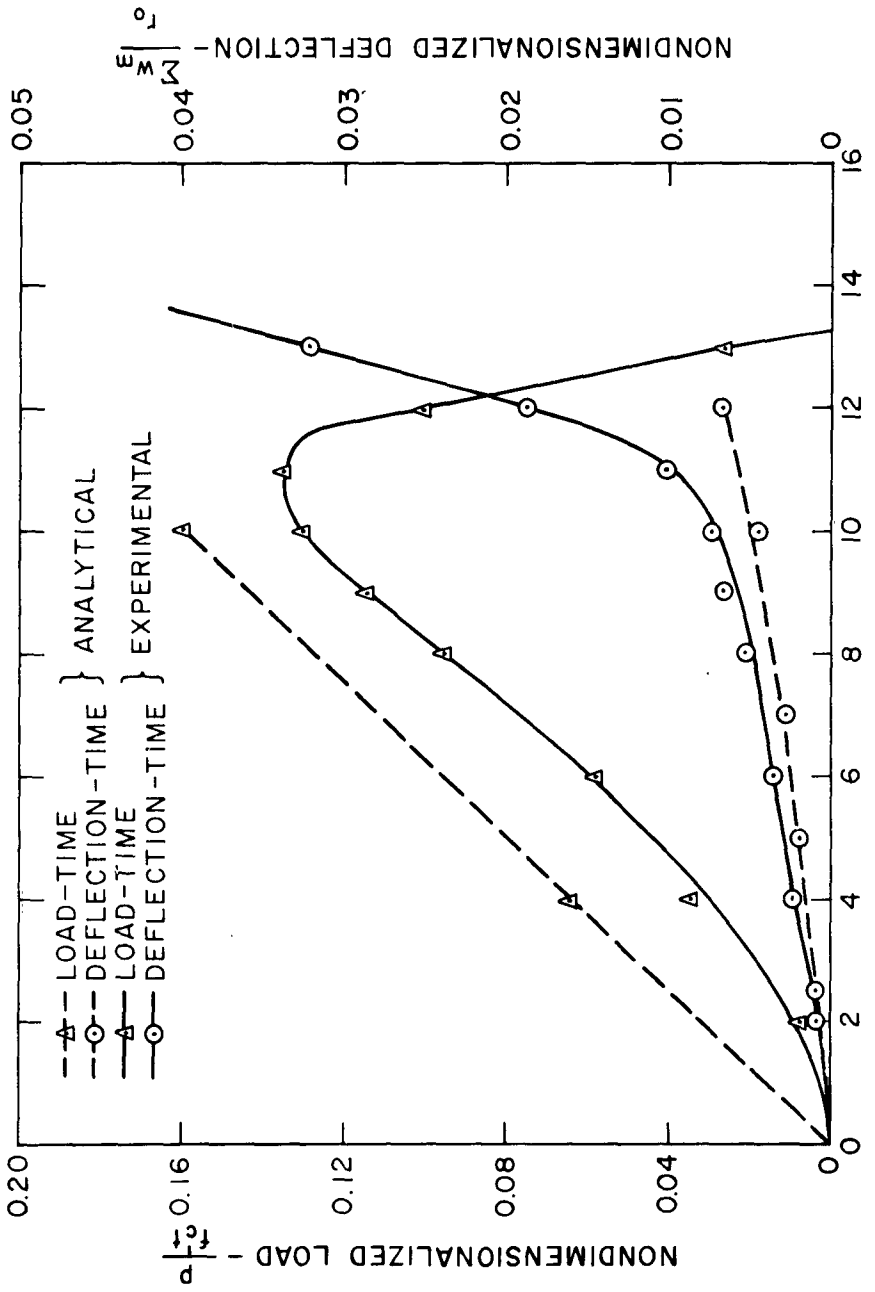

FIGURE 5.3-SPECIMEN A-17 (FAILURE PULSE)

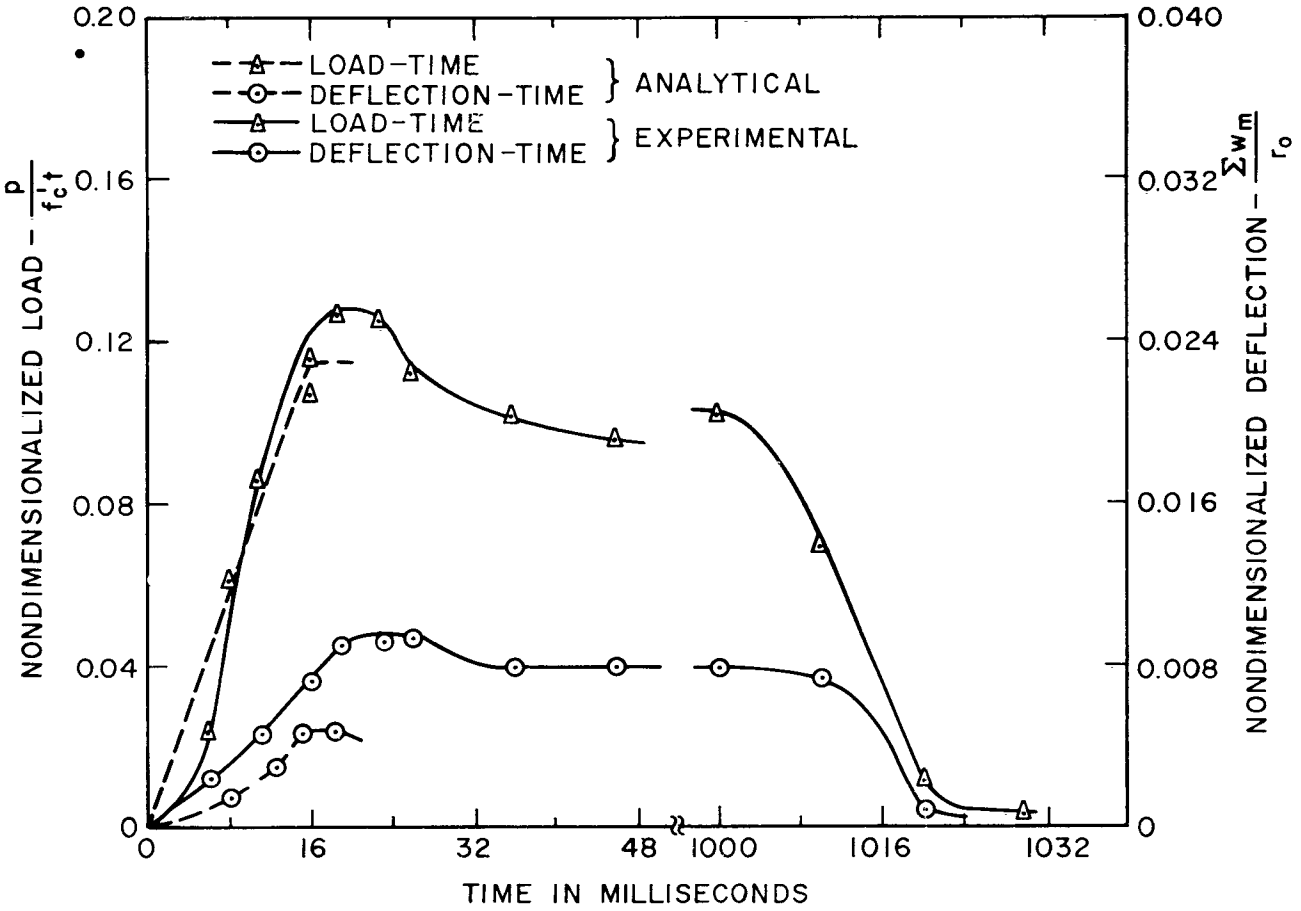

FIGURE 5.4-SPECIMEN A-17 (PARTIAL PULSE)

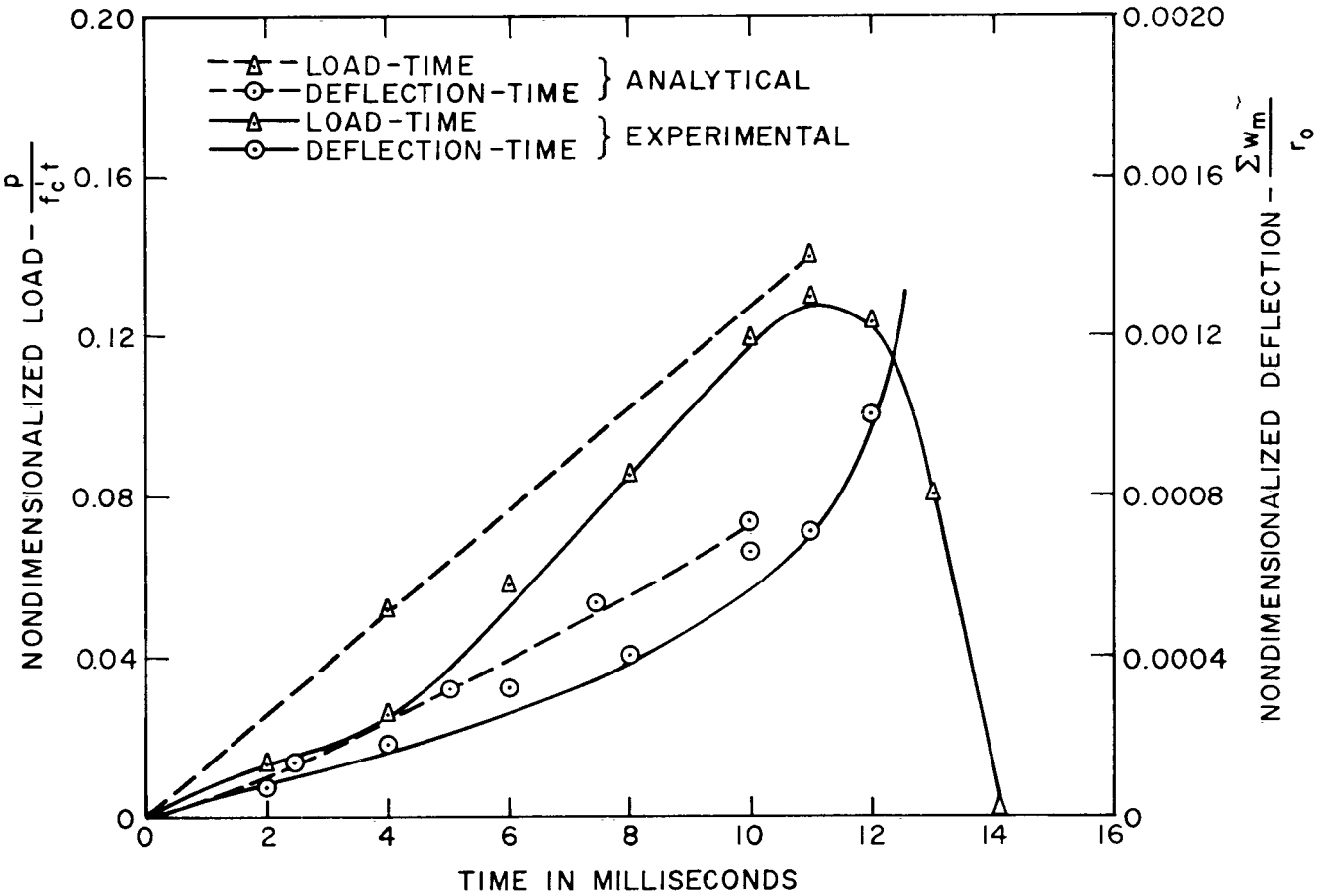

FIGURE 5.5-SPECIMEN B-14 (FAILURE PULSE)

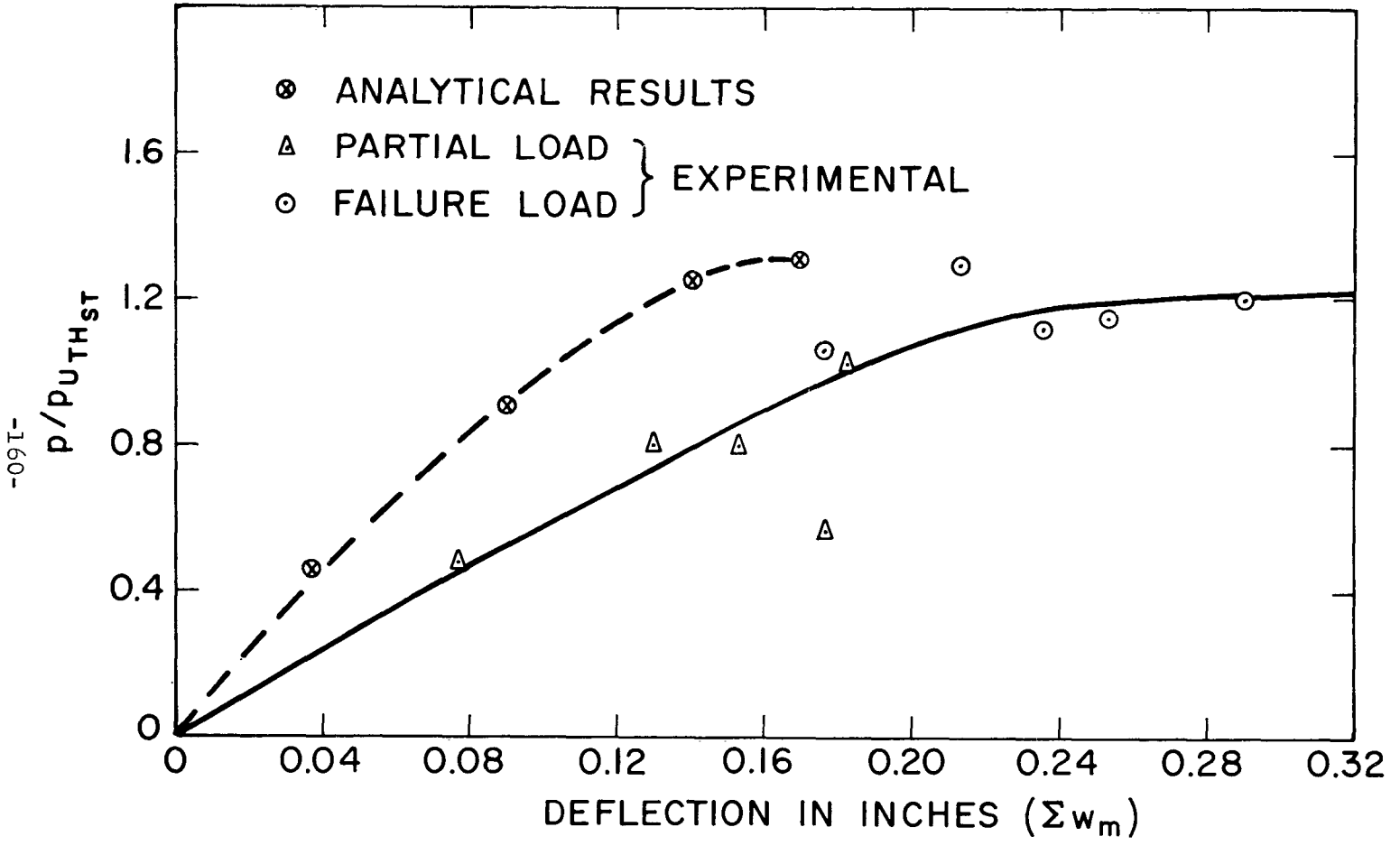

FIGURE 5.6 - LOAD-DEFLECTION (DYNAMIC CASE)

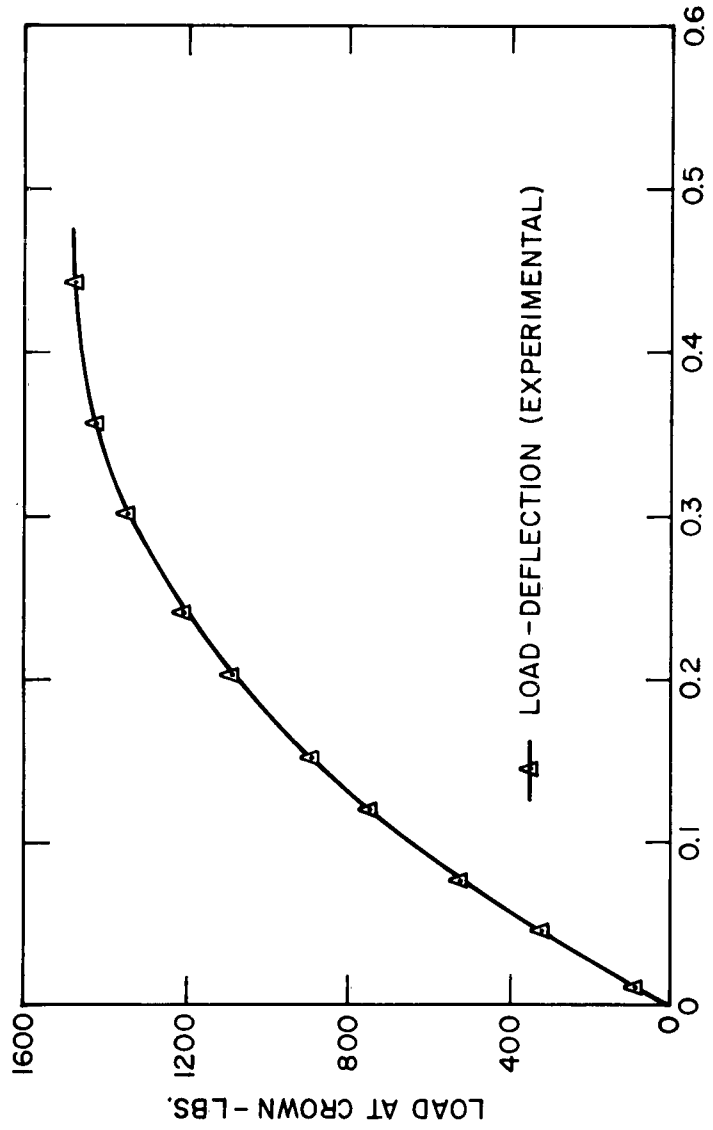

FIGURE 5.7-SPECIMEN A-21

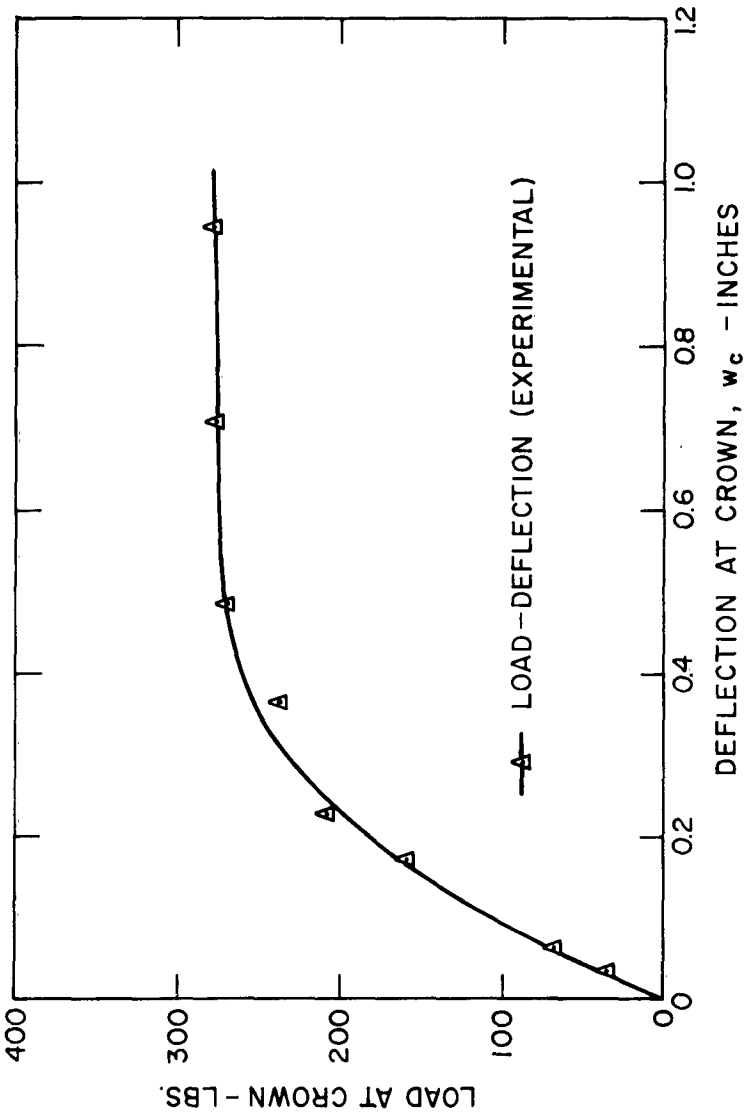

FIGURE 5.8-SPECIMEN B-21

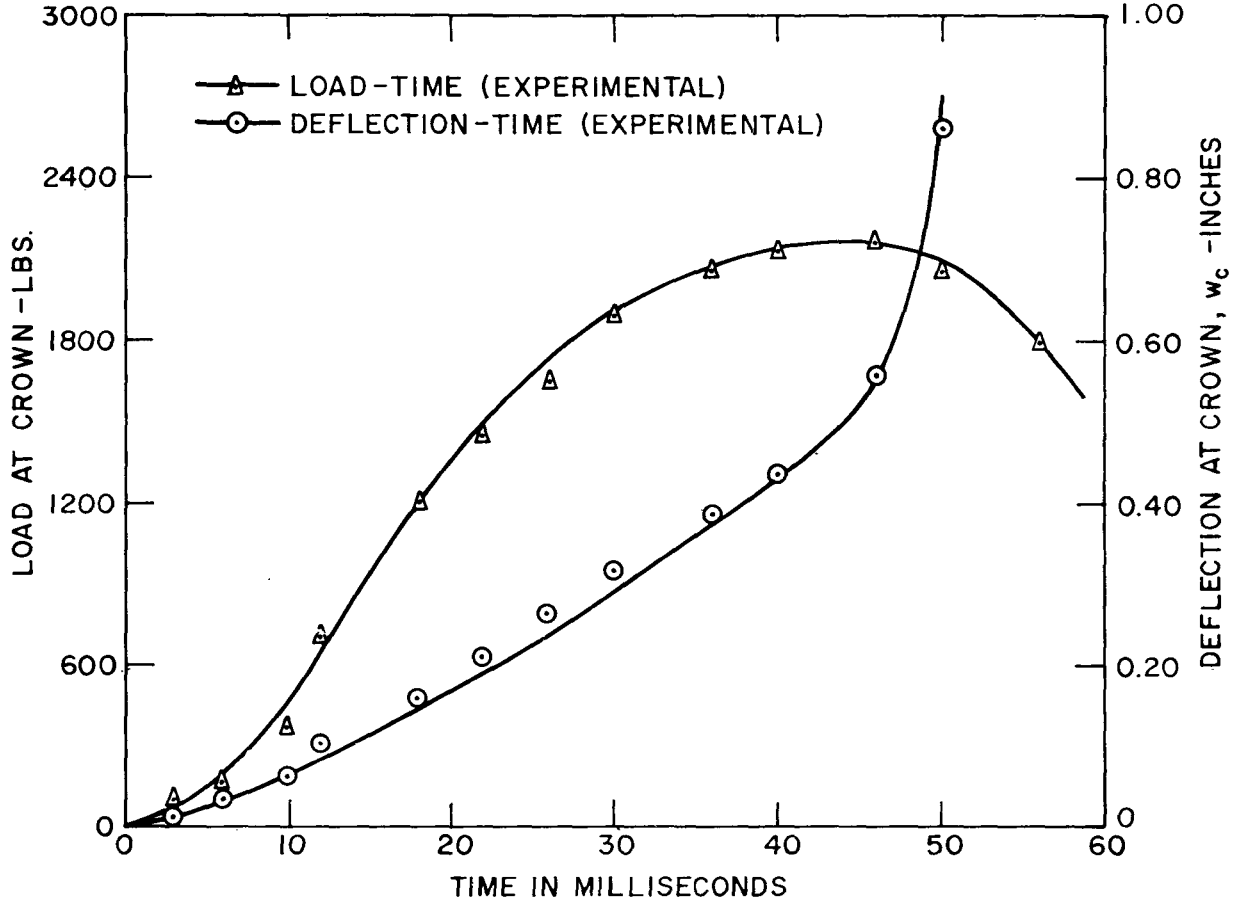

FIGURE 5.9 - SPECIMEN A - 24

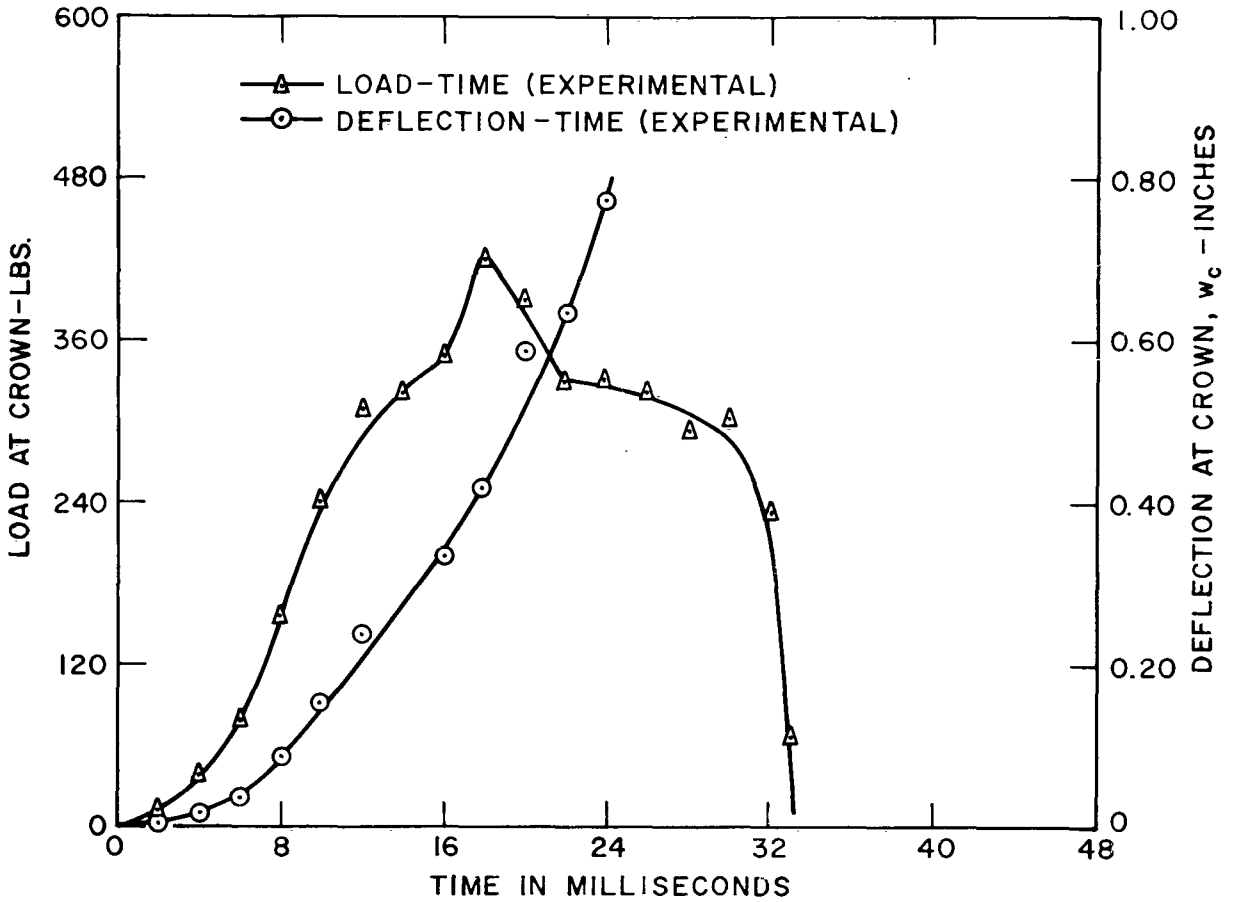

FIGURE 5.10-SPECIMEN B-24

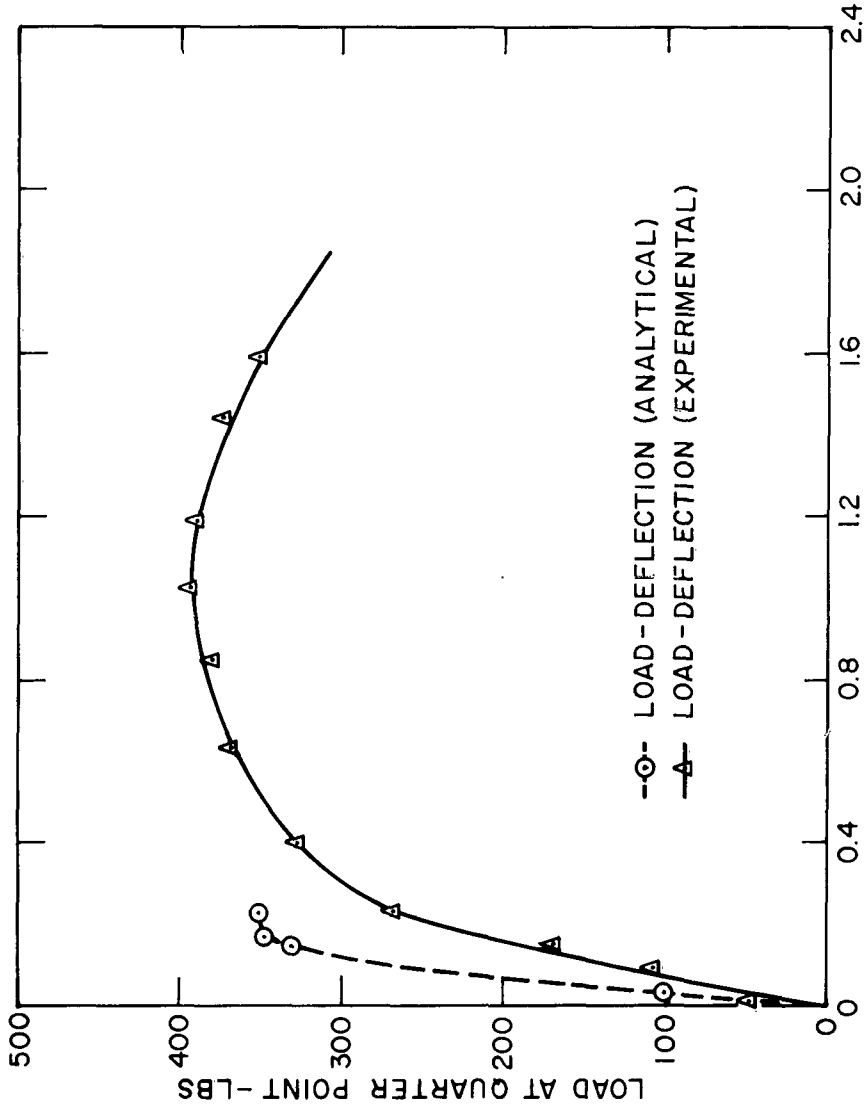

FIGURE 5.11 - SPECIMEN A-28

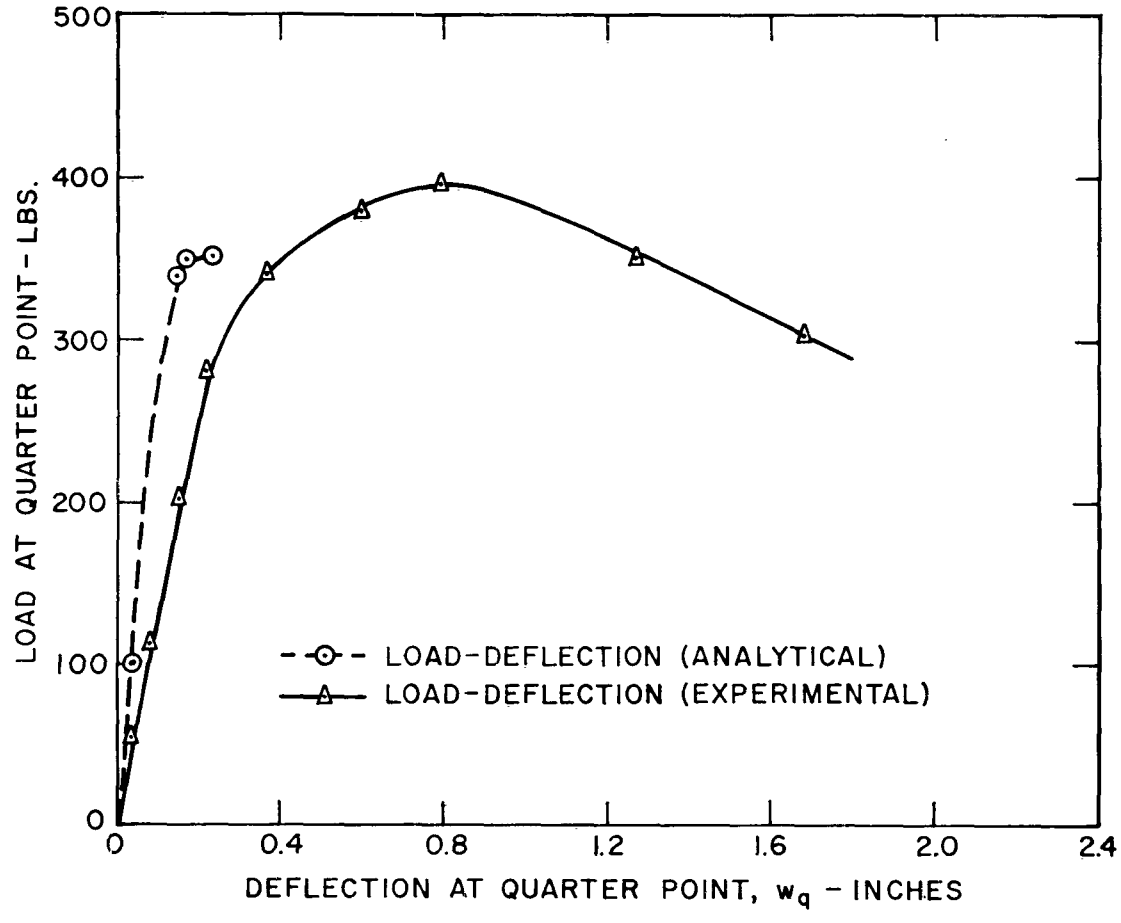

FIGURE 5.12-SPECIMEN A-34

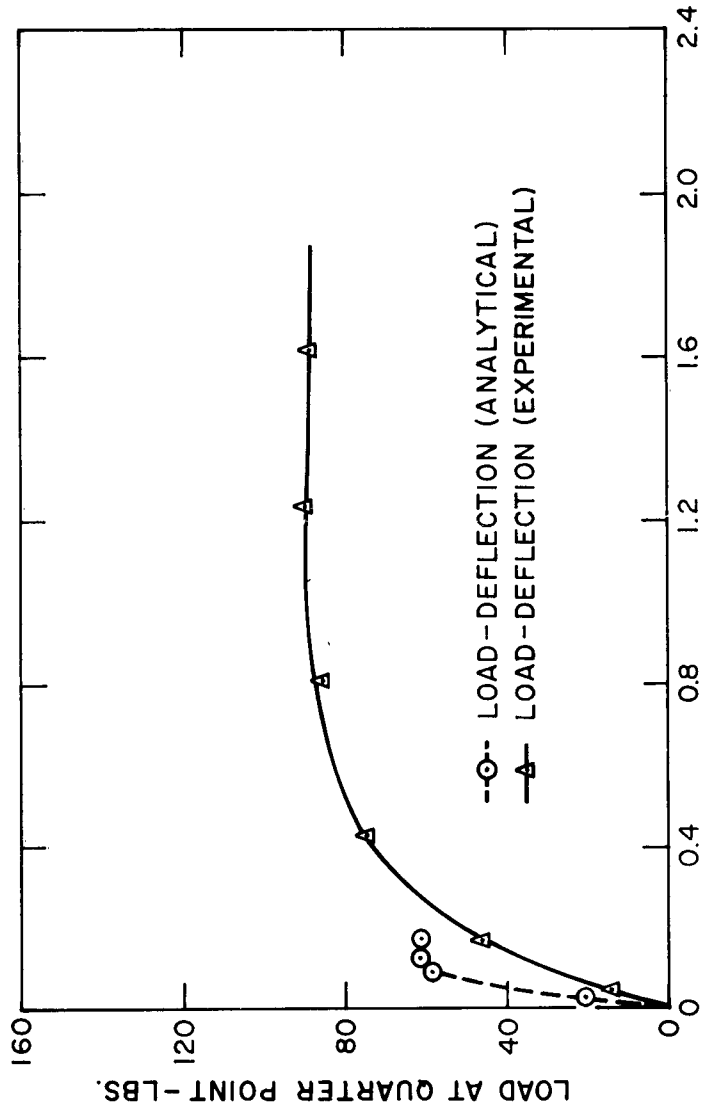

FIGURE 5.13-SPECIMEN B-26

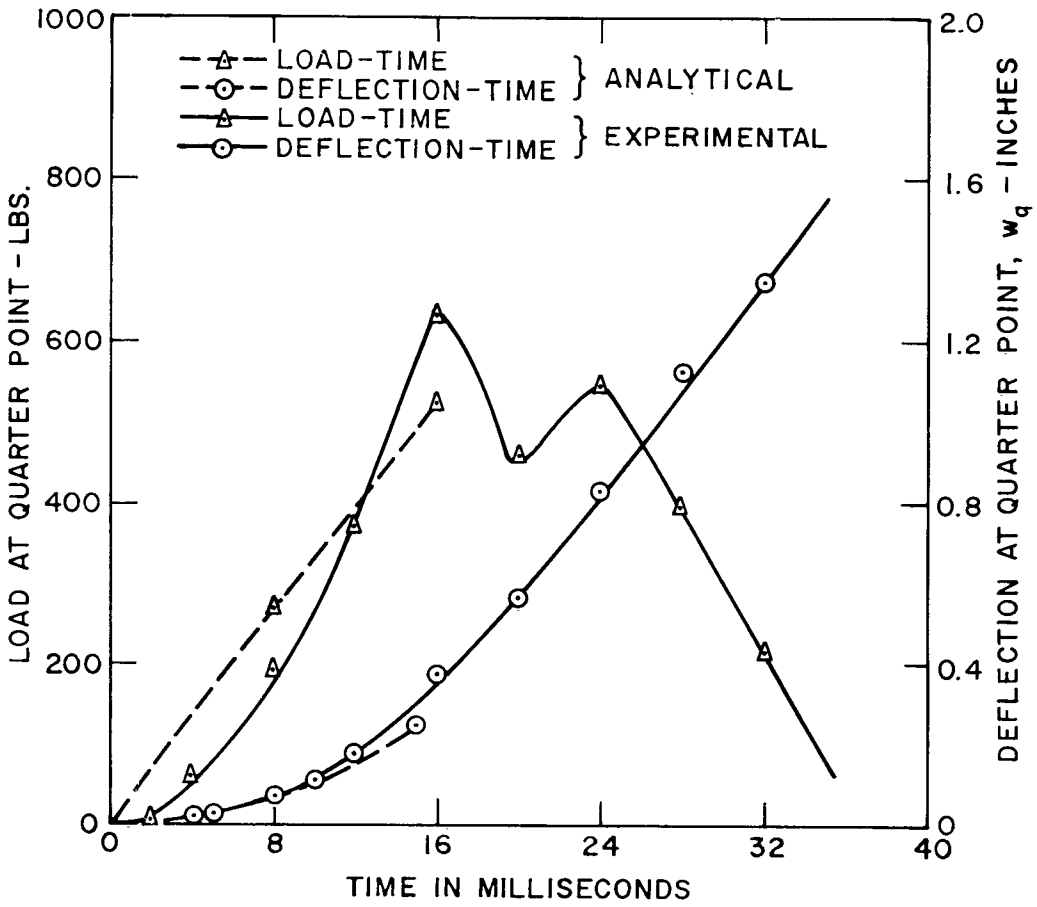

FIGURE 5.14 - SPECIMEN A-37

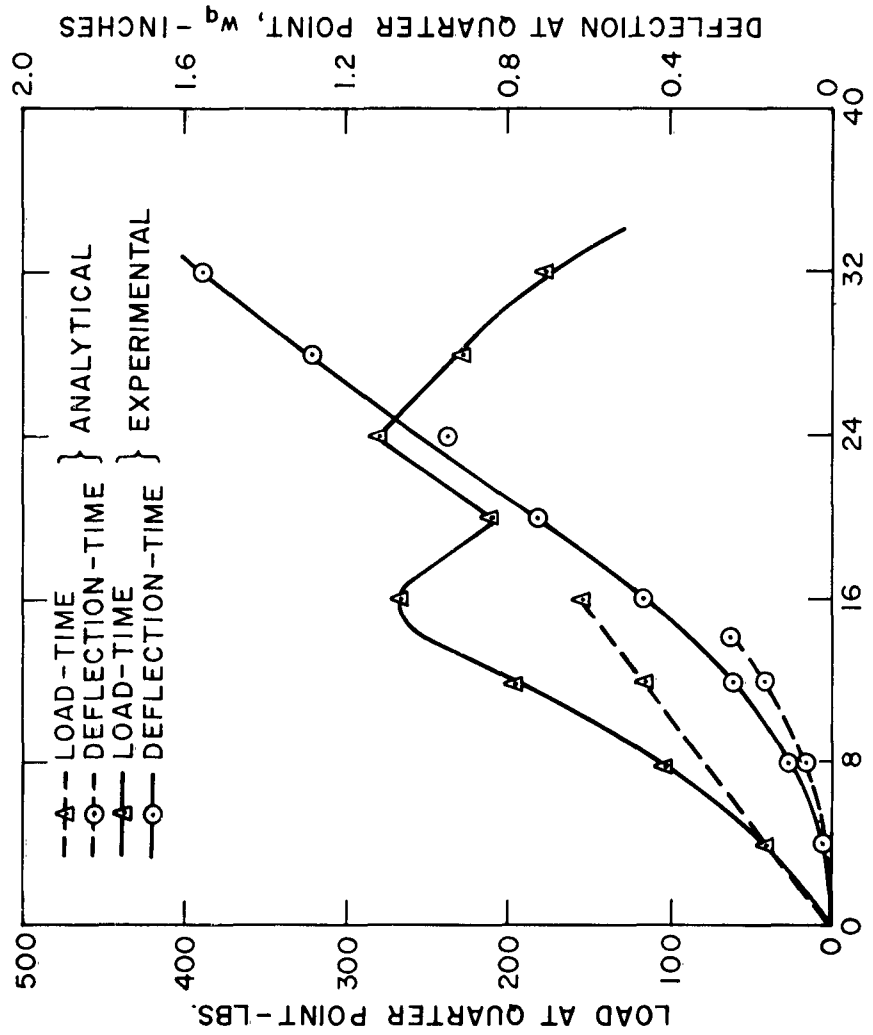

FIGURE 5.15-SPECIMEN B-32

CHAPTER 6

CONCLUSIONS

The following conclusions can be drawn on the basis of the analytical and experimental investigations as well as the approximate theoretical analysis.

1) The static ultimate loads obtained experimentally are in good agreement with both the conventional approximate theory and the non-linear theory developed herein.

2) In the compression mode loading, the dynamic increase in ultimate load is mainly due to the increase in properties of materials under very rapid strain rates. This increase is about 30 to 35%.

3) In the cases of a concentrated load at the crown and antisymmetric concentrated loads at quarter points, the natural periods of the arches in the flexural mode (and hence the inertial effects) have a significant influence on the dynamic increase. This increase is much higher than that in the case of compression mode loading.

4) In the compression mode loading the analytical and experimental values of μ are of the order of 1.5 to 2.5.

5) For a concentrated load at the crown the experimental value of μ is about 9 for the static case and about 7 for the dynamic case.

6) The experimental value of μ for antisymmetric concentrated loads at quarter points is of the order of 15 for the static case and varies between 3 and 7 for the dynamic case.

7) The analytical approach is adequate to compute the ultimate loads in most of the cases considered; however, it gives quite conservative results for the dynamic antisymmetric quarter point loading.

8) Experimental and analytical results indicate that the approximate static theory is quite adequate to predict the static ultimate loads for under-reinforced sections. The dynamic ultimate loads for compression mode loading can also be predicted by the approximate theory provided that an appropriate dynamic increase factor (based on the increase in material properties) is used.

9) From the comparison between the analytical results and those obtained from the approximate analysis based on a single degree freedom system (§ 2.7) it seems that the latter may give

unconservative dynamic failure loads, if the duration of loading is less than about half the natural period. However, clear reasons to explain this fact are not evident and further investigation is needed.

APPENDIX I

VARIOUS CONSIDERATIONS FOR FORCE-STRAIN RELATIONS BASED ON LINEAR CONCRETE STRESS-STRAIN CURVE

As explained in § 2.3.4, in order to solve the non-linear force-strain relations to obtain strains e_1 and e_4, it is necessary to have certain approximate values of these strains to start the 'Newton-Raphson iteration' (Appendix II). These approximate values of strains at the bottom and the top of the section denoted here by ee_1 and ee_4 are calculated by assuming that the stress-strain curve for concrete is linear with a modulus of elasticity $\bar{E}_c$, and that the tensile stresses in concrete are negligible. The value of $\bar{E}_c$ is assumed to be less than E_c, the initial tangent modulus, so that the linear stress-strain curve closely approximates the non-linear curve even at high stress levels. The following considerations are necessary to calculate the values of ee_1 and ee_4.

At any section i, $\bar{N}_i$ and $\bar{M}_i$ are known. From these are calculated,

$$N = \bar{N} \cdot f''_c bt \text{ and } \bar{M} = M f''_c bt^2 \qquad (A1.1)$$

Also are calculated the gross Area A_g and the gross moment of inertia I_g of the section.

$$\left.\begin{aligned} A_g &= bt + p_t bt(n-1) \\ \text{and}\quad I_g &= \frac{bt^3}{12} + p_t bt(n-1)\,\frac{d'^2}{4} \end{aligned}\right\} \qquad \text{(A1.2)}$$

The various possibilities of the strain distributions on the section are,

(i) N = 0 and M is positive or negative:

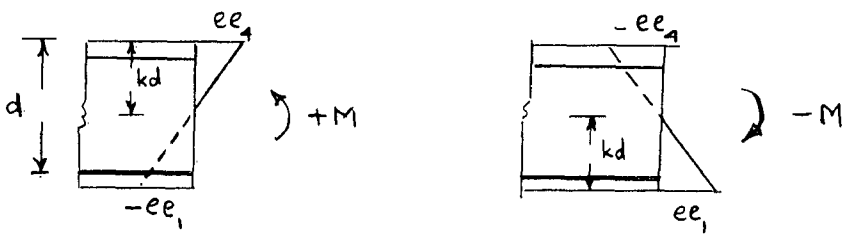

Figure A1.1 Strain Distribution - Case (i)

(ii) N is positive and M is positive or negative:

There exist two possibilities in this case.

If $\frac{|M|}{N} \leqslant \frac{2I_g}{tA_g}$, the entire section is under compression (Fig. A1.2); otherwise the section is partly in compression and partly in tension (Fig. A1.3).

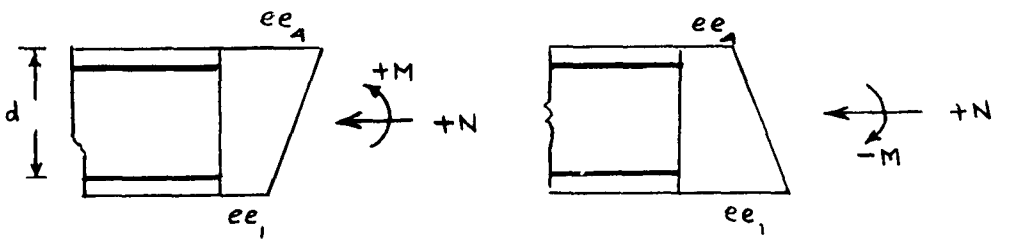

Figure A1.2 Strain Distribution - Case (ii)

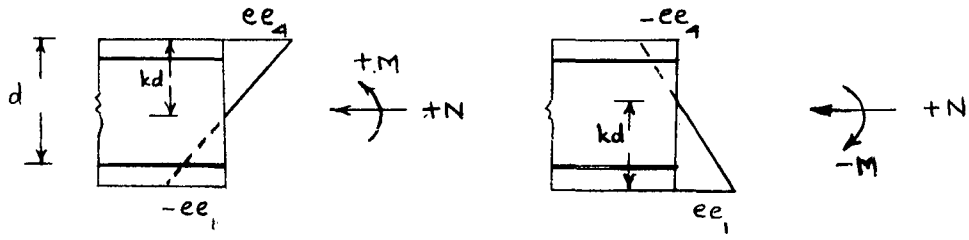

Figure A1.3 Strain Distribution - Case (ii)

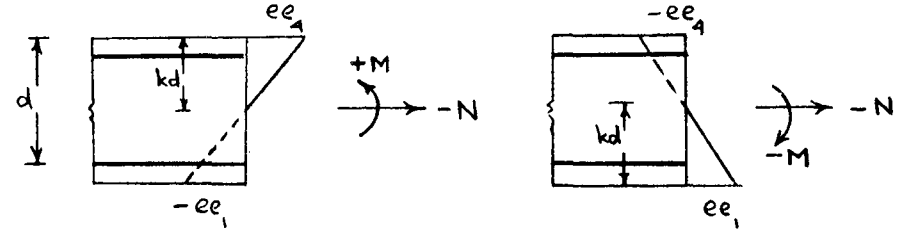

Figures A1.4 Strain Distribution - Case (iii)

(iii) N is negative and M is positive or negative:

Again there exist two possibilities. The first possibility is that the section is partly in compression and partly in tension (Fig. A1.4), while the second possibility is that the section is entirely under tension (Fig. A1.5). The criterion used for distinguishing these possibilities from each other is:

If $\frac{|N|}{2} - \frac{M}{t} \geqslant 0$, Fig. A1.5 is applicable, and if otherwise, Fig. A1.4 is to be used. This criterion

is approximate since $\frac{|N|}{2} - \frac{M}{t} < 0$ indicates that the strains in the concrete cover over the top steel (if M is positive) or in the concrete cover over the bottom steel (if M is negative) are compressive. This signifies that the section is not completely in tension until |N| is somewhat greater than that required by this criterion. However, since the depths of concrete covers are usually small as compared to the total depth of the section, this approximate criterion is accepted.

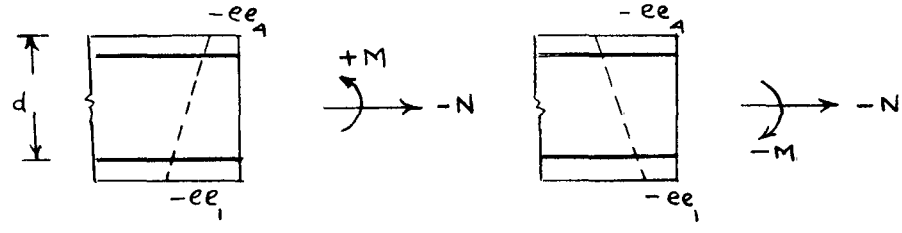

Figure A1.5 Strain Distribution - Case (iii)

The equations necessary to calculate the strains ee_1 and ee_4 in all the above cases are readily obtained by considering the equilibrium of the internal and external forces acting on the section. These equations and the criteria used to classify all the cases are incorporated in the computer program, (Appendix III).

APPENDIX II

'NEWTON-RAPHSON ITERATION' FOR SOLVING NONLINEAR SIMULTANEOUS ALGEBRAIC EQUATIONS

A2.1 'NEWTON-RAPHSON' METHOD

This method[12] affords an effective iterative procedure to obtain the solution of two or more simultaneous non-linear equations. For example, the two simultaneous equations of the form,

$$f(x,y) = 0 , \qquad g(x,y) = 0 \qquad \text{(A2.1)}$$

having (α,β) as one of its real solutions can be solved to obtain α and β as follows:

The two functions can be expanded in a Taylor series as,

$$\left.\begin{aligned} 0 = f(\alpha,\beta) &= f(x_k,y_k) + (\alpha - x_k) f_x(x_k,y_k) \\ &\quad + (\beta - y_k) f_y(x_k,y_k) + \cdots\cdots \\ 0 = g(\alpha,\beta) &= g(x_k,y_k) + (\alpha - x_k) g_x(x_k,y_k) \\ &\quad + (\beta - y_k) g_y(x_k,y_k) + \cdots \end{aligned}\right\} \qquad \text{(A2.2)}$$

where x_k and y_k are the values of the k^{th} iteration, If α and β in the terms on the right-hand side of the

expansion are replaced by x_{k+1} and y_{k+1}, respectively, and the terms nonlinear in $(x_{k+1} - x_k)$ and $(y_{k+1} - y_k)$ are neglected, the following recurrence formulae are obtained,

$$\left.\begin{aligned}(\Delta x_k) f_x(x_k, y_k) + (\Delta y_k) f_y(x_k, y_k) &= -f(x_k, y_k) \\ (\Delta x_k) g_x(x_k, y_k) + (\Delta y_k) g_y(x_k, y_k) &= -g(x_k, y_k)\end{aligned}\right\} \quad (A2.3)$$

$$\left.\begin{aligned}\text{where} \quad \Delta x_k &= x_{k+1} - x_k \\ \text{and} \quad \Delta y_k &= y_{k+1} - y_k\end{aligned}\right\} \quad (A2.4)$$

are the corrections of k^{th} iteration.

The iteration is started at a value (x_o, y_o) which is sufficiently near (α, β) and equations (A2.3) and (A2.4) are used to obtain successively better values of the roots of the equations (A2.1). The iteration is continued until the corrections become smaller than some assigned tolerance limit. The advantage of this method over others is that this is a 'second-order' process; that is, when the iteration converges, the errors in the $(k+1)^{th}$ iterate tend to be linear combinations of the 'squares' of the errors in the k^{th} iterate.

A2.2 APPLICATION OF THE METHOD TO THE PRESENT PROBLEM

As is explained in § 2.3.4, this method is used to solve the governing equations (2.26) and (2.27) or (2.28) and (2.29). The forms of equations used are as follows:

Using the notation

$$x = e_1 \ , \quad y = e_4 \ ,$$

$$k = \frac{E_s \ p_t}{2f_c''} \cdot \left(1-\frac{1}{n}\right) \quad \text{and} \quad k_1 = \frac{E_s \ p_t}{2f_c''}$$

and substituting

$$e_2 = e_1 + (e_4 - e_1) \cdot \frac{(t-d)}{t}$$

$$\text{and} \quad e_3 = e_1 + (e_4 - e_1) \cdot \frac{d}{t}$$

equations (2.26) and (2.27) become,

$$\left.\begin{aligned} f(x,y) &= k(x+y) + \frac{(x+y)}{e_c'} - \frac{(x^2 + xy + y^2)}{3e_c'^2} - \bar{N} = 0 \\ g(x,y) &= \frac{k}{2} \ \frac{d'^2}{t^2} \ (y-x)^2 + \frac{(y-x)^2}{6e_c'} - \frac{(y-x)^2(y+x)}{12e_c'^2} \\ &\quad - \bar{M}(y-x) = 0 \end{aligned}\right\} \quad (A2.5)$$

when $e_2 \leqslant e_y$ and $e_3 \leqslant e_y$,

$$
\left.
\begin{aligned}
f(x,y) &= k_1 e_y - \frac{k_1}{n}\left[x + (y-x)\frac{d}{t}\right] + kx + \frac{k}{t}(y-x)(t-d) \\
&\quad + \frac{(x+y)}{e'_c} - \frac{(x^2 + xy + y^2)}{3e'^2_c} - \bar{N} = 0 \\
g(x,y) &= -\frac{k_1}{2n}\frac{d'}{t}x(y-x) - \frac{k_1}{2n}\frac{d'}{t}\frac{d}{t}(y-x)^2 \\
&\quad + \frac{k_1}{2}\frac{d'}{t}e_y(y-x) - \frac{k}{2}\frac{d'}{t}x(y-x) \\
&\quad - \frac{k}{2}\frac{d'}{t}\frac{(t-d)}{t}(y-x)^2 + \frac{(y-x)^2}{6e'_c} \\
&\quad - \frac{(y-x)(y+x)}{12e'^2_c} - \bar{M}(y-x) = 0
\end{aligned}
\right\} \quad (A2.6)
$$

when $e_2 < e_y$ and $e_3 > e_y$,

and

$$
\left.
\begin{aligned}
f(x,y) &= 2k_1 e_y - \frac{k_1}{n}(x+y) + \frac{(x+y)}{e'_c} - \frac{(x^2+xy+y^2)}{3e'^2_c} \\
&\quad - \bar{N} = 0 \\
g(x,y) &= -\frac{k_1}{2n}\frac{d'^2}{t^2}(y-x) - \frac{(y-x)^2}{6e'_c} \\
&\quad - \frac{(y-x)^2(y+x)}{12e'^2_c} - \bar{M}(y-x) = 0
\end{aligned}
\right\} \quad (A2.7)
$$

when $e_2 \gg e_y$ and $e_3 \gg e_y$.

Similarly equations (2.28) and (2.29) become,

$$
\left.
\begin{aligned}
f(x,y) \;=\; & k_1 (y^2-x^2) - \frac{k_1}{n}\, xy + \frac{k_1}{n}\, x^2 - \frac{k_1}{n}\, \frac{d}{t}\, (y-x)^2 \\
& + \frac{y^2}{e_c'} - \frac{y^3}{3e_c'^2} - \bar{N}\,(y-x) \;=\; 0 \\
g(x,y) \;=\; & \frac{k_1}{2}\, \frac{d'^2}{t^2}\, (y-x)^3 - \frac{k_1}{2}\, \frac{d'}{t}\, \frac{x(y-x)^2}{n} \\
& - \frac{k_1}{2n}\, \frac{d'}{t}\, \frac{d}{t}\, (y-x)^3 + \frac{y^3}{6e_c'} - \frac{y^4}{12e_c'^2} \\
& - \frac{y^2 x}{2e_c'} + \frac{y^3 x}{6e_c'^2} - \bar{M}\,(y-x)^2 \;=\; 0
\end{aligned}
\right\} \text{(A2.8)}
$$

when $e_2 \ll e_y$ and $e_3 \ll e_y$,

$$
\left.
\begin{aligned}
f(x,y) \;=\; & -ke_y\,(y-x) + \left(k_1 - \frac{k_1}{n}\right) x\,(y-x) + \left(k_1 - \frac{k_1}{n}\right) \frac{d}{t}\, (y-x)^2 \\
& + \frac{y^2}{e_c'} - \frac{y^3}{3e_c'^2} - \bar{N}\,(y-x) \;=\; 0 \\
g(x,y) \;=\; & \frac{k_1}{2}\, \frac{d'}{t}\, \left(1 - \frac{1}{n}\right) x\,(y-x)^2 + \frac{k_1}{2}\, \frac{d'}{t}\, \frac{d}{t}\, \left(1 - \frac{1}{n}\right)(y-x)^3 \\
& + \frac{k_1}{2}\, \frac{d'}{t}\, e_y\,(y-x)^2 + \frac{y^3}{6e_c'} - \frac{y^4}{12e_c'^2} - \frac{y^2 x}{2e_c'} \\
& + \frac{y^3 x}{6e_c'^2} - \bar{M}\,(y-x)^2 \;=\; 0
\end{aligned}
\right\} \text{(A2.9)}
$$

when $|e_2| > |e_y|$ and $e_3 < e_y$,

$$
\left.
\begin{aligned}
f(x,y) \;=\; & k_1 x\,(y-x) + k_1 \frac{(t-d)}{t}\,(y-x)^2 + k_1 e_y\,(y-x) \\
& - \frac{k_1}{n}\,x(y-x) - \frac{k_1}{n}\,\frac{d}{t}\,(y-x)^2 + \frac{y^2}{e_c'} \\
& - \frac{y^3}{3e_c'^2} - \bar{N}\,(y-x) \;=\; 0 \\
\\
g(x,y) \;=\; & \frac{k_1}{2}\,\frac{d'}{t}\,e_y\,(y-x)^2 - \frac{k_1}{2n}\,\frac{d'}{t}\,x(y-x)^2 \\
& - \frac{k_1}{2n}\,\frac{d'}{t}\,\frac{d}{t}\,(y-x)^3 - \frac{k_1}{2}\,\frac{d'}{t}\,x(y-x)^2 \\
& - \frac{k_1}{2}\,\frac{d'}{t}\,\frac{(t-d)}{t}\,(y-x)^3 + \frac{y^3}{6e_c'} - \frac{y^4}{12e_c'^2} \\
& - \frac{y^2 x}{2e_c'} + \frac{y^3 x}{6e_c'^2} - \bar{M}\,(y-x)^2 \;=\; 0
\end{aligned}
\right\} \quad (A2.10)
$$

when $\quad |e_2| < |e_y| \quad$ and $\quad e_3 > e_y$,

$$
\left.
\begin{aligned}
f(x,y) \;=\; & -\frac{k_1}{n}\, x(y-x) - \frac{k_1}{n}\,\frac{d}{t}\,(y-x)^2 \\
& + \frac{y^2}{e'_c} - \frac{y^3}{3e'^2_c} - \bar{N}\,(y-x) = 0 \\
g(x,y) \;=\; & k_1\,\frac{d'}{t}\,e_y\,(y-x)^2 - \frac{k_1}{2n}\,\frac{d'}{t}\,x(y-x)^2 \\
& - \frac{k_1}{2n}\,\frac{d'}{t}\,\frac{d}{t}\,(y-x)^3 + \frac{y^3}{6e'_c} - \frac{y^4}{12e'^2_c} \\
& - \frac{y^2 x}{2e'_c} + \frac{y^3 x}{6e'^2_c} - \bar{M}\,(y-x)^2 = 0
\end{aligned}
\right\} \quad (A2.11)
$$

when $|e_2| \gg |e_y|$ and $e_3 \gg e_y$

The initial values (x_o, y_o) for starting the iterations of equations (A2.5) or (A2.8) are obtained as described in Appendix I (i.e., $x_o = ee_1$ and $y_o = ee_4$), while those for starting the iterations of equations (A2.6), (A2.7) or (A2.9), (A2.10), (A2.11) are obtained from the solutions of equations (A2.5) or (A2.8), respectively. If $\bar{M}$ is negative, the terms e_4 and e_1 are interchanged (i.e.,

$x = e_4$ and $y = e_1$) and the same equations then are employed along with the absolute value of $\bar{M}$.

A2.3 MODIFICATION OF THE METHOD

The method described above has been found to be adequate for most of the cases. However, it has to be slightly modified in two cases. Both of these cases occur when the load on the arch is near to the ultimate load. As described in §2.3.5, the method of obtaining the ultimate load consists of successively increasing the load by a small amount and checking for failure at each step. The following two types of difficulties can occur during this process.

a) If the load on the arch happens to exceed the ultimate load, the internal forces $\bar{N}$ and $\bar{M}$ acting at the critical section (i.e., the section at which the maximum concrete strain occurs) become too large and the solutions of the governing force-strain relations converge on erroneous values after going through a large number of iterations. In a normal case, it takes a maximum of only fifteen iterations to obtain the convergence. Therefore, if for any case it takes more than

say thirty iterations to obtain convergence it is certain that the internal forces are too large, caused by too large a load. Consequently, the occurence of thirty iterations or more is taken as a criterion to identify the case of too large a load and to stop further iterations.

b) In some cases when the load on the arch is slightly less than the ultimate, the functions $f(x,y) = 0$ and $g(x,y) = 0$ describing the force-strain relations exhibit a peculiar behavior. For clarity, this phenomenon is discussed here for a function having only one variable, say, $F(Z) = 0$. The recurrence formula for the 'Newton-Raphson iteration' in this case is[12],

$$\Delta Z_k = Z_{k+1} - Z_k = - \frac{F(Z_k)}{F'(Z_k)} \qquad (A2.12)$$

If the curve $F(Z) = Z$ is as shown in Fig. A2.1 and we are interested in a solution $Z = \gamma$, we must start the iteration at a value $Z_o > \gamma'$ such that $F'(Z_o) < 0$ If instead, we happen to start the iteration at $Z_o < \gamma'$, the solution will converge on some value of $Z \neq \gamma$, as shown in Fig. A2.1.

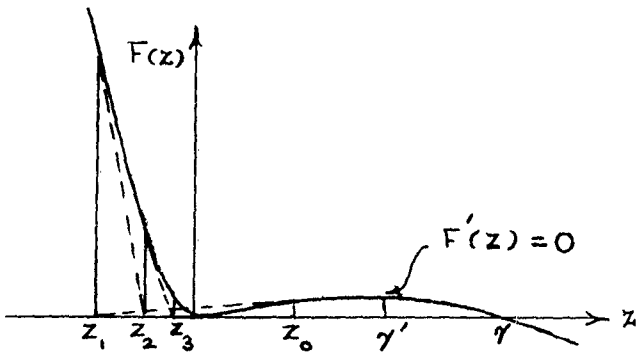

Figure A2.1 Function F (z) = z

In the present problem, under the action of loads which are near ultimate, steel at many sections yields and equations (A2.6), (A2.7), (A2.9), (A2.10) or (A2.11) have to be used for such cases. As explained before, the initial values for starting the iteration for the first two equations are obtained from the solution of equation (A2.5) while those for the last three equations are obtained from the solution of equation (A2.8). Both equations (A2.5) and (A2.8) consider no yielding of steel and hence the strains e_1 and e_4 obtained from these equations will be necessarily smaller than those obtained from solutions of equations (A2.6), (A2.7), (A2.9), (A2.10) or (A2.11). This means that the initial values used for starting the iteration are much smaller than the final values;

that is, a case similar to the one when $z < \gamma'$ (Fig.A2.1).

The situation is remedied as follows. It is seen from Fig. A2.1 that unless z_k, the value of z at any k^{th} iteration is positive, a convergence on $z = \gamma$ is not possible. If at the end of any iteration Δz_k turns out to be negative and larger in magnitude than z_k, instead of using $z_{k+1} = z_k + \Delta z_k$ [equation (A2.12)] we use,

$$z_{k+1} = z_k - 2(\Delta z_k) \qquad (A2.13)$$

This alteration in the method assures that z_k will always be positive and a convergence on $z = \gamma$ may be possible.

The above-mentioned technique is used to maintain the proper signs of the unknowns x and y (i.e., the strains e_1 and e_4 in the case of a positive $\bar{M}$ or the strains e_4 and e_1 in the case of a negative $\bar{M}$) by using formulae similar to equation (A2.13). The proper signs of the strains are known from the considerations presented in Appendix I.

APPENDIX III

CONCISED FLOW-CHART AND DIGITAL COMPUTER PROGRAM

STATIC CASE

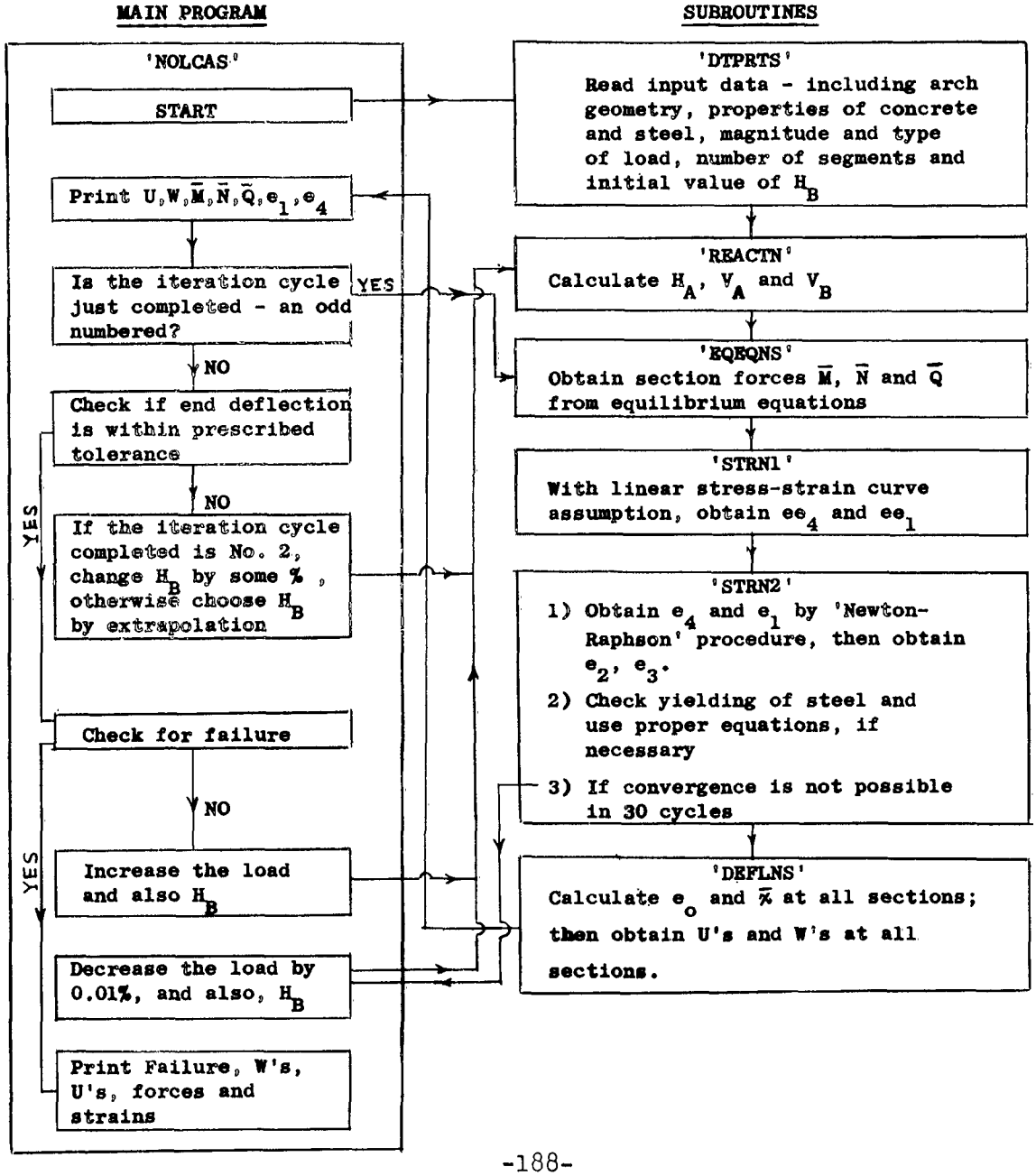

```
*      LIST
*      LABEL
CNOLCAS
C      ARCHES UNDER STATIC LOADING
C      VIJAY N. GUPCHUP
       DIMENSION PH(31),PV(31),PLN(31),W(31),U(31),CK(31),FRC(62),
      1FRCS(93),EE1(31),EE4(31),D2(62),E1(31),
      2E4(31),FRCSA(93),EO(31),CVTR(31),DEO(31),D2W(31),ADFL(62,62),
      3BDFL(62),FRCA(62),PRAD(29),PTGT(29),PLT(31),HC(25),COR(25)
      4,E2(31),E3(31),PINC(31),EEE4(20),WW(31),UU(31)
       COMMON B,D,DCVR,RO,PHIO,P,EBRC,EST,SPRC,NSEG,CVRG,HIN,
      1NPT,EC,EPRC,ERTO,ARG,AR2G,PHI2,THTA,TNO,QO,TNOO,QOO,FRCS,FRC,
      2FRCA,NPT3,CORTN,THTAA,U,W,EE1,EE4,E1,E4
      3,PH,PV,PLN,CK,D2,FRCSA,EO,CVTR,DEO,D2W,ADFL,BDFL
      4,PRAD,PTGT,SYLD,EPSY,PLT,NCHR,HC,COR,NOFL,EUTC,HINCR
  500 CALL DTPRTS
      NSEG=NSEG
      NPT=NSEG+1
      LRD=1
  502 N=0
  505 N=N+1
      NSAV=1
      DO 650 L=1,20
      NOFL=1
  510 CALL REACTN
      IF (L-1) 507,507,508
  507 HHIN=HIN
  508 CALL EQEQNS
      CALL STRN1
      CALL STRN2
      NOFL=NOFL
      IF (NOFL-2) 511,900,900
  900 IF (NSAV-1) 905,905,927
  905 PRINT 906
  906 FORMAT (3X,21HOVERCORRECTION CHECK.)
      IF (L-2) 927,927,910
  910 DLTH=HC(L)-HC(L-2)
      IF (DLTH) 912,912,913
  912 HIN=HC(L-2)-DLTH/2.
      L=L-1
```

```
      NSAV=2
      GO TO 650
  913 HIN=HC(L-2)+DLTH/2.
      L=L-1
      NSAV=2
      GO TO 650
  511 CALL DEFLNS
      HINN=HIN
  520 PRINT 525,((I,U(I)),I=1,NSEG)
  525 FORMAT (6(3X,1HU,I2,1H=,E12.4))
  530 PRINT 535,((I,W(I)),I=2,NPT)
  535 FORMAT (6(3X,1HW,I2,1H=,E12.4))
  540 PRINT 595,((I,E4(I),I,E1(I)),I=1,NPT)
  545 PRINT 550,((I,FRCS(I)),I=1,NPT3)
  550 FORMAT (3(3X,5HFRCS(,I2,2H)=,E12.4))
  596 IF (L-2) 597,600,620
  597 COR(L)=W(NPT)
      HC(L)=QOO
      GO TO 650
  600 COR(L)=W(NPT)
      HC(L)=QOO
      HIN=HINCR*HIN
      GO TO 624
  620 IF (L-4) 597,623,621
  621 IF (L-6) 597,623,622
  622 IF (L-8) 597,623,626
  626 IF (L-10) 597,623,627
  627 IF (L-12) 597,623,628
  628 IF (L-14) 597,623,629
  629 IF (L-16) 597,623,631
  631 IF (L-18) 597,623,632
  632 IF (L-20) 597,623,597
  623 COR(L)=W(NPT)
      HC(L)=QOO
      HIN=(HC(L)-(COR(L)*(HC(L)-HC(L-2))/(COR(L)-COR(L-2))))*SINF(PHIO)
     1+TNOO*COSF(PHIO)
  624 PRINT 625,HIN
  625 FORMAT (3X,3HHIN,1H=,6E15.6)
      CHK=W(NPT)*RO
      IF (CHK) 630,580,635
```

```
630   IF (CHK+0.005) 650,580,580
635   IF (CHK-0.005) 580,580,650
650   CONTINUE
      PRINT 655
655   FORMAT (3X,54HLOAD IN THE PREVIOUS CYCLE IS NEAREST TO THE ULTIMAT
     1E.)
      GO TO 500
580   DO 581 I=1,NPT3,3
      J=I/3+1
581   PRINT 585, J,FRCS(I),J,FRCS(I+1),J,FRCS(I+2)
585   FORMAT (3X,6HTHRUST,I2,1H=,E12.4,3X,5HSHEAR,I2,1H=,E12.4,
     13X,6HMOMENT,I2,1H=,E12.4)
590   PRINT 595,((I,E4(I),I,E1(I)),I=1,NPT)
595   FORMAT (3(3X,3HE4(,I2,2H)=,E12.4,3X,3HE1(,I2,2H)=,E12.4))
700   DO 730 I=1,NPT
      IF (E1(I)) 705,705,710
705   IF (E4(I)) 730,730,715
710   IF (E4(I)) 720,720,725
715   IF (E4(I)-EUTC) 730,735,735
720   IF (E1(I)-EUTC) 730,740,740
725   IF (E4(I)-EUTC) 726,735,735
726   IF (E1(I)-EUTC) 730,740,740
730   CONTINUE
      IF (LRD-2) 750,731,731
731   PRINT 732
732   FORMAT (3X,26HTHIS IS THE ULTIMATE LOAD.)
      GO TO 500
735   PRINT 737,I,E4(I)
737   FORMAT (3X,32HARCH FAILED. CONCRETE STRAIN E4(,I2,2H)=,E12.4)
      GO TO 500
740   PRINT 742,I,E1(I)
742   FORMAT (3X,32HARCH FAILED. CONCRETE STRAIN E1(,I2,2H)=,E12.4)
      GO TO 500
750   IF (N-2) 751,800,800
751   EEE4(N)=0.0
      PINCR=0.0
      DO 770 I=1,NPT
      IF (E4(I)) 755,755,752
752   IF (E4(I)-EEE4(N)) 755,755,753
753   EEE4(N)=E4(I)
```

```
      NCK=I
  755 E2(I)=E1(I)+(E4(I)-E1(I))*DCVR/D
      E3(I)=E1(I)+(E4(I)-E1(I))*(D-DCVR)/D
      PI=ABSF(E2(I))/EPSY
      PIN=ABSF(E3(I))/EPSY
      IF (PIN-PI) 757,757,756
  756 PINC(I)=PIN
      GO TO 760
  757 PINC(I)=PI
  760 IF (PINC(I)-PINCR) 770,770,765
  765 PINCR=PINC(I)
  770 CONTINUE
      PRINT 754,NCK
  754 FORMAT (3X,4HNCK=,I2)
  775 IF (NCHR-2) 805,779,779
  779 DO 780 I=1,NSEG
      PRAD(I)=PRAD(I)/PINCR
      PTGT(I)=PTGT(I)/PINCR
  780 CONTINUE
      HIN=HINN/PINCR
  785 PRINT 790,((I,PRAD(I),I,PTGT(I)),I=1,NSEG)
  790 FORMAT (2(3X,5HPRAD(,I2,2H)=,F12.6,3X,5HPTGT(,I2,2H)=,F12.6))
  795 PRINT 625,HIN.
      GO TO 505
  800 IF (NCHR-2) 805,803,803
  803 EEE4(N)=E4(NCK)
      IF (EEE4(N)-EEE4(N-1)) 801,805,805
  801 PRINT 802
  802 FORMAT (3X,83HARCH BEHAVIOUR UNREASONABLE. LOAD IN THE PREVIOUS CY
     1CLE IS NEAREST TO THE ULTIMATE.)
  805 DO 810 I=1,NSEG
      PRAD(I)=PRAD(I)+0.01*PRAD(I)
      PTGT(I)=PTGT(I)+0.01*PTGT(I)
  810 CONTINUE
      HIN=HINN+0.01*HINN
  815 PRINT 820,((I,PRAD(I),I,PTGT(I)),I=1,NSEG)
  820 FORMAT (2(3X,5HPRAD(,I2,2H)=,F12.6,3X,5HPTGT(,I2,2H)=,F12.6))
  825 PRINT 625,HIN
      GO TO 505
  927 DO 930 I=1,NSEG
```

```
      PRAD(I)=PRAD(I)-0.001*PRAD(I)
      PTGT(I)=PTGT(I)-0.001*PTGT(I)
  930 CONTINUE
      HIN=HHIN-0.001*HHIN
      LRD=2
      GO TO 815
      END

*     LIST
*     LABEL
      SUBROUTINE DTPRTS
      DIMENSION PH(31),PV(31),PLN(31),W(31),U(31),CK(31),FRC(62),
     1FRCS(93),EE1(31),EE4(31),D2(62),E1(31),
     2E4(31),FRCSA(93),EO(31),CVTR(31),DEO(31),D2W(31),ADFL(62,62),
     3BDFL(62),FRCA(62),PRAD(29),PTGT(29),PLT(31),HC(25),COR(25)
      COMMON B,D,DCVR,RO,PHIO,P,EBRC,EST,SPRC,NSEG,CVRG,HIN,
     1NPT,EC,EPRC,ERTO,ARG,AR2G,PHI2,THTA,TNO,QO,TNOO,QOO,FRCS,FRC,
     2FRCA,NPT3,CORTN,THTAA,U,W,EE1,EE4,E1,E4
     3,PH,PV,PLN,CK,D2,FRCSA,EO,CVTR,DEO,D2W,ADFL,BDFL
     4,PRAD,PTGT,SYLD,EPSY,PLT,NCHR,HC,COR,NOFL,EUTC,HINCR
C     READ INPUT
      READ 1,B,D,DCVR,RO
      READ 1,PHIO
      READ 1,P
      READ 1,EBRC,EST,SPC,SYLD
      READ 2,NCHR
      READ 2,NSEG
      READ 1,CVRG,EUTC
      READ 1,HI,HINCR
      READ 1,(PRAD(I),I=1,NSEG)
      READ 1,(PTGT(I),I=1,NSEG)
C     COMPUTE PROPERTIES
      SEGN=NSEG
      NPT=NSEG+1
      EPSY=SYLD/EST
      SPRC=0.85*SPC
      EC=1800.+460.*SPRC
      EPRC=2.*SPRC/EC
      ERTO=EST/EBRC
      ARG=B*D+P*B*D*(ERTO-1.)
```

```
      AR2G=((B*D**3)/12.)+P*B*D*(ERTO-1.)*((D-DCVR-DCVR)**2)/4.
      EI=EBRC*AR2G
      EA=EBRC*ARG
      PHI2=PHIO+PHIO
      THTA=PHI2/(SEGN*PHIO)
      THTAA=PHI2/SEGN
      HIN=HI/(SPRC*B*D)
      NPT3=3*NPT
      PRINT 3,B,D,DCVR,RO,PHIO,P
      PRINT 4,EBRC,EST,SPC,SYLD,EUTC,CVRG
      PRINT 5,HIN,NSEG,NCHR
      PRINT 6,((I,PRAD(I),I,PTGT(I)),I=1,NSEG)
    1 FORMAT (4F12.6)
    2 FORMAT (I2)
    3 FORMAT (3X,2HB=,F5.2,3X,2HD=,F5.2,3X,5HDCVR=,F5.3,3X,3HRO=,F6.2,
     13X,5HPHIO=,F8.6,3X,2HP=,F6.3)
    4 FORMAT (3X,5HEBRC=,F12.6,3X,4HEST=,F12.6,3X,4HSPC=,F8.6,3X,5HSYLD=
     1,F9.6,3X,5HEUTC=,F8.6,3X,5HCVRG=,F8.6)
    5 FORMAT (3X,4HHIN=,F9.6,3X,5HNSEG=,I2,3X,5HNCHR=,I2)
    6 FORMAT (2(3X,5HPRAD(,I2,2H)=,F9.6,3X,5HPTGT(,I2,2H)=,F9.6))
      RETURN
      END

*     LIST
*     LABEL
      SUBROUTINE REACTN
      DIMENSION PH(31),PV(31),PLN(31),W(31),U(31),CK(31),FRC(62),
     1FRCS(93),EE1(31),EE4(31),D2(62),E1(31),
     2E4(31),FRCSA(93),EO(31),CVTR(31),DEO(31),D2W(31),ADFL(62,62),
     3BDFL(62),FRCA(62),PRAD(29),PTGT(29),PLT(31),HC(25),COR(25)
      COMMON B,D,DCVR,RO,PHIO,P,EBRC,EST,SPRC,NSEG,CVRG,HIN,
     1NPT,EC,EPRC,ERTO,ARG,AR2G,PHI2,THTA,TNO,QO,TNOO,QOO,FRCS,FRC,
     2FRCA,NPT3,CORTN,THTAA,U,W,EE1,EE4,E1,E4
     3,PH,PV,PLN,CK,D2,FRCSA,EO,CVTR,DEO,D2W,ADFL,BDFL
     4,PRAD,PTGT,SYLD,EPSY,PLT,NCHR,HC,COR
      NPT2=(NPT+1)/2
      NPT1=NPT2+1
      DO 15 I=1,NSEG
      PLN(I)=PRAD(I)/(SPRC*D)
      PLT(I)=PTGT(I)/(SPRC*D)
```

```
15    CONTINUE
      IF (NCHR-2) 20,21,22
20    HOO=HIN
      HO=HOO
      VO=PLN(2)*SINF(PHIO)*RO/B
      VOO=VO
      GO TO 27
21    HOO=HIN
      SPH=2.*PLN(2)*(1.-COSF(PHIO))*RO/B
      HO=-SPH+HOO
      VO=PLN(2)*(SINF(PHIO/2.)*SINF(1.5*PHIO)
     1-SINF(PHIO/2.)**2)*RO/(B*SINF(PHIO))
      VOO=-VO
      GO TO 27
22    THT=-THTAA/2.
      SPH=0
      SPV=0
      VO=0
      DO 25 I=1,NSEG
      THT=THT+THTAA
      PV(I)=PLN(I)*(COSF(PHIO-THT))*THTAA*RO/B
     1-PLT(I)*(SINF(PHIO-THT))*THTAA*RO/B
      PH(I)=PLN(I)*(SINF(PHIO-THT))*THTAA*RO/B
     1+PLT(I)*(COSF(PHIO-THT))*THTAA*RO/B
      CST1=1.+COSF(THT)-SINF(THT)*COSF(PHIO)/SINF(PHIO)
      CST2=(COSF(THT)*COSF(PHIO)/SINF(PHIO))+SINF(THT)
     1-COSF(PHIO)/SINF(PHIO)
      CST3=PV(I)*CST1-PH(I)*CST2
      VO=VO+CST3/2.
      SPH=SPH+PH(I)
25    SPV=SPV+PV(I)
      VOO=SPV-VO
      HOO=HIN
      HO=-SPH+HOO
27    TNO=VO*SINF(PHIO)+HO*COSF(PHIO)
      QO=VO*COSF(PHIO)-HO*SINF(PHIO)
      TNOO=VOO*SINF(PHIO)+HOO*COSF(PHIO)
      QOO=HOO*SINF(PHIO)-VOO*COSF(PHIO)
      RETURN
      END
```

```
*      LIST
*      LABEL
       SUBROUTINE EQEQNS
       DIMENSION PH(31),PV(31),PLN(31),W(31),U(31),CK(31),FRC(62),
      1FRCS(93),EE1(31),EE4(31),D2(62),E1(31),
      2E4(31),FRCSA(93),EO(31),CVTR(31),DEO(31),D2W(31),ADFL(62,62),
      3BDFL(62),FRCA(62),PRAD(29),PTGT(29),PLT(31),HC(25),COR(25)
      4,SN(31),CS(31)
       COMMON B,D,DCVR,RO,PHIO,P,EBRC,EST,SPRC,NSEG,CVRG,HIN,
      1NPT,EC,EPRC,ERTO,ARG,AR2G,PHI2,THTA,TNO,QO,TNOO,QOO,FRCS,FRC,
      2FRCA,NPT3,CORTN,THTAA,U,W,EE1,EE4,E1,E4
      3,PH,PV,PLN,CK,D2,FRCSA,EO,CVTR,DEO,D2W,ADFL,BDFL
      4,PRAD,PTGT,SYLD,EPSY,PLT,NCHR,HC,COR
C      COMPUTE CONSTANTS
       C1=B/RO
       C2=C1*COTF(THTAA/2.)
       C3=PHIO*THTA/SINF(THTAA/2.)
       C4=RO*PHIO*THTA*COSF(THTAA/4.)/(2.*D)
       C5=RO*PHIO*THTA*SINF(THTAA/4.)/(2.*D)
       N3=3*(NSEG+1)
       FRCS(1)=TNO
       FRCS(2)=QO
       FRCS(3)=0
       FRCS(N3-2)=TNOO
       FRCS(N3-1)=QOO
       FRCS(N3)=0
       N1=NSEG-1
       DO 50 I=1,N1
       J=3*I
       CK(I)=(W(I+2)-2.*W(I+1)+W(I))/(PHIO*THTA)
       SN(I)=SINF(CK(I))
       CS(I)=COSF(CK(I))
       A1=C2*CS(I)-C1*SN(I)
       A2=-C2*SN(I)-C1*CS(I)
       A3=C2*CS(I)+C1*SN(I)
       A4=-C2*SN(I)+C1*CS(I)
       A5=A3*FRCS(J-1)+A4*FRCS(J-2)-2.*PLN(I)
       A6=-A4*FRCS(J-1)+A3*FRCS(J-2)+C3*PLT(I)
       FRCS(J+1)=(A1*A6+A2*A5)/(A1**2+A2**2)
```

```
      FRCS(J+2)=(A1*A5-A2*A6)/(A1**2+A2**2)
      FRCS(J+3)=FRCS(J)+C4*FRCS(J-1)+C4*FRCS(J+2)
     1-C5*FRCS(J+1)+C5*FRCS(J-2)
 50   CONTINUE
      RETURN
      END

*     LIST
*     LABEL
      SUBROUTINE STRN1
      DIMENSION PH(31),PV(31),PLN(31),W(31),U(31),CK(31),FRC(62),
     1FRCS(93),EE1(31),EE4(31),D2(62),E1(31),
     2E4(31),FRCSA(93),EO(31),CVTR(31),DEO(31),D2W(31),ADFL(62,62),
     3BDFL(62),FRCA(62),PRAD(29),PTGT(29),PLT(31),HC(25),COR(25)
      COMMON B,D,DCVR,RO,PHIO,P,EBRC,EST,SPRC,NSEG,CVRG,HIN,
     1NPT,EC,EPRC,ERTO,ARG,AR2G,PHI2,THTA,TNO,QO,TNOO,QOO,FRCS,FRC,
     2FRCA,NPT3,CORTN,THTAA,U,W,EE1,EE4,E1,E4
     3,PH,PV,PLN,CK,D2,FRCSA,EO,CVTR,DEO,D2W,ADFL,BDFL
     4,PRAD,PTGT,SYLD,EPSY,PLT,NCHR,HC,COR
      N2=2*NPT
      DO 92 I=1,NPT
      J=3*I
      K=2*I
      FRC(K-1)=FRCS(J-2)*SPRC*B*D
      FRC(K)=FRCS(J)*SPRC*B*D**2
 92   CONTINUE
      DO 130 I=1,NPT
      J=2*I
      IF (FRC(J)) 93,94,94
 93   FRCA(J)=-1.0*FRC(J)
      GO TO 103
 94   FRCA(J)=FRC(J)
 103  IF (FRC(J-1)) 97,98,95
 98   A1=ERTO*P*D+(ERTO-1.)*P*D
      A2=ERTO*P*D*(D-DCVR)+(ERTO-1.)*P*D*DCVR
      A6=(A1**2+4.*A2)
      A3=SQRTF(A6)
      DK=(-A1+A3)/2.
      A4=((ERTO-1.)*P*B*D*(DK-DCVR)*(D-2.*DCVR))/(2.*DK)
      A5=B*DK*(3.*(D-DCVR)-DK)/6.
```

```
      SGMC=FRCA(J)/(A4+A5)
      STR1=SGMC/EBRC
      STR2=-STR1*(D-DK)/DK
      GO TO 127
   97 A7=(-FRC(J-1)/2.-FRCA(J)/(D-2.*DCVR))
      IF (A7) 100,99,99
   99 EE2=((2.*FRC(J)/(D-2.*DCVR))-FRC(J-1))/(P*B*D*EST)
      EE3=(-FRC(J-1)-(2.*FRC(J)/(D-2.*DCVR)))/(P*B*D*EST)
      EE1(I)=-((EE2+EE3)/2.+(EE2-EE3)*D/(2.*(D-2.*DCVR)))
      EE4(I)=-((EE2+EE3)/2.-(EE2-EE3)*D/(2.*(D-2.*DCVR)))
      GO TO 130
   95 Y=((FRCA(J)*D*ARG)/(2.*FRC(J-1)*AR2G))-1.0
      IF (Y) 96,96,100
   96 EE1(I)=(FRC(J-1)/(EBRC*ARG))-((FRC(J)*D)/(2.*EBRC*AR2G))
      EE4(I)=(FRC(J-1)/(EBRC*ARG))+((FRC(J)*D)/(2.*EBRC*AR2G))
      GO TO 130
  100 ETY=FRCA(J)/FRC(J-1)
      ETYT=ETY+(D/2.)-DCVR
      PP=3.*(ETYT-D+DCVR)
      QQ=(3.*ERTO*P*D*ETYT)+(3.*(ERTO-1.)*P*D*(ETYT-D+DCVR+DCVR))
      RR1=-(ERTO*P*B*D*ETYT*(D-DCVR)/2.)
      RR2=-((ERTO-1.)*P*B*D*DCVR*(ETYT-D+DCVR+DCVR))/2.
      RR=(RR1+RR2)*6./B
      IF (RR) 101,101,120
  101 DK=0.
  102 XX=DK**3+PP*DK**2+QQ*DK+RR
      IF (XX) 105,125,115
  105 DK=DK+0.1
      GO TO 102
  115 DK=DK-0.01
      YY=DK**3+PP*DK**2+QQ*DK+RR
      IF (YY) 125,125,115
  120 DK=0.
  121 XX=DK**3+PP*DK**2+QQ*DK+RR
      IF (XX) 123,125,122
  122 DK=DK+0.1
      GO TO 121
  123 DK=DK-0.01
      YY=DK**3+PP*DK**2+QQ*DK+RR
      IF (YY) 123,125,125
```

```
  125  AA1=(ERTO*P*B*D*(D-DCVR-DK))/(2.*DK)
       AA2=((ERTO-1.0)*P*B*D*(DK-DCVR))/(2.*DK)
       AA3=B*DK/2.
       AA=-AA1+AA2+AA3
       SGMC=FRC(J-1)/AA
       STR1=SGMC/EBRC
       STR2=-STR1*(D-DK)/DK
  127  IF (FRC(J)) 126,128,128
  126  EE4(I)=STR2
       EE1(I)=STR1
       GO TO 130
  128  EE1(I)=STR2
       EE4(I)=STR1
  130  CONTINUE
       RETURN
       END

*      LIST
*      LABEL
       SUBROUTINE STRN2
       DIMENSION PH(31),PV(31),PLN(31),W(31),U(31),CK(31),FRC(62),
      1FRCS(93),EE1(31),EE4(31),D2(62),E1(31),
      2E4(31),FRCSA(93),EO(31),CVTR(31),DEO(31),D2W(31),ADFL(62,62),
      3BDFL(62),FRCA(62),PRAD(29),PTGT(29),PLT(31),HC(25),COR(25)
       COMMON B,D,DCVR,RO,PHIO,P,EBRC,EST,SPRC,NSEG,CVRG,HIN,
      1NPT,EC,EPRC,ERTO,ARG,AR2G,PHI2,THTA,TNO,QO,TNOO,QOO,FRCS,FRC,
      2FRCA,NPT3,CORTN,THTAA,U,W,EE1,EE4,E1,E4
      3,PH,PV,PLN,CK,D2,FRCSA,EO,CVTR,DEO,D2W,ADFL,BDFL
      4,PRAD,PTGT,SYLD,EPSY,PLT,NCHR,HC,COR,NOFL
       SK=(EST*P*(ERTO-1.))/(2.*ERTO*SPRC)
       SK1=(EST*P)/(2.*SPRC)
       DO 250 I=1,NPT
       LL=0
       J=3*I
       IF (EE1(I)) 131,131,135
  131  IF (EE4(I)) 132,132,135
  132  E1(I)=EE1(I)
       E4(I)=EE4(I)
       GO TO 250
  135  IF(FRCS(J)) 140,145,145
```

```
 140  FRCSA(J)=-1.0*FRCS(J)
      X=EE4(I)
      Y=EE1(I)
      GO TO 150
 145  FRCSA(J)=FRCS(J)
      X=EE1(I)
      Y=EE4(I)
 150  IF(X)155,180,180
C     CALCULATION OF STRAINS WHEN SECTION
C     IS PARTLY IN TENSION AND PARTLY IN COMPRESSION
 155  DLTX=0
      DLTY=0
 160  X=X+DLTX
      Y=Y+DLTY
      F1=SK1*(Y**2-X**2)
      F2=-SK1*X*Y/ERTO
      F3=SK1*X**2/ERTO
      F4=-SK1*(D-DCVR)*(Y-X)**2/(ERTO*D)
      F5=Y**2/EPRC
      F6=-Y**3/(3.*EPRC**2)
      F7=-FRCS(J-2)*(Y-X)
      FXY=F1+F2+F3+F4+F5+F6+F7
      FX1=-2.*SK1*X
      FX2=FRCS(J-2)
      FX3=-SK1*(Y-2.*X)/ERTO
      FX4=2.*SK1*(D-DCVR)*(Y-X)/(ERTO*D)
      FXYX=FX1+FX2+FX3+FX4
      FY1=2.*SK1*Y
      FY2=-SK1*X/ERTO
      FY3=-2.*SK1*(D-DCVR)*(Y-X)/(ERTO*D)
      FY4=2.*Y/EPRC
      FY5=-Y**2/EPRC**2
      FY6=-FRCS(J-2)
      FXYY=FY1+FY2+FY3+FY4+FY5+FY6
      G1=SK1*(D-DCVR-DCVR)**2*(Y-X)**3/(2.*D**2)
      G2=-SK1*(D-DCVR-DCVR)*X*(Y-X)**2/(2.*D*ERTO)
      G3=-SK1*(D-DCVR-DCVR)*(D-DCVR)*(Y-X)**3/(2.*D**2*ERTO)
      G4=Y**3/(6.*EPRC)
      G5=-Y**4/(12.*EPRC**2)
      G6=-X*Y**2/(2.*EPRC)
```

```
      G7=X*Y**3/(6.*EPRC**2)
      G8=-FRCSA(J)*(Y-X)**2
      GXY=G1+G2+G3+G4+G5+G6+G7+G8
      GX1=-3.*SK1*(D-DCVR-DCVR)**2*(Y-X)**2/(2.*D**2)
      GX2=-SK1*(D-DCVR-DCVR)*(Y-X)**2/(2.*D*ERTO)
      GX3=SK1*(D-DCVR-DCVR)*X*(Y-X)/(ERTO*D)
      GX4=3.*SK1*(D-DCVR-DCVR)*(D-DCVR)*(Y-X)**2/(2.*D**2*ERTO)
      GX5=-Y**2/(2.*EPRC)
      GX6=Y**3/(6.*EPRC**2)
      GX7=2.*FRCSA(J)*(Y-X)
      GXYX=GX1+GX2+GX3+GX4+GX5+GX6+GX7
      GY1=3.*SK1*(D-DCVR-DCVR)**2*(Y-X)**2/(2.*D**2)
      GY2=-SK1*(D-DCVR-DCVR)*X*(Y-X)/(D*ERTO)
      GY3=-3.*SK1*(D-DCVR-DCVR)*(D-DCVR)*(Y-X)**2/(2.*ERTO*D**2)
      GY4=Y**2/(2.*EPRC)
      GY5=-Y**3/(3.*EPRC**2)
      GY6=-X*Y/EPRC
      GY7=X*Y**2/(2.*EPRC**2)
      GY8=-2.*FRCSA(J)*(Y-X)
      GXYY=GY1+GY2+GY3+GY4+GY5+GY6+GY7+GY8
      DLTX=(FXYY*GXY-FXY*GXYY)/(FXYX*GXYY-FXYY*GXYX)
      DLTY=(FXY*GXYX-FXYX*GXY)/(FXYX*GXYY-FXYY*GXYX)
      IF(DLTX)161,162,162
  161 DLTXA=-1.0*DLTX
      GO TO 163
  162 DLTXA=DLTX
  163 IF(DLTY)164,165,165
  164 DLTYA=-1.0*DLTY
      GO TO 166
  165 DLTYA=DLTY
  166 IF(DLTXA-CVRG)168,168,160
  168 IF(DLTYA-CVRG)170,170,160
  170 XX=X+(Y-X)*DCVR/D
      YY=X+(Y-X)*(D-DCVR)/D
      IF(ABSF(XX)-EPSY) 200,200,201
  200 IF(ABSF(YY)-EPSY) 225,225,210
  201 IF(ABSF(YY)-EPSY) 205,205,215
C     TENSION STEEL YIELDED
  205 DLTX=0
      DLTY=0
```

```
206   X=X+DLTX
      Y=Y+DLTY
      LL=LL+1
      IF (X) 505,500,500
500   X=X-2.*DLTX
505   IF (Y) 510,510,514
510   Y=Y-2.*DLTY
514   IF (LL-30) 515,251,251
515   F1=-SK1*EPSY*(Y-X)
      F2=(ERTO*SK1-SK1)*X*(Y-X)/ERTO
      F3=(ERTO*SK1-SK1)*(D-DCVR)*(Y-X)**2/(ERTO*D)
      F4=Y**2/EPRC
      F5=-Y**3/(3.*EPRC**2)
      F6=-FRCS(J-2)*(Y-X)
      FXY=F1+F2+F3+F4+F5+F6
      FX1=SK1*EPSY
      FX2=(ERTO*SK1-SK1)*(Y-2.*X)/ERTO
      FX3=-(ERTO*SK1-SK1)*(D-DCVR)*(Y-X)*2./(D*ERTO)
      FX4=FRCS(J-2)
      FXYX=FX1+FX2+FX3+FX4
      FY1=-FX1
      FY2=(ERTO*SK1-SK1)*X/ERTO
      FY3=-FX3
      FY4=2.*Y/EPRC
      FY5=-Y**2/EPRC**2
      FY6=-FRCS(J-2)
      FXYY=FY1+FY2+FY3+FY4+FY5+FY6
      G1=SK1*(D-2.*DCVR)*(ERTO-1.)*X*(Y-X)**2/(2.*D*ERTO)
      G2=G1*(D-DCVR)*(Y-X)/(X*D)
      G3=SK1*(D-2.*DCVR)*EPSY*(Y-X)**2/(2.*D)
      G4=Y**3/(6.*EPRC)
      G5=-Y**4/(12.*EPRC**2)
      G6=-X*Y**2/(2.*EPRC)
      G7=X*Y**3/(6.*EPRC**2)
      G8=-FRCSA(J)*(Y-X)**2
      GXY=G1+G2+G3+G4+G5+G6+G7+G8
      GX1=G1/X
      GX2=-2.*G1/(Y-X)
      GX3=-3.*G2/(Y-X)
      GX4=-2.*G3/(Y-X)
```

```
      GX5=-Y**2/(2.*EPRC)
      GX6=Y**3/(6.*EPRC**2)
      GX7=2.*FRCSA(J)*(Y-X)
      GXYX=GX1+GX2+GX3+GX4+GX5+GX6+GX7
      GY1=-GX2
      GY2=-GX3
      GY3=-GX4
      GY4=-GX5
      GY5=-2.*GX6
      GY6=-X*Y/EPRC
      GY7=X*Y**2/(2.*EPRC**2)
      GY8=-GX7
      GXYY=GY1+GY2+GY3+GY4+GY5+GY6+GY7+GY8
      DLTX=(FXYY*GXY-FXY*GXYY)/(FXYX*GXYY-FXYY*GXYX)
      DLTY=(FXY*GXYX-FXYX*GXY)/(FXYX*GXYY-FXYY*GXYX)
      IF(ABSF(DLTX)-CVRG) 207,207,206
  207 IF(ABSF(DLTY)-CVRG) 208,208,206
  208 YY=X+(Y-X)*(D-DCVR)/D
      IF(ABSF(YY)-EPSY) 225,225,215
C     COMPRESSION STEEL YIELDED
  210 DLTX=0
      DLTY=0
  211 X=X+DLTX
      Y=Y+DLTY
      LL=LL+1
      IF (X) 605,600,600
  600 X=X-2.*DLTX
  605 IF (Y) 610,610,614
  610 Y=Y-2.*DLTY
  614 IF (LL-30) 615,251,251
  615 F1=SK1*X*(Y-X)
      F2=SK1*DCVR*(Y-X)**2/D
      F3=SK1*EPSY*(Y-X)
      F4=-SK1*X*(Y-X)/ERTO
      F5=-SK1*(D-DCVR)*(Y-X)**2/(ERTO*D)
      F6=Y**2/EPRC
      F7=-Y**3/(3.*EPRC**2)
      F8=-FRCS(J-2)*(Y-X)
      FXY=F1+F2+F3+F4+F5+F6+F7+F8
      FX1=SK1*(Y-2.*X)
```

```
FX2=-2.*SK1*DCVR*(Y-X)/D
FX3=-SK1*EPSY
FX4=-SK1*(Y-2.*X)/ERTO
FX5=2.*SK1*(D-DCVR)*(Y-X)/(ERTO*D)
FX6=FRCS(J-2)
FXYX=FX1+FX2+FX3+FX4+FX5+FX6
FY1=SK1*X
FY2=-FX2
FY3=-FX3
FY4=-SK1*X/ERTO
FY5=-FX5
FY6=2.*Y/EPRC
FY7=-Y**2/EPRC**2
FY8=-FRCS(J-2)
FXYY=FY1+FY2+FY3+FY4+FY5+FY6+FY7+FY8
G1=SK1*(D-2.*DCVR)*EPSY*(Y-X)**2/(2.*D)
G2=-SK1*(D-2.*DCVR)*X*(Y-X)**2/(2.*D*ERTO)
G3=G2*(D-DCVR)*(Y-X)/(X*D)
G4=G2*ERTO
G5=G3*ERTO*DCVR/(D-DCVR)
G6=Y**3/(6.*EPRC)
G7=-Y**4/(12.*EPRC**2)
G8=-X*Y**2/(2.*EPRC)
G9=X*Y**3/(6.*EPRC**2)
G10=-FRCSA(J)*(Y-X)**2
GXY=G1+G2+G3+G4+G5+G6+G7+G8+G9+G10
GX1=-G1*2./(Y-X)
GX2=G2/X
GX3=-2.*G2/(Y-X)
GX4=-3.*G3/(Y-X)
GX5=G4/X
GX6=-2.*G4/(Y-X)
GX7=-3.*G5/(Y-X)
GX8=-Y**2/(2.*EPRC)
GX9=Y**3/(6.*EPRC**2)
GX10=2.*FRCSA(J)*(Y-X)
GXYX=GX1+GX2+GX3+GX4+GX5+GX6+GX7+GX8+GX9+GX10
GY1=-GX1
GY2=-GX3
GY3=-GX4
```

```
      GY4=GY2*ERTO/2.
      GY5=-GX7
      GY6=Y**2/(2.*EPRC)
      GY7=-Y**3/(3.*EPRC**2)
      GY8=-X*Y/EPRC
      GY9=X*Y**2/(2.*EPRC**2)
      GY10=-GX10
      GXYY=GX1+GX2+GX3+GX4+GX5+GX6+GX7+GX8+GX9+GX10
      DLTX=(FXYY*GXY-FXY*GXYY)/(FXYX*GXYY-FXYY*GXYX)
      DLTY=(FXY*GXYX-FXYX*GXY)/(FXYX*GXYY-FXYY*GXYX)
      IF(ABSF(DLTX)-CVRG) 212,212,211
  212 IF(ABSF(DLTY)-CVRG) 213,213,211
  213 XX=X+(Y-X)*DCVR/D
      IF(ABSF(XX)-EPSY) 225,225,215
C     BOTH STEELS YIELDED
  215 DLTX=0
      DLTY=0
  216 X=X+DLTX
      Y=Y+DLTY
      LL=LL+1
      IF (X) 705,700,700
  700 X=X-2.*DLTX
  705 IF (Y) 710,710,714
  710 Y=Y-2.*DLTY
  714 IF (LL-30) 715,251,251
  715 F1=-SK1*X*(Y-X)/ERTO
      F2=-SK1*(D-DCVR)*(Y-X)**2/(ERTO*D)
      F3=Y**2/EPRC
      F4=-Y**3/(3.*EPRC**2)
      F5=-FRCS(J-2)*(Y-X)
      FXY=F1+F2+F3+F4+F5
      FX1=-SK1*(Y-2.*X)/ERTO
      FX2=2.*SK1*(D-DCVR)*(Y-X)/(D*ERTO)
      FX3=FRCS(J-2)
      FXYX=FX1+FX2+FX3
      FY1=-SK1*X/ERTO
      FY2=-FX2
      FY3=2.*Y/EPRC
      FY4=-Y**2/EPRC**2
      FY5=-FRCS(J-2)
```

```
      FXYY=FY1+FY2+FY3+FY4+FY5
      G1=SK1*(D-2.*DCVR)*EPSY*(Y-X)**2/D
      G2=-SK1*(D-2.*DCVR)*X*(Y-X)**2/(2.*D*ERTO)
      G3=G2*(D-DCVR)*(Y-X)/(X*D)
      G4=Y**3/(6.*EPRC)
      G5=-Y**4/(12.*EPRC**2)
      G6=-X*Y**2/(2.*EPRC)
      G7=X*Y**3/(6.*EPRC**2)
      G8=-FRCSA(J)*(Y-X)**2
      GXY=G1+G2+G3+G4+G5+G6+G7+G8
      GX1=-2.*G1/(Y-X)
      GX2=G2/X
      GX3=-2.*G2/(Y-X)
      GX4=-3.*G3/(Y-X)
      GX5=-Y**2/(2.*EPRC)
      GX6=Y**3/(6.*EPRC**2)
      GX7=2.*FRCSA(J)*(Y-X)
      GXYX=GX1+GX2+GX3+GX4+GX5+GX6+GX7
      GY1=-GX1
      GY2=-GX3
      GY3=-GX4
      GY4=-GX5
      GY5=-Y**3/(3.*EPRC**2)
      GY6=-X*Y/EPRC
      GY7=X*Y**2/(2.*EPRC**2)
      GY8=-GX7
      GXYY=GY1+GY2+GY3+GY4+GY5+GY6+GY7+GY8
      DLTX=(FXYY*GXY-FXY*GXYY)/(FXYX*GXYY-FXYY*GXYX)
      DLTY=(FXY*GXYX-FXYX*GXY)/(FXYX*GXYY-FXYY*GXYX)
      IF(ABSF(DLTX)-CVRG) 217,217,216
  217 IF(ABSF(DLTY)-CVRG) 225,225,216
  225 IF(FRCS(J)) 226,228,228
  226 E4(I)=X
      E1(I)=Y
      GO TO 250
  228 E1(I)=X
      E4(I)=Y
      GO TO 250
C     CALCULATION OF STRAINS WHEN SECTION IS COMPLETELY IN COMPRESSION
  180 DLTX=0
```

```
      DLTY=0
  185 X=X+DLTX
      Y=Y+DLTY
      F1=SK*(X+Y)
      F2=(X+Y)/EPRC
      F3=-(X**2+X*Y+Y**2)/(3.*EPRC**2)
      F4=-FRCS(J-2)
      FXY=F1+F2+F3+F4
      FX1=(SK*EPRC+1.0)/EPRC
      FX2=-(2.*X+Y)/(3.*EPRC**2)
      FXYX=FX1+FX2
      FY1=FX1
      FY2=-(X+2.*Y)/(3.*EPRC**2)
      FXYY=FY1+FY2
      G1=SK*(Y-X)**2*(D-DCVR-DCVR)**2/(2.*D**2)
      G2=-FRCSA(J)*(Y-X)
      G3=(Y-X)**2/(6.*EPRC)
      G4=-(Y+X)*(Y-X)**2/(12.*EPRC**2)
      GXY=G1+G2+G3+G4
      GX1=-SK*(Y-X)*(D-DCVR-DCVR)**2/D**2
      GX2=-(Y-X)/(3.*EPRC)
      GX3=(Y**2+2.*Y*X-3.*X**2)/(12.*EPRC**2)
      GX4=FRCSA(J)
      GXYX=GX1+GX2+GX3+GX4
      GY1=-GX1
      GY2=-GX2
      GY3=(X**2+2.*Y*X-3.*Y**2)/(12.*EPRC**2)
      GY4=-GX4
      GXYY=GY1+GY2+GY3+GY4
      DLTX=(FXYY*GXY-FXY*GXYY)/(FXYX*GXYY-FXYY*GXYX)
      DLTY=(FXY*GXYX-FXYX*GXY)/(FXYX*GXYY-FXYY*GXYX)
      IF(DLTX)186,187,187
  186 DLTXA=-1.0*DLTX
      GO TO 188
  187 DLTXA=DLTX
  188 IF(DLTY)189,190,190
  189 DLTYA=-1.0*DLTY
      GO TO 191
  190 DLTYA=DLTY
  191 IF(DLTXA-CVRG)193,193,185
```

```
  193  IF(DLTYA-CVRG)195,195,185
  195  XX=X+(Y-X)*DCVR/D
       YY=X+(Y-X)*(D-DCVR)/D
       IF(ABSF(YY)-EPSY)245,245,230
  230  IF(ABSF(XX)-EPSY)235,235,240
C      COMPRESSION STEEL YIELDED
  235  DLTX=0
       DLTY=0
  236  X=X+DLTX
       Y=Y+DLTY
       LL=LL+1
       IF (LL-30) 815,251,251
  815  F1=SK1*EPSY
       F2=SK*X
       F3=-SK1*(X*D+(Y-X)*(D-DCVR))/(ERTO*D)
       F4=(Y+X)/EPRC
       F5=-(Y**2+Y*X+X**2)/(3.*EPRC**2)
       F6=-FRCS(J-2)
       F7=SK*(Y-X)*DCVR/D
       FXY=F1+F2+F3+F4+F5+F6+F7
       FX1=SK*(D-DCVR)/D
       FX2=-SK1*DCVR/(ERTO*D)
       FX3=1.0/EPRC
       FX4=-(Y+2.*X)/(3.*EPRC**2)
       FXYX=FX1+FX2+FX3+FX4
       FY1=SK*DCVR/D
       FY2=-SK1*(D-DCVR)/(ERTO*D)
       FY3=1.0/EPRC
       FY4=-(2.*Y+X)/(3.*EPRC**2)
       FXYY=FY1+FY2+FY3+FY4
       G1=-SK*(D-2.*DCVR)*X*(Y-X)/(2.*D)
       G2=-SK*(D-2.*DCVR)*DCVR*(Y-X)**2/(2.*D**2)
       G3=SK1*(D-2.*DCVR)*EPSY*(Y-X)/(2.*D)
       G4=-G3*X/(ERTO*EPSY)
       G5=G4*(D-DCYR)*(Y-X)/(X*D)
       G6=(Y-X)**2/(6.*EPRC)
       G7=-(Y+X)*(Y-X)**2/(12.*EPRC**2)
       G8=-FRCSA(J)*(Y-X)
       GXY=G1+G2+G3+G4+G5+G6+G7+G8
       GX1=-SK*(D-2.*DCVR)*(Y-2.*X)/(2.*D)
```

```
      GX2=SK*(D-2.*DCVR)*DCVR*(Y-X)/(D**2)
      GX3=-SK1*(Y-2.*X)*(D-2.*DCVR)/(2.*ERTO*D)
      GX4=SK1*(D-DCVR)*(Y-X)*(D-2.*DCVR)/(ERTO*D**2)
      GX5=-SK1*(D-2.*DCVR)*EPSY/(2.*D)
      GX6=-(Y-X)/(3.*EPRC)
      GX7=(-3.*X**2+2.*X*Y+Y**2)/(12.*EPRC**2)
      GX8=FRCSA(J)
      GXYX=GX1+GX2+GX3+GX4+GX5+GX6+GX7+GX8
      GY1=-SK*(D-2.*DCVR)*X/(2.*D)
      GY2=-GX2
      GY3=-SK1*X*(D-2.*DCVR)/(2.*ERTO*D)
      GY4=-GX4
      GY5=-GX5
      GY6=-GX6
      GY7=(-3.*Y**2+2.*X*Y+X**2)/(12.*EPRC**2)
      GY8=-GX8
      GXYY=GY1+GY2+GY3+GY4+GY5+GY6+GY7+GY8
      DLTX=(FXYY*GXY-FXY*GXYY)/(FXYX*GXYY-FXYY*GXYX)
      DLTY=(FXY*GXYX-FXYX*GXY)/(FXYX*GXYY-FXYY*GXYX)
      IF(ABSF(DLTX)-CVRG)237,237,236
  237 IF(ABSF(DLTY)-CVRG)238,238,236
  238 XX=X+(Y-X)*DCVR/D
      IF(ABSF(XX)-EPSY)245,245,240
C     BOTH STEELS YIELDED
  240 DLTX=0
      DLTY=0
  241 X=X+DLTX
      Y=Y+DLTY
      LL=LL+1
      IF (LL-30) 915,251,251
  915 F1=2.*SK1*EPSY
      F2=-SK1*(X+Y)/ERTO
      F3=(X+Y)/EPRC
      F4=-(Y**2+Y*X+X**2)/(3.*EPRC**2)
      F5=-FRCS(J-2)
      FXY=F1+F2+F3+F4+F5
      FX1=(ERTO-SK1*EPRC)/(EPRC*ERTO)
      FX2=-(Y+2.*X)/(3.*EPRC**2)
      FXYX=FX1+FX2
      FY1=FX1
```

```
      FY2=-(2.*Y+X)/(3.*EPRC**2)
      FXYY=FY1+FY2
      G1=-SK1*(Y-X)*(D-2.*DCVR)**2/(2.*ERTO*D**2)
      G2=(Y-X)**2/(6.*EPRC)
      G3=-(Y+X)*(Y-X)**2/(12.*EPRC**2)
      G4=-FRCSA(J)*(Y-X)
      GXY=G1+G2+G3+G4
      GX1=SK1*(D-2.*DCVR)**2/(2.*ERTO*D**2)
      GX2=-(Y-X)/(3.*EPRC)
      GX3=(-3.*X**2+2.*X*Y+Y**2)/(12.*EPRC**2)
      GX4=FRCSA(J)
      GXYX=GX1+GX2+GX3+GX4
      GY1=-GX1
      GY2=-GX2
      GY3=(-3.*Y**2+2.*X*Y+X**2)/(12.*EPRC**2)
      GY4=-GX4
      GXYY=GY1+GY2+GY3+GY4
      DLTX=(FXYY*GXY-FXY*GXYY)/(FXYX*GXYY-FXYY*GXYX)
      DLTY=(FXY*GXYX-FXYX*GXY)/(FXYX*GXYY-FXYY*GXYX)
      IF(ABSF(DLTX)-CVRG)242,242,241
  242 IF(ABSF(DLTY)-CVRG)245,245,241
  245 IF(FRCS(J))246,248,248
  246 E4(I)=X
      E1(I)=Y
      GO TO 250
  248 E1(I)=X
      E4(I)=Y
  250 CONTINUE
      GO TO 253
  251 PRINT 252
  252 FORMAT (3X,47HLOAD IS TOO HIGH. IT IS REDUCED IN NEXT CYCLES.)
      NOFL=2
  253 RETURN
      END

*     LIST
*     LABEL
      SUBROUTINE DEFLNS
      DIMENSION PH(31),PV(31),PLN(31),W(31),U(31),CK(31),FRC(62),
     2E4(31),FRCSA(93),EO(31),CVTR(31),DEO(31),D2W(31),ADFL(62,62),
```

```
     1FRCS(93),EE1(31),EE4(31),D2(62),E1(31),
     3BDFL(62),FRCA(62),PRAD(29),PTGT(29),PLT(31),HC(25),COR(25)
     4,CW(30)
      COMMON B,D,DCVR,RO,PHIO,P,EBRC,EST,SPRC,NSEG,CVRG,HIN,
     1NPT,EC,EPRC,ERTO,ARG,AR2G,PHI2,THTA,TNO,QO,TNOO,QOO,FRCS,FRC,
     2FRCA,NPT3,CORTN,THTAA,U,W,EE1,EE4,E1,E4
     3,PH,PV,PLN,CK,D2,FRCSA,EO,CVTR,DEO,D2W,ADFL,BDFL
     4,PRAD,PTGT,SYLD,EPSY,PLT,NCHR,HC,COR
      DO 260 I=1,NPT
      EO(I)=0
      CVTR(I)=0
      DEO(I)=0
  260 D2W(I)=0
      DO 270 I=1,NPT
      CVTR(I)=(E1(I)-E4(I))*RO/D
  270 CONTINUE
      DO 275 I=2,NSEG
      EO(I)=(E1(I)+E4(I))/2.+(W(I+1)-W(I-1))**2/(8.*THTAA**2)+(U(I)*(W(I
     1+1)-W(I-1)))/(2.*THTAA)
  275 CONTINUE
      EO(1)=(E1(1)+E4(1))/2.+W(2)**2/(2.*THTAA**2)
      EO(NPT)=(E1(NPT)+E4(NPT))/2.-W(NSEG)**2/(2.*THTAA**2)
      DO 280 I=2,NSEG
      DEO(I)=(EO(I+1)-EO(I-1))/(2.*THTA)
  280 CONTINUE
      DEO(1)=(EO(2)-EO(1))/THTA
      DO 290 I=1,NPT
      D2W(I)=(PHIO**2)*(CVTR(I)-EO(I))
  290 CONTINUE
      CW(1)=0.0
      DO 295 I=2,NSEG
      CW(I)=CW(I-1)+D2W(I-1)*THTA
  295 CONTINUE
C     ADFL=COEFFICIENT MATRIX OF DEFLECTION EQUATIONS
      NN=NSEG-2
      N1=NSEG-1
      N2=2*NSEG
      DO 300 I=1,N2
      DO 300 J=1,N2
  300 ADFL(I,J)=0
```

```
      DO 320 I=2,N1
      J=2*I-1
      ADFL(J,1)=-THTA
      ADFL(J,J-1)=-1.0
      ADFL(J,J+1)=1.0
      ADFL(J+1,1)=-PHIO*THTA**2/2.
      ADFL(J+1,J-1)=-PHIO*THTA
      ADFL(J+1,J)=-1.
      ADFL(J+1,J+2)=1.
  320 CONTINUE
      ADFL(1,1)=-THTA
      ADFL(1,2)=1.
      ADFL(2,1)=-PHIO*THTA**2/2.
      ADFL(2,3)=1.
      ADFL(N2-1,1)=-THTA
      ADFL(N2-1,N2-2)=-1.
      ADFL(N2-1,N2)=1.0
      ADFL(N2,1)=ADFL(2,1)
      ADFL(N2,N2-2)=-PHIO*THTA
      ADFL(N2,N2-1)=-1.0
      DO 330 I=1,N2
  330 BDFL(I)=0
      DO 340 I=1,NSEG
      J=2*I
      BDFL(J-1)=CW(I)*THTA+D2W(I)*THTA**2/2.
      BDFL(J)=CW(I)*PHIO*THTA**2/2.-PHIO*EO(I)*THTA-PHIO*DEO(I)*THTA**2/
     12.
  340 CONTINUE
  345 FORMAT(5H  D1=,E16.9/(6F18.9))
  350 FORMAT(15H OVER/UNDERFLOW)
  355 FORMAT(14H A IS SINGULAR)
      D1=1.0
      M=XSIMEQF(62,N2,1,ADFL,BDFL,D1,D2)
      GO TO (360,365,370),M
  365 PRINT 350
      CALL EXIT
  370 PRINT 355
      CALL EXIT
  360 PRINT 345,D1,(ADFL(I,1),I=1,N2)
      DO 380 I=1,NPT
```

```
      U(I)=0
380   W(I)=0
      DO 390 I=1,NSEG
      J=2*I
      U(I)=ADFL(J-1,1)
      W(I+1)=ADFL(J,1)
390   CONTINUE
      RETURN
      END
```

APPENDIX IV

CONCISED FLOW-CHART AND DIGITAL COMPUTER PROGRAM

DYNAMIC CASE

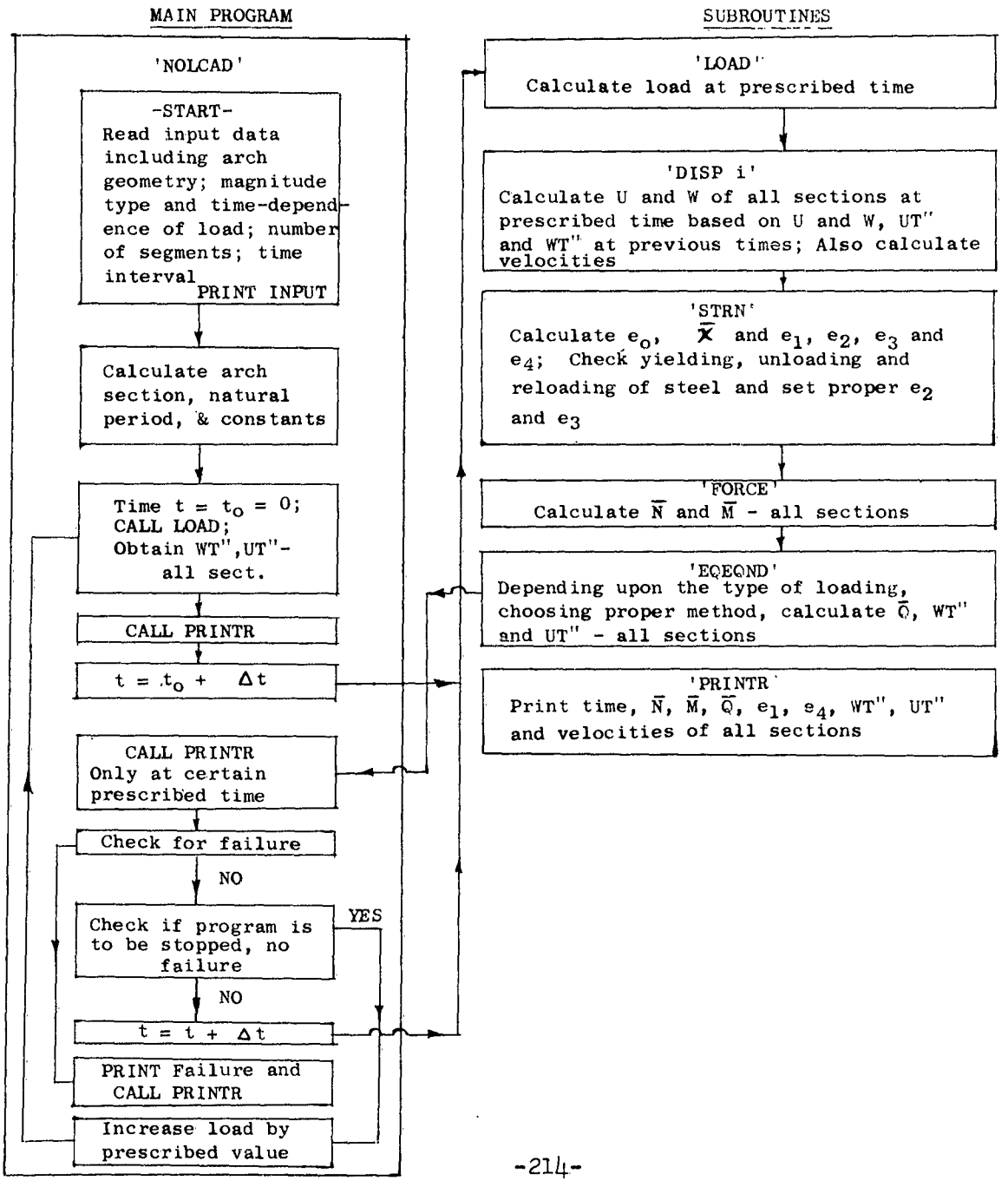

```
*       LIST
*       LABEL
CNOLCAD
C       DYNAMIC LOADING ON ARCHES
C       VIJAY N. GUPCHUP
        DIMENSION PRDPK(30),PTGPK(30),TRS(30),TLD(30),TDC(30),PLNPK(30),
       1PLTPK(30),TRSN(30),TLDN(30),TDCN(30),PLN(30,3),PLT(30,3),U(31,3),
       2W(31,3),DUT(30,3),DWT(30,3),D2UT(30,3),D2WT(30,3),D2UTX(30,20),
       3D2WTX(30,20),CHKU(30),CHKW(30),E4(31,3),E1(31,3),E2(31,3),E3(31,3)
       4,E2MX(31),E3MX(31),TN(31),BM(31),Q(31),CK(30),SN(30),
       5CS(30),EO(31,3),CVTR(31,3),A1(30),A2(30),A3(30),A4(30),QX(31,20),
       6EE2(31,3),EE3(31,3)
        COMMON B,D,DCVR,RO,PHIO,P,RHO,PI,EST,SYLD,SPC,EUTC,NSEG,NPT,PLNPK,
       1PLTPK,TRSN,TLDN,TDCN,EPSYS,SPRCS,EC,PHI2,THTA,THTAA,NSEG3,TNAT,
       2EPRCS,SPRCD,EPRCD,SYLDD,EPSYD,C1,C2,C3,C4,C5,C6,TM,JTM,KTR,PLN,PLT
       3,TINT,CVRG,U,W,DUT,DWT,D2UT,D2WT,D2UTX,D2WTX,E1,E2,E3,E4,E2MX,E3MX
       4,TN,BM,Q,EO,CVTR,A1,A2,A3,A4,QX,EE2,EE3,PRDPK,PTGPK,TRS,TLD,TDC,
       5NLOAD,CHKU,CHKW,NCHR
C       READ INPUT
  5     READ 1,B,D,DCVR,RO
        READ 1,PHIO,P,RHO,PI
        READ 1,EST,SYLDS,SPC,EUTC
        READ 1,TINTV,CVRG,TSTP,PINCR
        READ 1,SC,SST
        READ 2,NCHR,NLOAD,NSEG,MLT
        READ 1,(PRDPK(I),I=1,NSEG)
        READ 1,(PTGPK(I),I=1,NSEG)
        READ 1,(TRS(I),I=1,NSEG)
        READ 1,(TLD(I),I=1,NSEG)
        READ 1,(TDC(I),I=1,NSEG)
  1     FORMAT (4F12.6)
  2     FORMAT (4I3)
C       COMPUTE PROPERTIES
        SEGN=NSEG
        NPT=NSEG+1
        EPSYS=SYLDS/EST
        SPRCS=0.85*SPC
        EC=1800.+460.*SPRCS
        EPRCS=2.*SPRCS/EC
        PHI2=PHIO+PHIO
```

```
      THTA=PHI2/(SEGN*PHIO)
      THTAA=PHI2/SEGN
      NSEG3=3*NSEG
      IF (NCHR-2) 10,11,11
10    TNAT=RO/21.6
      GO TO 15
11    PSY=(PI**2+1.5*PHIO**2)/(PI**2-PHIO**2)
      X=SQRTF(P/2.)
      TNAT=(PHIO**2)*(RO**2)*PSY/(425.*D*X)
15    SPRCD=SC*SPRCS
      EPRCD=SC*EPRCS
      SYLDD=SST*SYLDS
      EPSYD=SST*EPSYS
      TINT=TINTV/TNAT
      MPI=MLT
      DO 16 I=1,NPT
      TN(I)=0
      Q(I)=0
      BM(I)=0
      U(I,1)=0
      W(I,1)=0
16    CONTINUE
      PRINT 20,B,D,DCVR,RO,PHIO,P
      PRINT 21,RHO,EST,SPC,SYLDS,EUTC,EPRCS
      PRINT 22,SPRCD,EPRCD,SYLDD,EPSYD,TNAT
      PRINT 23,NCHR,NSEG,MLT
      PRINT 24,TINT,CVRG,SC,SST,TSTP,PINCR
      PRINT 25,((I,PRDPK(I),I,PTGPK(I),I,TRS(I),I,TLD(I),I,TDC(I)),I=1,
     1NSEG)
20    FORMAT (3X,2HB=,F5.2,3X,2HD=,F5.2,3X,5HDCVR=,F5.3,3X,3HRO=,F6.2,
     13X,5HPHIO=,F8.6,3X,2HP=,F6.3)
21    FORMAT (3X,4HRHO=,F8.6,3X,4HEST=,F12.6,3X,4HSPC=,F8.6,3X,6HSYLDS=,
     1F9.6,3X,5HEUTC=,F8.6,3X,6HEPRCS=,F8.6)
22    FORMAT (3X,6HSPRCD=,F8.6,3X,6HEPRCD=,F8.6,3X,6HSYLDD=,F9.6,3X,
     16HEPSYD=,F8.6,3X,5HTNAT=,F8.4)
23    FORMAT (3X,5HNCHR=,I2,3X,5HNSEG=,I2,3X,4HMLT=,I2)
24    FORMAT (3X,5HTINT=,F8.6,3X,5HCVRG=,F8.6,3X,3HSC=,F8.6,3X,4HSST=,
     1F8.6,3X,5HTSTP=,F8.4,3X,6HPINCR=,F6.3)
25    FORMAT (3X,6HPRDPK(,I2,2H)=,F9.6,3X,6HPTGPK(,I2,2H)=,F9.6,3X,4HTRS
     1(,I2,2H)=,F9.6,3X,4HTLD(,I2,2H)=,F9.6,3X,4HTDC(,I2,2H)=,F9.6)
```

```
C       NONDIMENSIONALIZATION OF LOADS
        DO 30 I=1,NSEG
        PLNPK(I)=PRDPK(I)/(SPRCS*D)
        PLTPK(I)=PTGPK(I)/(SPRCS*D)
        TRSN(I)=TRS(I)/TNAT
        TLDN(I)=TLD(I)/TNAT
        TDCN(I)=TDC(I)/TNAT
 30     CONTINUE
C       COMPUTE CONSTANTS
        C1=B/RO
        C2=C1*COTF(THTAA/2.)
        C3=PHIO*THTA/SINF(THTAA/2.)
        C4=RO*PHIO*THTA*COSF(THTAA/4.)/(2.*D)
        C5=C4*TANF(THTAA/4.)
        C6=B*D*RHO*RO*PHIO*THTA/(SPRCS*D*SINF(THTAA/2.)*TNAT**2)
        DO 40 I=1,NPT
        E2MX(I)=0.0
        E3MX(I)=0.0
 40     CONTINUE
        TSTPN=TSTP/TNAT
 50     TM=0.0
        JTM=1
        MTM=0
        DO 55 I=1,NPT
        U(I,JTM)=0
        W(I,JTM)=0
        DUT(I,JTM)=0
 55     DWT(I,JTM)=0
        CALL LOAD
        CALL EQEQND
        CALL PRINTR
 60     IF (TM-TSTPN) 65,65,62
 62     PRINT 63,TSTP
 63     FORMAT (3X,24HARCH DID NOT FAIL AFTER ,F8.4,2X,24HMILLISECONDS FRO
       1M START.)
        DO 64 I=1,NSEG
        PRDPK(I)=PINCR*PRDPK(I)
        PTGPK(I)=PINCR*PTGPK(I)
 64     CONTINUE
        GO TO 15
```

```
65    TM=TM+TINT
      JTM=JTM+1
      MTM=MTM+1
      KTR=1
      IF (JTM-2) 100,70,100
70    IF (NLOAD-2) 75,100,100
75    CALL LOAD
      DO 80 I=2,NSEG
      D2UTX(I,KTR)=C3*(PLT(I,JTM)+PLT(I-1,JTM))/(2.*C6)
      D2WTX(I,KTR)=(PLN(I,JTM)+PLN(I-1,JTM))/C6
80    CONTINUE
82    CALL DISP1
      KTR=KTR+1
      CALL EQEQND
      DO 85 I=2,NSEG
      CHKU(I)=(D2UTX(I,KTR)-D2UTX(I,KTR-1))/D2UTX(I,KTR-1)
      CHKW(I)=(D2WTX(I,KTR)-D2WTX(I,KTR-1))/D2WTX(I,KTR-1)
      IF (ABSF(CHKU(I))-CVRG) 84,84,82
84    IF (ABSF(CHKW(I))-CVRG) 85,85,82
85    CONTINUE
      GO TO 105
100   CALL DISP1
      CALL STRN
      CALL FORCE
      CALL LOAD
      CALL EQEQND
105   DO 110 I=2,NSEG
      Q(I)=QX(I,KTR)
      D2UT(I,JTM)=D2UTX(I,KTR)
110   D2WT(I,JTM)=D2WTX(I,KTR)
      Q(1)=QX(1,KTR)
      Q(NPT)=QX(NPT,KTR)
      D2UT(1,JTM)=0.0
      D2WT(1,JTM)=0.0
      D2UT(NPT,JTM)=0.0
      D2WT(NPT,JTM)=0.0
      IF (JTM-2) 112,111,112
111   CALL PRINTR
      GO TO 115
112   IF (MTM-MPI) 115,114,115
```

```
114   CALL PRINTR
      MPI=MPI+MLT
115   DO 140 I=1,NPT
      IF (E1(I,JTM)) 117,117,120
117   IF (E4(I,JTM)) 140,140,125
120   IF (E4(I,JTM)) 130,130,135
125   IF (E4(I,JTM)-EUTC) 140,141,141
130   IF (E1(I,JTM)-EUTC) 140,144,144
135   IF (E4(I,JTM)-EUTC) 136,141,141
136   IF (E1(I,JTM)-EUTC) 140,144,144
140   CONTINUE
      GO TO 148
141   TIME=TM*TNAT
      PRINT 142,I,E4(I,JTM),TIME
142   FORMAT (3X,32HARCH FAILED. CONCRETE STRAIN E4(,I2,2H)=,E12.4,8HAT
     1TIME=,F8.4,2X,13HMILLISECONDS.)
      CALL PRINTR
      GO TO 5
144   TIME=TM*TNAT
      PRINT 145,I,E1(I,JTM),TIME
145   FORMAT (3X,32HARCH FAILED. CONCRETE STRAIN E1(,I2,2H)=,E12.4,8HAT
     1TIME=,F8.4,2X,13HMILLISECONDS.)
      CALL PRINTR
      GO TO 5
148   IF (JTM-2) 60,60,150
150   DO 170 I=1,NPT
      U(I,JTM-2)=U(I,JTM-1)
      U(I,JTM-1)=U(I,JTM)
      U(I,JTM)=0.0
      W(I,JTM-2)=W(I,JTM-1)
      W(I,JTM-1)=W(I,JTM)
      W(I,JTM)=0.0
      DUT(I,JTM-2)=DUT(I,JTM-1)
      DUT(I,JTM-1)=DUT(I,JTM)
      DUT(I,JTM)=0.0
      DWT(I,JTM-2)=DWT(I,JTM-1)
      DWT(I,JTM-1)=DWT(I,JTM)
      DWT(I,JTM)=0.0
      D2UT(I,JTM-2)=D2UT(I,JTM-1)
      D2UT(I,JTM-1)=D2UT(I,JTM)
```

```
      D2UT(I,JTM)=0.0
      D2WT(I,JTM-2)=D2WT(I,JTM-1)
      D2WT(I,JTM-1)=D2WT(I,JTM)
      D2WT(I,JTM)=0.0
  170 CONTINUE
      JTM=JTM-1
      GO TO 60
      END

*     LIST
*     LABEL
      SUBROUTINE LOAD
      DIMENSION PRDPK(30),PTGPK(30),TRS(30),TLD(30),TDC(30),PLNPK(30),
     1PLTPK(30),TRSN(30),TLDN(30),TDCN(30),PLN(30,3),PLT(30,3),U(31,3),
     2W(31,3),DUT(30,3),DWT(30,3),D2UT(30,3),D2WT(30,3),D2UTX(30,20),
     3D2WTX(30,20),CHKU(30),CHKW(30),E4(31,3),E1(31,3),E2(31,3),E3(31,3)
     4,E2MX(31),E3MX(31),TN(31),BM(31),Q(31),CK(30),SN(30),
     5CS(30),EO(31,3),CVTR(31,3),A1(30),A2(30),A3(30),A4(30),QX(31,20),
     6EE2(31,3),EE3(31,3)
      COMMON B,D,DCVR,RO,PHIO,P,RHO,PI,EST,SYLD,SPC,EUTC,NSEG,NPT,PLNPK,
     1PLTPK,TRSN,TLDN,TDCN,EPSYS,SPRCS,EC,PHI2,THTA,THTAA,NSEG3,TNAT,
     2EPRCS,SPRCD,EPRCD,SYLDD,EPSYD,C1,C2,C3,C4,C5,C6,TM,JTM,KTR,PLN,PLT
     3,TINT,CVRG,U,W,DUT,DWT,D2UT,D2WT,D2UTX,D2WTX,E1,E2,E3,E4,E2MX,E3MX
     4,TN,BM,Q,EO,CVTR,A1,A2,A3,A4,QX,EE2,EE3,PRDPK,PTGPK,TRS,TLD,TDC,
     5NLOAD,CHKU,CHKW
      DO 400 I=1,NSEG
      IF (TRSN(I)) 360,360,351
  351 IF (TRSN(I)-TM) 360,352,352
  352 PLN(I,JTM)=PLNPK(I)*TM/TRSN(I)
      PLT(I,JTM)=PLTPK(I)*TM/TRSN(I)
      GO TO 400
  360 IF (TLDN(I)-TRSN(I)) 370,370,361
  361 IF (TLDN(I)-TM) 370,370,362
  362 PLN(I,JTM)=PLNPK(I)
      PLT(I,JTM)=PLTPK(I)
      GO TO 400
  370 IF (TDCN(I)-TLDN(I)) 380,380,371
  371 IF (TDCN(I)-TM) 380,380,372
  372 PLN(I,JTM)=PLNPK(I)*(TDCN(I)-TM)/(TDCN(I)-TLDN(I))
      PLT(I,JTM)=PLTPK(I)*(TDCN(I)-TM)/(TDCN(I)-TLDN(I))
```

```
      GO TO 400
  380 PLN(I,JTM)=0.0
      PLT(I,JTM)=0.0
  400 CONTINUE
      RETURN
      END

*     LIST
*     LABEL
      SUBROUTINE DISP1
      DIMENSION PRDPK(30),PTGPK(30),TRS(30),TLD(30),TDC(30),PLNPK(30),
     1PLTPK(30),TRSN(30),TLDN(30),TDCN(30),PLN(30,3),PLT(30,3),U(31,3),
     2W(31,3),DUT(30,3),DWT(30,3),D2UT(30,3),D2WT(30,3),D2UTX(30,20),
     3D2WTX(30,20),CHKU(30),CHKW(30),E4(31,3),E1(31,3),E2(31,3),E3(31,3)
     4,E2MX(31),E3MX(31),TN(31),BM(31),Q(31),CK(30),SN(30),
     5CS(30),EO(31,3),CVTR(31,3),A1(30),A2(30),A3(30),A4(30),QX(31,20),
     6EE2(31,3),EE3(31,3)
      COMMON B,D,DCVR,RO,PHIO,P,RHO,PI,EST,SYLD,SPC,EUTC,NSEG,NPT,PLNPK,
     1PLTPK,TRSN,TLDN,TDCN,EPSYS,SPRCS,EC,PHI2,THTA,THTAA,NSEG3,TNAT,
     2EPRCS,SPRCD,EPRCD,SYLDD,EPSYD,C1,C2,C3,C4,C5,C6,TM,JTM,KTR,PLN,PLT
     3,TINT,CVRG,U,W,DUT,DWT,D2UT,D2WT,D2UTX,D2WTX,E1,E2,E3,E4,E2MX,E3MX
     4,TN,BM,Q,EO,CVTR,A1,A2,A3,A4,QX,EE2,EE3,PRDPK,PTGPK,TRS,TLD,TDC,
     5NLOAD,CHKU,CHKW
C     COMPUTE DISPLACEMENTS BY ACCELERATION PULSE METHOD
      IF (JTM-2) 200,200,210
  200 IF (NLOAD-2) 202,204,204
  202 DO 203 I=2,NSEG
      U(I,JTM)=D2UTX(I,KTR)*TINT**2/6.
      W(I,JTM)=D2WTX(I,KTR)*TINT**2/6.
  203 CONTINUE
      GO TO 225
  204 DO 205 I=2,NSEG
      U(I,JTM)=D2UT(I,JTM-1)*TINT**2/2.
      W(I,JTM)=D2WT(I,JTM-1)*TINT**2/2.
  205 CONTINUE
      GO TO 225
  210 DO 220 I=2,NSEG
      U(I,JTM)=2.*U(I,JTM-1)-U(I,JTM-2)+D2UT(I,JTM-1)*TINT**2
      W(I,JTM)=2.*W(I,JTM-1)-W(I,JTM-2)+D2WT(I,JTM-1)*TINT**2
  220 CONTINUE
```

```
  225  U(1,JTM)=0
       W(1,JTM)=0
       U(NPT,JTM)=0
       W(NPT,JTM)=0
       DUT(1,JTM)=0
       DWT(1,JTM)=0
       DUT(NPT,JTM)=0
       DWT(NPT,JTM)=0
       DO 260 I=2,NSEG
       DUT(I,JTM)=(U(I,JTM)-U(I,JTM-1))/TINT
       DWT(I,JTM)=(W(I,JTM)-W(I,JTM-1))/TINT
  260  CONTINUE
       RETURN
       END

*      LIST
*      LABEL
       SUBROUTINE STRN
       DIMENSION PRDPK(30),PTGPK(30),TRS(30),TLD(30),TDC(30),PLNPK(30),
      1PLTPK(30),TRSN(30),TLDN(30),TDCN(30),PLN(30,3),PLT(30,3),U(31,3),
      2W(31,3),DUT(30,3),DWT(30,3),D2UT(30,3),D2WT(30,3),D2UTX(30,20),
      3D2WTX(30,20),CHKU(30),CHKW(30),E4(31,3),E1(31,3),E2(31,3),E3(31,3)
      4,E2MX(31),E3MX(31),TN(31),BM(31),Q(31),CK(30),SN(30),
      5CS(30),EO(31,3),CVTR(31,3),A1(30),A2(30),A3(30),A4(30),QX(31,20),
      6EE2(31,3),EE3(31,3)
       COMMON B,D,DCVR,RO,PHIO,P,RHO,PI,EST,SYLD,SPC,EUTC,NSEG,NPT,PLNPK,
      1PLTPK,TRSN,TLDN,TDCN,EPSYS,SPRCS,EC,PHI2,THTA,THTAA,NSEG3,TNAT,
      2EPRCS,SPRCD,EPRCD,SYLDD,EPSYD,C1,C2,C3,C4,C5,C6,TM,JTM,KTR,PLN,PLT
      3,TINT,CVRG,U,W,DUT,DWT,D2UT,D2WT,D2UTX,D2WTX,E1,E2,E3,E4,E2MX,E3MX
      4,TN,BM,Q,EO,CVTR,A1,A2,A3,A4,QX,EE2,EE3,PRDPK,PTGPK,TRS,TLD,TDC,
      5NLOAD,CHKU,CHKW
       DO 300 I=2,NSEG
       EO(I,JTM)=W(I,JTM)-(U(I+1,JTM)-U(I-1,JTM))/(2.*PHIO*THTA)
      1-(W(I+1,JTM)-W(I-1,JTM))**2/(8.*THTAA**2)-(U(I,JTM)*(W(I+1,JTM)-
      2W(I-1,JTM)))/(2.*THTAA)
       CVTR(I,JTM)=EO(I,JTM)+(W(I+1,JTM)-2.*W(I,JTM)+W(I-1,JTM))/THTAA**2
  300  CONTINUE
       EO(1,JTM)=-U(2,JTM)/THTAA-(W(2,JTM)**2)/(2.*THTAA**2)
       EO(NPT,JTM)=U(NSEG,JTM)/THTAA+(W(NSEG,JTM))**2/(2.*THTAA**2)
       CVTR(1,JTM)=0.0
```

```
      CVTR(NPT,JTM)=0.0
      DO 310 I=1,NPT
      E4(I,JTM)=EO(I,JTM)-D*CVTR(I,JTM)/(2.*RO)
      E1(I,JTM)=EO(I,JTM)+D*CVTR(I,JTM)/(2.*RO)
      E2(I,JTM)=E1(I,JTM)+(E4(I,JTM)-E1(I,JTM))*DCVR/D
      E3(I,JTM)=E1(I,JTM)+(E4(I,JTM)-E1(I,JTM))*(D-DCVR)/D
  310 CONTINUE
      DO 340 I=1,NPT
      SGM2=EST*(E2(I,JTM)-E2MX(I))
      IF (SGM2-SYLDD) 315,315,313
  313 E2MX(I)=E2MX(I)+(SGM2-SYLDD)/EST
      EE2(I,JTM)=EPSYD
      GO TO 320
  315 IF (-SGM2-SYLDD) 319,319,317
  317 E2MX(I)=E2MX(I)+(SGM2+SYLDD)/EST
      EE2(I,JTM)=-EPSYD
      GO TO 320
  319 EE2(I,JTM)=SGM2/EST
  320 SGM3=EST*(E3(I,JTM)-E3MX(I))
      IF (SGM3-SYLDD) 325,325,323
  323 E3MX(I)=E3MX(I)+(SGM3-SYLDD)/EST
      EE3(I,JTM)=EPSYD
      GO TO 340
  325 IF (-SGM3-SYLDD) 329,329,327
  327 E3MX(I)=E3MX(I)+(SGM3+SYLDD)/EST
      EE3(I,JTM)=-EPSYD
      GO TO 340
  329 EE3(I,JTM)=SGM3/EST
  340 CONTINUE
      RETURN
      END

*     LIST
*     LABEL
      SUBROUTINE FORCE
      DIMENSION PRDPK(30),PTGPK(30),TRS(30),TLD(30),TDC(30),PLNPK(30),
     1PLTPK(30),TRSN(30),TLDN(30),TDCN(30),PLN(30,3),PLT(30,3),U(31,3),
     2W(31,3),DUT(30,3),DWT(30,3),D2UT(30,3),D2WT(30,3),D2UTX(30,20),
     3D2WTX(30,20),CHKU(30),CHKW(30),E4(31,3),E1(31,3),E2(31,3),E3(31,3)
     4,E2MX(31),E3MX(31),TN(31),BM(31),Q(31),CK(30),SN(30),
```

```
     5CS(30),EO(31,3),CVTR(31,3),A1(30),A2(30),A3(30),A4(30),QX(31,20),
     6EE2(31,3),EE3(31,3)
      COMMON B,D,DCVR,RO,PHIO,P,RHO,PI,EST,SYLD,SPC,EUTC,NSEG,NPT,PLNPK,
     1PLTPK,TRSN,TLDN,TDCN,EPSYS,SPRCS,EC,PHI2,THTA,THTAA,NSEG3,TNAT,
     2EPRCS,SPRCD,EPRCD,SYLDD,EPSYD,C1,C2,C3,C4,C5,C6,TM,JTM,KTR,PLN,PLT
     3,TINT,CVRG,U,W,DUT,DWT,D2UT,D2WT,D2UTX,D2WTX,E1,E2,E3,E4,E2MX,E3MX
     4,TN,BM,Q,EO,CVTR,A1,A2,A3,A4,QX,EE2,EE3,PRDPK,PTGPK,TRS,TLD,TDC,
     5NLOAD,CHKU,CHKW
      DO 1000 I=1,NPT
      IF (E1(I,JTM)) 860,850,855
  850 IF (E4(I,JTM)) 990,870,870
  855 IF (E4(I,JTM)) 950,870,870
  860 IF (E4(I,JTM)) 990,990,910
C     SECTION UNDER COMPRESSION
  870 IF (E4(I,JTM)-E1(I,JTM)) 875,880,875
  875 R=((E4(I,JTM)**2-E1(I,JTM)**2)/EPRCD)-(E4(I,JTM)**3-E1(I,JTM)**3)/
     1(3.*EPRCD**2)
      S=(2.*(E4(I,JTM)**3-E1(I,JTM)**3)/(3.*EPRCD))-(E4(I,JTM)**4-E1(I,
     1JTM)**4)/(4.*EPRCD**2)
      TN(I)=(P*(EST-EC)*(EE2(I,JTM)+EE3(I,JTM))/(2.*SPRCS))+SPRCD*R/
     1(SPRCS*(E4(I,JTM)-E1(I,JTM)))
      BM(I)=(P*(D-2.*DCVR)*(EST-EC)*(EE3(I,JTM)-EE2(I,JTM))/(4.*SPRCS*D)
     1)+(SPRCD*S/(SPRCS*(E4(I,JTM)-E1(I,JTM))**2))-(SPRCD*(E1(I,JTM)+
     2E4(I,JTM))*R/(2.*SPRCS*(E4(I,JTM) E1(I,JTM))**2))
      GO TO 1000
  880 TN(I)=(P*(EST-EC)*(EE2(I,JTM)+EE3(I,JTM))/(2.*SPRCS))+(SPRCD*(E4(I
     1,JTM)+E1(I,JTM))/(EPRCD*SPRCS))-(SPRCD*((E4(I,JTM))**2+(E4(I,JTM))
     2*(E1(I,JTM))+(E1(I,JTM))**2)/(3.*SPRCS*EPRCD**2))
      BM(I)=0.0
      GO TO 1000
C     SECTION PARTLY UNDER TENSION AND PARTLY UNDER COMPRESSION
  910 R=(E4(I,JTM)**2/EPRCD)-(E4(I,JTM)**3/(3.*EPRCD**2))
      S=(2.*E4(I,JTM)**3/(3.*EPRCD))-(E4(I,JTM)**4/(4.*EPRCD**2))
      TN(I)=(P*(EST*(EE3(I,JTM)+EE2(I,JTM))-EC*E3(I,JTM))/(2.*SPRCS))+
     1SPRCD*R/(SPRCS*(E4(I,JTM)-E1(I,JTM)))
      BM(I)=(P*(D-2.*DCVR)*(EST*(EE3(I,JTM)-EE2(I,JTM))-EC*E3(I,JTM))/
     1(4.*SPRCS*D))+(SPRCD*S/(SPRCS*(E4(I,JTM)-E1(I,JTM))**2))-(SPRCD*
     2(E1(I,JTM)+E4(I,JTM))*R/(2.*SPRCS*(E4(I,JTM)-E1(I,JTM))**2))
      GO TO 1000
  950 R=(E1(I,JTM)**2/EPRCD)-(E1(I,JTM)**3/(3.*EPRCD**2))
```

```
      S=(2.*E1(I,JTM)**3/(3.*EPRCD))-(E1(I,JTM)**4/(4.*EPRCD**2))
      TN(I)=(P*(EST*(EE2(I,JTM)+EE3(I,JTM))-EC*E2(I,JTM))/(2.*SPRCS))+
     1SPRCD*R/(SPRCS*(E1(I,JTM)-E4(I,JTM)))
      BM(I)=-(P*(D-2.*DCVR)*(EST*(EE2(I,JTM)-EE3(I,JTM))-EC*E2(I,JTM))/
     1(4.*SPRCS*D))-(SPRCD*S/(SPRCS*(E1(I,JTM)-E4(I,JTM))**2))+(SPRCD*
     2(E1(I,JTM)+E4(I,JTM))*R/(2.SPRCS*(E1(I,JTM)-E4(I,JTM))**2))
      GO TO 1000
C     SECTION COMPLETELY UNDER TENSION
 990  TN(I)=P*EST*(EE2(I,JTM)+EE3(I,JTM))/(2.*SPRCS)
      BM(I)=P*(D-2.*DCVR)*EST*(EE3(I,JTM)-EE2(I,JTM))/(4.*SPRCS*D)
1000  CONTINUE
      RETURN
      END

*     LIST
*     LABEL
      SUBROUTINE EQEQND
      DIMENSION PRDPK(30),PTGPK(30),TRS(30),TLD(30),TDC(30),PLNPK(30),
     1PLTPK(30),TRSN(30),TLDN(30),TDCN(30),PLN(30,3),PLT(30,3),U(31,3),
     2W(31,3),DUT(30,3),DWT(30,3),D2UT(30,3),D2WT(30,3),D2UTX(30,20),
     3D2WTX(30,20),CHKU(30),CHKW(30),E4(31,3),E1(31,3),E2(31,3),E3(31,3)
     4,E2MX(31),E3MX(31),TN(31),BM(31),Q(31),CK(30),SN(30),
     5CS(30),EO(31,3),CVTR(31,3),A1(30),A2(30),A3(30),A4(30),QX(31,20),
     6EE2(31,3),EE3(31,3)
     7,D2UTXX(30,20),D2WTXX(30,20),AEQ(90,90),BEQ(90),D2(90)
      COMMON B,D,DCVR,RO,PHIO,P,RHO,PI,EST,SYLD,SPC,EUTC,NSEG,NPT,PLNPK,
     1PLTPK,TRSN,TLDN,TDCN,EPSYS,SPRCS,EC,PHI2,THTA,THTAA,NSEG3,TNAT,
     2EPRCS,SPRCD,EPRCD,SYLDD,EPSYD,C1,C2,C3,C4,C5,C6,TM,JTM,KTR,PLN,PLT
     3,TINT,CVRG,U,W,DUT,DWT,D2UT,D2WT,D2UTX,D2WTX,E1,E2,E3,E4,E2MX,E3MX
     4,TN,BM,Q,EO,CVTR,A1,A2,A3,A4,QX,EE2,EE3,PRDPK,PTGPK,TRS,TLD,TDC,
     5NLOAD,CHKU,CHKW,NCHR
      IF (JTM-1) 590,590,615
 590  DO 592 I=1,NSEG
 592  D2WTXX(I,JTM)=2.*PLN(I,JTM)/C6
      DO 595 I=1,NSEG
 595  D2UTXX(I,JTM)=C3*PLT(I,JTM)/C6
      DO 610 I=2,NSEG
      D2UT(I,JTM)=(D2UTXX(I,JTM)+D2UTXX(I-1,JTM))/2.
      D2WT(I,JTM)=(D2WTXX(I,JTM)+D2WTXX(I-1,JTM))/2.
 610  CONTINUE
```

```
      GO TO 675
  615 NSEG1=NSEG-1
      DO 612 I=1,NSEG1
      CK(I)=(W(I+2,JTM)-2.*W(I+1,JTM)+W(I,JTM))/(PHIO*THTA)
  612 CONTINUE
      CK(NSEG)=CK(NSEG1)
      DO 630 I=1,NSEG
      SN(I)=SINF(CK(I))
      CS(I)=COSF(CK(I))
      A1(I)=-C2*CS(I)+C1*SN(I)
      A2(I)=-C2*SN(I)-C1*CS(I)
      A3(I)=C2*CS(I)+C1*SN(I)
      A4(I)=C2*SN(I)-C1*CS(I)
  630 CONTINUE
      IF (NCHR-2) 680,640,640
  640 R=A3(1)*TN(1)+A1(1)*TN(2)+C3*PLT(1)
      S=C5*TN(2)-C5*TN(1)+BM(2)-BM(1)
      T=A4(1)*TN(1)+A2(1)*TN(2)+2.*PLN(1)
      QX(1,KTR)=(T*C4-S*A1(1))/(A3(1)*C4-A1(1)*C4)
      QX(2,KTR)=(S*A3(1)-T*C4)/(A3(1)*C4-A1(1)*C4)
      D2UTXX(1,KTR)=(R+A4(1)*QX(1,KTR)+A2(1)*QX(2,KTR))/C6
      DO 650 I=2,NSEG
      J=I+1
      QX(J,KTR)=(C5*TN(J)-C5*TN(I)+BM(J)-BM(I)-C4*QX(I,KTR))/C4
      D2WTXX(I,KTR)=(A4(I)*TN(I)+A2(I)*TN(J)+2.*PLN(I,JTM)-A3(I)*QX(I,
     1KTR)-A1(I)*QX(J,KTR))/C6
      D2UTXX(I,KTR)=(A3(I)*TN(I)+A1(I)*TN(J)+C3*PLT(I,JTM)+A4(I)*QX(I,
     1KTR)+A2(I)*QX(J,KTR))/C6
  650 CONTINUE
      D2WTXX(1,KTR)=0.0
      D2WTXX(NSEG,KTR)=0.0
      GO TO 655
  680 NSEG2=NSEG/2
      NSEG12=NSEG2-1
      NSE23=3*NSEG2
      DO 685 I=1,NSE23
      DO 685 J=1,NSE23
  685 AEQ(I,J)=0
      DO 690 I=1,NSEG12
      J=3*I
```

```
      AEQ(J-2,J-2)=A3(I)
      AEQ(J-2,J-1)=C6
      AEQ(J-2,J+1)=A1(I)
      AEQ(J-1,J-2)=-A4(I)
      AEQ(J-1,J)=C6
      AEQ(J-1,J+1)=-A2(I)
      AEQ(J,J-2)=C4
      AEQ(J,J+1)=C4
  690 CONTINUE
      AEQ(NSE23-2,NSE23-2)=A3(NSEG2)
      AEQ(NSE23-2,NSE23-1)=C6
      AEQ(NSE23-1,NSE23-2)=-A4(NSEG2)
      AEQ(NSE23-1,NSE23)=C6
      AEQ(NSE23,NSE23-2)=C4
  700 DO 705 I=1,NSE23
  705 BEQ(I)=0
      DO 710 I=1,NSEG2
      J=3*I
      BEQ(J-2)=A4(I)*TN(I)+A2(I)*TN(I+1)+2.*PLN(I,JTM)
      BEQ(J-1)=A3(I)*TN(I)+A1(I)*TN(I+1)+C3*PLT(I,JTM)
      BEQ(J)=-C5*TN(I)+C5*TN(I+1)-BM(I) BM(I+1)
  710 CONTINUE
      D1=0.0
      M=XSIMEQF(90,NSE23,1,AEQ,BEQ,D1,D2)
      GO TO (725,720,715),M
  720 PRINT 730
      CALL EXIT
  715 PRINT 735
      CALL EXIT
  730 FORMAT(15H OVER/UNDERFLOW)
  735 FORMAT(14H A IS SINGULAR)
  725 DO 727 I=1,NSEG2
      J=3*I
      JJ=NPT-I+1
      QX(I,KTR)=AEQ(J-2,1)
      D2WTXX(I,KTR)=AEQ(J-1,1)
      D2UTXX(I,KTR)=AEQ(J,1)
      QX(JJ,KTR)=-AEQ(J-2,1)
      D2WTXX(JJ-1,KTR)=AEQ(J-1,1)
      D2UTXX(JJ-1,KTR)=-AEQ(J,1)
```

```
  727  CONTINUE
       KK=NSEG2+1
       QX(KK,KTR)=0.0
  655  DO 660 I=2,NSEG
       D2UTX(I,KTR)=(D2UTXX(I,KTR)+D2UTXX(I-1,KTR))/2.
       D2WTX(I,KTR)=(D2WTXX(I,KTR)+D2WTXX(I-1,KTR))/2.
  660  CONTINUE
  675  RETURN
       END

*      LIST
*      LABEL
       SUBROUTINE PRINTR
       DIMENSION PRDPK(30),PTGPK(30),TRS(30),TLD(30),TDC(30),PLNPK(30),
      1PLTPK(30),TRSN(30),TLDN(30),TDCN(30),PLN(30,3),PLT(30,3),U(31,3),
      2W(31,3),DUT(30,3),DWT(30,3),D2UT(30,3),D2WT(30,3),D2UTX(30,20),
      3D2WTX(30,20),CHKU(30),CHKW(30),E4(31,3),E1(31,3),E2(31,3),E3(31,3)
      4,E2MX(31),E3MX(31),TN(31),BM(31),Q(31),CK(30),SN(30),
      5CS(30),EO(31,3),CVTR(31,3),A1(30),A2(30),A3(30),A4(30),QX(31,20),
      6EE2(31,3),EE3(31,3)
       COMMON B,D,DCVR,RO,PHIO,P,RHO,PI,EST,SYLD,SPC,EUTC,NSEG,NPT,PLNPK,
      1PLTPK,TRSN,TLDN,TDCN,EPSYS,SPRCS,EC,PHI2,THTA,THTAA,NSEG3,TNAT,
      2EPRCS,SPRCD,EPRCD,SYLDD,EPSYD,C1,C2,C3,C4,C5,C6,TM,JTM,KTR,PLN,PLT
      3,TINT,CVRG,U,W,DUT,DWT,D2UT,D2WT,D2UTX,D2WTX,E1,E2,E3,E4,E2MX,E3MX
      4,TN,BM,Q,EO,CVTR,A1,A2,A3,A4,QX,EE2,EE3,PRDPK,PTGPK,TRS,TLD,TDC,
      5NLOAD,CHKU,CHKW
       TIME=TM*TNAT
  800  PRINT 802,TIME
  802  FORMAT (3X,7HTIME IS,F8.4,13HMILLISECONDS.)
  805  PRINT 810,((I,TN(I),I,Q(I),I,BM(I)),I=1,NPT)
  810  FORMAT (3X,7HTHRUST(,I2,2H)=,E12.4,3X,6HSHEAR(,I2,2H)=,E12.4,3X,
      17HMOMENT(,I2,2H)=,E12.4)
  815  PRINT 820,((I,E4(I,JTM),I,E1(I,JTM)),I=1,NPT)
  820  FORMAT (3(3X,3HE4(,I2,2H)=,E12.4,3X,3HE1(,I2,2H)=,E12.4))
  825  PRINT 830,((I,U(I,JTM),I,DUT(I,JTM),I,D2UT(I,JTM)),I=1,NPT)
  830  FORMAT (3X,2HU(,I2,2H)=,E12.4,3X,4HDUT(,I2,2H)=,E12.4,3X,5HD2UT(,
      1I2,2H)=,E12.4)
  835  PRINT 840,((I,W(I,JTM),I,DWT(I,JTM),I,D2WT(I,JTM)),I=1,NPT)
  840  FORMAT (3X,2HW(,I2,2H)=,E12.4,3X,4HDWT(,I2,2H)=,E12.4,3X,5HD2WT(,
      1I2,2H)=,E12.4)
```

```
      RETURN
      END
```

BIBLIOGRAPHY

1. Cross, H., and Morgan, N.D., "Continuous Frames of Reinforced Concrete", John Wiley and Sons, Inc. New York, 1932.

2. ACI Committee, "Plain and Reinforced Concrete Arches", J. ACI, Vol. 22, No. 9, May 1951.

3. Onat, E.T., and Prager, W., "Limit Analysis of Arches", J. Mechanics and Physics of Solids, Vol. 1, No. 2, January, 1953.

4. Jain, O. P., "Ultimate Strength of Reinforced Concrete Arches", J. ACI, December 1960.

5. Love, A.E.H., "A Treatise on the Mathematical Theory of Elasticity", Fourth Edition, Dover Publications, New York, 1944.

6. Eppink, R. T., and Veletsos, A. S., "Dynamic Analysis of Circular Elastic Arches", Second Conference on Electronic Computation, ASCE, September 1960.

7. Eppink, R. T., and Veletsos, A. S. "Response of Arches under Dynamic Loads", University of Illinois, Structural Research Series, No. 210, December 1960.

8. Hognestad, E., "A Study of Combined Bending and Axial Load in Reinforced Concrete Members", University of Illinois Engineering Experiment Station, Bulletin No. 399, 1951.

9. Watstein, E., "Effect of Straining Rate on the Compressive Strength and Elastic Properties of Concrete", J. ACI. Vol. 24, No. 8, April, 1953

10. Yang, C. Y., Tang, C. N., Ho, S., Parikh, K. S. Reinschmidt, K. F., Abbott, B. W., "The Dynamic Behavior of Reinforced Concrete Columns, Part II", Department of Civil Engineering, M.I.T., March 1962.

11. Norris, C. H., Hansen, R. J., Holley, M. J., Jr., Biggs, J. M., Namyet, S., Minami, J. K., "Structural Design for Dynamic Loads", McGraw-Hill, New York, 1959.

12. Hildebrand, F. B., "Introduction to Numerical Analysis", McGraw-Hill, New York, 1956.

13. "Protective Construction Review Guide (Hardening), Volume I", Department of Defense, June, 1961.

14. Crandall, S. H., "Engineering Analysis", McGraw-Hill, New York, 1956.

15. Wilson, W. M., "Laboratory Tests of Reinforced Concrete Arch Ribs", University of Illinois, Engg. Experiment Station, Bulletin No. 202 Feb. 1930.

16. Wilson, W. M., and Kluge, R. W. "Laboratory Tests of Three-Span Reinforced Concrete Arch Bridges with Deck on Slender Piers" Univ. of Illinois, Engg. Experiment Station, Bulletin No. 270, Dec. 1934.

17. "Design and Analysis of Underground Reinforced-Concrete Arches", Technical Report No. 2-590, U. S. Army Engineer Waterways Experiment Station, Vicksburg, January 1962.

18. Simpson, H., "Design and Construction of a Testing Machine for Large Dynamic Loads" Feb. 1959.

19. "Design of Structures to Resist Nuclear Weapons Effects", ASCE Manual No. 42.

20. Gupchup, V. N. "Nonlinear Response of Two-Hinged, Circular Reinforced Concrete Arches to Static and Dynamic Loads". Sc. D. Thesis, M.I.T. January, 1963.

DISTRIBUTION LIST
FOR BLAST & SHOCK
R & D REPORTS

ADDRESSEE	NO. OF CYS.
ARMY	
Chief of Research and Development, D/A, Washington 25, D. C. Attn: Atomic Division	1
Chief of Engineers, D/A, Washington 25, D.C.	
Attn: ENGCW-NE	1
ENGTE-E	1
ENGMC-E	1
Commanding General, U. S. Army Materiel Command, Washington, D. C. Attn: AMCRD-DE-N	2
Commandant, Command & General Staff College, Ft. Leavenworth, Kansas, Attn: Archieves	1
Commanding General, Aberdeen Proving Ground, Aberdeen, Md. Attn: Director, BRL	1
Commanding General, The Engineer Center, Ft. Belvoir, Va. Attn: Asst. Commandant, Engineer School	1
Director, U. S. Army Research and Development Laboratory Ft. Belvoir, Va. Attn: Chief, Tech. Support Branch	1
Commanding Officer, Picatinny Arsenal, Dover, New Jersey. Attn: ORDBB-TK	1
Commanding General, USA Electronic R&D Lab., Ft. Monmouth, N.J., Attn: Technical Documents Center, Evans Area	1
Director, Waterways Experiment Station, U. S. Army Corps of Engineers, Vicksburg, Mississippi, Attn: Library	1
Director, U. S. Army Corps of Engineers, Nuclear Cratering Group, Livermore, California	1
NAVY	
Chief of Naval Operations, ND, Washington 25, D.C.	
Attn: OP-75	2
Attn: OP-03EG	1

DISTRIBUTION LIST

ADDRESSEE	NAVY (Cont'd)	NO. OF CYS.
Chief, Bureau of Yards and Docks, ND, Washington 25, D. C.		
Attn: Code D-400		1
Attn: Code D-440		1
Chief of Naval Research, ND, Washington 25, D.C.		
Attn: Code 811		1
Superintendent, U. S. Naval Postgraduate School, Monterey, California		1
Commanding Officer, U. S. Naval Schools Command, U. S. Naval Station Treasure Island, San Francisco, California		1
Commanding Officer, Nuclear Weapons Training Center, Pacific, Naval Station, North Island, San Diego 35, California		2
Commanding Officer, U. S. Naval Damage Control Training Center, Naval Base, Philadelphia 12, Pa. Attn: ABC Defense Course		1
Commander, U. S. Naval Ordnance Laboratory, Silver Spring 19, Maryland,		
Attn: EA		1
EU		1
E		1
Commander, U. S. Naval Ordnance Test Station, China Lake, Calif.		1
Commanding Officer & Director, U. S. Naval Civil Engineering Laboratory, Port Hueneme, Calif., Attn: Code L31		1
Commanding Officer & Director, David W. Taylor Model Basin, Washington 7, D.C.,		
Attn: Library		1
	AIR FORCE	
Hq. USAF (AFDRC/NE - Maj. Lowry) Washington 25, D. C.		1

DISTRIBUTION LIST

ADDRESSEE	AIR FORCE	NO. OF CYS.
Air Force Intelligence Center, Hq. USAF ACS/I (AFCIN-3K2) Washington 25, D. C.		1
Commander, Air Force Logistics Command, Wright-Patterson AFB, Ohio		2
AFSC, Andrews Air Force Base, Washington 25, D. C. Attn: RDRWA		1
Director, Air University Library, Maxwell AFB, Alabama		2
AFSWC (SWRS) Kirtland AFB, New Mexico		1
Commandant, Institute of Technology, Wright-Patterson AFB, Ohio, Attn: MCLI-ITRIDL		1
BSD, Norton AFB, California		1
Director, USAF Project RAND, Via: U. S. Air Force Liaison Office, The Rand Corporation, 1700 Main Street, Santa Monica, California		1
Director of Civil Engineering, Hq. USAF, Washington 25, D. C. Attn: AFOCE		1
OTHERS		
Director, Weapons Systems Evaluation Group, OSD, Rm 1E880, The Pentagon, Washington 25, D. C.		1
Commandant, Armed Forces Staff College, Norfolk 11, Virginia. Attn: Library		1
Commander, Field Command, DASA, Sandia Base. Albuquerque, New Mexico		16
Commander, Field Command, DASA, Sandia Base. Albuquerque, New Mexico Attn:	FCWT	1
	FCTG	1
Chief, Defense Atomic Support Agency, Washington 25, D. C.		5

DISTRIBUTION LIST

ADDRESSEE	OTHERS (Cont'd)	NO. OF CYS.
Officer-in-Charge, U. S. Naval School, Civil Engineering Corps Officers, U. S. Naval Construction Battalion, Port Hueneme, California		1
Los Alamos Scientific Laboratory, P. O. Box 1663, Los Alamos, New Mexico, Attn: Report Librarian (for Dr. A. C. Graves)		1
Chief, Classified Technical Library, Technical Information Service, U. S. Atomic Energy Commission, Washington 25, D. C., Attn: Mrs. Jean o'Leary (for Dr. Paul C. Fine)		1
Chief, Classified Technical Library, Technical Information Service, U. S. Atomic Energy Commission, Washington 25, D. C., Attn: Mrs. Jean o'Leary		1
Dr. Robert J. Hansen, Rm. 1-238, Massachusetts Institute of Technology, 77 Mass. Ave. Cambridge, Massachusetts		1
Dr. Bruce G. Johnston, The University of Michigan, University Research Security Office, Lobby 1, East Engineering Bldg., Ann Arbor, Michigan		1
Sandia Corporation, Sandia Base, Albuquerque, New Mexico, Attn: Classified Document Division (for Dr. M. L. Merritt		1
Dr. Nathan M. Newmark, University of Illinois, Rm. 207, Talbot Laboratory, Urbana, Illinois		1
Commander, ASTIA, Arlington Hall Station, Arlington 12, Virginia, Attn: TIPDR		15
Holmes & Narver, Inc. AEC Facilities Division, 849 S. Broadway Los Angeles 14, California Attn: Mr. Frank Galbreth		1
Professor Robert V. Whitman, Massachusetts Institute of Technology, Rm. 1-346A Cambridge 39, Mass.		1

DISTRIBUTION LIST

ADDRESSEE	OTHERS (Cont'd)	NO. OF CYS.
Professor J. Neils Thompson, University of Texas, Structural Mechanics Research Laboratory, Austin, Texas		1
Dr. Neidhardt, General American Transportation Corporation, 7501 N. Natchez Avenue, Niles, Illinois		1
Mr. Sherwood Smith, Roland F. Beers, Inc., 2520 Oakville, Alexandria, Va.		1
Paul Weidlinger, Consulting Engineer, 770 Lexington Ave., New York 21, New York Attn: Dr. M. Baron		1
Mr. A. Weiderman, Armour Research Foundation, 10 West 35th St. Chicago 16, Illinois		1